

Hugo García Juan

Preparation of polymeric nanocarriers with response to visible light

Director/es

ORIO L LANGA, LUIS T
PIÑOL LACAMBRA, MILAGROS

<http://zaguan.unizar.es/collection/Tesis>



© Universidad de Zaragoza
Servicio de Publicaciones

ISSN 2254-7606



Universidad
Zaragoza

Tesis Doctoral

PREPARATION OF POLYMERIC NANOCARRIERS
WITH RESPONSE TO VISIBLE LIGHT

Autor

Hugo García Juan

Director/es

ORIO L LANGA, LUIS T
PIÑOL LACAMBRA, MILAGROS

UNIVERSIDAD DE ZARAGOZA
Escuela de Doctorado

2019

TESIS DOCTORAL

**PREPARATION OF POLYMERIC
NANOCARRIERS WITH RESPONSE
TO VISIBLE LIGHT**

Hugo García Juan

Directores:

Dr. Luis Oriol Langa

Dra. Milagros Piñol Lacambra

Dpto. de Química Orgánica

Universidad de Zaragoza-ICMA

Zaragoza, Octubre 2019



Departamento de
Química Orgánica
Universidad Zaragoza



TESIS DOCTORAL

**PREPARATION OF POLYMERIC
NANOCARRIERS WITH RESPONSE
TO VISIBLE LIGHT**

Memoria presentada en la Universidad de Zaragoza
para optar al grado de Doctor

Hugo García Juan

Dpto. de Química Orgánica

Universidad de Zaragoza-ICMA

Zaragoza, Octubre 2019



Departamento de
Química Orgánica
Universidad Zaragoza



icma
Instituto de Ciencia
de Materiales de Aragón



Los Drs. LUIS T. ORIOL LANGA, Catedrático del Departamento de Química Orgánica, y MILAGROS PIÑOL LACAMBRA, Profesora Titular del Departamento de Química Orgánica, pertenecientes a la Facultad de Ciencias y al Instituto de Ciencia de Materiales de Aragón de la Universidad de Zaragoza-CSIC

HACEN CONSTAR:

Que la memoria titulada: "Preparation of polymeric nanocarriers with response to visible light" ha sido realizada bajo nuestra dirección por D. Hugo García Juan en el Departamento de Química Orgánica de esta Universidad y reúne las condiciones requeridas para su presentación como tesis doctoral.

Zaragoza, Octubre de 2019

Fdo.: Dr. Luis Oriol Langa

Fdo.: Dra. Milagros Piñol Lacambra

RESUMEN

El uso de copolímeros bloque anfífilos para la preparación de micelas o vesículas poliméricas, capaces de actuar como nanotransportadores de fármacos para la encapsulación y liberación controlada de los mismos, ha sido ampliamente descrito en la bibliografía.

La introducción de moléculas con capacidad de responder a la luz en este tipo de autoensamblados es particularmente interesante ya que la luz es un estímulo que se puede controlar de forma espacio-temporal. En particular, los derivados de azobenceno (capaces de isomerizar de *trans* a *cis* al ser irradiados con luz de longitud de onda adecuada) han sido ampliamente descritos en la bibliografía. Este tipo de cromóforos han sido introducidos en copolímeros bloque pudiendo inducir cambios morfológicos en los nanotransportadores derivados de los mismos, al ser éstos irradiados, lo que puede conducir a la liberación controlada de moléculas previamente encapsuladas. Sin embargo, los sistemas descritos en la bibliografía hacen uso de la luz UV como fuente de excitación, la cual es dañina para los tejidos biológicos, lo que limita su aplicación. Una alternativa interesante podría ser el uso en copolímeros bloque anfífilos de nuevos cromóforos que presenten respuesta en la región visible o infrarroja cercana, puesto que son menos dañinas y tienen más penetración en los tejidos.

Por otro lado, en los últimos años se ha producido un auge en la aplicación de la química supramolecular a polímeros. Concretamente, los polímeros supramoleculares permiten el acceso a nuevos tipos de materiales basados en la naturaleza dinámica de las interacciones supramoleculares (principalmente sistemas “*host-guest*” y enlaces de hidrógeno). Otra gran ventaja de estos sistemas es la de poder preparar una gran cantidad de materiales distintos partiendo de unos pocos precursores, combinándolos mediante el uso de las interacciones supramoleculares mencionadas.

Con todo esto se plantean dos grandes objetivos. En primer lugar, la preparación de nanotransportadores poliméricos con respuesta a la luz fuera de la región UV y, en segundo lugar, el uso de la química supramolecular para preparar copolímeros bloque anfífilos, y su autoensamblaje para generar nanotransportadores con respuesta a la luz. En concreto para los distintos capítulos los objetivos han sido los siguientes:

- La preparación de copolímeros bloque anfífilos basados en unidades de *orto*-tetrametoxiazobenceno, con respuesta a la luz verde y roja, su autoensamblado en agua y el estudio de su fotorrespuesta a dichas longitudes de onda (**Capítulo 2**).
- La preparación de copolímeros bloque anfífilos basados en un sistema formado por derivados de 4-alkilaminoazobenceno, capaces de responder a longitudes de onda fuera de la región UV, y derivados de naftaleno que puede actuar como sensibilizador (a uno o dos fotones) para provocar la excitación de la unidad azobenceno. La incorporación de ambos derivados en los copolímeros bloque mediante dos aproximaciones: unión covalente en la misma unidad de ambos de tipos de derivados o incorporación independiente, como comonómeros, a la estructura polimérica. El autoensamblado en agua de los diferentes copolímeros bloque y el estudio de la fotorrespuesta de los mismos. El uso de la química supramolecular para introducir dichas unidades en polímeros con unidades complementarias (**Capítulo 3**).
- La preparación de copolímeros bloque basados en guanina, capaz de formar enlaces de hidrógeno con unidades complementarias de citosina, así como la introducción de derivados de azobenceno con grupos terminales de citosina y el autoensamblado de dichos sistemas en agua (**Capítulo 4**).

Acronyms list

2PA	Two-photon absorption
AIBN	2,2'-Azobis(2-methylpropionitrile)
ATRP	Atom transfer radical polymerization
BC	Block copolymer
CAC	Critical aggregation concentration
CD	Cyclodextrin
CMC	Critical micellar concentration
Cps	Counts per second
CRP	Control radical polymerization
CTA	Chain transfer agent
CuAAC	Copper-catalysed alkyne-azide cycloaddition
DAP	Diaminopyridine
DCM	Dichloromethane
DLS	Dynamic light scattering
DMAP	Dimethylaminopyridine
DMF	Dimethylformamide
DMSO	Dimethylsulfoxide
DOX	Doxorubicin
DP	Degree of polymerization
DPTS	1,4-Dimethylpyridinium p-toluenesulfonate
DR1	Disperse Red 1
DSC	Differential scanning calorimetry
EDC	N-(3-Dimethylaminopropyl)-N'-ethylcarbodiimide hydrochloride
GPC	Gel permeation chromatography
LCST	Lower critical solution temperature

MeOH	Methanol
M_n	Number average molar mass
M_w	Mass average molar mass
PCL	Polycaprolactone
PDAEMA	Poly(diehtylamino) methacrylate
PDAP	Poly diaminopyridine methacrylate
PEG	Poly(ethylene glycol)
PMMA	Poly(methylmethacrylate)
PNIPAM	Poly(N-isopropylacrylamide)
PS	Polystyrene
RAFT	Reversible addition fragmentation transfer
Rcf	Relative centrifugal field
RhB	Rhodamine B
SEC	Size exclusion chromatography
TBAF	Tetrabutylammonium fluoride
TBDMS	Tert-butyl dimethyl silyl group
TEM	Transmission electronic microscopy
T_g	Glass transition temperature
TGA	Thermogravimetric analysis
THF	Tetrahydrofuran
TLC	Thin layer chromatography

Contents

Chapter 1: General Introduction	1
1.1. Stimuli responsive polymers.....	3
1.1.1. Light responsive polymers	5
1.1.2. Visible and NIR responsive azobenzenes.....	7
1.2. Amphiphilic block copolymers	13
1.2.1. Synthesis of block copolymers.....	13
1.2.2. Polymeric nanocontainers based on amphiphilic block copolymers ...	19
1.2.2.1. Stimuli responsive polymer nanocarriers.....	25
1.2.2.2. Light responsive polymeric nanocarriers	26
1.3. Supramolecular polymers.....	37
1.3.1. H-bonded supramolecular polymers	40
1.4. References	51
Chapter 2: Amphiphilic BCs based on tetramethoxyazobenzene	63
2.1. Introduction and aims	65
2.2. Synthesis, characterisation and self-assembly in water	67
2.3. Visible light responsiveness	83
2.3.1. Photoisomerisation of the monomers in solution	83
2.3.2. Photoresponse of the polymeric self-assemblies.....	86
2.4. Conclusions.....	94
2.5. Experimental section	95
2.5.1. Synthesis and chemical characterisation	95
2.5.2. Preparation and characterisation of polymeric aggregates	100
2.5.3. Encapsulation and release studies	101
2.6. References	102

Chapter 3: Amphiphilic BCs based on 4-dialkylaminoazobenzene derivatives.....	105
3.1. Introduction and aims	107
3.2. Synthesis and characterisation of the block copolymers	110
3.2.1. Covalent amphiphilic block copolymer having the AZO-Naph bichromophore.....	110
3.2.2. Supramolecular amphiphilic block copolymer having the AZO-Naph bichromophore.....	116
3.2.3. Covalent amphiphilic block copolymers with AZO-NO ₂	119
3.2.4. Supramolecular amphiphilic block copolymers with AZO-NO ₂	127
3.3. Light responsiveness.....	134
3.3.1. Study of the photoresponse of PEG5k- <i>b</i> -p(AZO-NAPH).....	134
3.3.2. Study of the photoresponse of AZO-NO ₂ /Naph BCs.....	138
3.4. Conclusions.....	150
3.5. Experimental section	151
3.5.1. Synthesis and chemical characterisation	151
3.5.2. Preparation and characterisation of polymer aggregates.....	170
3.6. References	173
Chapter 4: Amphiphilic BCs based on guanine.....	175
4.1. Introduction and aims	177
4.2. Synthesis and characterisation of amphiphilic block copolymers	179
4.2.1. Synthesis of guanine and cytosine monomers.....	179
4.2.2. Synthesis of amphiphilic block copolymers.....	184
4.3. Self-assembly in water of amphiphilic block copolymers	188
4.3.1 Self-assembly of block copolymers.....	188
4.3.2. Self-assembly of supramolecular block copolymers	191

4.4. Conclusions.....	198
4.5. Experimental section	199
4.5.1. Synthesis and chemical characterisation	199
4.5.2. Preparation and characterisation of polymer aggregates.....	207
4.6. References	209
Conclusions.....	211
Appendix: Techniques and instruments.....	215

CHAPTER 1: GENERAL INTRODUCTION

1.1. STIMULI RESPONSIVE POLYMERS

Stimuli responsive or 'smart' polymers have been defined as polymers that suffer changes in their structures when an appropriate stimulus is applied. These changes can go from an alteration of the polymer polarity to a modification of the chemical connectivity. Regarding stimuli, examples include pH, temperature, light, mechanical forces or oxidizing/reducing agents, amongst others. In last years, these polymers have gained interest for different applications such as data storage, biosensing, controlled drug delivery, actuators, artificial muscles or nanoreactors.¹

Temperature responsive polymers are amongst the most studied stimuli responsive polymer because changes in temperature are relatively easy to control. The majority of the polymers included in this category are soluble below a temperature named lower critical solution temperature (LCST) above which the polymer is not soluble and collapses into a globular state (**Figure 1.1**). The LCST depends on the polymer composition and the solvent, being water the most interesting solvent for biomedical applications. In water, this type of polymers change from hydrophilic to hydrophobic upon this transition. Poly(*N*-isopropylacrylamide) (PNIPAM) is a representative example that has a LCST closed to the physiological temperature.² Copolymers of oligoethylene glycol methacrylate and diethylene glycol methacrylate are interesting because they present a tuneable LCST depending on the relative proportion of both monomers.³ This type of copolymers have been used in our group for the preparation of polymeric vesicles capable of modifying their morphology when they are heated above LCST.⁴

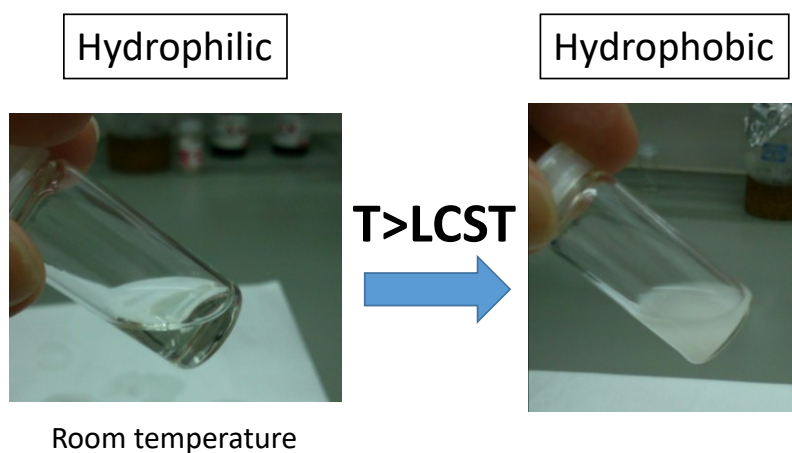


Figure 1.1. Visual changes observed in a temperature responsive polymer below (left) and above (right) its lower critical solution temperature (LCST)

pH is also a widely used stimulus that modifies the solubility of a polymer.⁵ The incorporation of pH sensitive units (e.g. amine groups) in a polymer chain can induce a transition from a non-soluble to a soluble polymer in water. When pH is higher than pK_a , the amine groups are neutral but when it is lower they are protonated and the polymer becomes soluble in water (**Figure 1.2**).

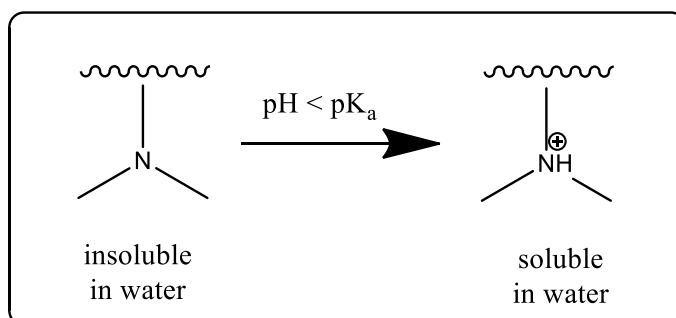


Figure 1.2. Example of a pH responsive group

In recent years, relevant achievements on new synthetic methodologies attained in Polymer Chemistry together with the large variety of available stimuli have launched the enormous progress on stimuli-responsive polymers with tailored properties for different purposes observed during last decade. This General Introduction will be focused on light responsive polymers mainly for bioapplications.

1.1.1. LIGHT RESPONSIVE POLYMERS

Light is a very interesting stimulus that can be controlled in time and space. Usually, light response is associated with the presence of chromophores capable to isomerise or being able to undergo a chemical reaction when they are irradiated with light of a proper wavelength. In **Figure 1.3**, examples of chromophores commonly used in light responsive materials are shown.

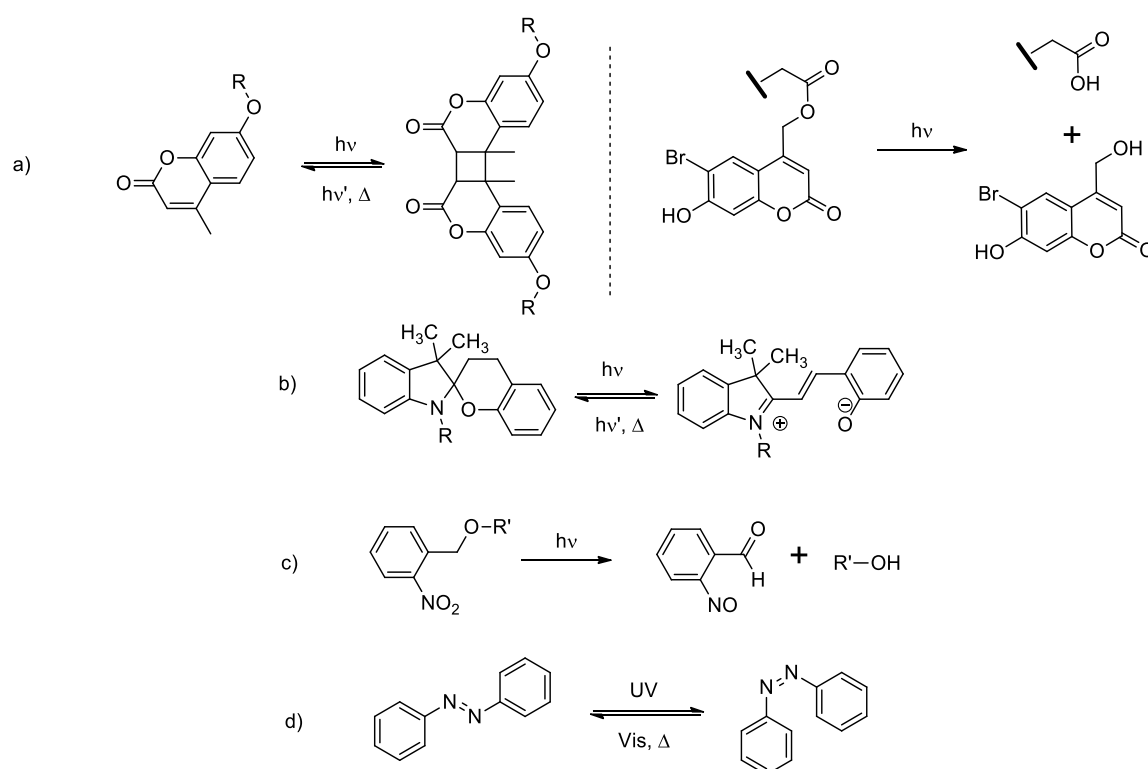


Figure 1.3. Examples of light responsive units:
a) coumarin, b) spiropyran, c) 2-nitrobenzyl and d) azobenzene

Coumarins can dimerise upon light irradiation in a reversible way.⁶ In addition, with specific coumarin molecules it is possible to dissociate photolabile bonds in an irreversible way.⁷ Spiropyran is a neutral molecule that can be transformed into a charged molecule (merocyanine) through a photoinduced ring-opening reaction, increasing dramatically its polarity.⁸ 2-Nitrobenzyl is a photolabile group that is dissociated upon illumination.⁹ Nevertheless, azobenzene is by far the most studied chromophore for preparing light responsive materials.¹⁰ Azobenzene has

two geometric isomers: *trans* and *cis* (or *E* and *Z*, respectively). The *trans* azobenzene is the thermodynamically stable isomer and can be transformed into the *cis* isomer when irradiated with UV light. Conversely, the *cis* azobenzene reverts to the *trans* isomer when irradiated with visible light, when heated or spontaneously over time. The changes of geometry and polarity of the molecule that go with the *trans to cis* isomerisation are the basis of the light responsiveness of azobenzene materials. The required irradiation wavelength depends on the substituents of the azobenzene unit. Isomerisation process is associated to modifications on the UV-Vis spectra. Azobenzene has two bands: a high intensity $\pi\text{-}\pi^*$ band in UV region and a low intensity $n\text{-}\pi^*$ band in the visible region. Upon *trans to cis* photoisomerisation, the $\pi\text{-}\pi^*$ band decreases, while the $n\text{-}\pi^*$ band increases. This process follows the opposite way if *cis* isomer is irradiated with visible light and transformed into *trans*.

Azobenzene derivatives can be classified in three different families: azobenzene type derivatives, aminoazobenzenes and the pseudostilbenes. Azobenzene type derivatives are the most similar to azobenzene regarding their electronic nature. Aminoazobenzenes include a donor group at the azobenzene and have $\pi\text{-}\pi^*$ and $n\text{-}\pi^*$ bands close to the UV-Vis region. Pseudostilbene azobenzenes (or push-pull azobenzenes) have a donor group in one of the benzene rings and a withdrawing group in the other. This provokes the shift of both bands to the visible region of spectrum and in many cases the overlap of both bands.

The incorporation of azobenzenes into polymers makes them good candidates in different applications that require light-responsive behaviour, from optical storage or molecular actuators to light-induced drug delivery.^{10–13}

The main weakness of most of azobenzenes is that photoisomerisation occurs under UV light illumination. Indeed, UV light presents problems when bioapplications are anticipated because of its limited penetration into biological tissues and the damage that produces in them. Despite the fact that UV active azobenzenes can be used in proofs of concept, the use of light stimuli responsive polymers in biological systems requires the use of chromophore sensitive to less harmful wavelengths.

1.1.2. VISIBLE AND NIR RESPONSIVE AZOBENZENES

A suitable alternative to overcome the limitation of UV light while preserving the adequate performance of azobenzenes is the use of visible and near infrared (NIR) sensitive azobenzene moieties.^{14,15} Visible and NIR light have a deeper penetration (e.g. on rat skin surface: 1 mm for 408 nm light, 6.3 mm for 633 nm and 8 mm for 808 nm)¹⁶ and are less harmful than UV light for bioapplications.

In the last few years, different structurally modified azobenzenes have been reported with photoresponse out of the UV region. Depending on the structural modification of the azobenzenes, four families can be identified:

1. BF₂ bridged azobenzenes
2. Push-pull type azobenzenes (or pseudostilbenes)
3. NIR switchable azobenzenes based on two-photon absorption
4. Tetra *ortho*-substituted azobenzenes

Aprahamian and co-workers developed a new type of azobenzene complexes with a BF₂ bridge (**Figure 1.4**). The formation of the complex modifies the electronic structure by extending the π -conjugation and giving a new dominating band in the absorption spectrum at 530 nm. The *trans* to *cis* photoisomerisation was induced by irradiation at 570 nm and reverted at 450 nm light or storing the azobenzene in dark for several hours. In addition, the half lifetime of the *cis* state was determined to be 12.5 h, which was quite large in comparison with other azobenzenes.¹⁷ The influence on the absorption properties and on the photoisomerisation process of substituents located at the *para* position was also investigated.¹⁸ The modification led to a bathochromic shift of the absorption band allowing the isomerisation in NIR region. Nevertheless, these azobenzenes presented an important drawback as they are not stable in water because of the hydrolysis of BF₂ bridge and its conversion into hydrazones, limiting their bioapplications.¹⁵

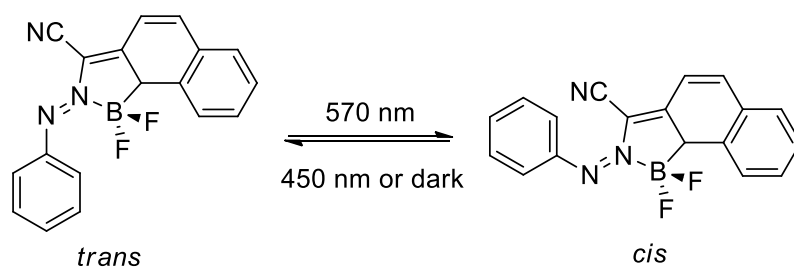


Figure 1.4. Light induced isomerisation of a BF_2 bridged azobenzene

Push-pull azobenzenes have a donor group at one side of the azobenzene and a withdrawing substituent at the other. This might shift the π - π^* band to the visible region. In these azobenzenes, the π - π^* band of the *trans* isomer usually overlaps the n - π^* band of the *cis* isomer, so continuous *trans* to *cis* to *trans* transitions might be induced when irradiated, being difficult to obtain a *cis* rich state. Furthermore, because lifetime of *cis* isomer in solution is in the nanosecond scale, this isomer is hard to detect.¹⁹ This behaviour is useful in applications that requires a continuous isomerisation of azobenzene, like applications based on the orientation of azobenzene moieties by *trans* to *cis* to *trans* cycles.¹⁴ Disperse Red 1 (DR1) belongs to this type of azo compounds (**Figure 1.5**).²⁰ Despite the fact that the *cis* isomer has a very short lifetime in solution, films of DR1 based polymers have been irradiated observing a decrease in its main absorption band due to the *trans* to *cis* photoisomerisation. In this case, *cis* lifetime was increased because of the confinement of the DR1 units into the films.^{21,22}

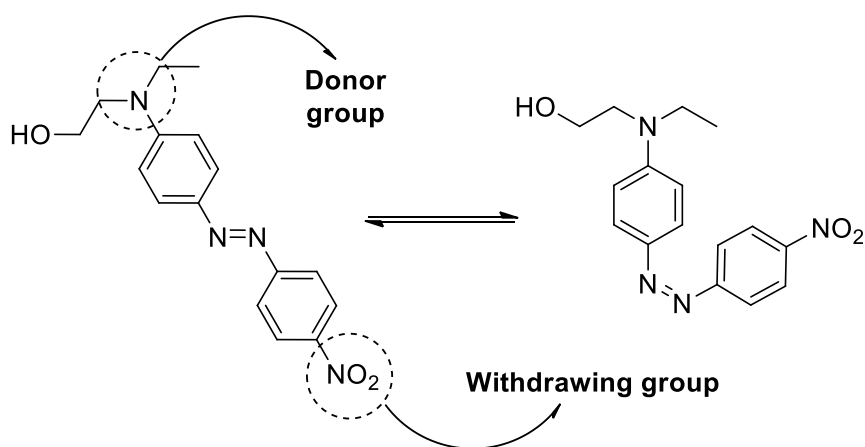


Figure 1.5. *Trans* to *cis* isomerisation of DR1

An alternative to avoid UV light is the use of two-photon absorption (2PA) process to photoinduce the isomerisation of the azo compounds. 2PA consists in the simultaneous absorption of two photons by a molecule to promote the excitation from the ground to an excited state. 2PA usually occurs at the double wavelength of the analogous one-photon absorption process, shifting the excitation wavelength from the UV to the NIR region. Unfortunately, not all molecules are able to experience efficient 2PA and chromophores have to be carefully designed. In general terms, the requirements to maximize 2PA include molecules with an extended π -conjugation and strong donor and acceptor groups. 2PA cross section value gives an idea about the ability of some chromophores to be excited properly using this phenomenon.²³ Some push-pull azobenzenes (DR1 among others) have been tested for 2PA. Mendonça et al. showed the potential of push-pull azobenzenes for NIR response using two-photon excitation.²⁴

Gorostiza and co-workers developed a novel azobenzene photoswitch that can be excited using NIR light *via* 2PA. They synthesised a system formed by a push-pull type azobenzene bonded to a naphthalene fluorophore as a sensitiser, with good 2PA properties, to promote the azobenzene photoisomerisation (**Figure 1.6**).²⁵ Under two-photon excitation at 740 nm, the naphthalene emitted at 475 nm, which overlapped the azobenzene absorption inducing its isomerisation by an energy transfer process. Additionally, direct two-photon activation of the azobenzene (at approx. 880 nm) was also observed. This naphthalene-azobenzene system was successfully used to control the activation of neurons and astrocytes with subcellular resolution.²⁶ Additionally, Isacoff and co-workers demonstrated that push-pull azobenzene described by Gorostiza showed a good 2PA cross section by itself without the need of naphthalene, allowing its two-photon isomerisation irradiating *ca.* 840 nm. Moreover, they found that only *trans* isomer can be excited by 2PA.²⁷

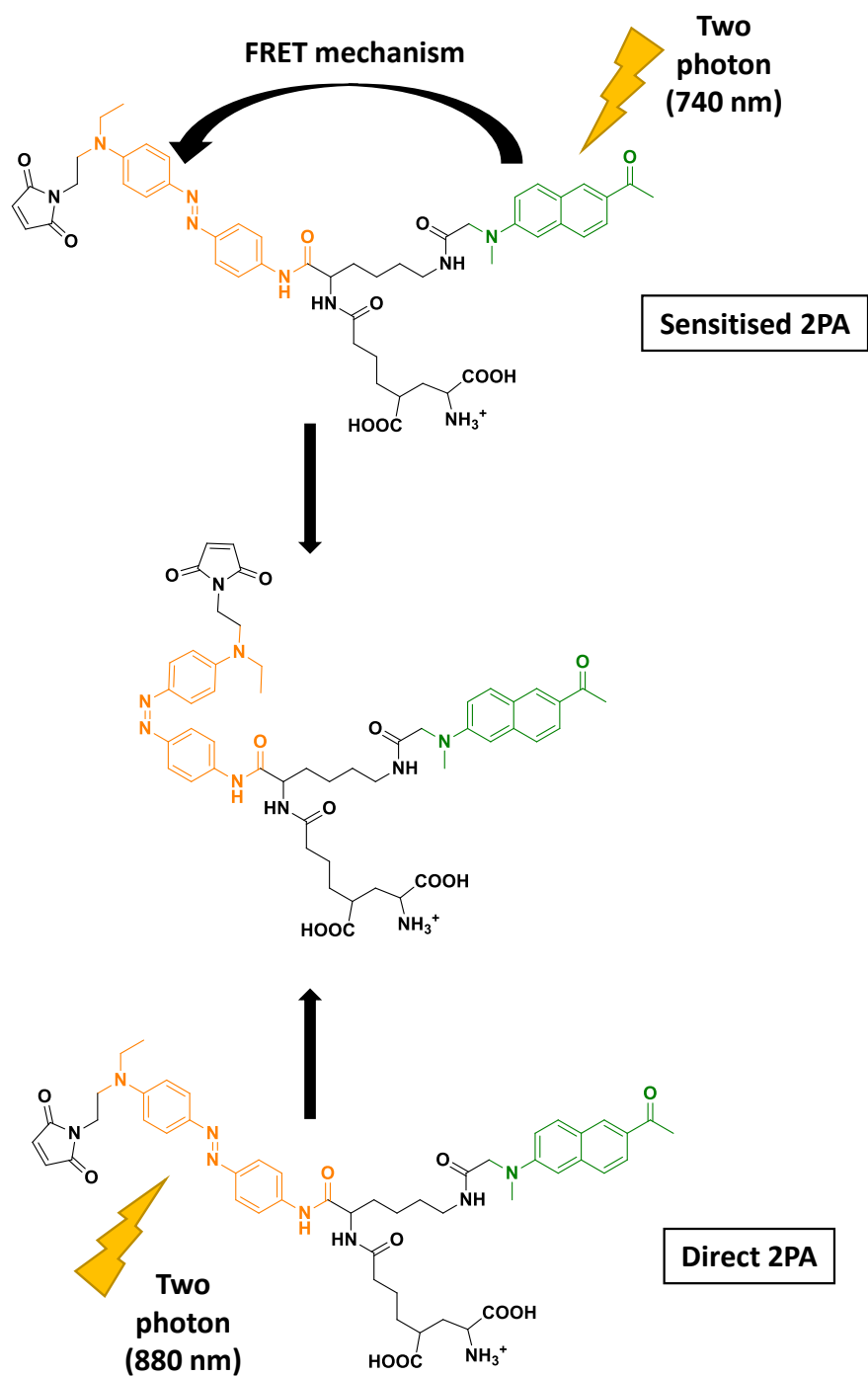


Figure 1.6. Schematic representation of the *trans* to *cis* isomerisation of the azobenzene—naphthalene system used by Gorostiza et al. for two-photon excitation

Despite of the benefits of exciting at the NIR region, 2PA processes have an important drawback: two-photon excitation requires high-power femtosecond lasers to generate a high density of photons. In addition, it is a spot-by-spot process

that limits its application in large areas. Additionally, two-photon processes are produced at the focus of high-intensity pulsed lasers. Taking into account that laser beam will defocus passing through biological tissues, 2PA presents limitations for deep-tissue applications but it is still of interest in superficial applications.²⁸

Tetra *ortho*-tetramethoxyazobenzenes were explored by Wooley and co-workers (**Figure 1.7**) observing in the UV-spectrum that the π - π^* band of the *trans* isomer was blue-shifted as well as the n - π^* band was red-shifted when compared with the same molecule without substituents. This was attributed to twisting (non-planarity) of aromatic rings in the *trans* isomer and interaction of the methoxy groups with the N lone electrons pair. Because the n - π^* band of the *cis* isomer was less affected by this substitution, n - π^* bands of both isomers were sufficiently separated to induce *cis* to *trans* isomerisation with blue light, and *trans* to *cis* isomerisation with green light.²⁹

They also found out that the *trans* n - π^* band of the *trans* isomer extend beyond 600 nm having a very small absorption coefficient but not zero. In spite of the reduced absorption, it was several times greater than *cis* absorption, allowing the *trans* to *cis* isomerisation using red light.³⁰

These tetra *ortho*-methoxyazobenzenes still presented problems regarding reduction by thiols in bioenvironments. Actually, they were reduced by glutathione in a few hours. Then, methoxy groups were replaced by chloro atoms and by thioether groups, avoiding this problem while n - π^* band is still red-shifted for *trans* isomer (**Figure 1.7**).³¹

Wooley's group also reported how the introduction of these methoxy groups stabilised the azonium ion at neutral pH, since they are usually formed at pH below 3.5. This stabilisation was produced because of the formation of hydrogen bonds between the methoxy group and the H⁺ located at the azo bridge. These azonium ions could be isomerised using visible light, but their *cis* lifetimes were of nanoseconds. However, in tetramethoxy substituted azonium ions, this lifetimes were increased up to a few seconds.³²

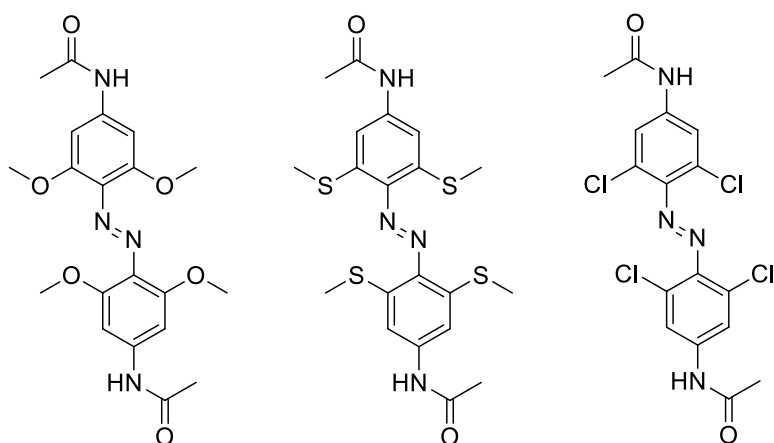


Figure 1.7. Examples of tetra ortho-substituted azobenzenes syntetised by Wooley's group

Wu and co-workers used this strategy to prepare red-sensitive materials. They reported a cyclodextrin-azobenzene complex, which was disrupted under red light due to azobenzene isomerisation.³³ They also photopatterned a film using this type of azobenzenes and red light, which can be applied to optical storage of information.³⁴

1.2. AMPHIPHILIC BLOCK COPOLYMERS

A block copolymer (BC) can be defined as a kind of copolymer in which the different repetitive units are disposed in segregated segments, not necessarily of the same length (**Figure 1.8**).



Figure 1.8. Schematic representation of a diblock copolymer

Probably, the most interesting feature of BCs is their ability to segregate and self-assemble if the blocks are different enough in their chemical and physical properties, giving rise to a wide range of nanostructures. The control over these nanostructures depends on the total control of the BC synthesis, as well as other factors such as the topology or the functionalities of the different blocks.^{35,36}

This ability has been used in several material applications ranging from thermoplastic elastomers to functional materials in optics or electronics, for example. However, the emergence of nanoscience and nanotechnology boosted the search of new BCs to prepare nanostructured materials. In nanoscience, one of the most important applications of these materials is the ability of amphiphilic BCs to self-assemble into polymeric aggregates when they are dispersed in water.³⁷

1.2.1. SYNTHESIS OF BLOCK COPOLYMERS

Synthetic tools have improved greatly in the last few decades to make the synthesis of BCs with tailored properties more accessible.^{38,39} In particular, development of new controlled polymerisation techniques, such as atom transfer radical polymerisation (ATRP) or reversible addition–fragmentation chain-transfer

polymerisation (RAFT), and click chemistry reactions have facilitated the access to novel polymeric architectures with either new or improved properties.

Acrylates and methacrylates have been commonly prepared by free radical polymerisation. Nevertheless, this type of conventional polymerisation has a great drawback: propagating macroradicals tend to react between them (termination reactions) giving dead polymer chains that are not able to propagate. This makes not possible the control over the dispersity (in terms of low dispersity) or terminal groups. This contrasts with anionic polymerisation where bimolecular termination reactions between anionic propagating species do not occur preserving the activity of the macromolecule end group if impurities or chain transfer are avoided on the polymerisation media. Due to this peculiarity, polymerisation can be paused by neutralizing the propagation anion and restarted afterwards. This is why anionic polymerisation is called a living polymerisation. On this basis, BCs can be approached by sequential polymerisation of different monomers by polymerising first one monomer and, once consumed, restart the polymerisation by adding a second monomer.

In an attempt to imitate the advantageous characteristics of anionic living polymerisation and since not all monomers can be polymerised using this technique, controlled radical polymerisation (CRP) techniques were developed. The main objective of CRPs is to minimize termination reactions through sophisticated mechanisms of polymerisation. This allows a precise control over molecular masses, dispersity values and terminal groups.⁴⁰

ATRP was mainly developed by Matyjaszewski.⁴¹ In this polymerisation, an alkyl halide (R-X) acts as initiator forming a propagating radical (R·), that reacts with monomers to form polymeric chains, *via* reversible homolytic transfer of the halogen atom to a transition metal complex (usually Cu(I) in combination with nitrogenous ligands), which is oxidised in this process (**Figure 1.9**). The polymerisation is controlled by an equilibrium between dormant species (R-X) and propagating radicals (R·) in such a way that dormant species are predominant in the equilibrium keeping propagating species in minimum values ($k_d \gg \gg k_a$), minimising termination reactions and leading to well controlled weight distributions. The most common catalytic system consists of a Cu(I) metal salt in combination with nitrogenous

ligands, such as *N,N,N',N'',N''',N''''*-hexamethyltriethylenetetramine (HMTETA), *N,N,N',N'',N'''*-pentamethyldiethylenetriamine (PMDETA) or bipyridine, and 2-bromoisobutyrate derivatives as alkyl halide.

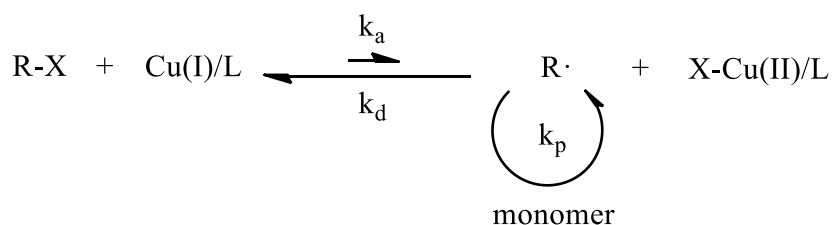
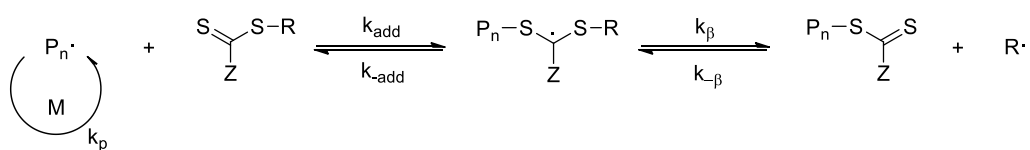
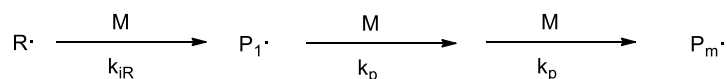
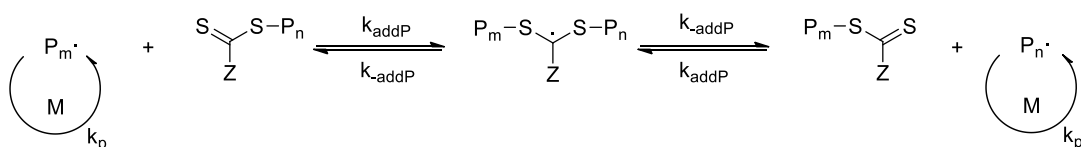


Figure 1.9. Scheme of ATRP mechanism

RAFT polymerisation was developed in Commonwealth Scientific and Industrial Research Organisation (CSIRO).⁴² The key point of this polymerisation is the use of a called RAFT agent in addition to the thermal initiator and the monomer used in free radical polymerisation. The role of this RAFT agent is to mediate in the polymerisation *via* a reversible chain-transfer process. Common RAFT agents are thiocarbonylthio compounds such as dithioesters, thiocarbamates and xanthates. The accepted mechanism for RAFT polymerisation is schematically represented in **Figure 1.10**. Polymerisation is initiated by a radical thermal initiator (2,2'-azobis(2-methylpropionitrile), AIBN, is the most common) that generates the propagating species ($P_n\cdot$) by addition of a few number of monomers. Then, these propagating species react with the RAFT agent to give an intermediate whose fragmentation produces new radicals $R\cdot$ (initiation step), which by addition of monomers generate new propagating species $P_m\cdot$ (reinitiation step). Finally, a main equilibrium is reached where $P_m\cdot$ and $P_n\cdot$ have an equal probability to leave the dormant species and so propagate and grow polymers of controlled masses with narrow dispersities.

Initiation:**Reinitiation:****Main equilibrium:****Figure 1.10. Scheme of RAFT mechanism**

In RAFT polymerisation, the selection of the RAFT agent (*i.e.* Z and R groups) is crucial and depends on different factors. First, the selection should take into account the type of monomer. R has to generate more stable radical species than P_n in order to get an efficient fragmentation of the intermediate species in initiation step ($k_{\beta} \gg k_{-add}$). In other words, R has to be a better leaving group than P_n. The Z group stabilises radical species in the equilibria, controlling the equilibrium constants (k_{addP} and k_{-addP}). In order to keep a good control over polymer growth, for more active monomers with high k_p , Z has to be chosen so that $k_{addP} \gg k_{-addP}$. For less active monomers, it should be the opposite. Therefore, taking into account the role of Z and R, specific RAFT or CTA agents are recommended for each type of monomer (**Figure 1.11**).

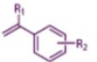
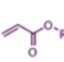
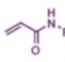
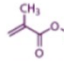
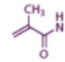
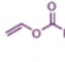
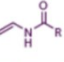
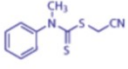
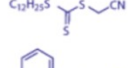

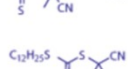
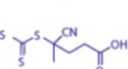
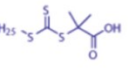

	 styrenes	 acrylates	 acrylamides	 methacrylates	 methacrylamides	 vinyl esters	 vinyl amides
	—	—	—	—	—	+++	+++
	+++	+++	+++	—	—	—	—
	++	+	—	+++	+++	—	—
	++	+	+	+++	+++	—	—
	+++	++	++	+++	+++	—	—
	+++	++	++	+++	+++	—	—
	+++	+++	+++	+	+	—	—

Figure 1.11. RAFT agents compatibility table (reproduced from Sigma-Aldrich website)

The ‘click chemistry’ is a concept coined by Sharpless in 2001.⁴³ It identifies a group of reactions with a set of specific characteristics such as good yields, mild reaction conditions, high selectivity or absence of side reactions, among others. Click chemistry includes Diels-Alder, thiol-ene or thiol-yne reactions, but there is a reaction that stands out: copper(I) catalysed alkyne-azide cycloaddition (CuAAC). In contrast to non-catalysed cycloaddition between azides and terminal alkynes in which mixtures of 1,4 and 1,5-regioisomers are obtained, in CuAAC only the 1,4-isomer is generated (**Figure 1.12**). CuAAC has been widely used in polymer chemistry for the efficient coupling of polymeric blocks or post-polymerisation modification of properly functionalized polymers.⁴⁴

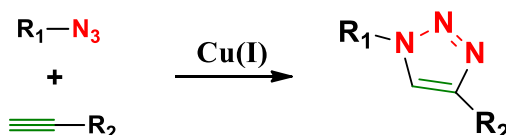


Figure 1.12. General scheme for CuAAC coupling

Considering CRP and click chemistry, there are three main strategies to approach the synthesis of BCs, using these synthetic tools:

1. Sequential polymerisation of monomers
2. Polymerisation of a monomer using a macroinitiator
3. Coupling of preformed blocks

The first approach is appropriate for monomers able of polymerising according to the same mechanism. Hence, a monomer is first polymerised by a CRP until consumption and then the polymerisation is reactivated in the same reaction vessel by adding a second monomer. The first polymerised block acts as a macroinitiator for polymerising the second one, using the same polymerisation technique. This operation can be, at least theoretically, repeated as many times as blocks are required. This strategy has been employed in our research group to prepare diblock copolymers of poly(methyl methacrylate) and azopolymethacrylates by ATRP.⁴⁵

The second strategy is very closely related and, in this case a previously synthesised polymer is used as a macroinitiator for polymerising the second monomer. It differs from the first strategy that the macroinitiator is isolated and purified and consequently it has not to be necessarily polymerised using the same technique. Besides, macro-RAFT agents and macro-ATRP initiators are commercially available. This strategy has also been used in our group to prepare amphiphilic BCs containing 2,6-diacylaminopyridine polymethacrylates by RAFT using a hydrophilic poly(ethylene glycol) (PEG) as macro-RAFT agent.⁴⁶⁻⁴⁸

The final alternative implies the coupling of preformed blocks with complementary terminal groups using click chemistry reactions. Advantages of this approach are the possibility of purifying and characterising the blocks before their conjugation and that the blocks can be produced by different polymerisation techniques. In our group, this strategy has been used for the preparation of different BCs.⁴⁹

An example of each strategy is represented in **Figure 1.13**.

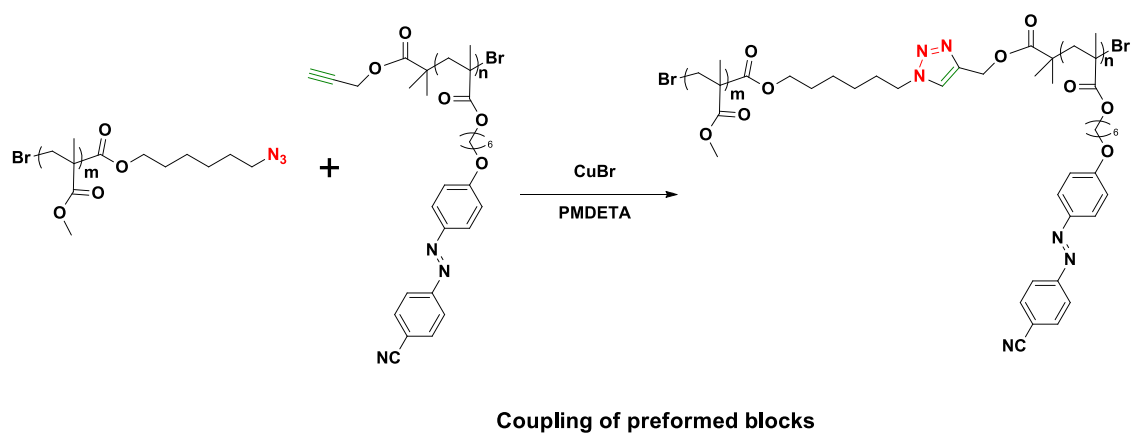
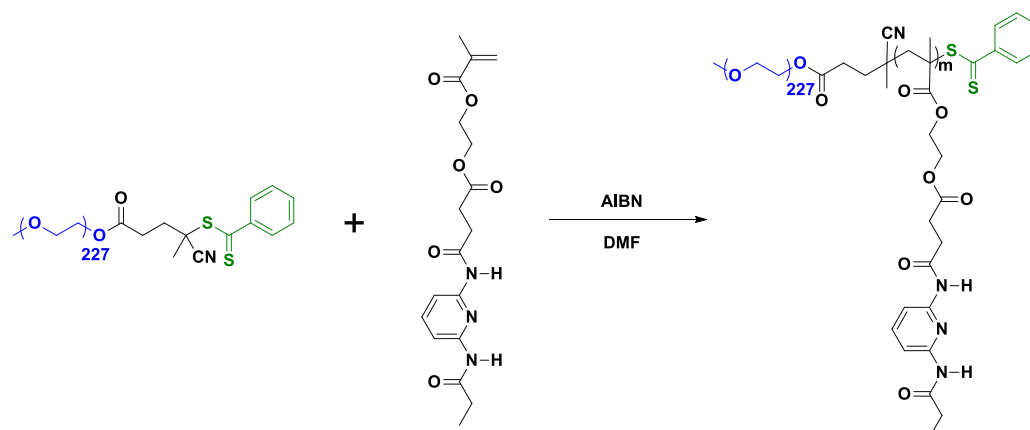
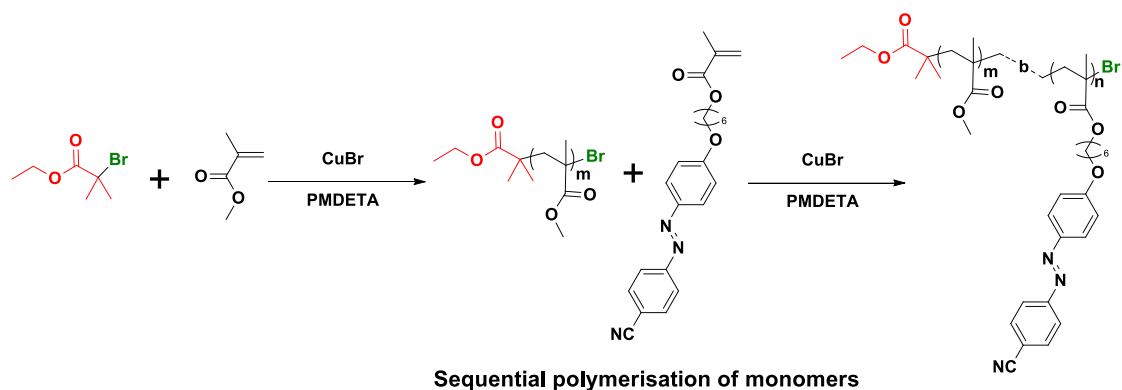


Figure 1.13. Different strategies to prepare BCs

1.2.2. POLYMERIC NANOCONTAINERS BASED ON AMPHIPHILIC BLOCK COPOLYMERS

As it was mentioned in **Section 1.2.**, one of the most interesting features of BCs is their ability to undergo phase segregation at the nanoscale when the blocks are immiscible.

The simplest assumption is the segregation in bulk, in which BCs can self-assemble into different morphologies such as spheres, cylinders or lamellas. The morphology depends on the volume fraction of each block (f), the degree of polymerisation of each block (n), the overall degree of polymerisation ($N=\sum n$) and the Flory-Huggins parameter (χ), which gives us an idea about how blocks interact between them. Matsen and Bates determined a theoretical phase diagram for linear-linear diblock copolymers that is used in practice to predict the morphology in bulk.³⁶

In the last years, a huge effort has been made to the preparation of polymeric self-assemblies from BCs in selective solvents, being the simplest case a diblock copolymer in which a segment is soluble in a certain solvent, while the other segment is not. Under this circumstance, the BC might self-assemble adopting different morphologies when the soluble block attempts to shield to the non-soluble from the solvent in a process that minimizes the interfacial area of the insoluble block lowering the interfacial free energy. This self-assembly process is driven by an enthalpic gain (because of the diminution of unfavourable interactions) that compensates the entropic loss due to the aggregation of chains. Despite the fact that this phenomenon can occur in any solvent, self-assembly of amphiphilic BCs in water is particularly appealing. This is because the obtained nanostructures can be used in biological systems for several applications, such as bioimaging, solubilisation of poorly water soluble drugs or controlled drug delivery.^{37,50}

Among the different existing morphologies, micelles and vesicles have interesting potential as carriers of nanometric dimensions. In aqueous media, micelles consist on a hydrophobic core and a hydrophilic corona, while vesicles are formed by a hydrophobic membrane and a hydrophilic inner cavity (**Figure 1.14**). There are several factors that control the self-assembly but the relative length of the blocks, their topology or the chemical composition are probably the most important. In general, a transition from micelles to vesicles is observed as hydrophobic/hydrophilic ratio increases.^{37,51}

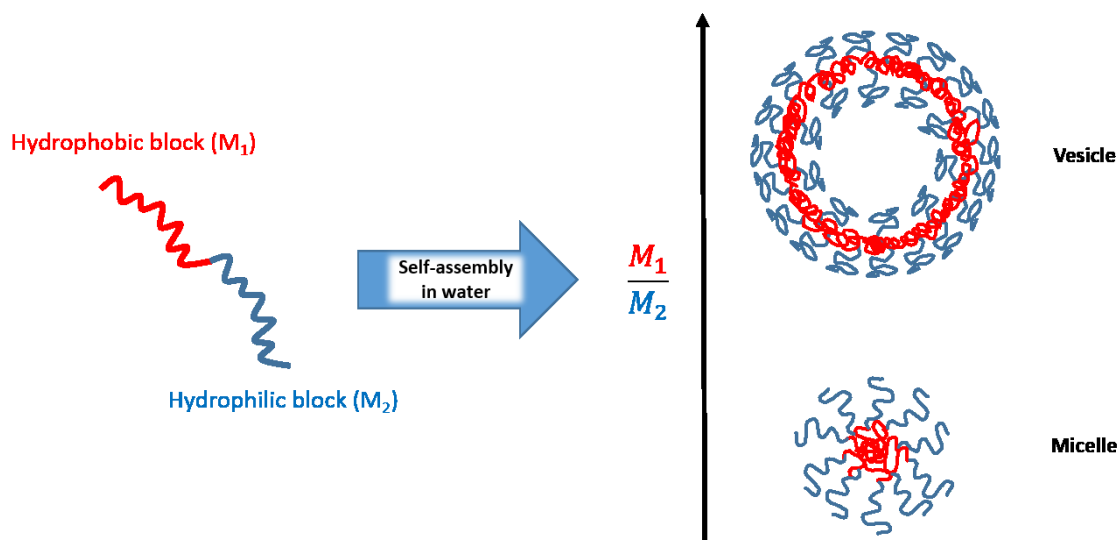


Figure 1.14. Transition from micelles to vesicles when hydrophobic/hydrophilic ratio increases (adapted from ref. 51)

Polymeric nanocarriers can be prepared using various methods. Amongst the most used in literature are co-solvent method and film re-hydration method.^{50,52}

Co-solvent method (also called solvent switch method) is a bottom-up approach. In this technique, a common organic solvent for hydrophobic and hydrophilic blocks is used to dissolve the polymer and then water is added slowly (drop by drop or in a continuous flow). Since only hydrophilic block is soluble in water, a critical point is reached in which hydrophobic block is not soluble anymore and it collapses giving rise to self-assembled structures (**Figure 1.15**). Organic solvent is then removed by dialysis against water. This purification step is a drawback, since it is time consuming and can affect the morphology of the nanocarriers. It is necessary to remark that the organic solvent has to be miscible with water in order to avoid phase separation. This is why solvents like THF, DMF or DMSO are the most used in solvent switch method.

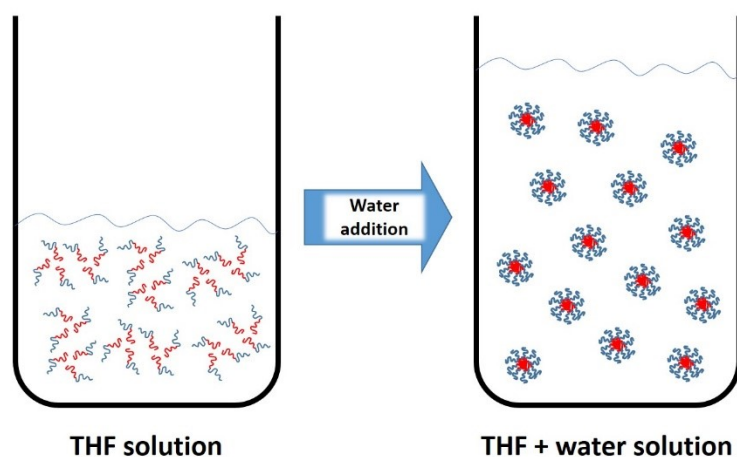


Figure 1.15. Schematic representation of solvent switch method

Film re-hydration method is a top-down approach. First, a polymer film is casted onto the bottom of a vial. For this purpose, the polymer is dissolved in a volatile organic solvent, such as chloroform or THF. The organic solvent is removed and the film dried. The subsequent addition of water hydrates the film yielding to self-assembled structures (**Figure 1.16**). Most of times, vigorous agitation or sonication is required in order to completely hydrate the film.⁵³ Generally, broad size distributions and structures with defects are obtained and it is frequently necessary to purify the sample to obtain a narrow and homogeneous distribution. Purification techniques include size exclusion chromatography (SEC), centrifugation or filtration, among others.⁵⁴ The main advantage of this method is the absence of organic solvent during self-assembly process.

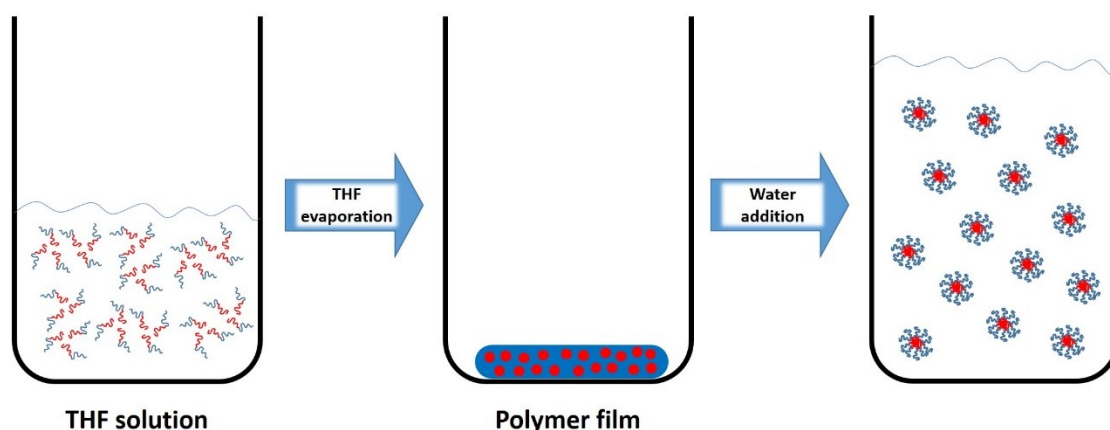


Figure 1.16. Schematic representation of re-hydration method

Micelles can encapsulate hydrophobic compounds into its hydrophobic core. On the other hand, vesicles are able to encapsulate hydrophobic and hydrophilic compounds into the hydrophobic membrane and into the hydrophilic inner cavity, respectively (**Figure 1.17**).

The use of micelles and vesicles as nanocarriers exhibits some important advantages: the solubilisation of poorly water soluble drugs exceeding its normal solubility value in water, the protection of the drug until it is delivered into the targeted place and the possibility of a controlled release into a specified tissue. Also, micelles or vesicles can accumulate in tumorous tissues due to a mechanism called enhanced permeability and retention (EPR effect), that is a physiological mechanism by which tumorous tissues tend to accumulate particles ranging from 10 to 500 nm (depending on the tumour) due to the new vascularisation, created for the nutritional support of the tumorous cells, that have bigger porous than regular vascularisation. This increases the accumulation of the nanocarrier at tumour sites and opens the possibility of using these systems for drug delivery.⁵⁵

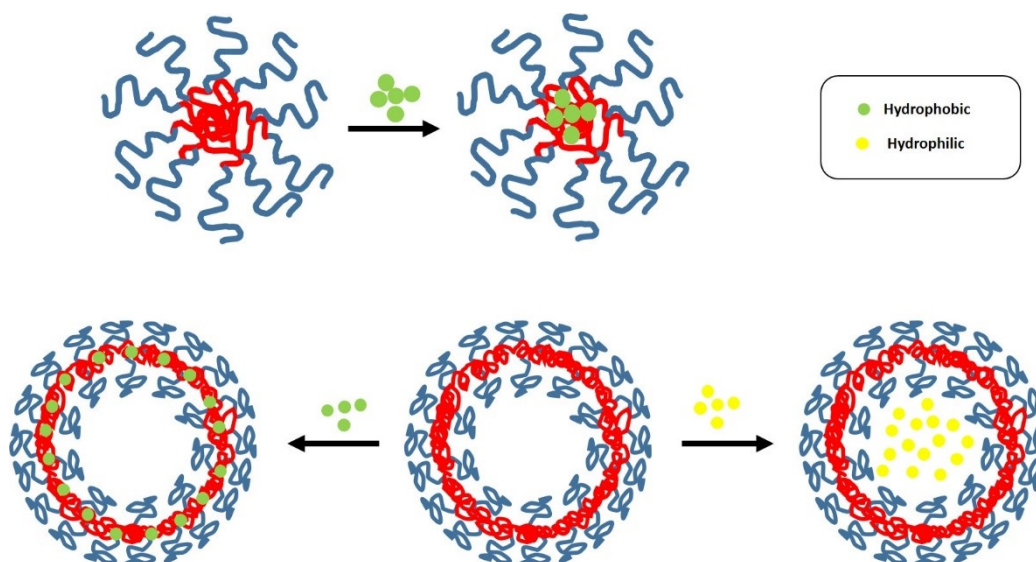


Figure 1.17. Schematic representation of encapsulation of molecules into micelles (top) and vesicles (bottom)

For drug delivery purpose, it is very important to control both the morphology and size of nanostructures. Depending on them, nanocarriers may vary its effectivity. It is described that optimum sizes are around 10 and 100 nm, although this should be optimized for each application.^{56,57}

Another important factor is the critical aggregation concentration (CAC) value, which is the concentration above which BC starts to self-assemble forming nanostructures. This value gives information about the stability of the system against dissociation, which is very important because when micelles or vesicles are introduced into a biological system, they are inevitably diluted and they have to be stable enough to avoid their dissociation. According to CAC values, it is described that BCs are much more stable than traditionally used low MW surfactants.⁵⁸ The reason is that being longer the hydrophobic block in BC than in low-MW surfactants, the free energy derived from the self-assembly interactions is greater.⁵⁷ This value can be determined using conductimetry or surface tension measurements, but probably fluorometry is the most used method for BCs.⁵⁹

1.2.2.1. STIMULI RESPONSIVE POLYMER NANOCARRIERS

As it was described in **Section 1.1.**, stimuli responsive polymers can vary a property (or properties) when a determined stimulus is applied. This is very useful in controlled drug release with polymeric nanocarriers because the modification of these properties might induce changes in the morphology that eventually can allow the release of a previously encapsulated molecular cargo such as a drug.

For instance, Pietrangelo and co-workers prepared thermoresponsive micelles derived from an amphiphilic block copolymer formed by PNIPAM and three different hydrophobic blocks. They found out how micelles tended to aggregate when heated above LCST (ca. 38 °C), being that PNIPAM block became hydrophobic. They also loaded doxorubicin (DOX) into the micelles and described how it was released when temperature was above LCST (**Figure 1.18**).⁶⁰

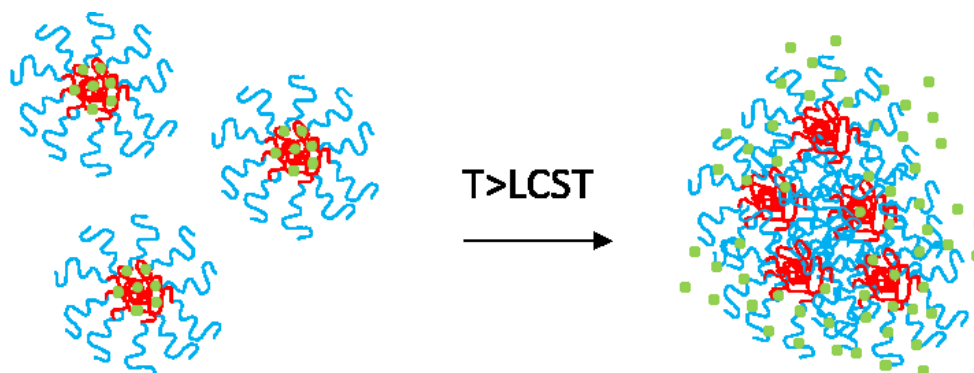


Figure 1.18. Schematic representation of a thermoresponsive micelle and the release of doxorubicin (green)

As another example, Gao and co-workers prepared a series of pH-responsive amphiphilic BCs with tertiary amine groups in the hydrophobic blocks. These BCs formed micelles when self-assembled into water. When pH was minor than the pK_a values of amine groups, they got protonated and micelles were partially disassembled and suffered a decrease in their diameter according to TEM and DLS experiments (**Figure 1.19**).⁶¹

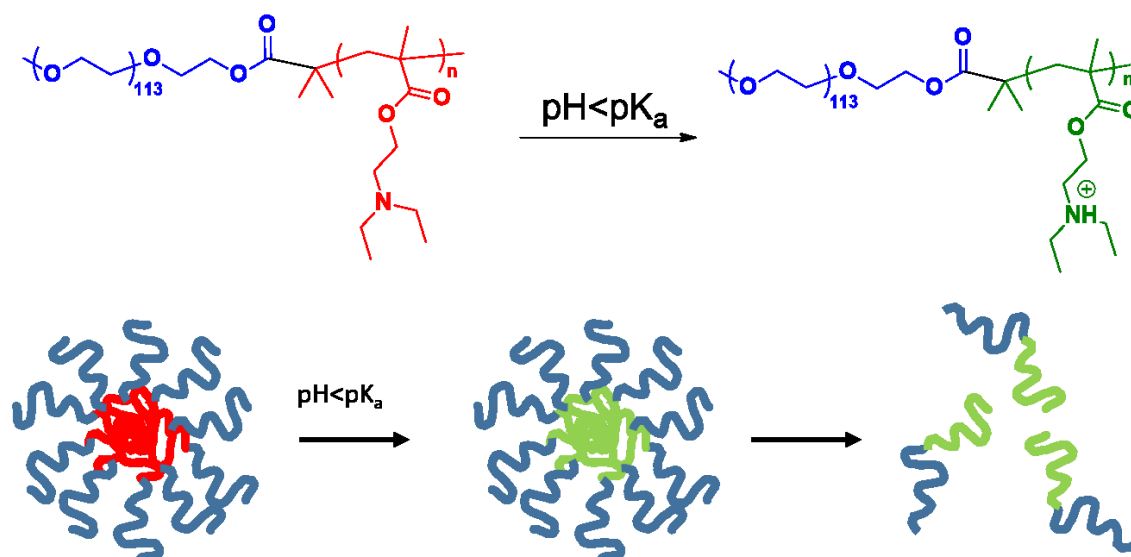


Figure 1.19. Schematic representation of a pH responsive micelle

Matsumura and co-workers have reported a BC composed by PEG, as the hydrophilic block, and a poly(4-phenyl butyl aspartate) as hydrophobic segment, able to respond to pH releasing paclitaxel at acidic pH conditions. This BC is in preclinical studies due to their good results in controlled drug release.⁶²

Among the multiple stimuli available, light is of interest as it can be manipulated from an external source, allowing spatial and time control over the stimulus. This possibility increases the selectivity of the stimulus regarding both parameters, inducing the release of the cargo molecules when and where it is desired. This makes light a powerful tool in stimuli responsive materials.

1.2.2.2. LIGHT RESPONSIVE POLYMERIC NANOCARRIERS

The inclusion of light responsive units into the amphiphilic BCs can undergo light responsive polymeric self-assemblies. Under light irradiation, amphiphilic BCs might suffer a change on the hydrophilic-hydrophobic balance that might result in the disruption of the self-assembled polymeric aggregates or even its disassembly, releasing the previously encapsulated molecules.⁶³ Some examples of these systems, including the chromophores described in **Section 1.1.1.**, are described

below in order to show their potential to induce photoresponse in polymeric nanocarriers.

Matyjaszewski and co-workers described the reversible light induced formation-disruption of micelles derived from spiropyran. They prepared an amphiphilic BC that becomes hydrophilic after irradiation with UV light because of the photoinduced ring opening of spiropyran (**Figure 1.20**). The conversion of the spiropyran into merocyanine provoked a great increase in polarity that permitted the total solubilisation of the amphiphilic BC and therefore the disruption of the micelles. Irradiation with visible light reversed the process converting the merocyanine form back into the spiropyran, the hydrophobicity was recovered and micelles were reassembled. A hydrophobic coumarin fluorescent probe was used to demonstrate the loading/releasing ability of the system observing its liberation after UV irradiation and the partial re-encapsulation after visible light irradiation.⁶⁴

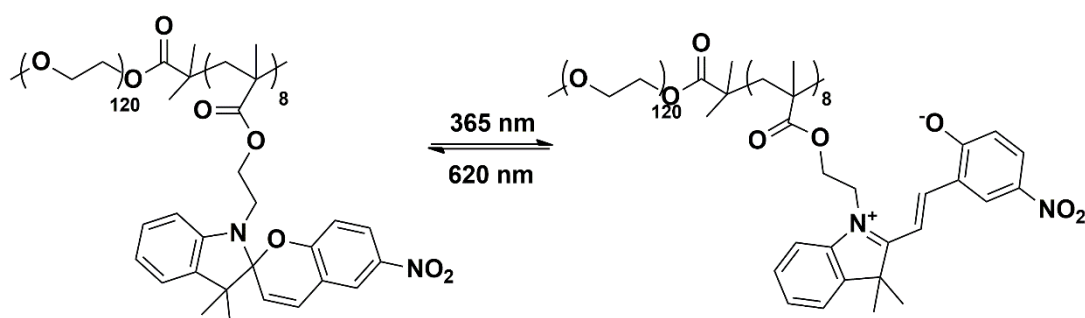


Figure 1.20. Structures of spiropyran based polymer and its photoinduced ring opening product

Using a different approach, Burdick and co-workers prepared a diblock copolymer formed by PEG as hydrophilic block and polycaprolactone (PCL) as hydrophobic block, with a photolabile 2-nitrophenylalanine group at the juncture point of the blocks. In this case, irradiation with 365 nm tore both blocks apart. This rupture was corroborated by gel permeation chromatography (GPC), in which two peaks at mayor elution times (corresponding to minor molar masses) appeared after irradiation. This BC self-assembled into vesicles that disassembled after irradiation giving rise to PCL precipitation. Biocytin was encapsulated into the vesicles and its light-induced release was followed by fluorescence spectroscopy.⁶⁵

One of the most outstanding groups in this topic is Zhao's one.^{63,66} They have described the light stimulated release abilities of nanocarriers with different chromophores at wavelengths ranging from UV to NIR. For example, they worked with NIR responsive coumarin moieties. In particular, 7-(Diethylamino)-4-(hydroxymethyl)coumarin was incorporated onto the side chains of a BC backbone. This coumarin has a large 2PA cross-section and allowed its photo cleavage upon NIR illumination (794 nm) (**Figure 1.21**). This polymer formed micelles of around 55 nm of diameter in aqueous dispersion and Nile Red was encapsulated into them. Both the release of coumarin and Nile Red were followed using fluorescence spectroscopy upon NIR irradiation with a Ti:sapphire laser.⁷

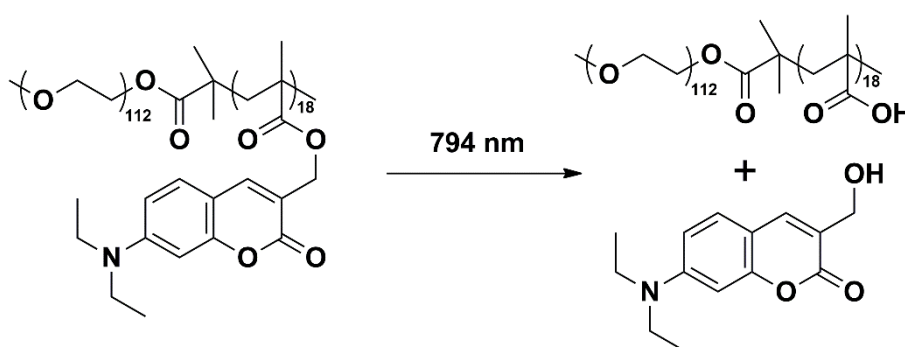


Figure 1.21. NIR induced release of coumarin from an amphiphilic block copolymer

Besides, they incorporated a different NIR responsive coumarin in a biocompatible BC formed by PEG and a polypeptide (**Figure 1.22**). This polymer formed micelles of around 73 nm of diameter in aqueous solution that were smaller after irradiation with 794 nm, according to TEM and DLS observations, proving the potential of the NIR-sensitive coumarin to provoke changes on the initial micelles. Rifampicin and Paclitaxel were encapsulated into the micelles and properly released using NIR light as stimulus.⁶⁷

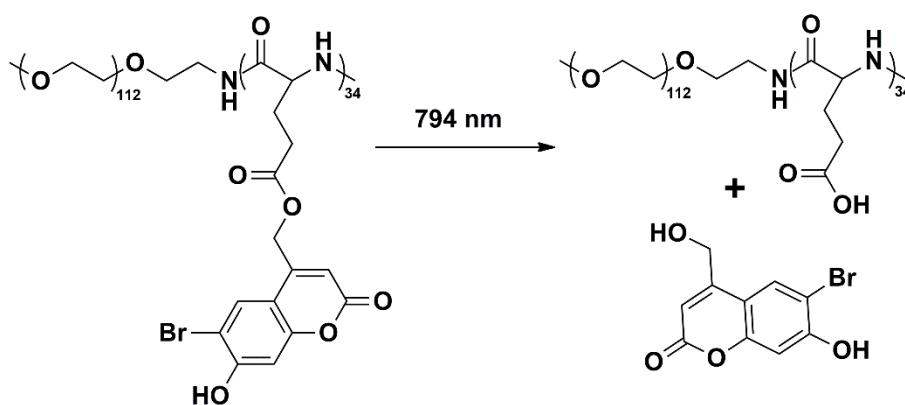


Figure 1.22. NIR induced release of coumarin from the polypeptide block of an amphiphilic BC

They also prepared an amphiphilic BC formed by a hydrophilic PEG and a polymetracrylate with *ortho*-nitrobenzyl pendant groups. The BC formed micelles of 20 nm of diameter. *Ortho*-nitrobenzyl was removed from the polymer chain *via* either one-photon (365 nm) or two-photon (700 nm) irradiation (**Figure 1.23**). As a consequence of this photo cleavage, the hydrophobic block became hydrophilic and micelles were disrupted. Nile Red was encapsulated into the micelles. Its encapsulation and photoinduced release was followed by fluorescence spectroscopy. The irradiation time needed for two-photon process was longer than in one-photon case due to the low 2PA cross-section of *ortho*-nitrobenzyl group.⁶⁸

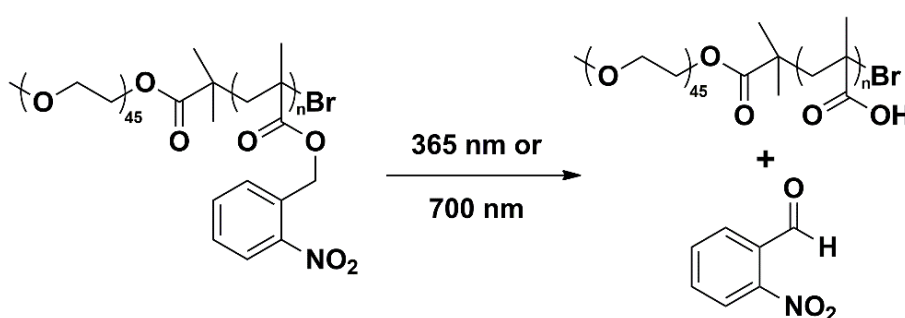


Figure 1.23. Structures of *ortho*-nitrobenzyl based polymers and its photo cleavage

Using the same chromophore, they also prepared a hydrophilic-hydrophobic-hydrophilic triblock copolymer in which the hydrophobic block was a polyurethane

with *ortho*-nitrobenzyl units forming part of the polymer backbone. *Ortho*-nitrobenzyl were cleaved off irradiating at 300 nm, degrading the hydrophobic block in small molecules and provoking the disruption of the micelles (**Figure 1.24**). Nile Red was encapsulated into the hydrophobic core of micelles and its release into the aqueous media was followed by fluorescence spectroscopy. They proved how Nile Red suffered a fast release in a few seconds upon UV illumination.⁶⁹

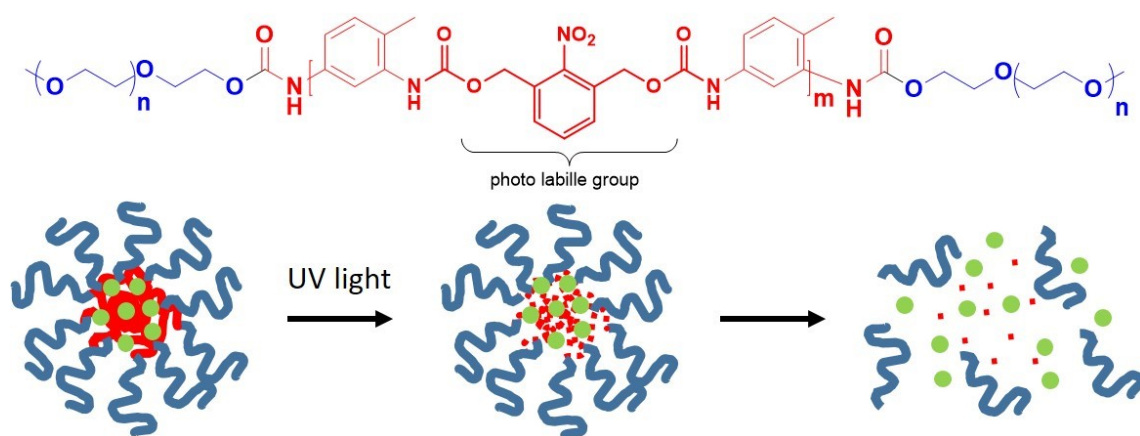


Figure 1.24. Schematic representation of the disruption of a micelle because of the degradation of the hydrophobic block (in red) and the subsequent release of Nile Red (in green)

Apart from proving the photoresponse of many polymeric nanocarriers with different chromophores, Zhao and co-workers described the first azobenzene containing nanocarriers, thus showing the potential of azobenzene to induce morphological changes in these structures. Since *cis* isomer is more polar than *trans* isomer, the hydrophobic/hydrophilic balance can be modified in amphiphilic azopolymers, resulting in morphological changes of the self-assemblies. They prepared several diblock copolymers formed by a hydrophilic block of poly(methacrylic acid) and a polymethacrylate derived from azobenzene. After the addition of water into dioxane solutions of both BCs, micelles and vesicles were formed. These self-assembled structures were irradiated alternatively with UV and visible light showing reversible morphological changes (**Figure 1.25**).⁷⁰

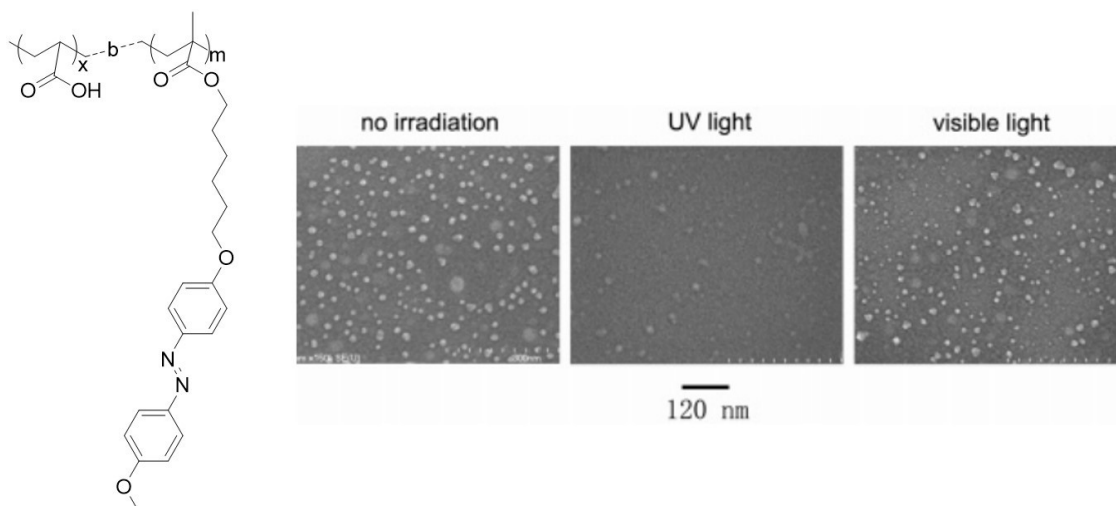


Figure 1.25. General structure of the azopolymers prepared by Zhao and TEM images showing the photoresponse of one of these azopolymers (adapted from ref. 70)

Recently, Yuan and co-workers prepared a series of BCs consisting on a hydrophilic poly(*N,N*-dimethylaminoethyl methacrylate) and an azobenzene containing hydrophobic random copolymer of poly[(benzyl methacrylate)-co-(4-phenylazophenyl methacrylate)]. These BCs were able to self-assemble into different morphologies, from wormlike micelles to vesicles, depending on the length of the hydrophobic block. Moreover, the wormlike micelles showed a reversible transition to vesicles upon UV or visible light irradiation (**Figure 1.26**). While UV irradiation, intermediate structures such as octopus and jellyfish morphologies were observed. According to the authors, this is the first light stimulated reversible worm to vesicle transition and it shows the potential of azobenzene to modify the morphology of polymeric aggregates.⁷¹

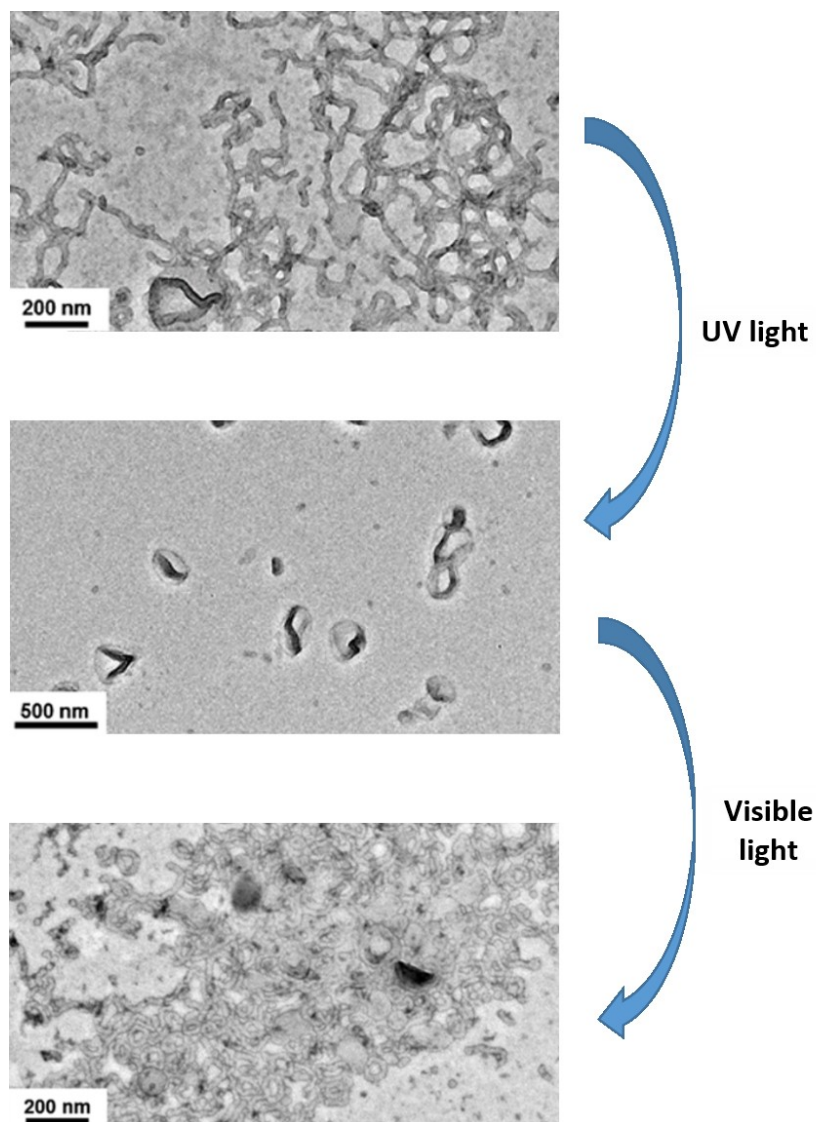


Figure 1.26. Worms to vesicles photoinduced transition (adapted from ref. 71)

As another example of light-induced morphological modifications induced by azobenzene, Zhang and co-workers self-assembled together an amphiphilic BC, formed by PEG and PS, and different azobenzene containing homopolymers, forming core-shell-corona (CSC) structures, composed by a core of azobenzene homopolymer isolated from water by the amphiphilic BC. Depending on the proportion between the azobenzene homopolymer and the BC, micelles, vesicles or cylindrical CSC were obtained. All the evaluated systems showed photoresponse according to the changes in UV-Vis spectra. Taking advantage of the possibility of align azobenzene using linear polarised light, these CSC were elongated using this technique.⁷²

In our group, several azobenzene based light-responsive polymeric vesicles have been reported.^{48,73,74} First, several linear-dendritic BCs composed by an azobenzene functionalised bis-MPA dendron and a PEG chain were prepared. Bis-MPA generation was varied from 1st to 4th keeping the same chain length for PEG and the corresponding self-assembled structures in water varied from nanofibers to vesicles, showing again the importance of hydrophobic/hydrophilic balance in amphiphilic BCs self-assembly.⁷⁵ Among these structures, the focus was put on vesicles and its photoresponse was evaluated. Upon 365 nm irradiation, the distortion produced by the *trans* to *cis* isomerisation of azobenzene produced perturbations on the membrane that provoked the total or partial disruption of vesicles (**Figure 1.27**). It was also demonstrated how these vesicles were able to encapsulate and release Nile Red and Rhodamine B, as hydrophobic and hydrophilic model compounds respectively, as consequence of UV irradiation.

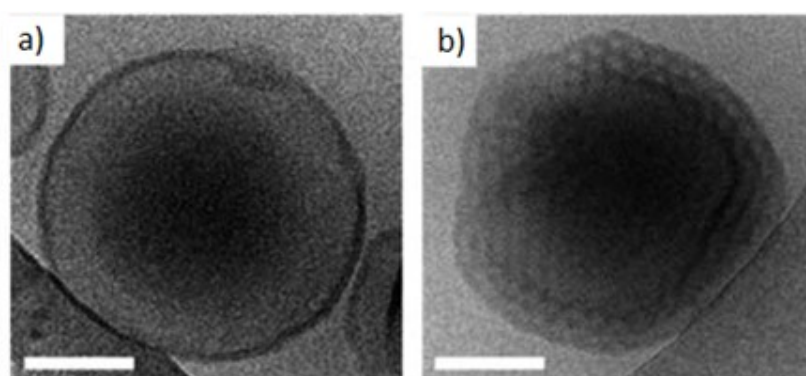


Figure 1.27. Cryo-TEM images of an azobenzene-containing vesicle a) before and b) after irradiation (adapted from ref. 73)

Besides, a star shaped BC formed by three arms of PEG and one arm of azopolymer was prepared (**Figure 1.28**). Hydrophobic/hydrophilic ratio was adjusted to 78/22, leading to the formation of vesicles when the BC was self-assembled in water. Photoresponse behaviour upon 365 nm irradiation was evaluated and both spectroscopic and morphological changes were observed in the vesicles, according to UV-Vis spectra and TEM images. These modifications were used to release in a controlled way organic compounds previously encapsulated. In particular, Nile Red was encapsulated into the hydrophobic

membrane of vesicles and Rhodamine B was trapped into the hydrophilic cavity. Both were properly released after irradiation, showing the potential of this system as drug nanocarrier.⁷⁶

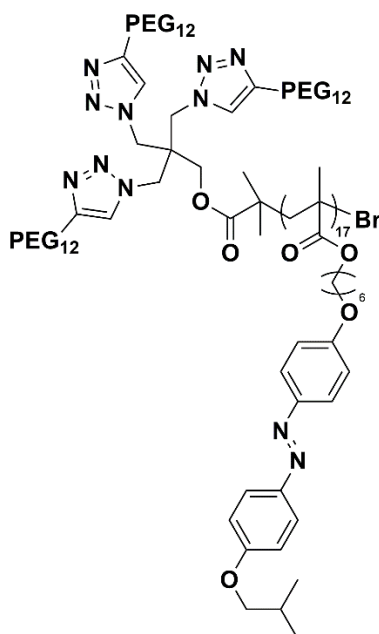


Figure 1.28. Star shaped azopolymer used for Nile Red and Rhodamine B encapsulation

Most of the azobenzene systems described above are very interesting proofs of concept, but they still have a problem: the use of UV light as exciting source. As it was mentioned before, UV light is harmful for biological tissues beyond its little penetration into them. Alternatively, red and NIR light do not present these problems, thus moving from UV to red or NIR wavelengths might be interesting for its use in light-responsive systems.

Regarding azobenzene, there are still no published papers of azopolymers acting as drug delivery systems excited by red or NIR light, to the best of our knowledge, but some examples with visible light are shown below.

Zhu and co-workers prepared a novel visible responsive azopolymer. They used an azobenzene with an electro-donating amino group at one extreme of the molecule. This shifted the main absorption band of azobenzene to visible region. After 450 nm irradiation of a polymer solution in THF, π - π^* band of azobenzene

decreased as consequence of *trans* to *cis* isomerisation (**Figure 1.29**). Self-assembly experiments were performed and vesicles of 120 nm of diameter were observed in TEM images. Similar changes to those for THF solution were observed in UV-Vis spectra for the vesicles and morphological changes were determined by TEM and DLS.⁷⁷

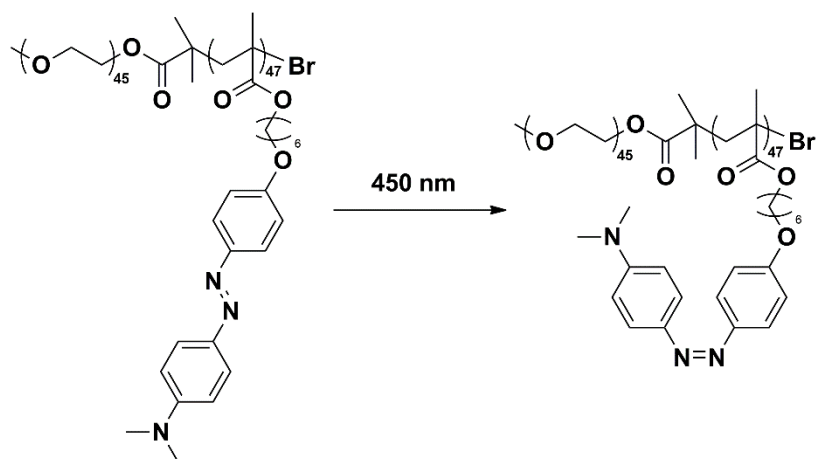


Figure 1.29. Visible responsive amphiphilic azopolymer

As another example of the use of visible light to isomerise azobenzenes, Zink and co-workers used blue light to induce continuously a *trans* to *cis* to *trans* isomerisation of azobenzene. Mesoporous silica was grafted with azobenzene moieties on the interior of the pores and the silica was loaded with small molecules. They demonstrated how the continuous isomerisation allowed the azobenzene to act as an impeller able to expel the cargo molecules when the particles were irradiated (**Figure 1.30**).⁷⁸

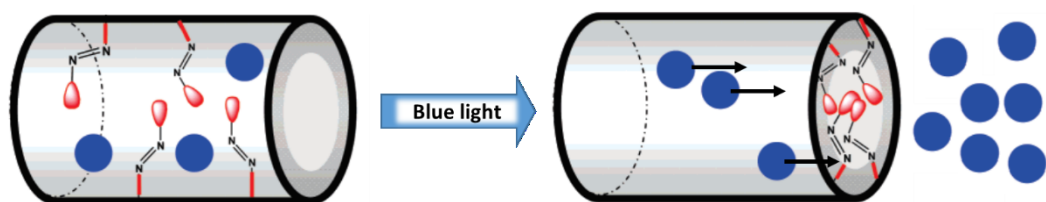


Figure 1.30. Schematic representation of a mesoporous silica functionalized with azobenzene acting as nanoimpellers (adapted from ref. 78)

All these examples open the possibility of preparing novel amphiphilic BCs based on the visible and NIR responsive azobenzene described in **Section 1.1.2**.

1.3. SUPRAMOLECULAR POLYMERS

Supramolecular chemistry can be defined as the chemistry beyond the covalent bond. It comprises different types of interactions, such as hydrogen bonds, hydrophobic and hydrophilic interactions, π - π stacking or electrostatic interactions. Usually, these interactions are weaker than covalent bonds. For instance, a covalent C-C bond has a bond energy of 86 kcal/mol, while H-bonding usually lies between 1 – 10 kcal/mol. It is worth noticing that these interactions are dynamic and reversible. Nevertheless, supramolecular motifs can be designed in order to increase their strengths and stabilities, combining different interactions like H-bonds and hydrophobic forces, for example.

Supramolecular polymers can be defined as polymers built using supramolecular interactions as driving forces. Because of the weakness of these interactions in comparison to the covalent ones, supramolecular polymers usually present worse mechanical and chemical stability than the corresponding covalent polymers.⁷⁹ Besides, small variations on temperature, solvent or pH can weaken the supramolecular interactions. This, which might be seen as a drawback, is a great opportunity to build new dynamic materials for novel applications. Supramolecular polymers have been used in different applications such as self-healing materials^{80,81} or biomedical applications.^{82–84}

Regarding structure, supramolecular polymers can be roughly classified as main chain polymers, side chain polymers and supramolecular polymeric networks. In the main chain polymers, the supramolecular motifs are located along the backbone, which is formed by repeating units with complementary supramolecular functionalities. Side chain supramolecular polymers are formed by a covalent backbone with supramolecular motifs pending from it. Supramolecular networks are formed by multifunctional molecules with complementary units that form large cross linked structures (**Figure 1.31**).

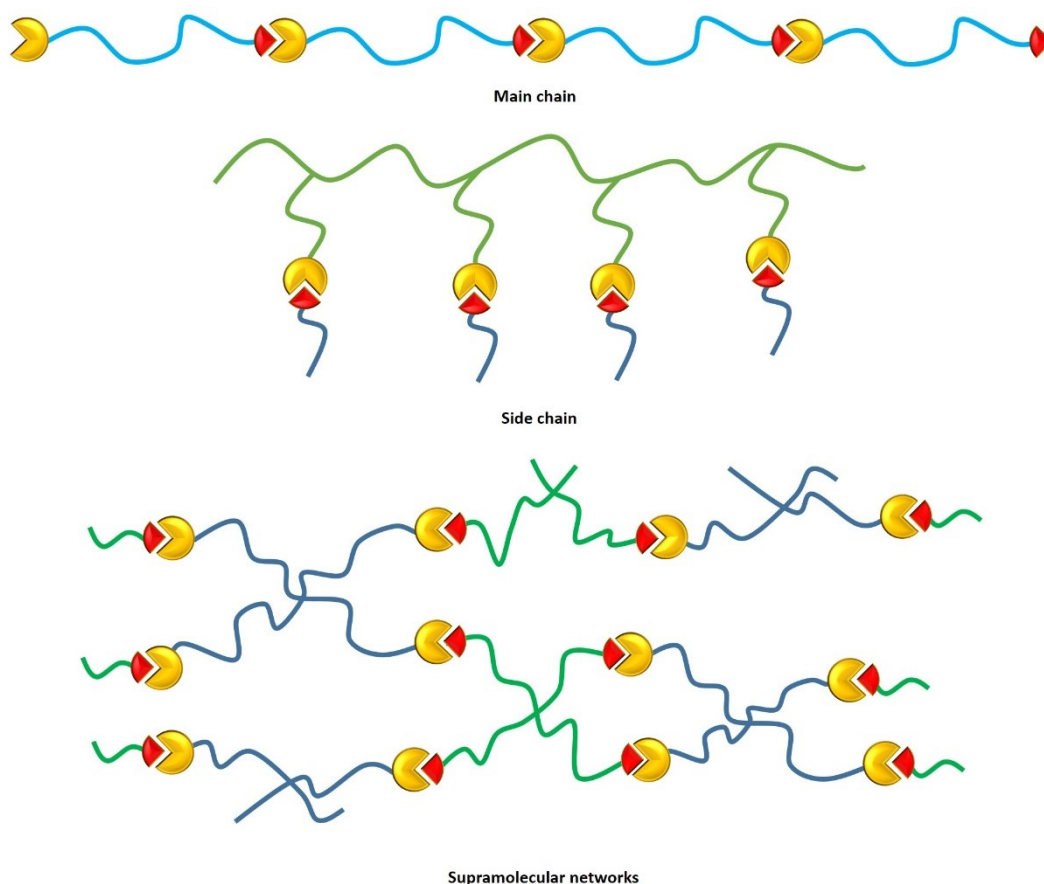


Figure 1.31. Schematic representation of a main and a side chain supramolecular polymer and a supramolecular network

With respect to the supramolecular interactions that govern the formation of the supramolecular polymers, host-guest complexation and H-bonding are the most reported for the preparation of this type of polymeric materials.

Supramolecular materials have been widely used in the preparation of drug nanocarriers. In particular, the formation of host-guest systems can give rise to amphiphilic systems able to self-assemble into micelles or vesicles and some examples are shown below.⁸⁵

Zhang and co-workers prepared supramolecular vesicles *via* interaction of a hydrophobic palmitate functionalized with pyrene, which was able to form a host-guest complex with a γ -CD (**Figure 1.32**). The hydroxyl groups of γ -CD acted as hydrophilic moieties. The system was UV-responsive because of the cleavage of the ester group that joins palmitate chain and pyrene. This caused the collapse of

the vesicles. It was also demonstrated how doxorubicin (DOX) was loaded into vesicles and released after irradiation with 365 nm.⁸⁶

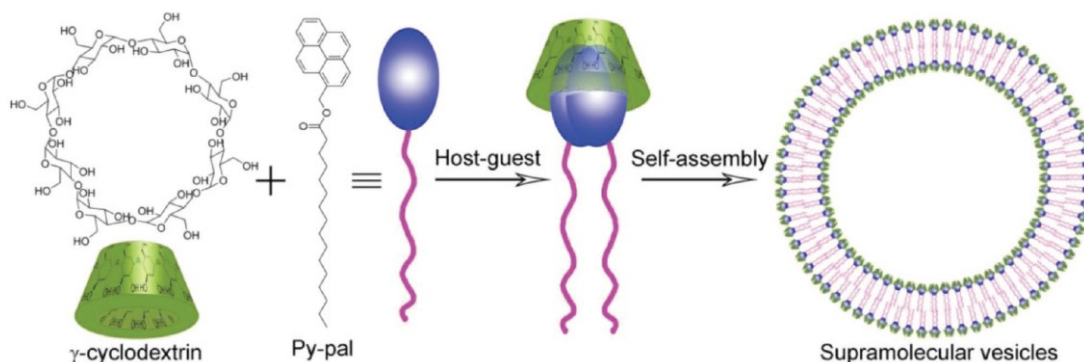


Figure 1.32. Pyrene-CD host-guest system forming UV- responsive vesicles (reproduced from ref. 86)

Micelles have also been prepared using this supramolecular approach. A diblock copolymer formed by PS and an azobenzene containing polyacrylate was synthesised. This copolymer formed micelles in water after complexation of *trans* isomer of azobenzene units with a CD that converts the block into hydrophilic due to the hydroxyl groups of the CD. Micelles were disassembled when irradiated with UV because *cis* isomer is not able to form a host-guest complex with the CD and then micelles were not stable. After irradiation with visible light, *trans* isomer was recovered and the micelles were reassembled.⁸⁷

Huang and co-workers prepared an azobenzene-containing copolymer able to form a host-guest system with a water soluble pillar[7]arene. The resulting supramolecular polymer was amphiphilic and it formed vesicles in water solution. They demonstrated how light disrupted vesicles (because of the rupture of the host-guest systems when the azobenzene isomerised from *trans* to *cis*) and how this can be used to induce a controlled release of previously encapsulated Calcein.⁸⁸

Wu and co-workers have used tetramethoxy substituted azobenzene in red light responsive valves to control drug release from mesoporous silica nanoparticles. For this purpose, they took advantage of the host-guest complex formed between

azobenzene and β -cyclodextrin. This complex worked as a capping agent in mesoporous silica nanoparticles containing DOX, closing the nanopores. This supramolecular host-guest complex can be broken isomerising the azobenzene unit with red light (because *cis* isomer does not fit in the β -CD) and therefore opening the nanopores releasing the previously loaded molecules (**Figure 1.33**).⁸⁹

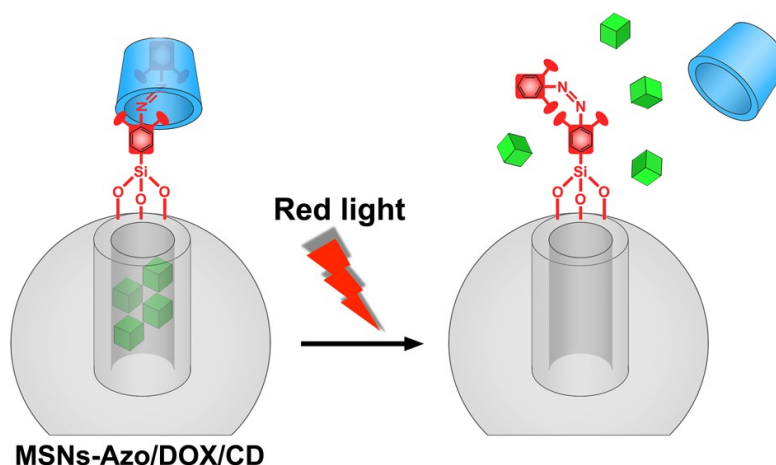


Figure 1.33. Use of azobenzene in a host-guest complex acting as capping agent for controlled drug release (reproduced from ref. 89)

Many other examples of host-guest supramolecular systems can be found in literature.^{82,90–92} However, in this Introduction we will focus on hydrogen bonded supramolecular polymers.

1.3.1. H-BONDED SUPRAMOLECULAR POLYMERS

Among the different supramolecular interactions, H-bonding has been widely used in the preparation of supramolecular materials. This interaction is strongly directional as well as temperature and pH dependant. As a sign of its importance, H-bonds are the responsible of anomalous properties of water and one of the main driving forces in DNA double helix.⁹³ Since H-bonds are drastically weakened by the presence of water, multivalent or hydrophobic protected H-bonding motifs have to be used in aqueous systems to ensure a stronger interaction.⁷⁹

Probably, the most important H-bonding based motifs are nitrogenous bases. DNA (or RNA) is composed by four nitrogenous bases. As it is well known, cytosine is complementary to guanine and adenine is complementary to thymine (or uracil). Although these are the main nitrogenous bases, there are some others as 2,6-diaminopyridine (DAP), complementary to thymine, or ureidopyrimidone that forms homodimers, used on the design of the H-bonding supramolecular materials (**Figure 1.34**).

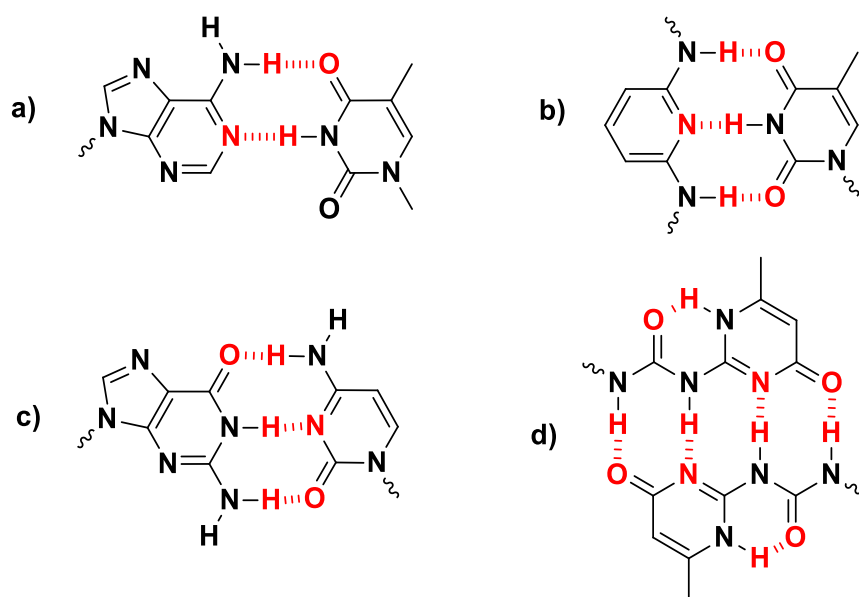


Figure 1.34. Different types of complementary nitrogenous bases
 a) adenine-thymine, b) 2,6-diaminopyridine-thymine, c) guanine-thymine and
 d) ureidopyrimidone dimer. In red, atoms involved in H-bonding.

The strength of these interactions depends on different factors, such as the number of H-bonds involved in the interaction, the solvent, the temperature, the pH or the secondary interactions existing between the atoms that form the whole motif. In this manner, the interaction of thymine with DAP is stronger than the interaction with adenine, since three and two H-bonds are formed respectively. Moreover, guanine-cytosine interaction is stronger than DAP-thymine, even though both are formed by three H-bonding.⁹⁴ The reason is that in the first case, there are secondary crossed interactions that are favourable, while in the second case these secondary interactions are repulsive (**Figure 1.35**).

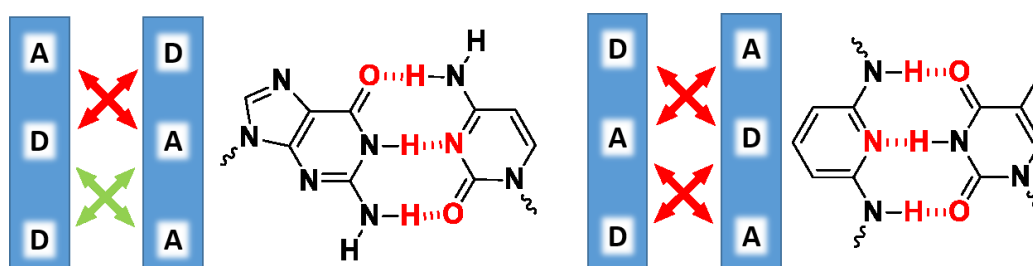


Figure 1.35. Schematic representations of secondary crossed interactions (red = unfavourable; green = favourable; A = acceptor; D = donor) in guanine-cytosine and diaminopyridine-thymine motifs

On the other hand, the increase of temperature weakens the strength of H-bonding based motifs.⁴⁸ In the same way, the polarity of the solvent, as well as its ability to suppress H-bonds, should be taken into account in the stability of polymeric architectures based on supramolecular interactions. It is described how nucleobases interactions are stronger in halogenated solvents as chloroform or DCM than in polar solvents as THF, DMF or DMSO.^{95,96} Since nucleobases can be protonated, the strength of the interaction can be modulated varying pH. In this manner, when pH decreases nitrogen groups can be protonated and, consequently, less H-bonds can be formed, weakening the interaction. This might be useful in the design of pH responsive materials.⁹⁷

Taking into account all these factors, nucleobases have been widely introduced in polymer structures. They have been used in different applications, from self-healing materials to polymeric nanocarriers.^{98,99} In particular, some examples are shown below in order to illustrate the potential of nucleobases in the preparation of H-bonding supramolecular polymers.

Kim and co-workers prepared polymers derived from guanine, cytosine, uracil and thymine *via* postfunctionalisation. For this purpose, they prepared a polymer with hydroxyl groups in the side chains. Then, they postfunctionalised this polymer with different nucleobases containing acid groups using the Steglich reaction. The physicochemical properties of the resulting polymers were studied, as well as their selective protein adsorption and their suppressed bacterial adherence.¹⁰⁰

Van Hest and co-workers polymerised adenine, thymine, cytosine and guanine methacrylate monomers using ATRP polymerisation. They described the synthesis of monomers as well as their polymerisation processes in DMSO. In the case of guanine and cytosine this was the first time they were polymerised.¹⁰¹

Rotello and co-workers have published several works related to supramolecular polymers. In particular, they have prepared styrenic polymers randomly postfunctionalised with DAP units able to recognize thymine derivatives through specific interactions.¹⁰² They also described the preparation of polymersomes based on the molecular recognition of both components *via* self-assembly of the DAP-functionalized PS with a thymine functionalised PS in chloroform (**Figure 1.36**). These recognition-induced polymersomes were stable several days, but they were disassembled when heated above 60 °C, showing the dynamic and reversible nature of hydrogen bonds.¹⁰³ Bis-thymines units were also used to crosslink these recognition-induced polymersomes in a noncovalent way. The self-assembled structures could be disaggregated when heated above 50 °C and re-assembled when cooling down. They found out how depending on the structure of the spacer, recognition induced polymersomes diameter varied.¹⁰⁴

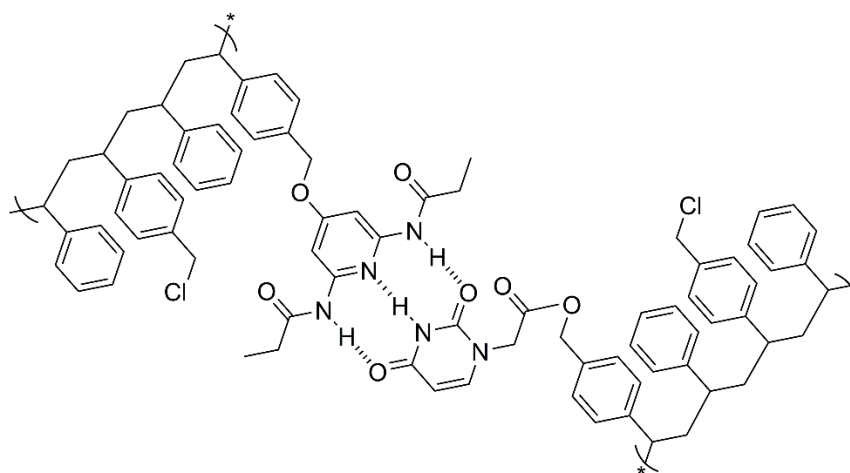


Figure 1.36. DAP and thymine-functionalized styrenic polymers prepared by Rotello's group

Nucleobases have also been used in the preparation of BCs. There are two main strategies in their preparation: the recognition of complementary motifs to create

the juncture point of both blocks and the introduction of the nucleobases in the polymeric side chains.

Following the first approach, BCs may be prepared by coupling different blocks having complementary nucleobases as terminal groups. Using this strategy, Zhu and co-workers prepared an amphiphilic BC formed by PEG and PCL, functionalised at the terminal group with uracil and with adenine, respectively. The complementarity of these groups allowed to obtain the final BC, which formed micelles in aqueous dispersion. These micelles were pH responsive, since uracil-adenine motif could be disrupted modifying the pH due to its basic nitrogens. The acidification of the medium resulted in a disruption of micelles. DOX was encapsulated in the micelles core and released after pH modification (**Figure 1.37**).⁹⁷

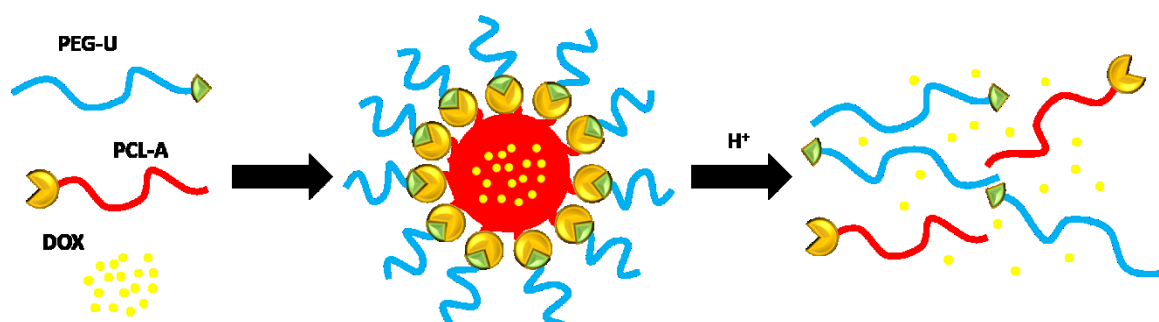


Figure 1.37. Schematic representation of supramolecular micelles encapsulating DOX (yellow) and its release under acidic conditions reported by Zhu and co-workers (adapted from ref. 97)

Regarding the side chain approach, Van Hest and co-workers prepared thymine and adenine containing amphiphilic BCs by ATRP polymerisation of monomers derived from these nucleobases using PEG as macroinitiator in a pioneering work. CAC were determined using fluorescence spectroscopy, using a solvatochromic dye, obtaining values of 8 $\mu\text{g}/\text{mL}$ for both polymers separately and 12 $\mu\text{g}/\text{mL}$ for a mixture of both. Aggregates from each amphiphilic BC in water were studied by DLS experiments, obtaining particles of around 20 nm of diameter.¹⁰⁵ O'Reilly and co-workers prepared amphiphilic BCs containing adenine and thymine by RAFT polymerisation using a poly[oligo(ethylene glycol) methacrylate] macro-CTA to

polymerise a hydrophobic block consisting of polymethacrylate functionalised with thymine and/or adenine (**Figure 1.38**). The BCs were self-assembled by adding water to a solution of the polymer in either DMF or DMSO. Self-assemblies presented great differences depending on the starting organic solvent that were related to the strong interaction between the nucleobases as well as the interaction with solvents. These interactions played a fundamental role in the stability and morphologies of the nanocarriers. Moreover, different annealing processes were performed by heating from 15 °C to 85 °C at different rates and then cooled down to room temperature, or varying the number of heating-cooling cycles. They observed variations in morphologies of some of the structures as well as narrower distributions. These variations were associated to the effect of temperature in polymer chains mobility that could reorganise themselves in the nanostructures as a consequence of the dynamic nature of hydrogen bonds.¹⁰⁶

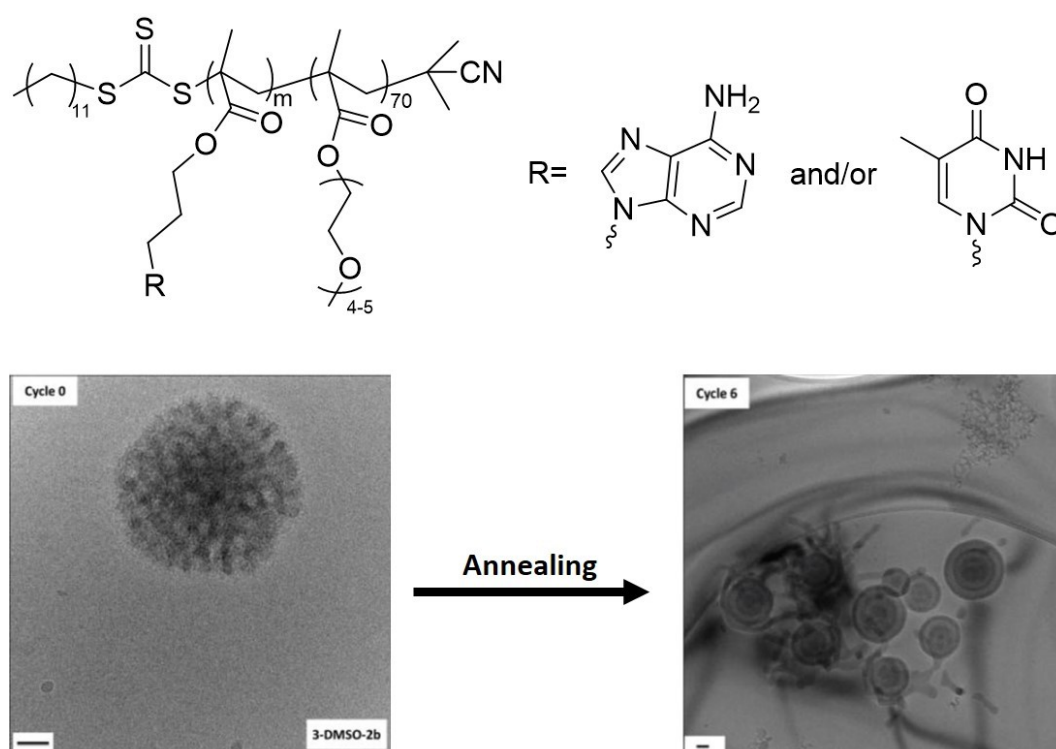


Figure 1.38. General structures of the nucleobase based BC and TEM images of self-assembled structures before and after annealing (adapted from ref. 106)

Taking advantage of the poor solubility of nucleobases containing polymers in organic solvents (except in high polarity solvents like DMF or DMSO), they have also prepared self-assemblies *via* RAFT dispersion polymerisation in chloroform and dioxane. For this purpose, they performed the polymerisation of a thymine monomer starting from a PMMA macro-CTA on both solvents. Due to the poor solubility of nucleobases, these polymers self-assembled throughout the polymerisation, giving rise to a heterogeneous polymerisation. These self-assembled structures formed in both chloroform and dioxane were studied by TEM and DLS, and they described how both the degree of polymerisation and solvent could affect morphologies, which ranged from micelles to vesicles depending on these factors. In particular, a transition from spherical micelles to vesicles was observed as degree of polymerisation was increased.¹⁰⁷

O'Reilly's group has also reported a template radical polymerisation using a block of polythymine (polyT) as template. For this purpose, a BC formed by PS and polyT was self-assembled in chloroform giving rise to spherical micelles with a polyT core. Then, a complementary adenine monomer was added and it was dissolved into the micelles through dynamic exchange. Finally, AIBN was added and the solution heated to initiate the polymerisation of adenine monomer using polyT as template (**Figure 1.39**). Efficiency of this template polymerisation was evaluated using GPC. The 'daughter adenine polymer' presented high MW (up to 400000 g/mol) and low dispersity (below 1.08).¹⁰⁸

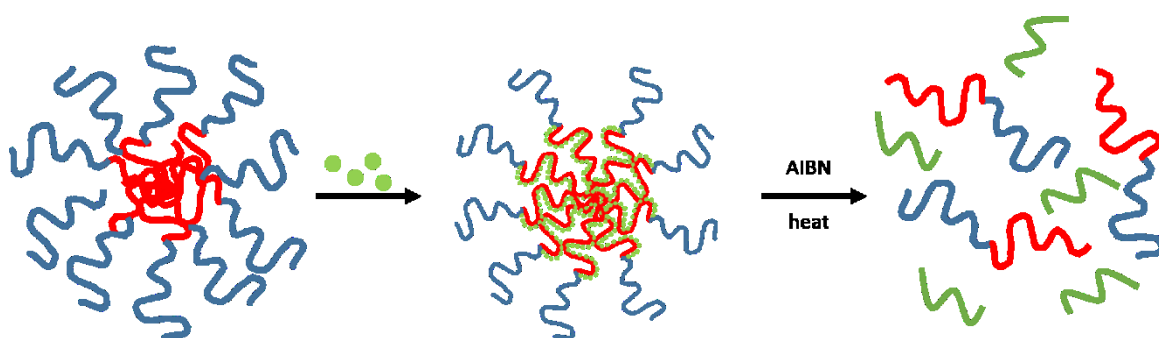


Figure 1.39. Schematic representation of template polymerisation. In blue, PS; in red, polyT; in green, adenine monomer/polymer

Liu and co-workers prepared several amphiphilic BCs formed by a hydrophobic block of PS and a hydrophilic block of poly(acryloylthymine) (PS-*b*-PAT). Spherical micelles were formed when the BCs were dispersed in water. According to the authors, micelle sizes were from 113 to 227 nm depending on hydrophobic/hydrophilic ratio between both blocks. Due to the formation of three hydrogen bonds, micelles aggregated after the addition of melamine (**Figure 1.40**). This interaction was studied by ¹H NMR, and the aggregation of micelles was studied by TEM, observing the apparition of micelles aggregates which is in concordance with the increase of turbidity observed with the naked eye.¹⁰⁹

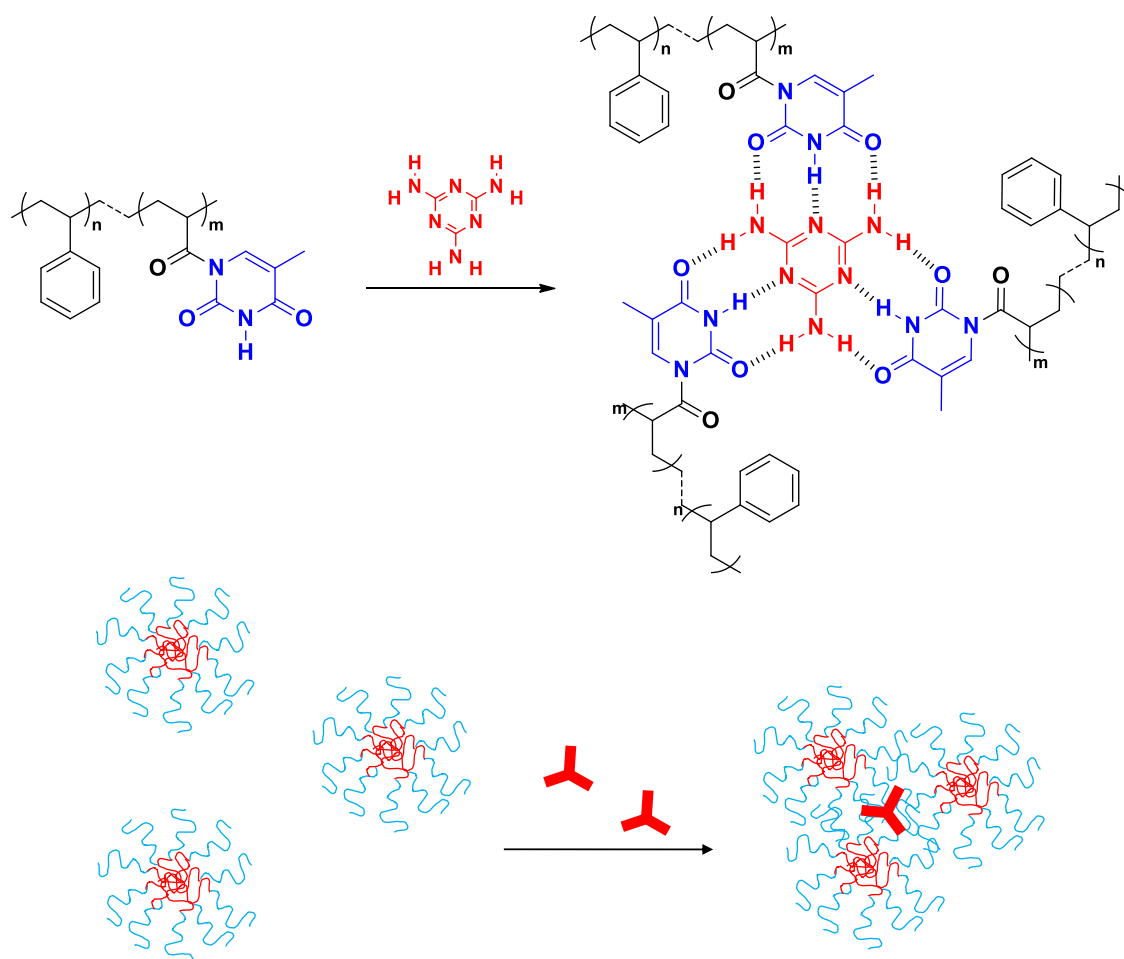


Figure 1.40. PS-*b*-PAT aggregation after addition of melamine

In our group, some supramolecular side chain BCs-related work has also been described. Firstly, a DAP-containing methacrylic monomer was polymerised using

a PMMA macro-CTA to form a BC. These polymers were easily postfunctionalised taking advantage of the DAP-thymine interactions. Some azobenzene derivatives, containing thymine units, were attached to the DAP units and the resultant polymers were properly characterised. Thermal and optical properties were evaluated, founding out that optical anisotropy could be photoinduced in these materials.⁴⁶

In a later work, amphiphilic BCs based on DAP were prepared following the same strategy, but using commercial PEG macro-CTAs of 2000 and 10000 g/mol to build two different amphiphilic BCs (**PEG2k-*b*-PDAP** and **PEG10k-*b*-PDAP**). Both formed micelles in water dispersion that were able to encapsulate camptothecin in their cores. Antiviral activity was evaluated on Huh 5-2 cells, demonstrating the potential of these systems as drug nanocarriers.⁴⁷

Finally, these **PEG-*b*-PDAP** polymers were functionalized with a thymine terminated azobenzene unit (**tAZO**) *via* multiple H-bonding (**Figure 1.41**). In case of **PEG2k-*b*-PDAP-tAZO** a transition from micelles to vesicles was observed in contrast with **PEG2k-*b*-PDAP** micelles. This is because the hydrophobic/hydrophilic ratio was increased. **PEG10k-*b*-PDAP-tAZO** still formed micelles despite of the post-functionalisation step. Light-responsive behaviour was checked in both systems as well as the ability of the self-assembled structures to respond to light stimulus, modifying their morphology in a similar way than covalent analogues (**Figure 1.42**).

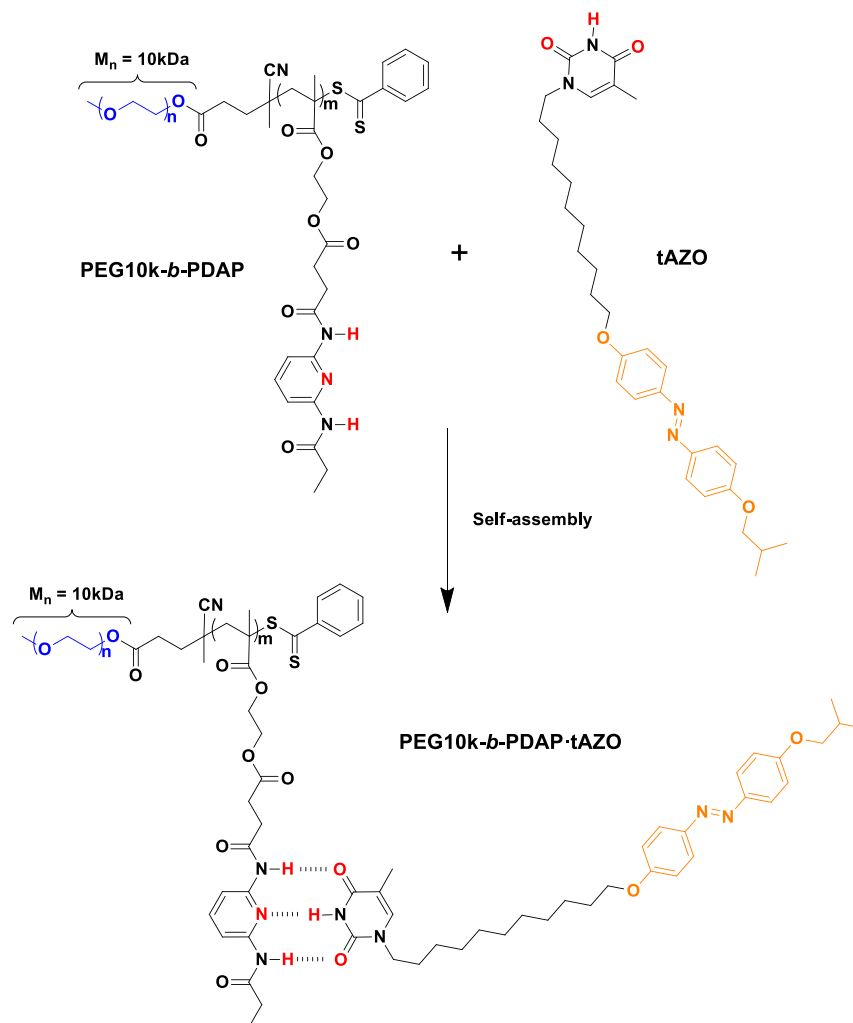


Figure 1.41. Self-assembly process and chemical structure of PEG10k-b-PDAP-tAZO

In both **PEG2k-b-PDAP-tAZO** and **PEG10k-b-PDAP-tAZO**, Nile Red was encapsulated into the hydrophobic parts of the polymer aggregates and released upon illumination. Rhodamine B was encapsulated into the hydrophilic inner cavity of **PEG2k-b-PDAP-tAZO** vesicles, as it was corroborated by fluorescence confocal microscopy. This technique was also used to study its light induced release in a similar way than in covalent BCs.⁴⁸

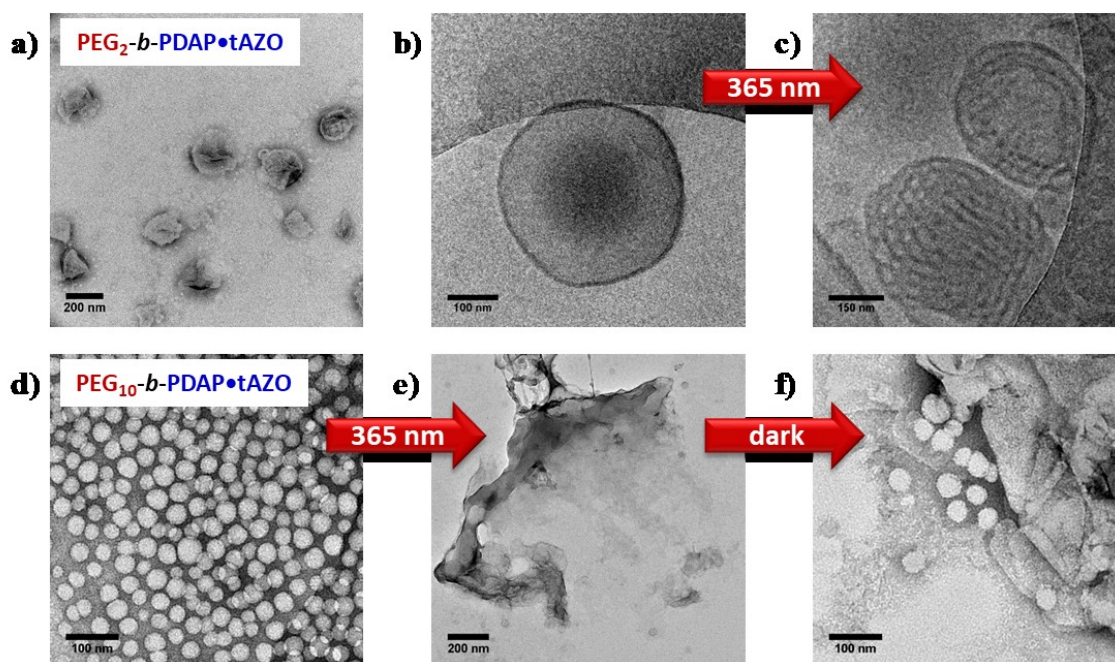


Figure 1.42. a) dry-state TEM image of PEG₂k-b-PDAP-tAZO vesicles, b) cryo-TEM image of PEG₂k-b-PDAP-tAZO, c) cryo-TEM image of PEG₂k-b-PDAP-tAZO after irradiation with UV light. d) dry-state TEM image of PEG₁₀k-b-PDAP-tAZO micelles, e) TEM image of PEG₁₀k-b-PDAP after irradiation with UV light and f) TEM image of PEG₁₀k-b-PDAP after some hours in dark

As a conclusion, there are not many examples of nucleobases based light-responsive amphiphilic BCs, in particular containing guanine, for the preparation of drug nanocarriers and it still remains a field of interest in Polymer Science.

1.4. REFERENCES

1. Wei, M., Gao, Y., Li, X. & Serpe, M. J. Stimuli-responsive polymers and their applications. *Polym. Chem.* **8**, 127–143 (2017).
2. Schild, H. G. Poly(N-isopropylacrylamide): experiment, theory and application. *Prog. Polym. Sci.* **17**, 163–249 (1992).
3. Vancoillie, G., Frank, D. & Hoogenboom, R. Thermoresponsive poly(oligo ethylene glycol acrylates). *Prog. Polym. Sci.* **39**, 1074–1095 (2014).
4. García-Juan, H. *et al.* Self-assembly of thermo and light responsive amphiphilic linear dendritic block copolymers. *Eur. Polym. J.* **81**, 621–633 (2016).
5. Schmaljohann, D. Thermo- and pH-responsive polymers in drug delivery☆. *Adv. Drug Deliv. Rev.* **58**, 1655–1670 (2006).
6. Park, S., Palai, A. K., Park, J., Jung, J. H. & Pyo, S. Synthesis and characterization of photo-crosslinkable coumarin-containing polymer dielectric for organic transistors. *Org. Electron.* **66**, 169–174 (2019).
7. Babin, J. *et al.* A New Two-Photon-Sensitive Block Copolymer Nanocarrier. *Angew. Chem. Int. Ed.* **48**, 3329–3332 (2009).
8. Jia, S., Fong, W.-K., Graham, B. & Boyd, B. J. Photoswitchable Molecules in Long-Wavelength Light-Responsive Drug Delivery: From Molecular Design to Applications. *Chem. Mater.* **30**, 2873–2887 (2018).
9. Il'ichev, Y. V., Schwörer, M. A. & Wirz, J. Photochemical Reaction Mechanisms of 2-Nitrobenzyl Compounds: Methyl Ethers and Caged ATP. *J. Am. Chem. Soc.* **126**, 4581–4595 (2004).
10. Wang, D. & Wang, X. Amphiphilic azo polymers: Molecular engineering, self-assembly and photoresponsive properties. *Prog. Polym. Sci.* **38**, 271–301 (2013).

11. Bruder, F.-K., Hagen, R., Rölle, T., Weiser, M.-S. & Fäcke, T. From the Surface to Volume: Concepts for the Next Generation of Optical-Holographic Data-Storage Materials. *Angew. Chem. Int. Ed.* **50**, 4552–4573 (2011).
12. Gelebart, A. H. *et al.* Making waves in a photoactive polymer film. *Nature* **546**, 632–636 (2017).
13. Yu, Y., Nakano, M. & Ikeda, T. Directed bending of a polymer film by light: Photomechanics. *Nature* **425**, 145–145 (2003).
14. Weis, P. & Wu, S. Light-Switchable Azobenzene-Containing Macromolecules: From UV to Near Infrared. *Macromol. Rapid Commun.* 1700220 (2017). doi:10.1002/marc.201700220
15. Dong, M., Babalhavaeji, A., Samanta, S., Beharry, A. A. & Woolley, G. A. Red-Shifting Azobenzene Photoswitches for in Vivo Use. *Acc. Chem. Res.* **48**, 2662–2670 (2015).
16. Wu, S. & Butt, H.-J. Near-Infrared-Sensitive Materials Based on Upconverting Nanoparticles. *Adv. Mater.* **28**, 1208–1226 (2016).
17. Yang, Y., Hughes, R. P. & Aprahamian, I. Visible Light Switching of a BF₂-Coordinated Azo Compound. *J. Am. Chem. Soc.* **134**, 15221–15224 (2012).
18. Yang, Y., Hughes, R. P. & Aprahamian, I. Near-Infrared Light Activated Azo-BF₂ Switches. *J. Am. Chem. Soc.* **136**, 13190–13193 (2014).
19. Poprawa-Smoluch, M. *et al.* Photoisomerization of Disperse Red 1 Studied with Transient Absorption Spectroscopy and Quantum Chemical Calculations. *J. Phys. Chem. A* **110**, 11926–11937 (2006).
20. Cinar, M., Coruh, A. & Karabacak, M. FT-IR, UV–vis, ¹H and ¹³C NMR spectra and the equilibrium structure of organic dye molecule disperse red 1 acrylate:

- A combined experimental and theoretical analysis. *Spectrochim. Acta. A. Mol. Biomol. Spectrosc.* **83**, 561–569 (2011).
21. Chen, M., Yu, L., Dalton, L. R., Shi, Y. & Steier, W. H. New polymers with large and stable second-order nonlinear optical effects. *Macromolecules* **24**, 5421–5428 (1991).
22. Sekkat, Z., Morichère, D., Dumont, M., Loucif-Saïbi, R. & Delaire, J. A. Photoisomerization of azobenzene derivatives in polymeric thin films. *J. Appl. Phys.* **71**, 1543–1545 (1992).
23. Pawlicki, M., Collins, H. A., Denning, R. G. & Anderson, H. L. Two-Photon Absorption and the Design of Two-Photon Dyes. *Angew. Chem. Int. Ed.* **48**, 3244–3266 (2009).
24. De Boni, L., Misoguti, L., Zilio, S. C. & Mendonça, C. R. Degenerate Two-Photon Absorption Spectra in Azoaromatic Compounds. *ChemPhysChem* **6**, 1121–1125 (2005).
25. Kim, H. M. *et al.* Environment-Sensitive Two-Photon Probe for Intracellular Free Magnesium Ions in Live Tissue. *Angew. Chem. Int. Ed.* **46**, 3460–3463 (2007).
26. Izquierdo-Serra, M. *et al.* Two-Photon Neuronal and Astrocytic Stimulation with Azobenzene-Based Photoswitches. *J. Am. Chem. Soc.* **136**, 8693–8701 (2014).
27. Carroll, E. C. *et al.* Two-photon brightness of azobenzene photoswitches designed for glutamate receptor optogenetics. *Proc. Natl. Acad. Sci.* **112**, E776–E785 (2015).
28. Sun, W. *et al.* Photoactivation of Anticancer Ru Complexes in Deep Tissue: How Deep Can We Go? *Chem. - Eur. J.* **23**, 10832–10837 (2017).

29. Beharry, A. A., Sadovski, O. & Woolley, G. A. Azobenzene Photoswitching without Ultraviolet Light. *J. Am. Chem. Soc.* **133**, 19684–19687 (2011).
30. Samanta, S. *et al.* Photoswitching Azo Compounds in Vivo with Red Light. *J. Am. Chem. Soc.* **135**, 9777–9784 (2013).
31. Samanta, S., McCormick, T. M., Schmidt, S. K., Seferos, D. S. & Woolley, G. A. Robust visible light photoswitching with ortho-thiol substituted azobenzenes. *Chem. Commun.* **49**, 10314 (2013).
32. Samanta, S., Babalhavaeji, A., Dong, M. & Woolley, G. A. Photoswitching of ortho-Substituted Azonium Ions by Red Light in Whole Blood. *Angew. Chem. Int. Ed.* **52**, 14127–14130 (2013).
33. Wang, D., Wagner, M., Butt, H.-J. & Wu, S. Supramolecular hydrogels constructed by red-light-responsive host–guest interactions for photo-controlled protein release in deep tissue. *Soft Matter* **11**, 7656–7662 (2015).
34. Weis, P., Wang, D. & Wu, S. Visible-Light-Responsive Azopolymers with Inhibited π – π Stacking Enable Fully Reversible Photopatterning. *Macromolecules* **49**, 6368–6373 (2016).
35. Epps, III, T. H. & O'Reilly, R. K. Block copolymers: controlling nanostructure to generate functional materials – synthesis, characterization, and engineering. *Chem Sci* **7**, 1674–1689 (2016).
36. Kim, J. K., Yang, S. Y., Lee, Y. & Kim, Y. Functional nanomaterials based on block copolymer self-assembly. *Prog. Polym. Sci.* **35**, 1325–1349 (2010).
37. Smart, T. *et al.* Block copolymer nanostructures. *Nano Today* **3**, 38–46 (2008).
38. Blasco, E., Piñol, M. & Oriol, L. Responsive Linear-Dendritic Block Copolymers. *Macromol. Rapid Commun.* **35**, 1090–1115 (2014).

39. Keddie, D. J. A guide to the synthesis of block copolymers using reversible-addition fragmentation chain transfer (RAFT) polymerization. *Chem Soc Rev* **43**, 496–505 (2014).
40. Braunecker, W. A. & Matyjaszewski, K. Controlled/living radical polymerization: Features, developments, and perspectives. *Prog. Polym. Sci.* **32**, 93–146 (2007).
41. Matyjaszewski, K. Atom Transfer Radical Polymerization (ATRP): Current Status and Future Perspectives. *Macromolecules* **45**, 4015–4039 (2012).
42. Keddie, D. J., Moad, G., Rizzardo, E. & Thang, S. H. RAFT Agent Design and Synthesis. *Macromolecules* **45**, 5321–5342 (2012).
43. Kolb, H. C., Finn, M. G. & Sharpless, K. B. Click Chemistry: Diverse Chemical Function from a Few Good Reactions. *Angew. Chem. Int. Ed Engl.* **40**, 2004–2021 (2001).
44. Such, G. K., Johnston, A. P. R., Liang, K. & Caruso, F. Synthesis and functionalization of nanoengineered materials using click chemistry. *Prog. Polym. Sci.* **37**, 985–1003 (2012).
45. Forcén, P. *et al.* Synthesis, characterization and photoinduction of optical anisotropy in liquid crystalline diblock azo-copolymers. *J. Polym. Sci. Part Polym. Chem.* **45**, 1899–1910 (2007).
46. Concellón, A. *et al.* Photoresponsive polymers and block copolymers by molecular recognition based on multiple hydrogen bonds. *J. Polym. Sci. Part Polym. Chem.* **52**, 3173–3184 (2014).
47. Concellón, A. *et al.* Polymeric micelles from block copolymers containing 2,6-diacylaminopyridine units for encapsulation of hydrophobic drugs. *RSC Adv* **6**, 24066–24075 (2016).

48. Concellón, A. *et al.* Light-Responsive Self-Assembled Materials by Supramolecular Post-Functionalization via Hydrogen Bonding of Amphiphilic Block Copolymers. *Macromolecules* **49**, 7825–7836 (2016).
49. Berges, C. *et al.* Photoinduced optical anisotropy in azobenzene containing block copolymer–homopolymer blends. Influence of microstructure and molecular weight. *Eur. Polym. J.* **48**, 613–620 (2012).
50. Tang, Z. *et al.* Polymeric nanostructured materials for biomedical applications. *Prog. Polym. Sci.* **60**, 86–128 (2016).
51. Blanazs, A., Madsen, J., Battaglia, G., Ryan, A. J. & Armes, S. P. Mechanistic Insights for Block Copolymer Morphologies: How Do Worms Form Vesicles? *J. Am. Chem. Soc.* **133**, 16581–16587 (2011).
52. Zhu, Y., Yang, B., Chen, S. & Du, J. Polymer vesicles: Mechanism, preparation, application, and responsive behavior. *Prog. Polym. Sci.* **64**, 1–22 (2017).
53. Messenger, L. *et al.* Biomimetic Hybrid Nanocontainers with Selective Permeability. *Angew. Chem. Int. Ed.* **55**, 11106–11109 (2016).
54. Robertson, J. D. *et al.* Purification of Nanoparticles by Size and Shape. *Sci. Rep.* **6**, (2016).
55. Torchilin, V. Tumor delivery of macromolecular drugs based on the EPR effect. *Adv. Drug Deliv. Rev.* **63**, 131–135 (2011).
56. Bleul, R., Thiermann, R. & Maskos, M. Techniques To Control Polymersome Size. *Macromolecules* **48**, 7396–7409 (2015).
57. Cabral, H., Miyata, K., Osada, K. & Kataoka, K. Block Copolymer Micelles in Nanomedicine Applications. *Chem. Rev.* **118**, 6844–6892 (2018).
58. Adams, M. L., Lavasanifar, A. & Kwon, G. S. Amphiphilic block copolymers for drug delivery. *J. Pharm. Sci.* **92**, 1343–1355 (2003).

59. Scholz, N., Behnke, T. & Resch-Genger, U. Determination of the Critical Micelle Concentration of Neutral and Ionic Surfactants with Fluorometry, Conductometry, and Surface Tension—A Method Comparison. *J. Fluoresc.* **28**, 465–476 (2018).
60. Sun, X.-L. *et al.* Thermoresponsive block copolymer micelles with tunable pyrrolidone-based polymer cores: structure/property correlations and application as drug carriers. *J Mater Chem B* **3**, 814–823 (2015).
61. Li, Y. *et al.* Non-covalent interactions in controlling pH-responsive behaviors of self-assembled nanosystems. *Polym. Chem.* **7**, 5949–5956 (2016).
62. Hamaguchi, T. *et al.* NK105, a paclitaxel-incorporating micellar nanoparticle formulation, can extend in vivo antitumour activity and reduce the neurotoxicity of paclitaxel. *Br. J. Cancer* **92**, 1240–1246 (2005).
63. Zhao, Y. Light-Responsive Block Copolymer Micelles. *Macromolecules* **45**, 3647–3657 (2012).
64. Lee, H. *et al.* Light-Induced Reversible Formation of Polymeric Micelles. *Angew. Chem. Int. Ed.* **46**, 2453–2457 (2007).
65. Katz, J. S. *et al.* Modular Synthesis of Biodegradable Diblock Copolymers for Designing Functional Polymersomes. *J. Am. Chem. Soc.* **132**, 3654–3655 (2010).
66. Gohy, J.-F. & Zhao, Y. Photo-responsive block copolymer micelles: design and behavior. *Chem. Soc. Rev.* **42**, 7117 (2013).
67. Kumar, S. *et al.* Near-infrared light sensitive polypeptide block copolymer micelles for drug delivery. *J. Mater. Chem.* **22**, 7252 (2012).

68. Jiang, J., Tong, X., Morris, D. & Zhao, Y. Toward Photocontrolled Release Using Light-Dissociable Block Copolymer Micelles. *Macromolecules* **39**, 4633–4640 (2006).
69. Han, D., Tong, X. & Zhao, Y. Fast Photodegradable Block Copolymer Micelles for Burst Release. *Macromolecules* **44**, 437–439 (2011).
70. Wang, G., Tong, X. & Zhao, Y. Preparation of Azobenzene-Containing Amphiphilic Diblock Copolymers for Light-Responsive Micellar Aggregates. *Macromolecules* **37**, 8911–8917 (2004).
71. Ye, Q. *et al.* Photoinduced Reversible Worm-to-Vesicle Transformation of Azo-Containing Block Copolymer Assemblies Prepared by Polymerization-Induced Self-Assembly. *Macromolecules* **51**, 3308–3314 (2018).
72. Wu, S. *et al.* Block copolymers of PS-*b*-PEO co-assembled with azobenzene-containing homopolymers and their photoresponsive properties. *Soft Matter* **7**, 11535 (2011).
73. Blasco, E., Serrano, J. L., Piñol, M. & Oriol, L. Light Responsive Vesicles Based on Linear–Dendritic Block Copolymers Using Azobenzene–Aliphatic Codendrons. *Macromolecules* **46**, 5951–5960 (2013).
74. Blasco, E., Barrio, J. del, Sánchez-Somolinos, C., Piñol, M. & Oriol, L. Light induced molecular release from vesicles based on amphiphilic linear-dendritic block copolymers. *Polym. Chem.* **4**, 2246 (2013).
75. del Barrio, J. *et al.* Self-Assembly of Linear–Dendritic Diblock Copolymers: From Nanofibers to Polymersomes. *J. Am. Chem. Soc.* **132**, 3762–3769 (2010).
76. Blasco, E., Schmidt, B. V. K. J., Barner-Kowollik, C., Piñol, M. & Oriol, L. A Novel Photoresponsive Azobenzene-Containing Miktoarm Star Polymer: Self-

- Assembly and Photoresponse Properties. *Macromolecules* **47**, 3693–3700 (2014).
77. Dong, R., Zhu, B., Zhou, Y., Yan, D. & Zhu, X. Reversible photoisomerization of azobenzene-containing polymeric systems driven by visible light. *Polym. Chem.* **4**, 912 (2013).
78. Angelos, S., Choi, E., Vögtle, F., De Cola, L. & Zink, J. I. Photo-Driven Expulsion of Molecules from Mesoporous Silica Nanoparticles. *J. Phys. Chem. C* **111**, 6589–6592 (2007).
79. Krieg, E., Bastings, M. M. C., Besenius, P. & Rybtchinski, B. Supramolecular Polymers in Aqueous Media. *Chem. Rev.* **116**, 2414–2477 (2016).
80. Amaral, A. J. R. & Pasparakis, G. Stimuli responsive self-healing polymers: gels, elastomers and membranes. *Polym. Chem.* **8**, 6464–6484 (2017).
81. Herbst, F., Döhler, D., Michael, P. & Binder, W. H. Self-Healing Polymers via Supramolecular Forces. *Macromol. Rapid Commun.* **34**, 203–220 (2013).
82. Liu, G. *et al.* Cyclodextrin-based host–guest supramolecular hydrogel and its application in biomedical fields. *Polym. Chem.* **9**, 3436–3449 (2018).
83. Dong, R. *et al.* Functional Supramolecular Polymers for Biomedical Applications. *Adv. Mater.* n/a-n/a (2014). doi:10.1002/adma.201402975
84. Ma, X. & Zhao, Y. Biomedical Applications of Supramolecular Systems Based on Host–Guest Interactions. *Chem. Rev.* 141121152923008 (2014). doi:10.1021/cr500392w
85. Zhang, X. *et al.* Recent Advances in Cyclodextrin-Based Light-Responsive Supramolecular Systems. *Macromol. Rapid Commun.* **39**, 1800142 (2018).

86. Zhang, X., Dai, Y., Chen, X. & Zhuo, R. UV-Responsive Supramolecular Vesicles with Double Hydrophobic Chains. *Macromol. Rapid Commun.* **37**, 888–893 (2016).
87. Wang, S., Shen, Q., Nawaz, M. H. & Zhang, W. Photocontrolled reversible supramolecular assemblies of a diblock azo-copolymer based on β -cyclodextrin–Azo host–guest inclusion complexation. *Polym. Chem.* **4**, 2151 (2013).
88. Chi, X., Ji, X., Xia, D. & Huang, F. A Dual-Responsive Supra-Amphiphilic Polypseudorotaxane Constructed from a Water-Soluble Pillar[7]arene and an Azobenzene-Containing Random Copolymer. *J. Am. Chem. Soc.* **137**, 1440–1443 (2015).
89. Wang, D. & Wu, S. Red-Light-Responsive Supramolecular Valves for Photocontrolled Drug Release from Mesoporous Nanoparticles. *Langmuir* **32**, 632–636 (2016).
90. Schmidt, B. V. K. J. & Barner-Kowollik, C. Dynamic Macromolecular Material Design-The Versatility of Cyclodextrin-Based Host-Guest Chemistry. *Angew. Chem. Int. Ed.* **56**, 8350–8369 (2017).
91. Wang, D., Zhao, W., Wei, Q., Zhao, C. & Zheng, Y. Photoswitchable Azobenzene/Cyclodextrin Host-Guest Complexes: From UV- to Visible/Near-IR-Light-Responsive Systems. *ChemPhotoChem* **2**, 403–415 (2018).
92. Zhang, H., Liu, Z. & Zhao, Y. Pillararene-based self-assembled amphiphiles. *Chem. Soc. Rev.* **47**, 5491–5528 (2018).
93. Watson, J. D. & Crick, F. H. C. Molecular Structure of Nucleic Acids: A Structure for Deoxyribose Nucleic Acid. *Nature* **171**, 737 (1953).

94. Jorgensen, W. L. & Pranata, J. Importance of secondary interactions in triply hydrogen bonded complexes: guanine-cytosine vs uracil-2,6-diaminopyridine. *J. Am. Chem. Soc.* **112**, 2008–2010 (1990).
95. Kang, Y., Lu, A., Ellington, A., Jewett, M. C. & O'Reilly, R. K. Effect of Complementary Nucleobase Interactions on the Copolymer Composition of RAFT Copolymerizations. *ACS Macro Lett.* **2**, 581–586 (2013).
96. Cook, J. L., Hunter, C. A., Low, C. M. R., Perez-Velasco, A. & Vinter, J. G. Solvent Effects on Hydrogen Bonding. *Angew. Chem. Int. Ed.* **46**, 3706–3709 (2007).
97. Wang, D. *et al.* Supramolecular Copolymer Micelles Based on the Complementary Multiple Hydrogen Bonds of Nucleobases for Drug Delivery. *Biomacromolecules* **12**, 1370–1379 (2011).
98. Lin, Y. & Li, G. An intermolecular quadruple hydrogen-bonding strategy to fabricate self-healing and highly deformable polyurethane hydrogels. *J Mater Chem B* **2**, 6878–6885 (2014).
99. Xu, J.-F. *et al.* Hydrogen Bonding Directed Self-Assembly of Small-Molecule Amphiphiles in Water. *Org. Lett.* **16**, 4016–4019 (2014).
100. Kim, J. C. *et al.* Synthesis, physicochemical characteristics, and biocompatibility of self-assemble polymers bearing guanine, cytosine, uracil, and thymine moieties. *J. Polym. Sci. Part Polym. Chem.* **53**, 1151–1160 (2015).
101. Spijker, H. J., van Delft, F. L. & van Hest, J. C. M. Atom Transfer Radical Polymerization of Adenine, Thymine, Cytosine, and Guanine Nucleobase Monomers. *Macromolecules* **40**, 12–18 (2007).

102. Ilhan, F., Gray, M. & Rotello, V. M. Reversible Side Chain Modification through Noncovalent Interactions. "Plug and Play" Polymers. *Macromolecules* **34**, 2597–2601 (2001).
103. Ilhan, F., Galow, T. H., Gray, M., Clavier, G. & Rotello, V. M. Giant Vesicle Formation through Self-Assembly of Complementary Random Copolymers. *J. Am. Chem. Soc.* **122**, 5895–5896 (2000).
104. Thibault, R. J., Hotchkiss, P. J., Gray, M. & Rotello, V. M. Thermally Reversible Formation of Microspheres through Non-Covalent Polymer Cross-Linking. *J. Am. Chem. Soc.* **125**, 11249–11252 (2003).
105. Spijker, H. J., Dirks, A. J. & van Hest, J. C. M. Synthesis and assembly behavior of nucleobase-functionalized block copolymers. *J. Polym. Sci. Part Polym. Chem.* **44**, 4242–4250 (2006).
106. Kang, Y. *et al.* Use of complementary nucleobase-containing synthetic polymers to prepare complex self-assembled morphologies in water. *Polym Chem* **7**, 2836–2846 (2016).
107. Kang, Y., Pitto-Barry, A., Maitland, A. & O'Reilly, R. K. RAFT dispersion polymerization: a method to tune the morphology of thymine-containing self-assemblies. *Polym. Chem.* **6**, 4984–4992 (2015).
108. McHale, R., Patterson, J. P., Zetterlund, P. B. & O'Reilly, R. K. Biomimetic radical polymerization via cooperative assembly of segregating templates. *Nat. Chem.* **4**, 491–497 (2012).
109. Tao, Y. *et al.* Micelles formation of polystyrene-co-poly (N-acryloylthymine) and its aggregation behavior induced by triple hydrogen bonding. *Polymer* **53**, 1551–1557 (2012).

**CHAPTER 2: AMPHIPHILIC
BCs BASED ON
TETRAMETHOXYAZOBENZENE**

2.1. INTRODUCTION AND AIMS

The work compiled in this chapter aimed the preparation of amphiphilic BCs self-assemblies that can act as nanocarriers for controlled release of payloads under visible light stimulation. On the basis of literature reports, the chromophore *ortho*-tetramethoxyazobenzene was selected because of its ability to isomerise upon green and red light illumination.^{1,2} This particular selection combines the knowledge about the chemistry and properties of azobenzenes of the Liquid Crystal and Polymers Group with the possibility of provoking photostimulation using a region of the electromagnetic spectrum more adequate for bioapplications, as UV light is harmful for biological tissues.

With this purpose, amphiphilic linear-linear BCs were devised consisting of poly(ethylene glycol) (PEG) as the hydrophilic segment and an azobenzene polymethacrylate as the hydrophobic block. Because the morphology of the self-assembled structures is determined by the polymer architecture, to gain an adequate control on structural parameters, polymers were prepared by RAFT polymerisation using the macroinitiator approach with two different PEG macro-CTAs of 2000 and 10000 g/mol ($n = 45$ and 227, respectively) (**Figure 2.1**).

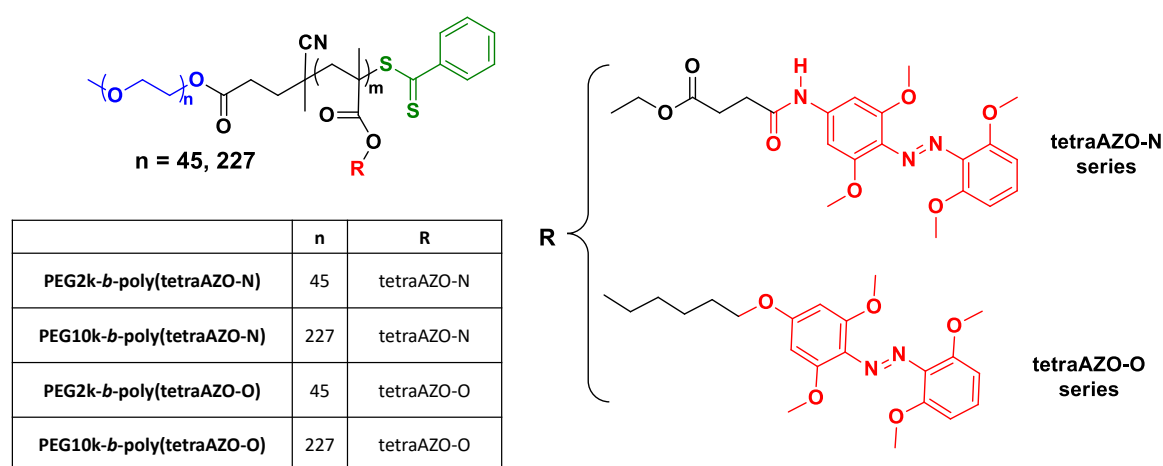


Figure 2.1. General structure and nomenclature of the target BCs

The proposed tasks were:

- Synthesis and characterisation of *ortho*-tetramethoxyazobenzene monomers and evaluation of their photoresponse
- Preparation of amphiphilic BCs by RAFT polymerisation using two PEG macro-CTA agents
- Structural and thermal characterisation
- Preparation of polymeric self-assemblies using the *co*-solvent method. Characterisation of self-assembled structures by transmission electronic microscopy (TEM) and dynamic light scattering (DLS)
- Study of the photoresponse of the self-assemblies by spectroscopic techniques
- Structural characterisation of the irradiated self-assemblies
- Evaluation of the encapsulation and light stimulated release properties of self-assemblies

2.2. SYNTHESIS, CHARACTERISATION AND SELF-ASSEMBLY IN WATER

Since *ortho*-tetramethoxyazobenzenes have proven being chromophores suitable to gain light responsiveness in the visible region of the electromagnetic spectrum, the *ortho*-tetramethoxyazobenzene based methacrylate **meth(tetraAZO-N)** was prepared in two steps (**Figure 2.2**).¹ First, the 4-amino substituted *ortho*-tetramethoxyazobenzene **1** was obtained by azo coupling between 2,6-dimethoxyaniline and 3,5-dimethoxyaniline. Then, reaction of **1** with mono-2-(methacryloyloxy)ethyl succinate *via* Steglich reaction gave the desired monomer.

Amphiphilic BCs were prepared by RAFT polymerisation using two commercial PEG macro-CTAs with the 4-cyano-4-(phenylthiocarbonylthio)pentanoate end group, which has been described as an appropriate chain transfer agent for the polymerisation of methacrylic monomers (**Figure 2.2**).³ RAFT polymerisations were conducted under argon atmosphere in freshly distilled DMF at 70 °C using AIBN as radical initiator in a 10% molar proportion respect to macro-CTA. Polymers were precipitated into cold diethyl ether and further purified by preparative size exclusion chromatography (SEC) using a BioBeads® resin to remove the unreacted monomer. Relevant characterisation data are collected in **Table 2.1**.

Table 2.1. Molar masses of BCs of the **tetraAZO-N** series

Polymer	m_{th}^a	m^b	$M_{n,NMR}^c$	$M_{n,SEC}$	\mathcal{D}
PEG10k- <i>b</i> -poly(tetraAZO-N)	40	15	17900	42105	1.12
PEG2k- <i>b</i> -poly(tetraAZO-N)	20	17	10900	32028	1.14

^a Theoretical degree of polymerisation calculated from the $[monomer]_0/[macro-CTA]_0$ assuming full monomer conversion

^b Experimental degree of polymerisation of the poly(tetraAZO-N) block estimated by ¹H NMR end group analysis

^c Molar mass of BC given as the sum of the molar mass of PEG and poly(tetraAZO-N) blocks calculated using m determined by $^1\text{H NMR}$ ($M_n = M_{\text{PEG}} + m \times M_{\text{monomer}}$). For PEG, commercial value was used

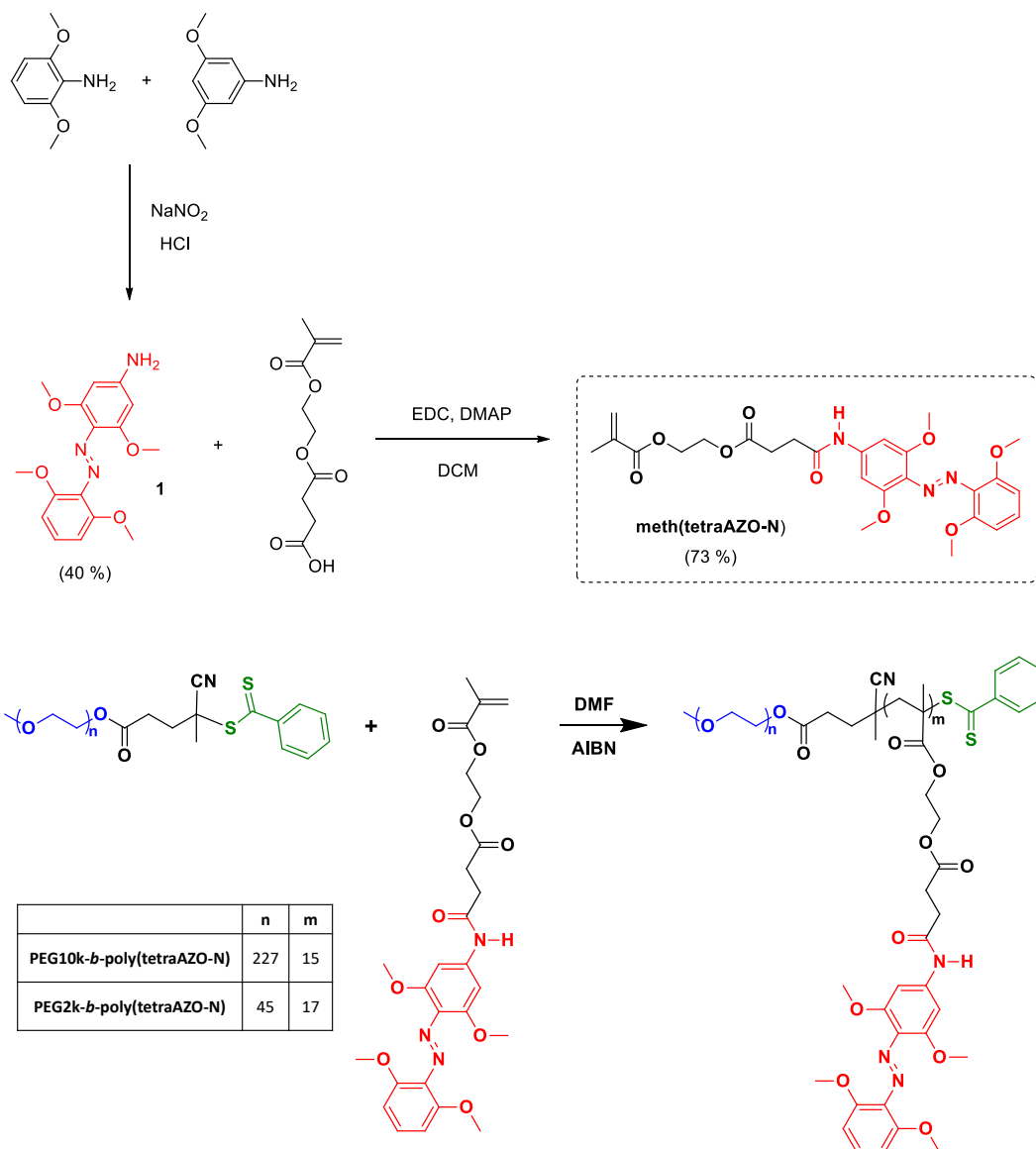


Figure 2.2. Synthesis and polymerisation of meth(tetraAZO-N)

Polymerisation was first accomplished with a macro-CTA of an average molar mass of a 10000 g/mol ($n = 227$) using a ratio $[\text{monomer}]_0/[\text{macro-CTA}]_0 = 40$, *i.e.* a targeted polymerisation degree (m_{th}) of 40. However, a significant lower degree of polymerisation was achieved (see below). Therefore, RAFT polymerisation was repeated using a macro-CTA of an average molar mass of a 2000 g/mol ($n = 45$)

and a targeted degree of polymerisation (m_{th}) of 20. The polymerisation degree of the final BC was in acceptable agreement with the theoretical value (**Table 2.1**). When analysed by size exclusion chromatography (SEC) in DMF, using polystyrene standards for calibration and a UV-Vis detector, BCs of **tetraAZO-N** series showed monomodal molar mass distributions with the peak shifted to lower elution time respect to the corresponding macro-CTA due to the increase of the molar mass. Traces of residual macro-CTA or monomer were not detected. As an example, SEC traces of **PEG2k-CTA** and **PEG2k-*b*-poly(tetraAZO-N)** are compared in **Figure 2.3**.

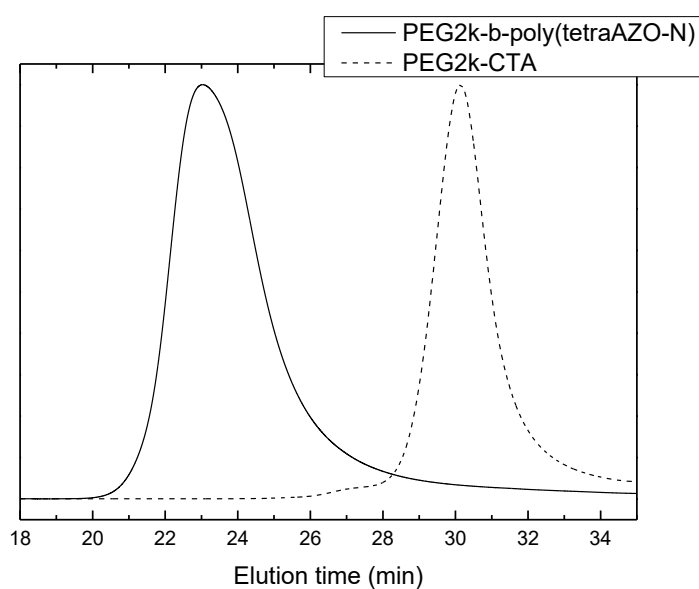


Figure 2.3. SEC curves of PEG2k-CTA and PEG2k-*b*-poly(tetraAZO-N)

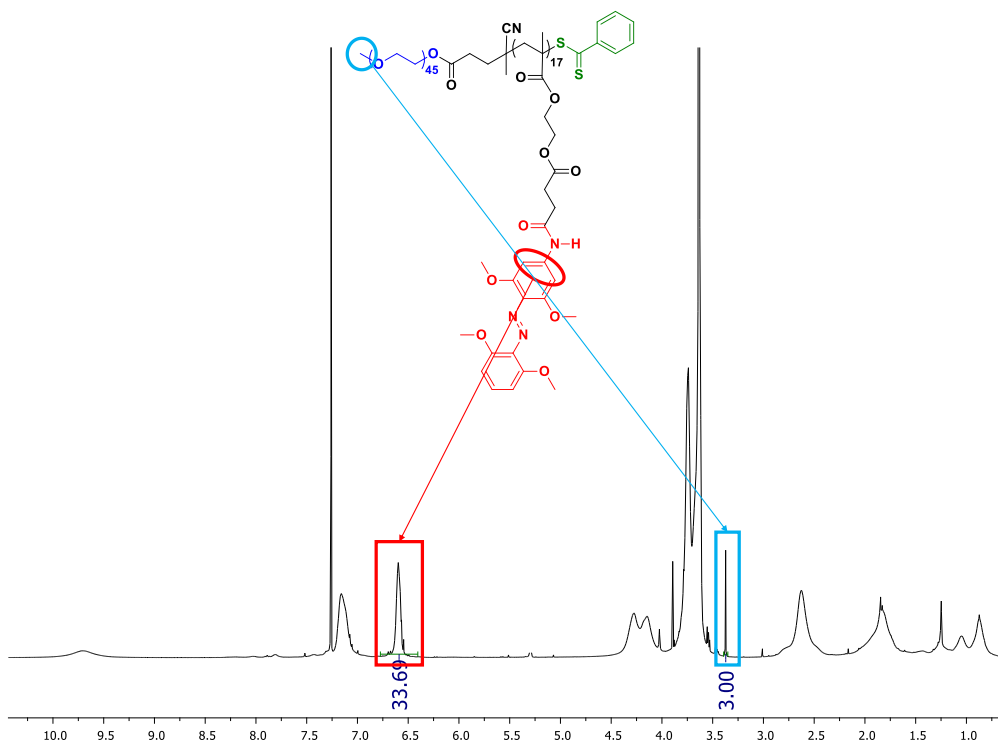


Figure 2.4. ^1H NMR spectrum in CDCl_3 of PEG2k-*b*-poly(tetraAZO-N)

Average number molar masses of the BCs ($M_{n,\text{NMR}}$ in **Table 2.1**) were calculated as the sum of the molar masses of **PEG** and **poly(tetraAZO-N)** blocks which in turn were calculated using the degree of polymerisation (m) values. These values were determined for the **poly(tetraAZO-N)** block by ^1H NMR end group analysis from the relative integration of the peak at 3.37 ppm corresponding to the CH_3O -terminal group of the PEG and the one at 6.53 ppm due to the azobenzene repeating unit (that corresponds to 2 protons). The ^1H NMR spectrum of **PEG2k-*b*-poly(tetraAZO-N)** is shown as an example in **Figure 2.4** for which an average degree of polymerisation of the hydrophobic block (m) of approx. 17 was determined that provides a $M_{n,\text{NMR}}$ of 10900 g/mol. For **PEG10k-*b*-poly(tetraAZO-N)**, a rather large difference between m and m_{th} was observed, in contrast with **PEG2k-*b*-poly(tetraAZO-N)** for which a better concordance was obtained after the conditions of the polymerisation were adjusted.

Thermal characterisation of BCs was performed by TGA and DSC and compared to that of the PEG-CTAs precursors taken as reference. Relevant data are gathered in **Table 2.2**. All polymers showed a good stability as determined by TGA

having decomposition temperatures associated with mass loss above 200 °C. Evolution of volatiles due to the presence of residual solvents or water was not observed. Thermal transitions were evaluated by DSC at 10 °C/min rate scan. Data were obtained from the first heating scan. For **PEG10k-*b*-poly(tetraAZO-N)**, only a melting transition was observed at $T_m = 61$ °C (no glass transitions were detected) that can be associated with the PEG block by comparing with **PEG10k-CTA**, which has a $T_m = 58$ °C. On the other hand, **PEG2k-*b*-poly(tetraAZO-N)** was amorphous and only exhibited a glass transition (T_g) at 68 °C, in contrast with **PEG2k-CTA** that was crystalline with a melting temperature (T_m) of 48 °C. Differences could be related to the larger wt% fraction of PEG in **PEG10k-*b*-poly(tetraAZO-N)** than in **PEG2k-*b*-poly(tetraAZO-N)**. The existence of a unique transition in both polymers might be indicative of a degree of compatibility between blocks, although it should be taken into account that both transitions appear in a similar temperature region.

Table 2.2. Thermal properties of BCs of the tetra(AZO-N) series

Polymer	TGA ^a	T_g ^b	T_m (ΔH_m) ^c
PEG10k-CTA	310	---	58 (142)
PEG2k-CTA	210	---	48 (163)
PEG10k-<i>b</i>-poly(tetraAZO-N)	263	---	61 (110)
PEG2k-<i>b</i>-poly(tetraAZO-N)	200	68	---

^a Decomposition temperature (in °C) associated to mass loss determined by TGA given at the onset of the weight loss curve

^b Glass transition temperature (in °C) determined by DSC on the first heating scan at 10 °C/min given at the half height of the baseline jump

^c Melting temperature (in °C) given at the maximum of the peak and associated melting enthalpy (in J/g), in brackets, determined by DSC on the first heating scan at 10 °C/min

Self-assembly of BCs was tested by the co-solvent method considering first the pair THF/water on the basis of our previous experience.⁴⁻⁸ However, both polymers were almost insoluble in THF, probably due to the amide bond connector group at the **tetraAZO-N** unit. Therefore, self-assembly was examined using DMSO and

DMF as better solvents of both blocks that are miscible with water. However, precipitation was eventually observed throughout the addition of water to the solutions of the polymers in both solvents. In the case of **PEG10k-*b*-poly(tetraAZO-N)**, the DMF/water mixture was poured into a large amount of water trying to freeze the possible self-assemblies formed before precipitation occurred. However, TEM inspection of the samples showed undefined structures (**Figure 2.5**). Due to these difficulties, **PEG10k-*b*-poly(tetraAZO-N)** and **PEG2k-*b*-poly(tetraAZO-N)** were discarded for further investigations.

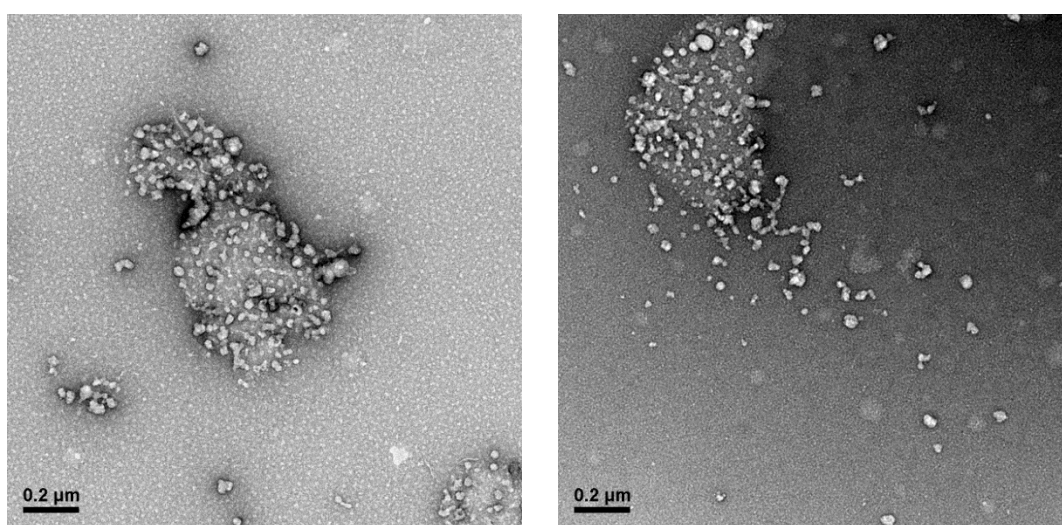


Figure 2.5. Representative TEM images of PEG10k-*b*-poly(tetraAZO-N)

To improve the limited solubility of the BCs with the **tetraAZO-N** chromophore, a new *ortho*-tetramethoxyazobenzene methacrylate was synthesised where the amide linking group was replaced by an ether bond (**Figure 2.6**). The 4-hydroxy substituted *ortho*-tetramethoxyazobenzene **2** was prepared by azo coupling between 2,6-dimethoxyaniline and 3,5-dimethoxyphenol. Then, a substitution reaction of **2** with 6-bromohexan-1-ol gave compound **3**, which further reacted with methacryloyl chloride to yield the targeted **meth(tetraAZO-O)**.²

This monomer was polymerised using the RAFT conditions described for **meth(tetraAZO-N)** (**Figure 2.6**) and m_{th} was adjusted to 30. Relevant characterisation data are collected in **Table 2.3**.

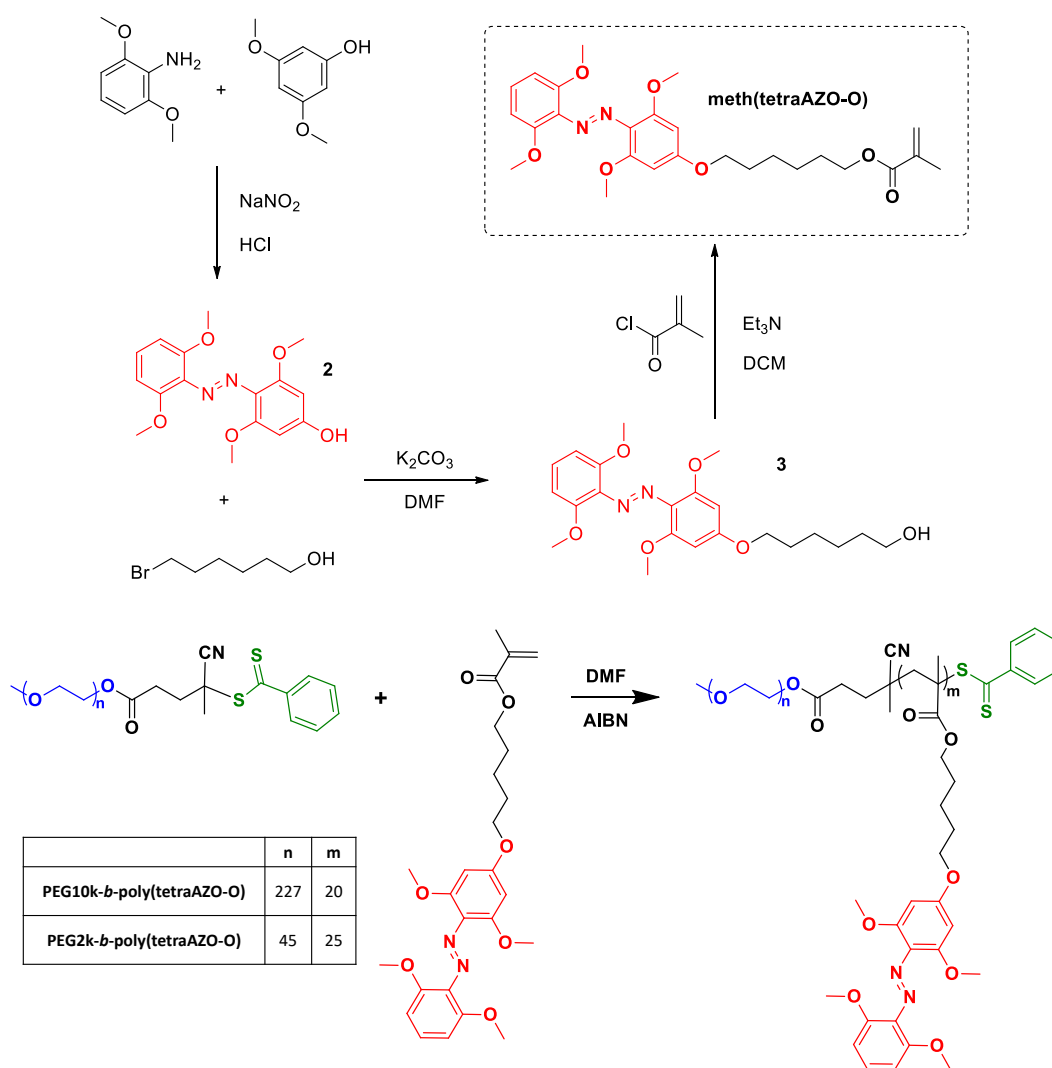


Figure 2.6. Synthesis and polymerisation of meth(tetraAZO-O)

Table 2.3. Molar masses of PEG10k-*b*-poly(tetraAZO-O) and PEG2k-*b*-poly(tetraAZO-O)

Polymer	m_{th}^a	m^b	$M_{n,NMR}^c$	$M_{n,SEC}$	\bar{D}
PEG10k- <i>b</i> -poly(tetraAZO-O)	30	20	19700	12015	1.07
PEG2k- <i>b</i> -poly(tetraAZO-O)	30	25	14100	10370	1.07

^a Theoretical degree of polymerisation calculated from the $[monomer]_0/[macro-CTA]_0$ assuming full monomer conversion

^b Experimental degree of polymerisation of the poly(tetraAZO-N) block estimated by ¹H NMR end group analysis

° Molar mass of BC as the sum of the molar mass of PEG and poly(tetraAZO-N) blocks calculated using m determined by $^1\text{H NMR}$ ($M_n = M_{\text{PEG}} + m \cdot M_{\text{monomer}}$). For PEG, commercial value was used

The average number molar masses ($M_{n,\text{SEC}}$) and dispersities (\mathcal{D}) of the BCs were characterised by SEC in THF, using poly(methyl methacrylate) (PMMA) standards for calibration and light scattering as detector. As an example, SEC curve registered for **PEG2k-*b*-poly(tetraAZO-O)** is compared to that of for **PEG2k-CTA** in **Figure 2.7**. Again, the molar mass distribution peaks shifted to lower elution times when compared to the **PEG-CTA** precursors, according to the increase on the average molar mass. Recorded \mathcal{D} values of 1.07 are in agreement with a polymerisation with living characteristics.

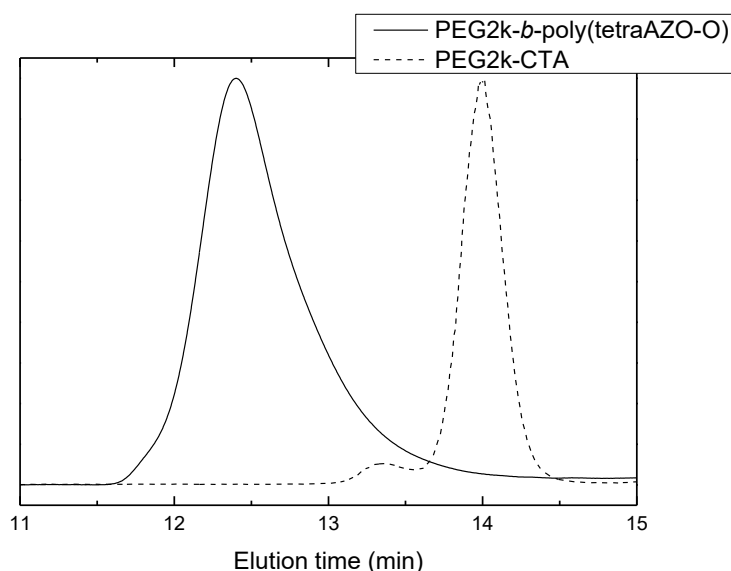


Figure 2.7. SEC curves of PEG2k-CTA and PEG2k-*b*-poly(tetraAZO-O)

Polymerisation degree (m) of the **poly(tetraAZO-O)** block was calculated by $^1\text{H NMR}$ end group analysis comparing the relative integration of resonances at 3.35 and 7.13 ppm (**Figure 2.8**). From these values, average number molar masses ($M_{n,\text{NMR}}$) were determined as the sum of the molar mass of PEG and **poly(tetraAZO-O)** blocks. When compared, $M_{n,\text{SEC}}$ values are slightly lower than $M_{n,\text{NMR}}$ but it must be taken into account that $M_{n,\text{SEC}}$ are values associated to the

hydrodynamic volume in solution and referred to PMMA standards used for calibrating the columns.

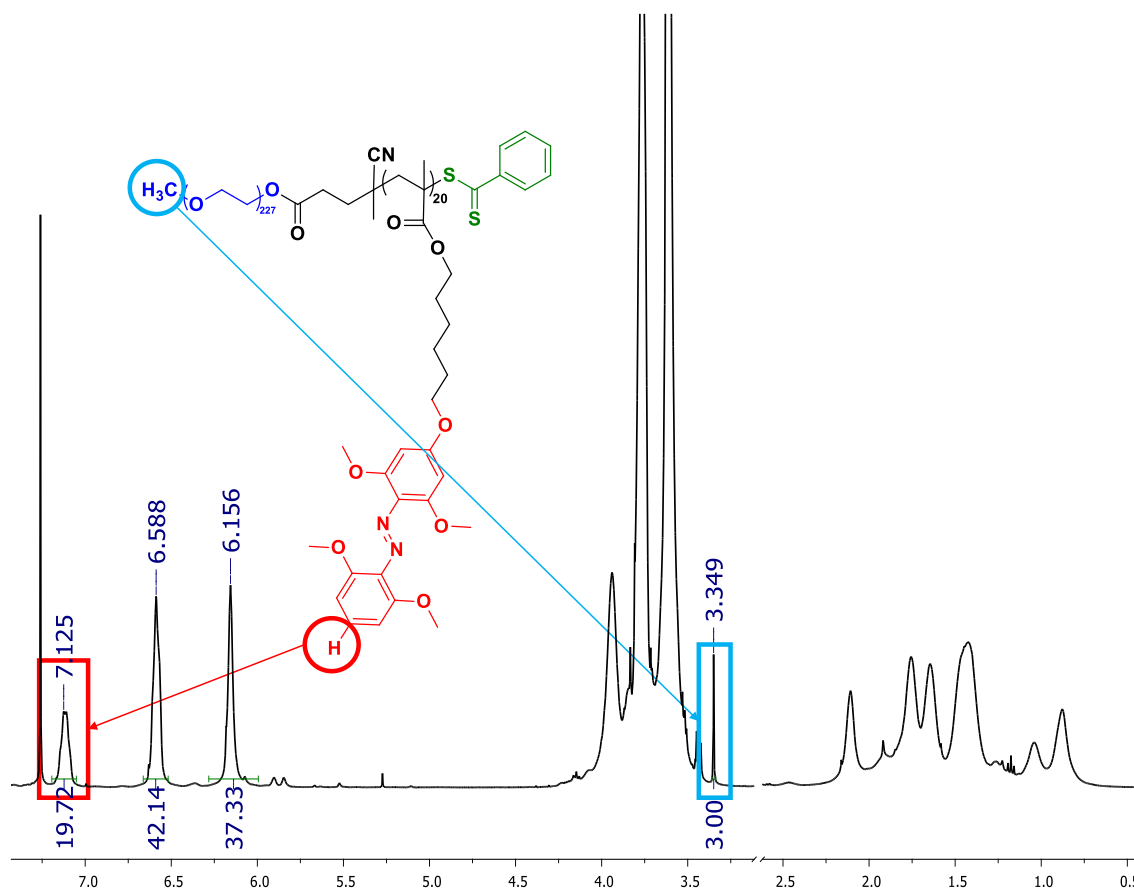


Figure 2.8. ^1H NMR spectrum in CDCl_3 of PEG10k-b-poly(tetraAZO-O)

Acceptable concordance between m and m_{th} values was observed in both polymers. This, together with the low D values, pointed to a good control over the polymerisation process. Nevertheless, **PEG10k-CTA** macroinitiator still yielded a smaller degree of polymerisation (m) as in the tetraAZO-N series.

Thermal characterisation of the polymers by TGA and DSC is summarised in **Table 2.4**. All polymers showed a good thermal stability up to 280 °C without traces of low molar mass volatiles. DSC curves registered for **PEG2k-b-poly(tetraAZO-N)** and **PEG2k-b-poly(tetraAZO-O)** were very similar to those of tetraAZO-N series BCs. **PEG2k-b-poly(tetraAZO-N)** was essentially amorphous with a $T_g = 54$ °C, while **PEG10k-b-poly(tetraAZO-O)** had a larger tendency to crystallise with $T_m =$

59 °C. Again, only a thermal transition was observed for both BC which might indicate that both blocks are at least, partially miscible in bulk.

Table 2.4. Thermal properties of the tetra(AZO-O) series

Polymer	TGA ^a	T _g ^b	T _m (ΔH _m) ^c
PEG10k-<i>b</i>-poly(tetraAZO-O)	296	---	59 (91)
PEG2k-<i>b</i>-poly(tetraAZO-O)	285	54	---

^a Decomposition temperature (in °C) associated to mass loss determined by TGA given at the onset of the weight loss curve

^b Glass transition temperature (in °C) determined by DSC on the first heating scan at 10 °C/min given at the half height of the baseline jump

^c Melting temperature (in °C) given at the maximum of the peak and associated melting enthalpy (in J/g), in brackets, determined by DSC on the first heating scan at 10 °C/min

Self-assembly ability of **PEG10k-*b*-poly(tetraAZO-O)** and **PEG2k-*b*-poly(tetraAZO-O)** was evaluated by the co-solvent method. Since BCs were not fully soluble in THF, self-assemblies were prepared starting from a solution of the polymer in THF/methanol (9/1) at a concentration of 5 mg/mL. The addition of 10% of methanol increased the solubility until reaching the required concentration, which was a clear improvement in comparison with BCs of series **tetraAZO-N**. In **Figure 2.9**, turbidity of the samples is represented when milli-Q water was slowly added to the solutions of the BCs. From the plots, it was observed that when a critical content of water was reached, turbidity increased indicating that the polymer started to self-assemble. Water was added until an almost constant value of turbidity was reached. At this point it was assumed that stable self-assemblies were formed. Samples were then dialysed against water to remove the organic solvents. The final aqueous dispersions were characterised by TEM and DLS.

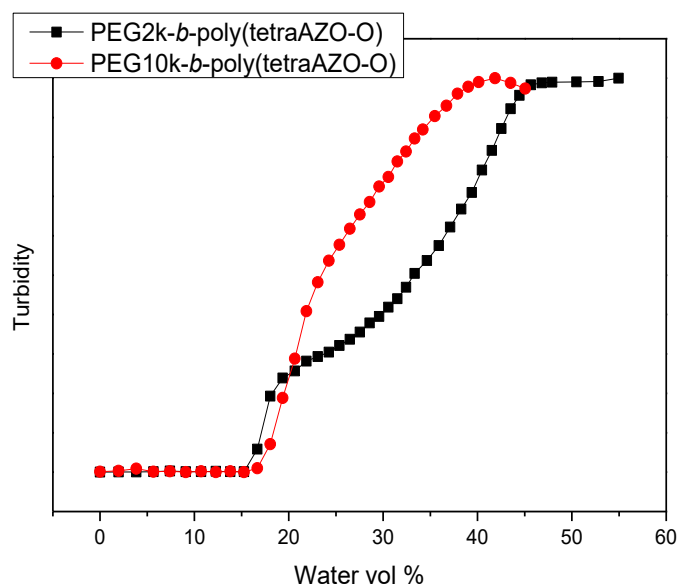


Figure 2.9. Turbidity curves for *PEG2k-b-poly(tetraAZO-O)* and *PEG10k-b-poly(tetraAZO-O)*

Inspection of **PEG10k-b-poly(tetraAZO-O)** self-assemblies, stained with uranyl acetate during 30 s, revealed well defined spherical micelles with uniform diameters along the TEM grid. Some representative images are shown in **Figure 2.10**. DLS experiments were done, obtaining a hydrodynamic diameter (D_h) of 33 ± 5 nm, showing a low dispersity (**Figure 2.10**).

In the TEM images of **PEG2k-b-poly(tetraAZO-O)** shown in **Figure 2.11**, vesicles were observed. Conventional TEM analysis was performed in dry state, for this reason, vesicles appeared as deflated or broken in some cases. Nevertheless, vesicles morphology was still appreciable. These vesicles were also studied by DLS and D_h of 902 ± 227 nm were determined (**Figure 2.11**). Differences in the self-assemblies morphology between **PEG2k-b-poly(tetraAZO-O)** and **PEG10k-b-poly(tetraAZO-O)** are consistent with differences in the hydrophilic/hydrophobic balance. For **PEG2k-b-poly(tetraAZO-O)** the hydrophilic/hydrophobic weight ratio is 14/86 while for **PEG10k-b-poly(tetraAZO-O)** is 51/49 and it is widely described that vesicles are more likely to be formed when the hydrophilic/hydrophobic ratio decreases.⁹

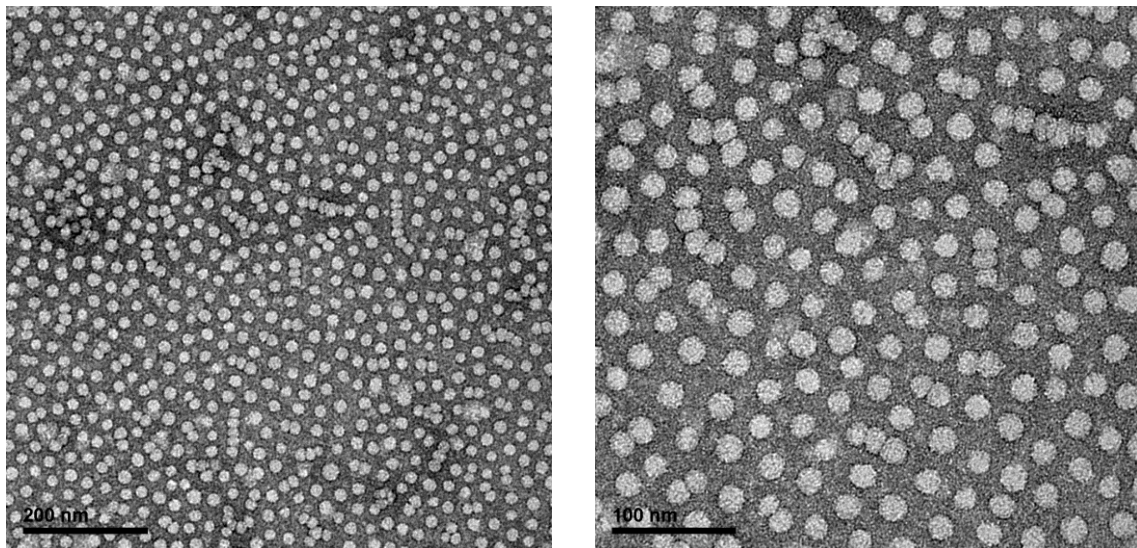
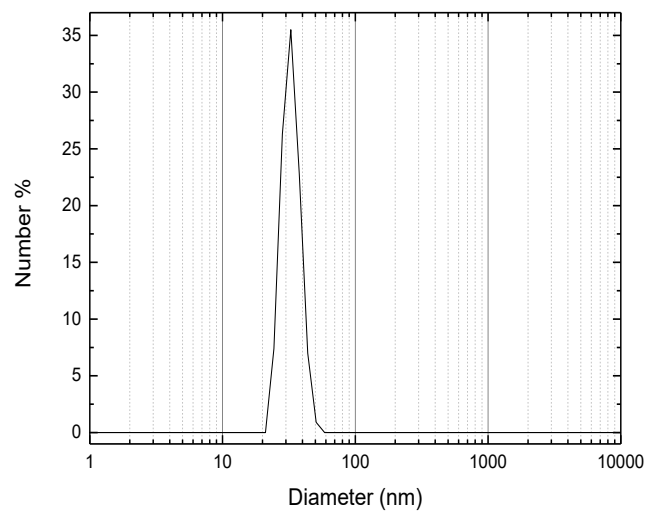


Figure 2.10. Representative TEM images and DLS of PEG10k-b-poly(tetraAZO-O) micelles in water dispersion

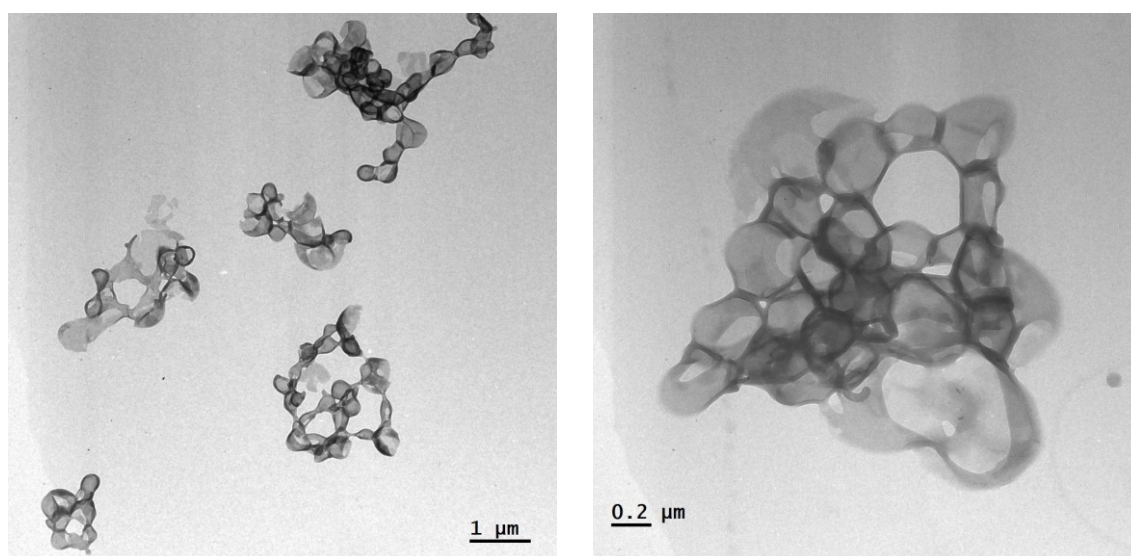
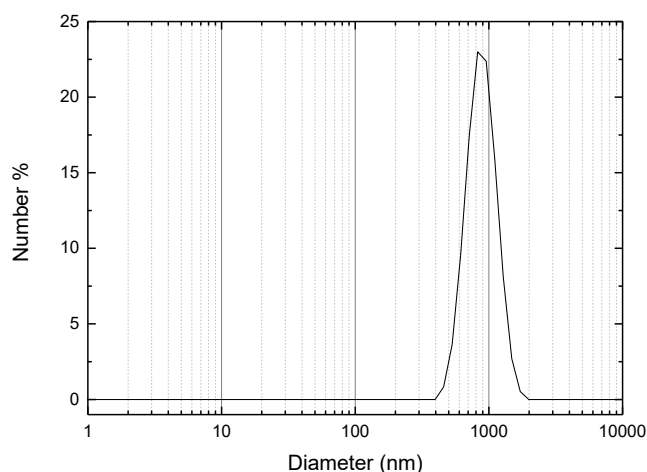


Figure 2.11. Representative TEM images and DLS of PEG2k-*b*-poly(tetraAZO-O) vesicles in water dispersion

Due to the interest of the micelles as nanocarriers of hydrophobic cargoes,¹⁰ **PEG10k-*b*-poly(tetraAZO-O)** self-assemblies were prepared by film hydration as an alternative method. Film hydration method allows to prepare polymeric self-assemblies in absence of organic solvent. For this purpose, a film was casted onto the bottom of a vial by evaporating a solution of **PEG10k-*b*-poly(tetraAZO-O)** in chloroform (5 mg/mL). The film was dried under vacuum before adding Milli-Q water until polymer concentration was 1 mg/mL. Vials were stirred with a magnetic bar for several weeks and aliquots were taken every few weeks to follow the self-assembly process by TEM. Evolution can be seen in the representative TEM images and DLS experiments represented in **Figure 2.12**.

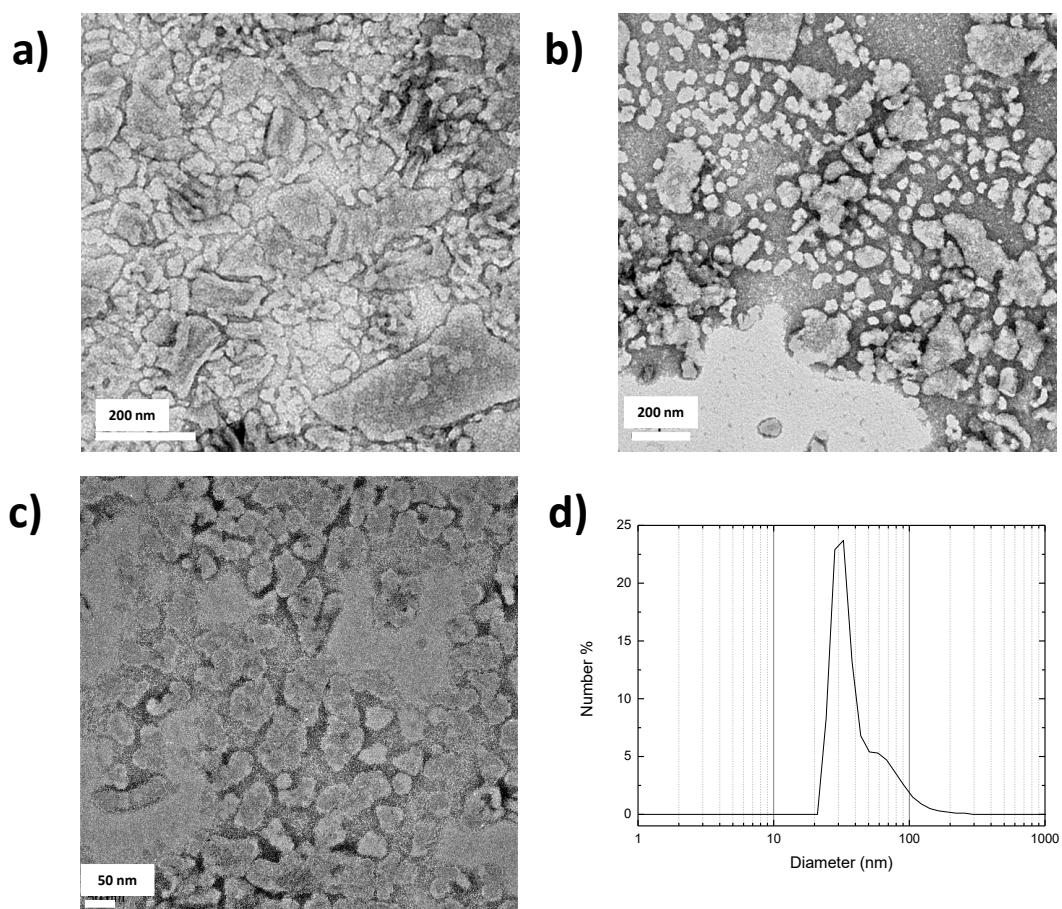


Figure 2.12. Representative TEM images of self-assemblies of PEG10k-b-poly(tetraAZO-O) prepared by film hydration taken after (a) 2 weeks, (b) 6 weeks and (c) 4 months and d) DLS distribution taken after 4 months

After 2 weeks, a milky solution was observed at the naked eye, however, micelles were not completely formed according to the TEM images. Some micelles were observed but most of the material was still amorphous.

After 6 weeks, an aliquot taken from the sample was centrifuged at 2000 rcf (relative centrifugal field) for 5 min to remove some amorphous material. The supernatant clear solution was analysed by TEM observing a large population of micelles. However, amorphous material was still appreciable.

After 4 months, a new aliquot was centrifuged again at 2000 rcf for 5 min. Despite the fact that almost no precipitate was observed after centrifugation, clear differences were not observed respect to the 6 weeks sample and amorphous

material was still present. Regarding DLS, a bimodal distribution was perceptible with a main population of micelles having D_h values around 30 nm.

In view of these results co-solvent method is a faster and more suitable way than film hydration to prepare homogenous micelles from **PEG10k-*b*-poly(tetraAZO-O)**.

CAC values are usually determined by fluorescence using a solvent sensitive fluorescent probe such as Nile Red. The method is based on the Nile Red solvatochromism, which is only fluorescent in hydrophobic environments. Unfortunately, in this case the overlap between excitation-emission wavelengths of Nile Red and the *ortho*-tetramethoxyazobenzene restricts the use of the technique. Nile Red emission is usually observed when exciting at 550 nm, but at this wavelength there is some overlapping with the $n-\pi^*$ absorption band of the *ortho*-tetramethoxyazobenzene chromophore. Therefore, CAC was determined by DLS, measuring the count rate or counts per seconds (cps), which is the number of photons scattered each second, at different concentrations of BC in water solution. When there are not nanoparticles in solution, count rate should be zero. When BC self-assembles light is dispersed and count rate increases as the concentration of nanoparticles increases (the more nanoparticles, the more photons are dispersed). Being that count rate is proportional to the number of nanoparticles fitting in an exponential function, these values are represented against concentration in a logarithmic scale and the onset determines the CAC value.¹¹ In **Figure 2.13, PEG10k-*b*-poly(tetraAZO-O)** graph is shown. CAC value was 26 $\mu\text{g/mL}$, which is in concordance with values reported for amphiphilic BCs.¹² Unfortunately, using this method, it was not possible to determine CAC for **PEG2k-*b*-poly(tetraAZO-O)** because a non-linear regression was obtained probably due to intermediate aggregates during the vesicles disassembly.

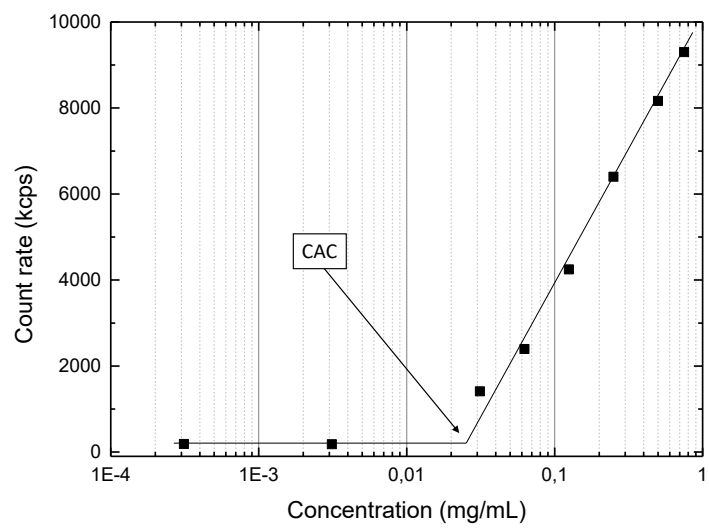


Figure 2.13. Count rate determined by DLS of the PEG10k-b-poly(tetraAZO-O) water solution vs. concentration (mg/mL)

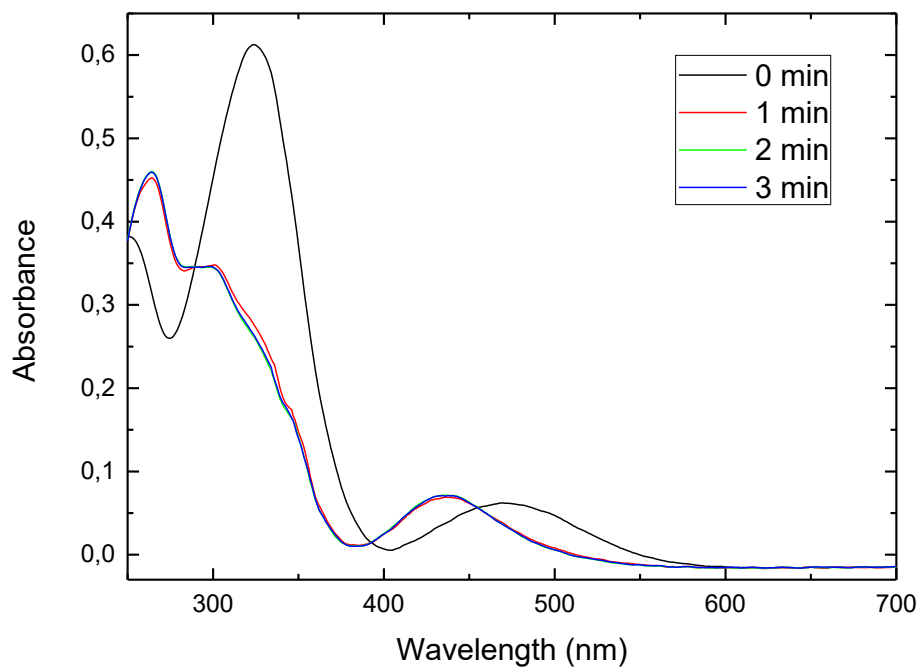
2.3. VISIBLE LIGHT RESPONSIVENESS

2.3.1. PHOTOISOMERISATION OF THE MONOMERS IN SOLUTION

Photoisomerisation of **meth(tetraAZO-N)** and **meth(tetraAZO-O)** monomers under 530 and 625 nm light in THF solutions was first investigated by UV-vis spectroscopy. Spectra are collected in **Figure 2.14** and **Figure 2.15**. Before irradiation, both monomers present identical features with two absorption bands at *ca.* 320 and 465 nm, being the **meth(tetraAZO-O)** bands slightly red-shifted, which corresponds with π - π^* and n - π^* bands of azobenzene, respectively. The n - π^* band of *trans* isomer in these tetramethoxyazobenzenes, when compared with conventionally used 4,4'-substituted azobenzenes, is red-shifted respect to n - π^* band of *cis* isomer due to the presence of methoxy groups in *ortho* positions respect to the azo bridge, that induce a non-planarity of the compound, allowing the *trans* to *cis* isomerisation using green and red light.¹³

Under light illumination a remarkable spectral modifications were registered concomitant to the *trans* to *cis* photoisomerisation. A notable decrease of the absorbance at *ca.* 320 nm was observed together with a hypsochromic shift of the n - π^* band. From the spectra, it was deduced that isomerisation was faster under irradiation at 530 nm since the absorbance of the *trans* azobenzene is much higher at this wavelength than at 625 nm. In fact, even if the absorbance at 625 nm is almost negligible, it is still enough to promote the photoisomerisation of the chromophore. Consequently, a photostationary state was reached at approx. 1-2 min at 530 nm but above 2 h at 625 nm. When comparing **meth(tetraAZO-N)** and **meth(tetraAZO-O)**, at 530 nm, isomerisation rates were similar. However, at 625 nm, **meth(tetraAZO-N)** isomerised slightly faster than **meth(tetraAZO-O)**. For **meth(tetraAZO-N)** a photostationary state was reached after 120 min of irradiation, while for **meth(tetraAZO-O)** above than 150 min.

a)



b)

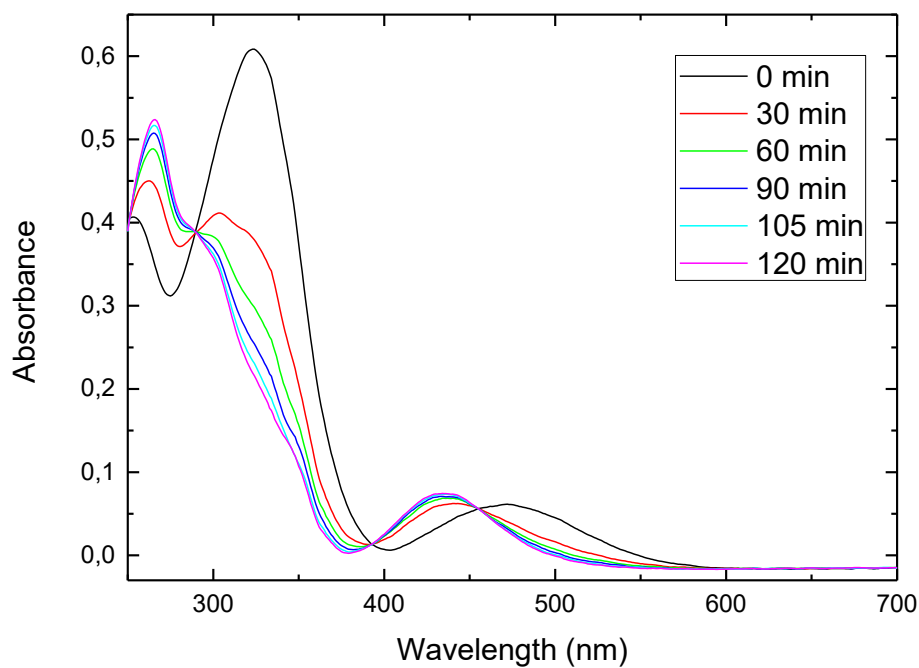
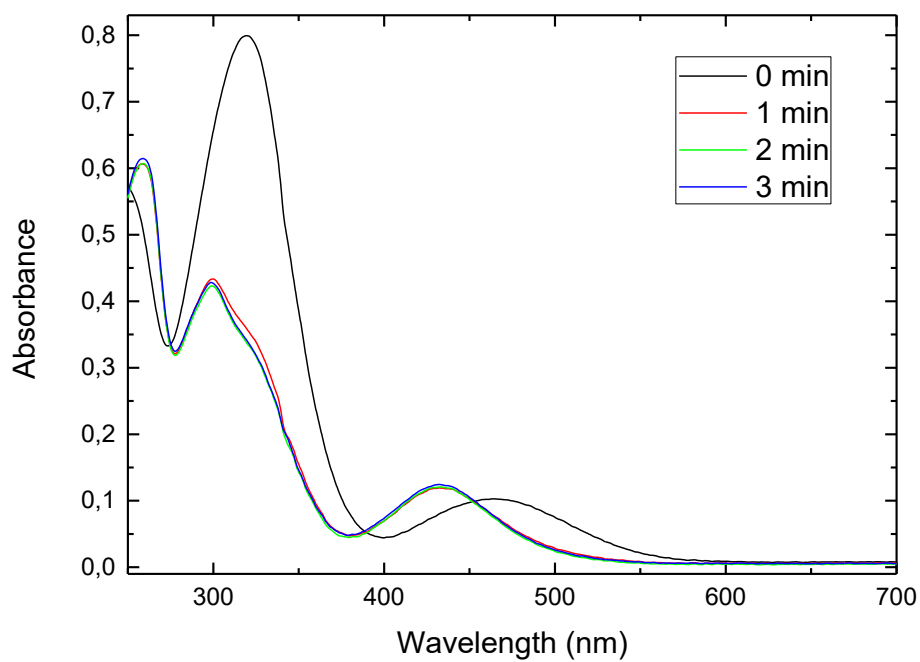


Figure 2.14. UV-Vis spectra of meth(tetraAZO-N) in THF (0.25 mg/mL) at different times of irradiation with a) 530 and b) 625 nm light

a)



b)

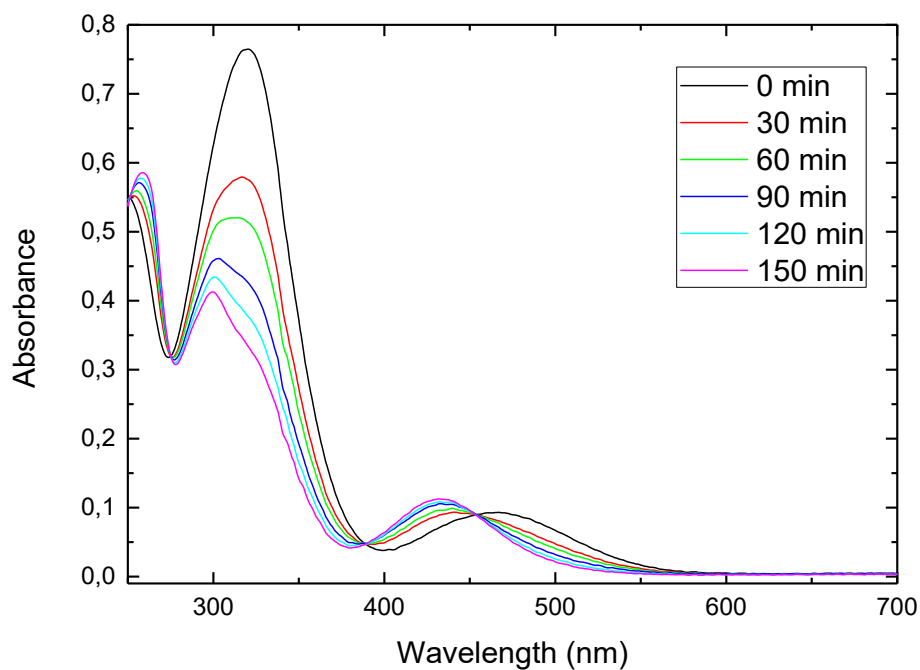


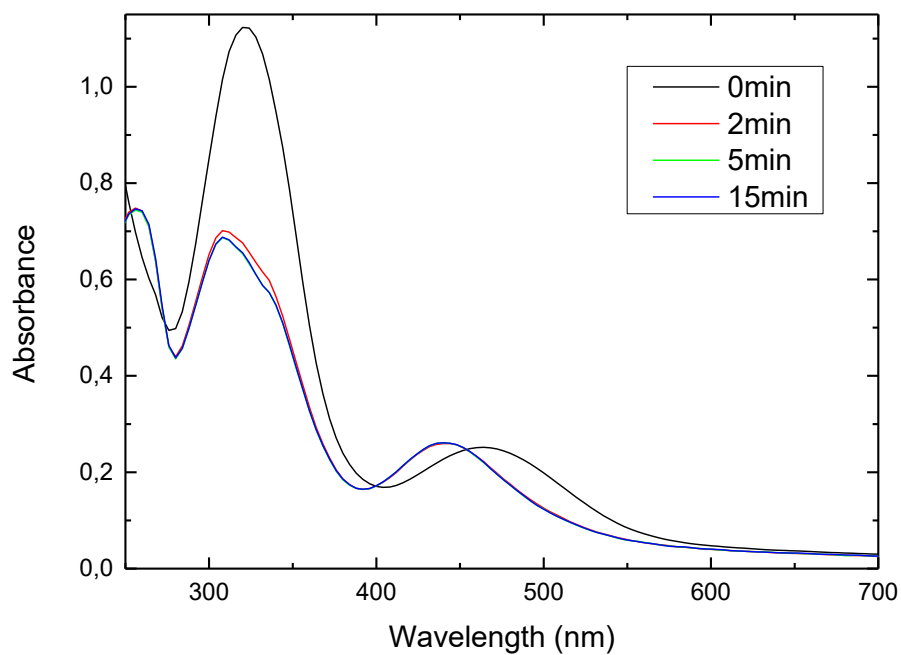
Figure 2.15. UV-Vis spectra of meth(tetraAZO-O) in THF (0.35 mg/mL) at different times of irradiation with a) 530 and b) 625 nm light

2.3.2. PHOTORESPONSE OF THE POLYMERIC SELF-ASSEMBLIES

Taking into account the studies described in the previous section, irradiation experiments were performed with the polymeric self-assemblies of **tetraAZO-O BCs series** in order to investigate their photoresponse under exposure to 530 and 625 nm light. Although photoisomerisation of the monomers in solution was faster when 530 nm light was used, 625 nm is still a wavelength of particular interest because it is less harmful for biological tissues and has a deeper penetration into them.

Before irradiation, UV-Vis spectrum of polymeric micelles of **PEG10k-b-poly(tetraAZO-O)** was similar to that of the monomer in THF solution, both $\pi-\pi^*$ band and $n-\pi^*$ band maxima were located at about the same wavelengths. The aqueous dispersions of the micelles were irradiated with light of 530 and 625 nm and spectra were registered at different times (**Figure 2.16**). After irradiation, a decrease in the $\pi-\pi^*$ band and a hypsochromic shift in $n-\pi^*$ band were observed with a photoinduced response faster when illuminating at 530 nm than at 625 nm. Despite the fact that azobenzene isomerised, no morphological changes were observed after irradiation at both wavelengths, 530 or 625 nm, and micelles maintained their morphology according to the TEM images of samples prepared from the irradiated solutions after the photostationary state was reached (**Figure 2.17**). Neither significant changes were observed from DLS experiments.

a)



b)

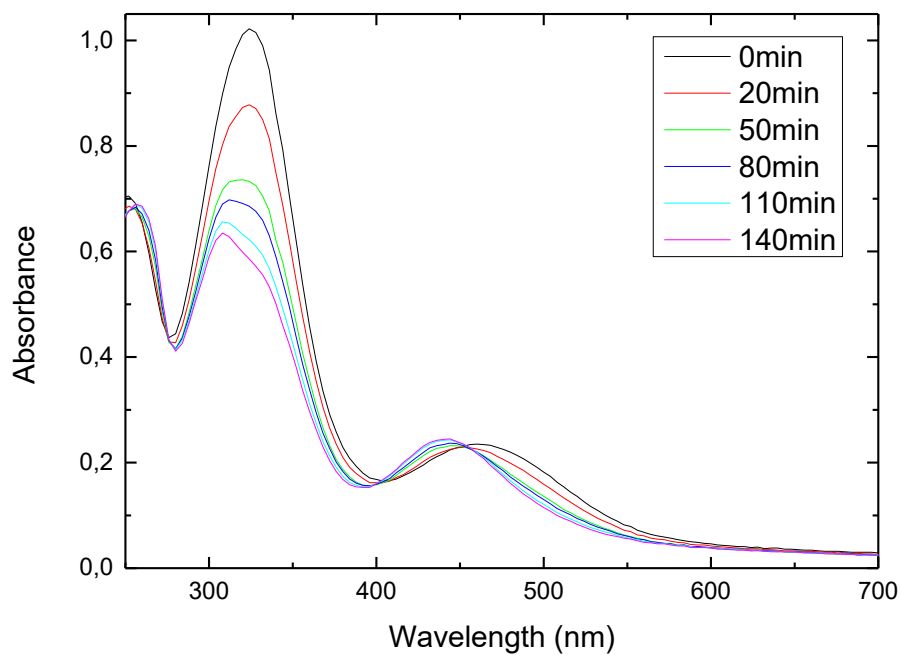


Figure 2.16. Spectra of PEG10k-b-poly(tetraAZO-O) micelles in water dispersion (1 mg/mL) at different times of irradiation with a) 530 and b) 625 nm light

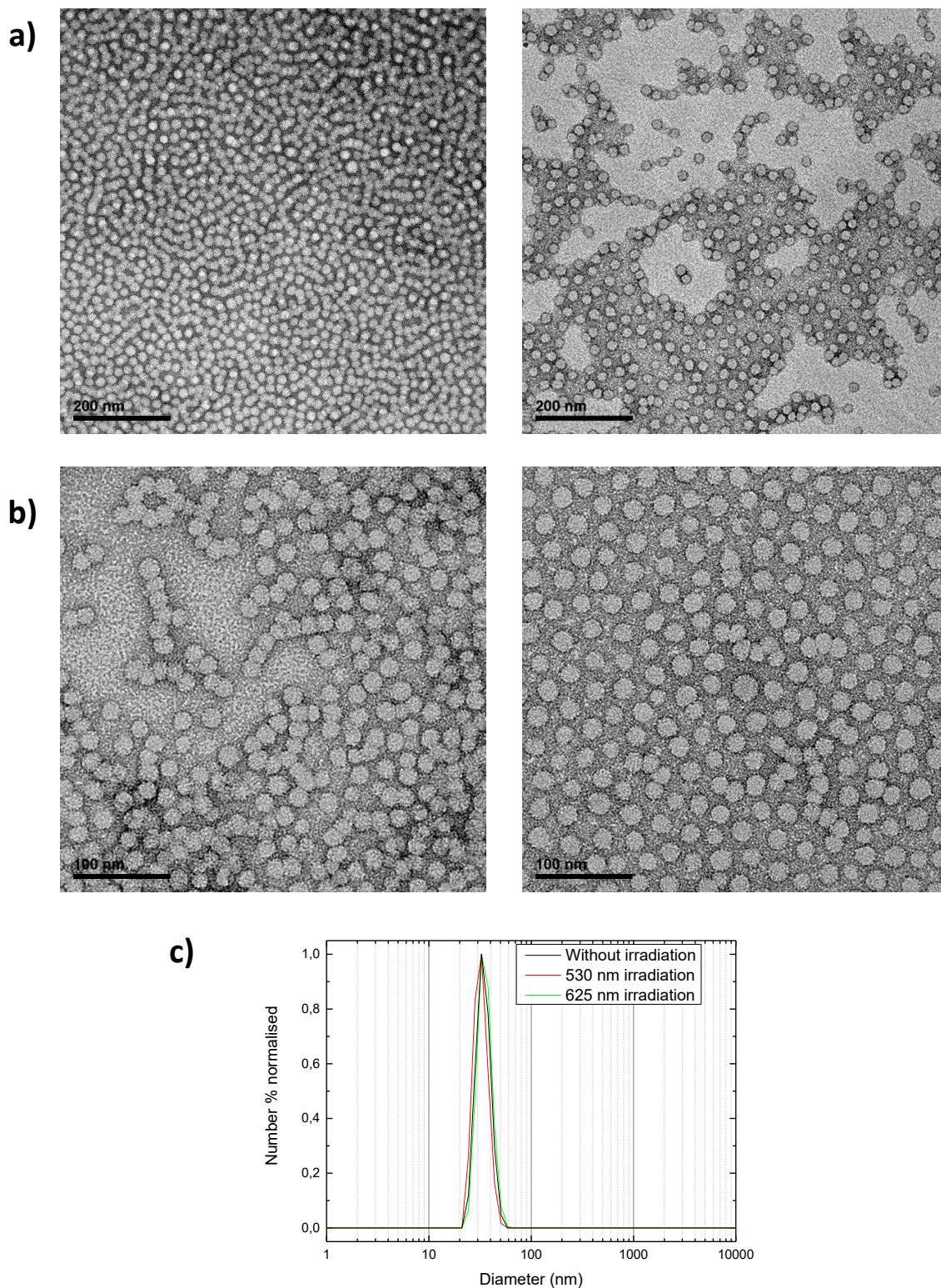


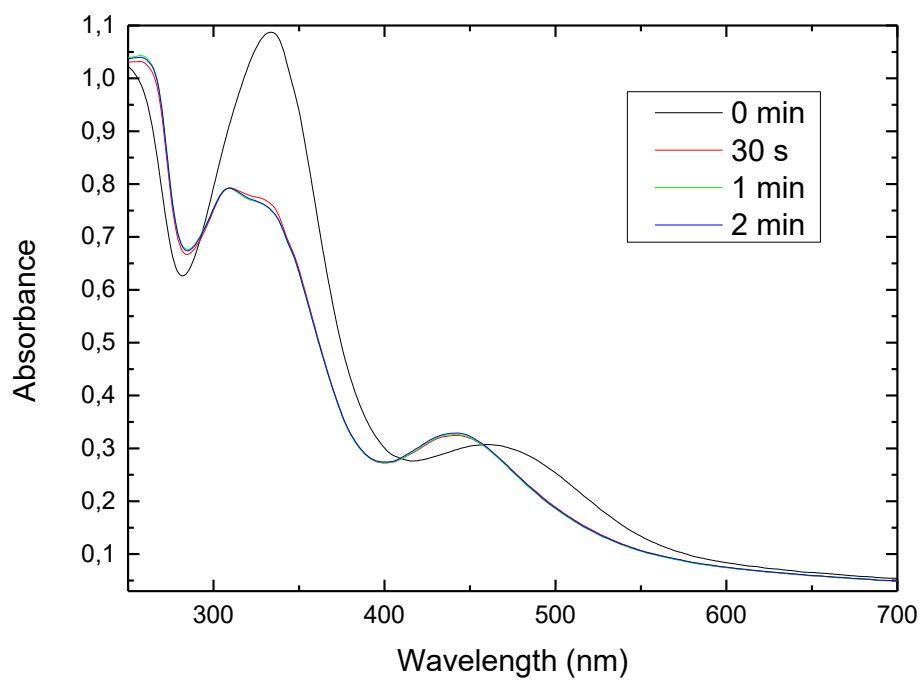
Figure 2.17. Representative TEM images of PEG10k-b-poly(tetraAZO-O) micelles in water dispersion a) after 530 nm irradiation, b) after 625 nm irradiation and c) DLS studies of PEG10k-b-poly(tetraAZO-O) micelles in water dispersion after 530 and 625 nm irradiation

Nile Red was attempted to be encapsulated into the hydrophobic core of the micelles but overlapping between the dye and the azobenzene absorption hindered to follow the photoinduced release of this probe

On the other hand, the UV-Vis spectrum of the aqueous dispersion of the **PEG2k-*b*-poly(tetraAZO-O)** polymeric vesicles presented some differences compared with that of micelles. The maximum of the $\pi-\pi^*$ band was red-shifted from 320 nm to 340 nm, probably due to the presence of *J*-aggregates, while $n-\pi^*$ band maximum remained at a similar position.

After irradiation with either 530 or 625 nm light, a decrease of the $\pi-\pi^*$ band intensity, as well as an evident hypsochromic shift in $n-\pi^*$ band were observed in both cases (**Figure 2.18**) due to the *trans* to *cis* isomerisation. After 530 nm irradiation a photostationary state was reached faster than after 625 nm irradiation, but with a less content in *trans* isomer since $\pi-\pi^*$ band relative decrease seemed to be minor (even after irradiation for 30 minutes) when compared to 625 nm irradiation, which was much slower but yielded more *trans* isomer according to UV-Vis spectra.

a)



b)

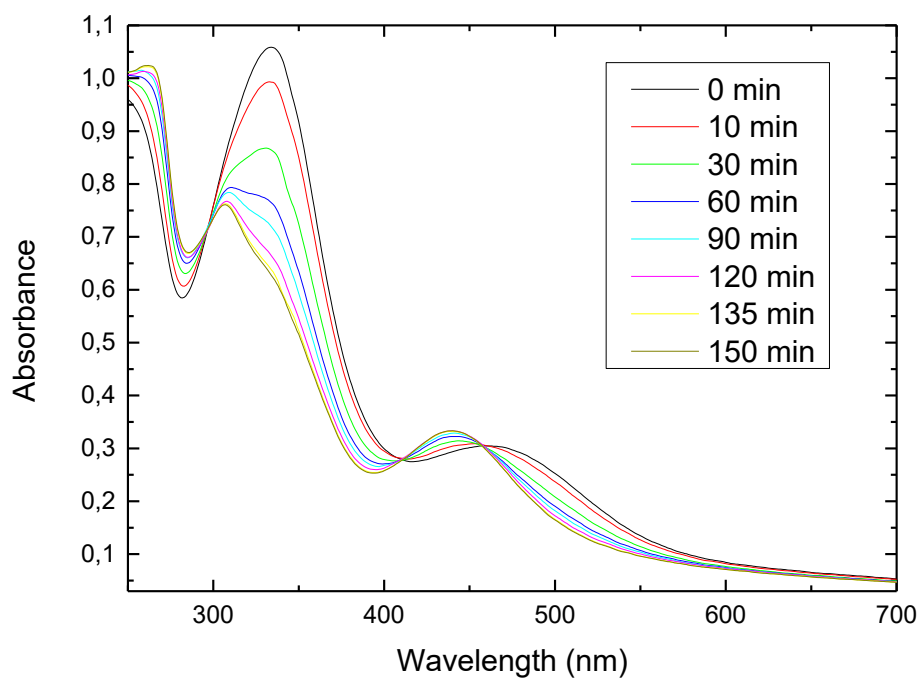


Figure 2.18. Spectra of PEG2k-b-poly(tetraAZO-O) vesicles in water dispersion (0.5 mg/mL) at different times of irradiation with a) 530 and b) 625 nm light

Once verified by UV-Vis spectroscopy the photoisomerisation of azobenzene moieties on the polymeric vesicles, it was checked if irradiation was able to produce any detectable change in their morphologies. For this purpose, samples were studied by TEM and DLS after irradiation, once the corresponding photostationary states were reached. In both cases, by TEM measurements, vesicles morphology was still appreciable although they seemed to be present in smaller number (**Figure 2.19**). Regarding DLS, shifts in size distributions from 902 ± 227 nm to 708 ± 275 nm and 692 ± 315 nm after 530 and 625 nm irradiations, respectively, were observed, which might be indicative of modifications that were not clearly observed in TEM images.

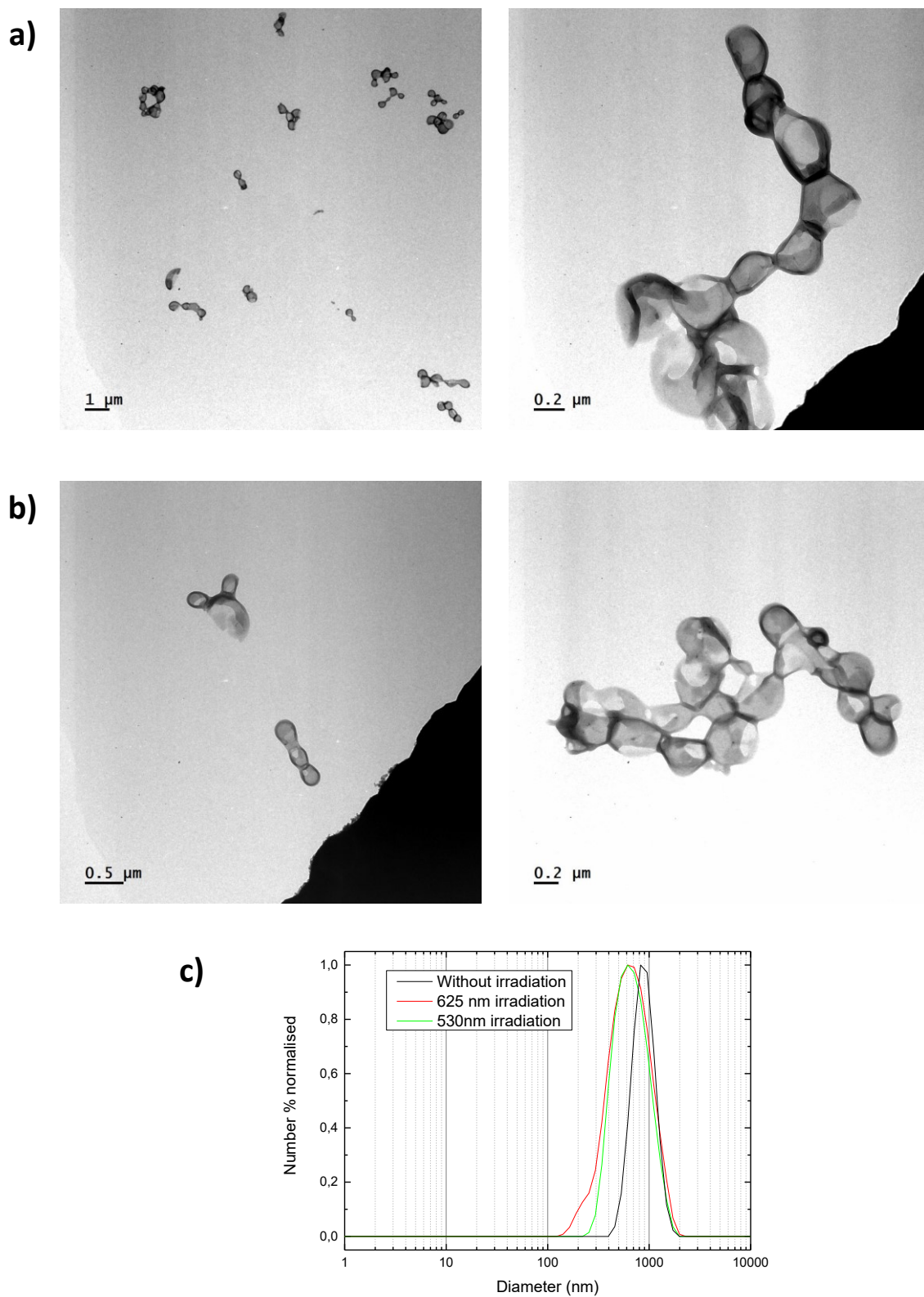


Figure 2.19. Representative TEM images of PEG2k-b-poly(tetraAZO-O) micelles in water dispersion a) after 530 nm irradiation, b) after 625 nm irradiation and c) DLS studies of PEG2k-b-poly(tetraAZO-O) micelles in water dispersion after 530 and 625 nm irradiation

Loading and photoinduced release of these self-assemblies were examined using Rhodamine B (RhB), which is a hydrophilic fluorescent molecule that exhibits emission at 575 nm upon excitation at 554 nm. For this purpose, polymeric vesicles were formed adding dropwise water to a solution of the polymer (5 mg/mL) and RhB (1 mg/mL) in THF and methanol (in proportion 9/1). Being hydrophilic, RhB should be entrapped at the internal aqueous cavity of the vesicles. Non encapsulated RhB was removed by dialysis against water until dialysis water was colourless (RhB solutions in water are intensely pink). RhB loaded vesicles were irradiated either at 530 nm for 10 min or at 625 nm for 1 h, respectively, inside a dialysis bag immerse in water. After 24 h the emission spectra of the dialysis water was registered and compared with that of a non-irradiated reference sample. A significant emission due to the presence of RhB was detected after irradiating at 530 nm when compared with the reference sample. The emission was certainly lower but still appreciable after irradiating at 625 nm (**Figure 2.20**). Therefore, despite the fact that morphological changes were not clearly observable in TEM, the release of the molecular probe was stimulated by light illumination.

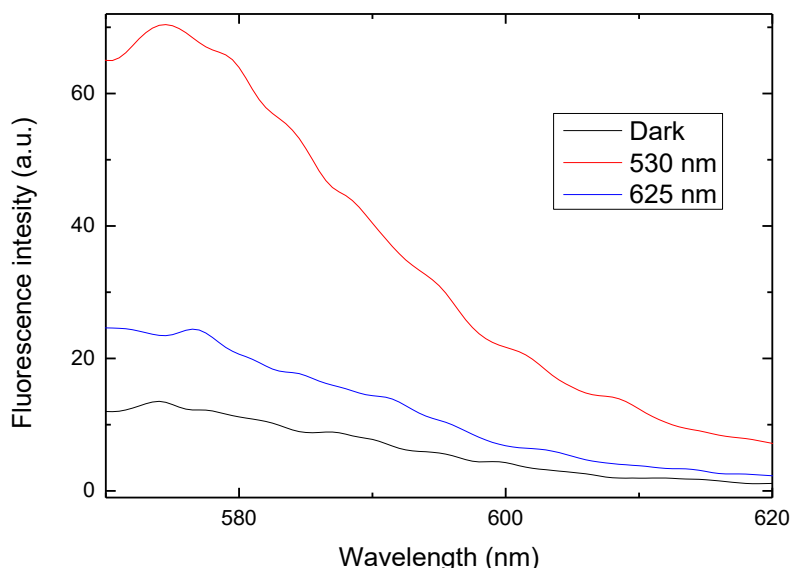


Figure 2.20. RhB fluorescence ($\lambda_{exc}=554$ nm) in water after irradiation and dialysis of RhB-loaded polymeric vesicles

2.4. CONCLUSIONS

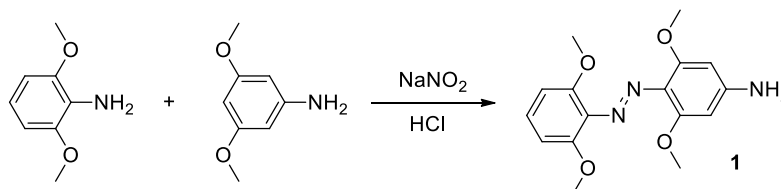
Summary of results and conclusions of this Chapter are the following:

- Novel amphiphilic block copolymers, having a hydrophobic block containing visible-light responsive azobenzene moieties, have been prepared by RAFT polymerisation of azobenzene methacrylates and PEG macro-CTAs.
- BCs tend to self-assemble in a selective solvent (water), although the formation of BC aggregates depends on the chemical structure of the azobenzene. BCs containing **meth(tetraAZO-O)** yielded stable polymeric micelles or vesicles, depending of the hydrophilic/hydrophobic ratio. However, incorporation of amide groups results on the eventual precipitation probably promoted by the H-bonding aggregation of chromophores.
- The photoresponse in solution and in micelle/vesicle water dispersions have been evaluated, and the photoisomerisation of the azobenzenes has been observed upon irradiation at 530 and 625 nm, being slower for 625 nm but still of interest for bioapplications.
- Although no morphological changes were observed for self-assembled structures, RhB light induced release experiments have been performed showing the potential of these systems for controlled cargo release using visible light.

2.5. EXPERIMENTAL SECTION

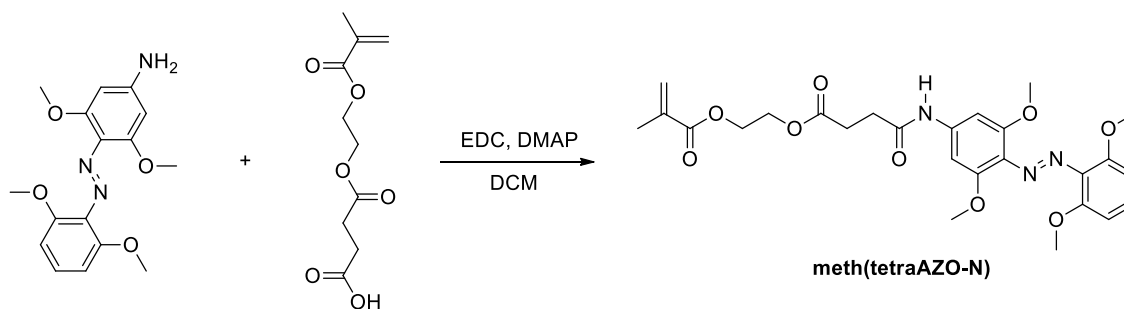
2.5.1. SYNTHESIS AND CHEMICAL CHARACTERISATION

Synthesis of 4-((2,6-dimethoxyphenyl)diazenyl)-3,5-dimethoxyaniline (1)



2,6-Dimethoxyaniline (459 mg, 3 mmol) was dissolved in 21% w/w HCl (1.3 mL) and the solution was cooled to 0 °C. NaNO₂ (207 mg, 3 mmol) in water (2.0 mL) was added dropwise and the reaction mixture was stirred for 20 min while keeping the temperature below 5 °C. Then, this solution was added dropwise over a suspension of 3,5-dimethoxyaniline (459 mg, 3 mmol) in water (20 mL) below 5 °C. Once the addition was completed, the pH was adjusted to 8 with saturated NaHCO₃ solution and the reaction was stirred overnight. The formed solid was isolated by filtration and further purified by silica flash chromatography using ethyl acetate/methanol (1/1) as eluent. The product was obtained as a red solid. Yield: 40 %. ¹H NMR (400 MHz, DMSO) δ 7.16 (t, *J* = 8.4 Hz, 1H), 6.72 (d, *J* = 8.4 Hz, 2H), 5.96 (s, 2H), 3.70 (s, 6H), 3.68 (s, 6H). ¹³C NMR (100 MHz, DMSO) δ 156.1, 153.4, 151.0, 126.6, 123.4, 105.3, 89.9, 55.9, 55.4.

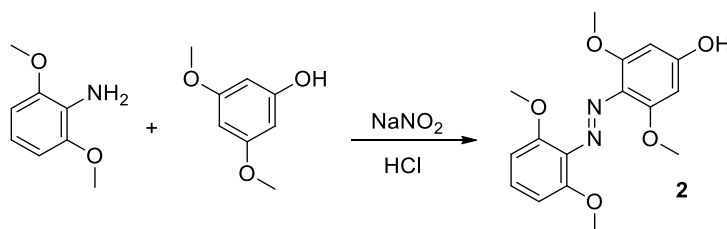
Synthesis of 2-(methacryloyloxy)ethyl 4-((4-((2,6-dimethoxyphenyl)diazenyl)-3,5-dimethoxyphenyl)amino)-4-oxobutanoate (meth(tetraAZO-N))



Compound 1 (800 mg, 2.52 mmol), mono-2-(methacryloyloxy)ethyl succinate (580 mg, 2.52 mmol) and DPTS (236 mg, 0.76 mmol) were dissolved in

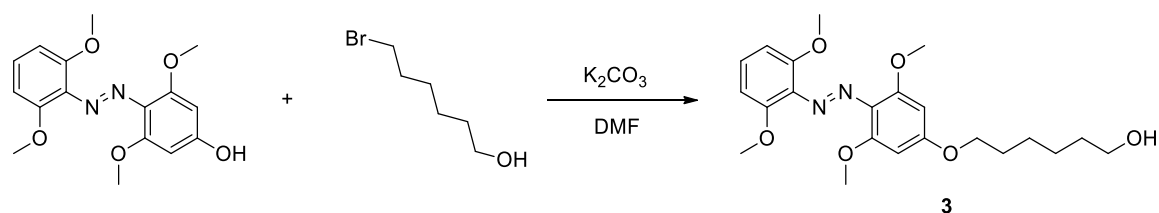
dichloromethane (30.0 mL) and the solution was cooled to 0 °C in an ice bath. Then, EDC (578 mg, 3.02 mmol) was added. The ice bath was removed after 30 min and the reaction was allowed to proceed at room temperature overnight. The reaction mixture was washed with water (50 mL) and brine (50 mL), and the organic phase was dried over MgSO₄, filtered and evaporated under reduced pressure. The crude was purified by silica flash chromatography using dichloromethane/ethyl acetate (3/2) as eluent. The product was further purified by recrystallisation in methanol, obtaining the product as a red solid. Yield: 73 %. IR (KBr), ν (cm⁻¹): 3276, 2941, 1742, 1711, 1699, 1599, 1546, 1475, 1454, 1406, 1256, 1157, 1129, 1109. ¹H NMR (400 MHz, CDCl₃) δ 8.65 (s, 1H), 7.20 (t, *J* = 8.4 Hz, 1H), 6.95 (s, 2H), 6.64 (d, *J* = 8.5 Hz, 2H), 6.12 (dq, *J* = 1.4, 1.0 Hz, 1H), 5.57 (dq, *J* = 1.6, 0.9 Hz, 1H), 4.33 (s, 4H), 3.77 (s, 6H), 3.66 (s, 6H), 2.61 (t, *J* = 6.6 Hz, 2H), 2.46 (t, *J* = 6.7 Hz, 2H), 1.93 (dd, *J* = 1.5, 1.0 Hz, 3H). ¹³C NMR (101 MHz, CDCl₃) δ 172.68, 170.45, 167.32, 153.79, 152.35, 136.00, 134.03, 129.31, 126.31, 105.22, 96.14, 62.53, 62.46, 56.52, 56.32, 31.56, 29.06, 18.38.

Synthesis of 4-((2,6-dimethoxyphenyl)diazenyl)-3,5-dimethoxyphenol (**2**)



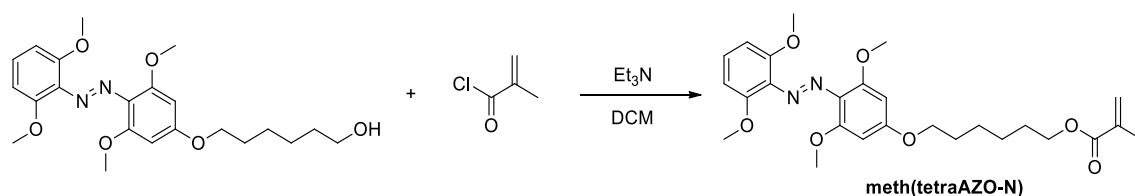
2,6-Dimethoxyaniline (300 mg, 1.96 mmol) was placed in a round-bottomed flask, dissolved in 10% w/w HCl (0.8 mL) and cooled below 5 °C. Then, NaNO₂ (138 mg, 1.96 mmol) was dissolved in water (2 mL) and added dropwise into the flask at 0 °C. After 10 min, a solution of 3,5-dimethoxyphenol (300 mg, 1.96 mmol) dissolved together in 0.75% w/w NaOH (20 mL) was added dropwise below 5 °C. The reaction was stirred during 3 days at room temperature and then acidified to pH = 6. The solid was obtained by filtration and purified by silica flash chromatography, eluting with dichloromethane/methanol (9.5/0.5), yielding a red solid. Yield: 50%. ¹H NMR (400 MHz, CD₃OD, δ): 7.36 (t, *J* = 8.4 Hz, 1H), 6.86 (d, *J* = 8.5 Hz, 2H), 6.13 (s, 2H), 4.04 (s, 6H), 3.96 (s, 6H).

Synthesis of 6-(4-((2,6-dimethoxyphenyl)diazenyl)-3,5-dimethoxyphenoxy)hexan-1-ol (**3**)



Compound **2** (900 mg, 2.83 mmol), K_2CO_3 (2 g, 14.5 mmol) and 6-bromohexan-1-ol (700 mg, 3.8 mmol) were suspended in dry DMF (30 mL). The reaction was allowed to stir at $80^\circ C$ during 12 h and then diluted with dichloromethane (150 mL). Organic solvent was washed with water (200 mL), brine (200 mL) and dried with $MgSO_4$. Dichloromethane was filtered and evaporated under reduced pressure. The residue was purified using silica flash chromatography eluting with dichloromethane/ethyl acetate (8/2) obtaining a red solid. Yield: 60%. 1H NMR (300 MHz, $CDCl_3$) δ 7.17 (t, $J = 8.4$ Hz, 1H), 6.64 (d, $J = 8.4$ Hz, 2H), 6.21 (s, 2H), 4.02 (t, $J = 6.5$ Hz, 2H), 3.86 (s, 6H), 3.83 (s, 6H), 3.65 (t, $J = 6.4$ Hz, 2H), 1.87 – 1.76 (m, 2H), 1.67 – 1.39 (m, 6H).

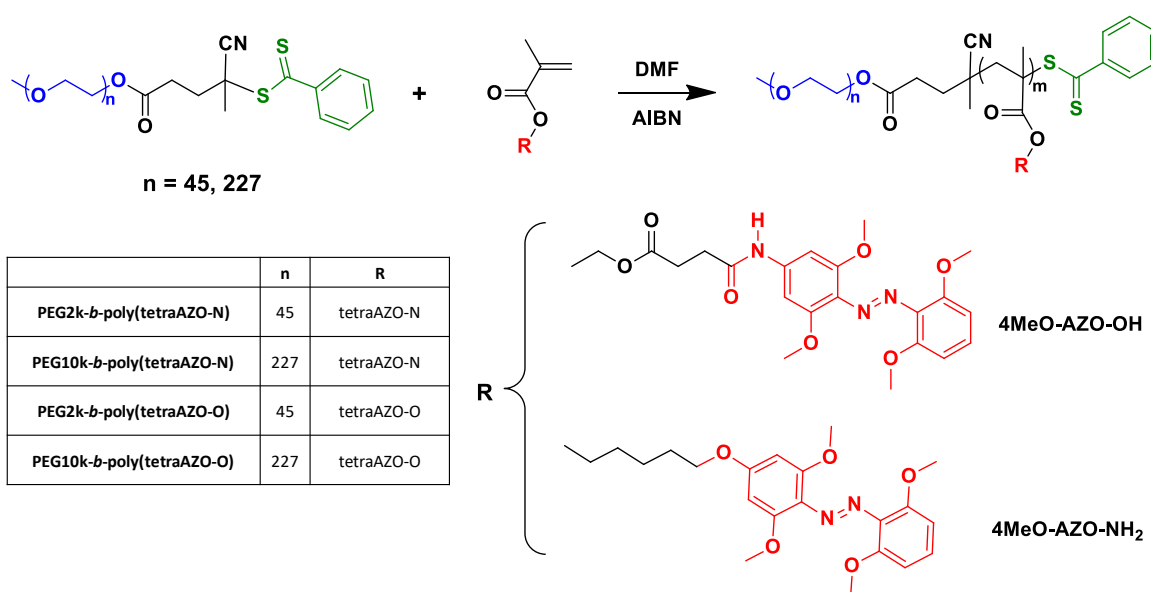
Synthesis of 6-(4-((2,6-dimethoxyphenyl)diazenyl)-3,5-dimethoxyphenoxy)hexyl methacrylate (meth(tetraAZO-N))



Compound **3** (500 mg, 1.2 mmol) and trimethylamine (181 mg, 1.8 mmol) were dissolved in dichloromethane (30 mL) and the flask was placed into an ice bath. Then, methacryloyl chloride (186 mg, 1.5 mmol) in dichloromethane (5 mL) was added dropwise under inert atmosphere. The reaction was allowed to proceed for 12 h. Then, organic phase was washed with NH_4Cl 10% and brine, and dried over $MgSO_4$ and the solvent evaporated. The residue was purified using silica flash chromatography, eluting with dichloromethane/acetone (9/1) to obtain a red solid. Yield: 70%. IR (KBr), ν (cm^{-1}): 2946, 1707, 1586, 1476, 1331, 1303, 1254, 1111,

771, 506. ^1H NMR (400 MHz, CDCl_3) δ 7.17 (t, $J = 8.4$ Hz, 1H), 6.64 (d, $J = 8.4$ Hz, 2H), 6.21 (s, 2H), 6.09 (dq, $J = 1.6, 0.9$ Hz, 1H), 5.54 (dq, $J = 1.6, 0.9$ Hz, 1H), 4.16 (t, $J = 6.6$ Hz, 2H), 4.01 (t, $J = 6.4$ Hz, 2H), 3.86 (s, 6H), 3.83 (s, 6H), 1.95 – 1.92 (m, 3H), 1.86 – 1.77 (m, 2H), 1.77 – 1.68 (m, 2H), 1.59 – 1.43 (m, 4H). ^{13}C NMR (101 MHz, CDCl_3) δ 167.60, 161.55, 154.83, 152.42, 136.56, 134.55, 128.72, 128.65, 125.31, 105.36, 92.15, 68.18, 64.67, 56.72, 56.66, 29.19, 28.62, 25.88, 25.81, 18.40.

General procedure for RAFT polymerisation



Monomer, macro-CTA agent and AIBN (see the table below for further details) were dissolved in freshly distilled DMF (1 mL/100 mg of reagents) in a Schlenk flask under inert atmosphere. The flask was degassed via three freeze-pump-thaw cycles and the polymerisation was allowed to stir at 70°C for 24 h. The crude was precipitated into cold diethyl ether (100 mL/mL of DMF) and the solid was isolated by filtration obtaining a red solid that was further purified using preparative size exclusion chromatography (SEC) in dichloromethane with Biobeads® SX-1 to remove the residual monomer. Then, pure fractions were evaporated under reduced pressure and precipitated into cold diethyl ether. Finally, the solid was filtered to obtain the polymer as a red powder.

Polymer	Macro-CTA mass (mmol)	Monomer mass (mmol)	AIBN mass (mmol)
PEG2k-<i>b</i>-poly(tetraAZO-N)	38 mg (0.0189) ¹	200 mg (0.378)	0.3 mg (0.00189)
PEG10k-<i>b</i>-poly(tetraAZO-N)	100 mg (0.01) ²	211 mg (0.4)	0.16 mg (0.001)
PEG2k-<i>b</i>-poly(tetraAZO-O)	27 mg (0.0137) ¹	200 mg (0.41)	0.74 mg (0.00137)
PEG10k-<i>b</i>-poly(tetraAZO-O)	137 mg (0.013) ²	200 mg (0.41)	0.74 mg (0.00137)

¹ PEG of 2000 g/mol

² PEG of 10000 g/mol

*Characterisation data for PEG2k-**b**-poly(tetraAZO-N):* IR (KBr), ν (cm⁻¹): 2935, 1736, 1695, 1598, 1540, 1475, 1407, 1256, 1127, 1109. ¹H NMR (400 MHz, CDCl₃) δ 9.48, 7.16, 7.07, 6.59, 4.27, 4.14, 3.62, 3.36, 2.60, 1.04, 0.87.

*Characterisation data for PEG10k-**b**-poly(tetraAZO-N):* IR (KBr), ν (cm⁻¹): 2889, 1735, 1695, 1599, 1467, 1342, 1280, 1242, 1108, 962, 842. ¹H NMR (400 MHz, DMSO-d⁶) δ 10.13, 7.19, 7.08, 6.69, 4.26, 4.13, 3.51, 3.24, 2.63, 1.06, 0.88.

*Characterisation data for PEG2k-**b**-poly(tetraAZO-O):* IR (KBr), ν (cm⁻¹): 2937, 1726, 1597, 1474, 1336, 1255, 1109. ¹H NMR (400 MHz, CDCl₃) δ 7.14, 6.62, 6.21, 3.96, 3.82, 3.64, 3.38 (s, 3H), 1.78, 1.67, 1.47, 1.44, 1.06, 0.89.

*Characterisation data for PEG10k-**b**-poly(tetraAZO-O):* IR (KBr), ν (cm⁻¹): 2886, 1727, 1598, 1474, 1342, 1256, 1109, 962, 841. ¹H NMR (400 MHz, CDCl₃) δ 7.13, 6.61, 6.17, 3.94, 3.78, 3.61, 3.35 (s, 3H), 1.76, 1.65, 1.47, 1.42, 1.04, 0.87.

2.5.2. PREPARATION AND CHARACTERISATION OF POLYMERIC AGGREGATES

Preparation of polymeric aggregates *via* co-solvent method

The corresponding BC (5 mg) was dissolved in the selected solvent (1 mL) (either THF, THF/methanol 9:1, DMSO or DMF) and then, Milli-Q water was added dropwise (10 μ L per drop) while turbidity changes were monitored by UV-Vis spectroscopy measuring the absorbance of the solution at 650 nm (light scattering due to polymeric aggregation gives rise to an apparent increase of absorbance). Once turbidity reached an almost constant value, the mixture was dialysed against water using a Spectra/Por® membrane (MWCO = 1000 g/mol) during 3 days. The dispersion was diluted with Milli-Q water to obtain a 1 mg/mL concentration of polymeric aggregates.

Preparation of polymeric aggregates *via* film rehydration method

5 mg of BC was dissolved in a vial with chloroform (5 mL) and the solvent was allowed to evaporate at room temperature. The resulting film deposited at the bottom of the vial was deeply dried under vacuum overnight. Then, Milli-Q water (5 mL) was added, the vial closed and the mixture was stirred during several weeks. Samples were purified *via* centrifugation at 2000 rcf (relative centrifugal field) for 5 min in an Eppendorf tube.

Preparation of TEM samples

10 μ L of a 1 mg/mL polymeric aggregates dispersion were deposited onto a TEM grid. After 30 s, the drop was removed with filter paper by capillarity. A 10 μ L of a uranyl acetate solution was applied following the same procedure and removed in the same way. Finally, the TEM grid was dried using a micropipette tip joined to a vacuum pump.

Determination of CAC using DLS

DLS measurements of nanoparticles in water solution were performed at different concentrations (from 0.0001 to 1 mg/mL). Attenuator was set in such a way that count rate at 0.1 mg/mL was around 2000-4000 kcps and kept in that configuration for all the experiments as well as the laser beam was positioned in a fixed position, in order to assure the same conditions in every measurement. Then, count rate was represented against concentration in logarithmic scale. The onset corresponded to the CAC value.

Irradiation experiments

The solution to be irradiated was introduced in UV cuvettes and placed at a distance of 10 cm from a LED light source of a proper wavelength depending on the experiment. UV-Vis spectra were registered at different times of irradiation.

2.5.3. ENCAPSULATION AND RELEASE STUDIES

Encapsulation of Rhodamine B

Rhodamine B (1 mg) and the desired polymer (5 mg) were dissolved in THF/methanol (0.9 + 0.1 mL) (Note: a drop of water may be necessary to dissolve completely the mixture). Then, Milli-Q water was added dropwise while turbidity was registered in the same way than **Section 2.5.2**. Once turbidity reached a plateau, the sample was dialysed against water several times until dialysis water had no colour at all.

Release of Rhodamine B under light illumination

An aliquot (1 mL) of RhB loaded vesicles (1 mg/mL) was sealed into a dialysis bag (MWCO = 1000 g/mol) and immerse inside a vial with water (20 mL). The sample was irradiated at 530 nm for 10 min or at 625 nm for 1 h and stand in the dark for 24 h. After taking out the dialysis bag, emission of the vial water content was registered.

2.6. REFERENCES

1. Wang, D., Wagner, M., Butt, H.-J. & Wu, S. Supramolecular hydrogels constructed by red-light-responsive host–guest interactions for photo-controlled protein release in deep tissue. *Soft Matter* **11**, 7656–7662 (2015).
2. Weis, P., Wang, D. & Wu, S. Visible-Light-Responsive Azopolymers with Inhibited π – π Stacking Enable Fully Reversible Photopatterning. *Macromolecules* **49**, 6368–6373 (2016).
3. Moad, G., Chong, Y. K., Postma, A., Rizzardo, E. & Thang, S. H. Advances in RAFT polymerization: the synthesis of polymers with defined end-groups. *Polymer* **46**, 8458–8468 (2005).
4. Blasco, E., Piñol, M. & Oriol, L. Responsive Linear-Dendritic Block Copolymers. *Macromol. Rapid Commun.* **35**, 1090–1115 (2014).
5. Blasco, E., Barrio, J. del, Sánchez-Somolinos, C., Piñol, M. & Oriol, L. Light induced molecular release from vesicles based on amphiphilic linear-dendritic block copolymers. *Polym. Chem.* **4**, 2246 (2013).
6. Concellón, A. *et al.* Light-Responsive Self-Assembled Materials by Supramolecular Post-Functionalization via Hydrogen Bonding of Amphiphilic Block Copolymers. *Macromolecules* **49**, 7825–7836 (2016).
7. García-Juan, H. *et al.* Self-assembly of thermo and light responsive amphiphilic linear dendritic block copolymers. *Eur. Polym. J.* **81**, 621–633 (2016).
8. Concellón, A. *et al.* Polymeric micelles from block copolymers containing 2,6-diacylaminopyridine units for encapsulation of hydrophobic drugs. *RSC Adv* **6**, 24066–24075 (2016).
9. Smart, T. *et al.* Block copolymer nanostructures. *Nano Today* **3**, 38–46 (2008).

10. Soukasene, S. *et al.* Antitumor Activity of Peptide Amphiphile Nanofiber-Encapsulated Camptothecin. *ACS Nano* **5**, 9113–9121 (2011).
11. Pearson, S. *et al.* Light-responsive azobenzene-based glycopolymer micelles for targeted drug delivery to melanoma cells. *Eur. Polym. J.* **69**, 616–627 (2015).
12. Mynar, J. L. *et al.* Two-photon degradable supramolecular assemblies of linear-dendritic copolymers. *Chem. Commun.* 2081 (2007). doi:10.1039/b701681f
13. Beharry, A. A., Sadovski, O. & Woolley, G. A. Azobenzene Photoswitching without Ultraviolet Light. *J. Am. Chem. Soc.* **133**, 19684–19687 (2011).

**CHAPTER 3: AMPHIPHILIC
BCs BASED ON 4-
DIALKYLAMINOAZOBENZENE
DERIVATIVES**

3.1. INTRODUCTION AND AIMS

In this Chapter, two systems are studied to obtain BCs with visible light response and a potential NIR response. The first one (**Figure 3.1a**) is a bichromophoric system (coded as **AZO-Naph**) based on the described by Gorostiza and co-workers where the azobenzene, with dialkylamino and aminocarbonyl groups, and the naphthalene moieties are bound together.¹ The *trans* to *cis* isomerisation can be achieved by direct excitation of the *trans* azobenzene upon blue light (473 nm) illumination but also under one photon (365 nm) or two photon excitation (740 nm) of the naphthalene moiety.

The second system, **AZO-NO₂/Naph**, (**Figure 3.1b**) combines a derivative of a well-known azobenzene chromophore combining a dialkylamino and a nitro group (Disperse Red 1) coded as **AZO-NO₂** with a naphthalene sensitiser (**Naph**). In this case, both functional moieties are independently incorporated into the polymeric structure. Again, **Naph** (when excited at 365 nm, or 730 nm for two photon) might be used to stimulate the photoisomerisation of the azobenzene whose absorbance is minimal at naphthalene band. This system is synthetically more accessible than **AZO-Naph**.

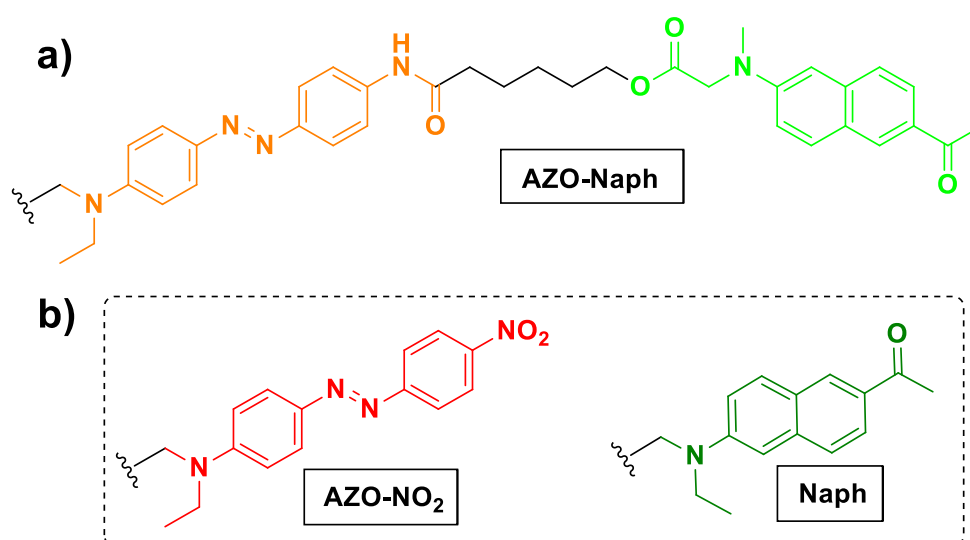


Figure 3.1. a) Bichromophoric azobenzene-naphthalene system and b) AZO-NO₂ based and Naph moieties units to be incorporated to the polymeric structure

Two different approaches have been used to incorporate these photoresponsive systems into BCs. First, covalent BCs shown in **Figure 3.2** were prepared via RAFT polymerisation from the corresponding methacrylic monomers. In the case of the BCs based on the **AZO-NO₂/Naph** system, the reference BCs having only either azobenzene (m=0) or naphthalene (p=0) moieties were also synthesised.

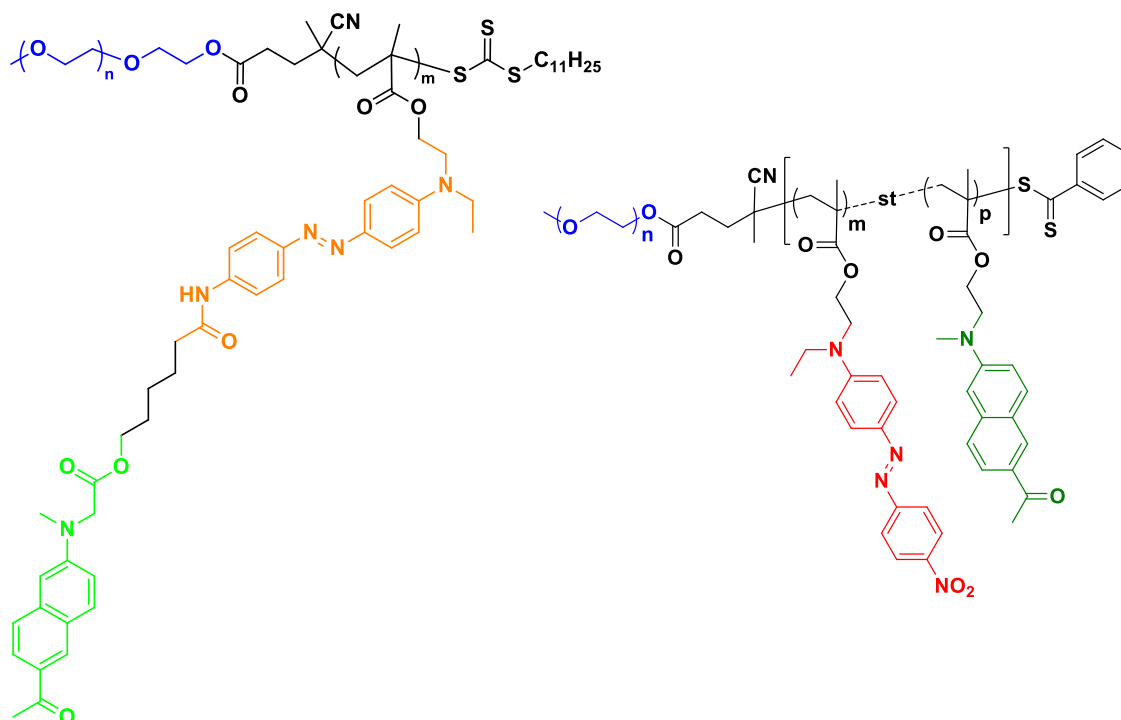


Figure 3.2. General structures of the covalent BCs synthesised

As an alternative to covalent chemistry, supramolecular BCs were also prepared where the photoresponsive moieties were anchored by H-bonding recognition. The main advantage of this strategy is the possibility of preparing a large number of BCs from a single BC scaffold. Therefore, chromophores functionalised with thymine units were attached to amphiphilic BCs having complementary 2,6-diacylaminopyridine (DAP) side pendant groups by forming three H-bonds as it is shown in **Figure 3.3**.

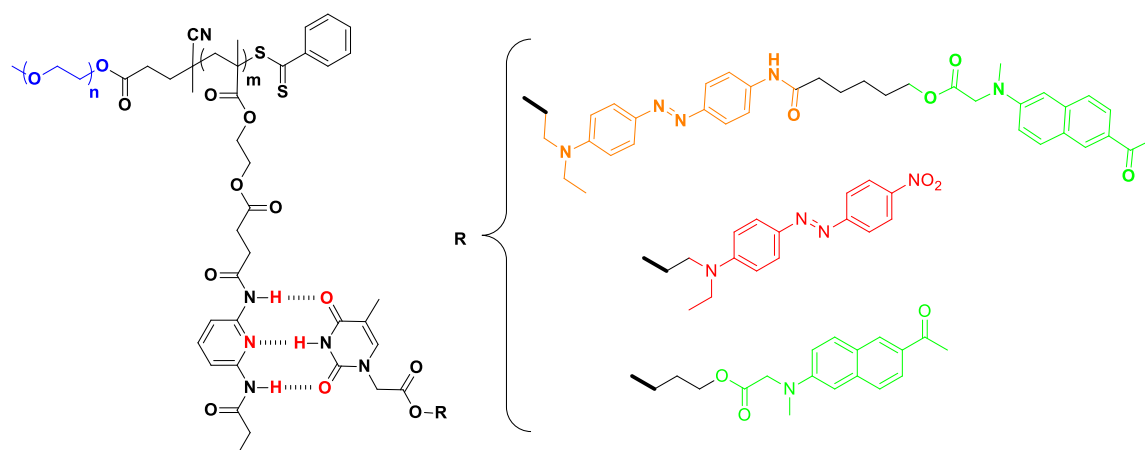


Figure 3.3. General structures of the supramolecular BCs prepared

Self-assembly in water of the covalent and the supramolecular BCs was investigated and the obtained nanostructures were characterised before and after irradiation with light of the appropriate wavelength.

The tasks were the following:

- Synthesis of methacrylic monomers and thymine derivatives
- Preparation and characterisation of amphiphilic BCs *via* RAFT polymerisation
- Preparation and characterisation of supramolecular BCs *via* DAP-thymine H-bonding
- Study of the self-assembly properties in water of the amphiphilic BCs
- Irradiation of BCs in solution
- Study of the photoresponse of the self-assembled BCs to different wavelengths.
- Encapsulation and controlled release experiments

3.2. SYNTHESIS AND CHARACTERISATION OF THE BLOCK COPOLYMERS

3.2.1. COVALENT AMPHIPHILIC BLOCK COPOLYMER HAVING THE AZO-NAPH BICHROMOPHORE

The synthesis of the covalent amphiphilic BC having the azobenzene-naphthalene functional moiety was approached by RAFT polymerisation of the methacrylic monomer **m(AZO-Naph)**, which was prepared by the multistep synthetic path shown in **Figure 3.4**. The azobenzene fragment was prepared starting from **AZO-NO₂**. In spite of its commercial availability and due to the simplicity of its preparation, **AZO-NO₂** was obtained by azo coupling between *para*-nitroaniline and 2-(ethyl(phenyl)amino)ethanol. The hydroxyl group was protected with allyl bromide obtaining compound **2**, that was transformed in the corresponding 4-aminoazobenzene **3** by a Zinin reduction. Compound **3** was subjected to a Steglich reaction with 6-hydroxyhexanoic acid with the hydroxyl group protected with the *tert*-butyl dimethyl silyl group (TBDMS).² Subsequent cleavage of TBDMS using tetrabutyl ammonium fluoride (TBAF) gave rise to the azobenzene fragment **4**. The naphthalene fragment was synthesised starting from 1-(6-methoxynaphthalen-2-yl)ethanone which was deprotected using HBr giving rise to compound **5** that reacted with methylamine and sodium metabisulfite in water at 140 °C, yielding **6**. Then compound **7** was obtained by reacting with methyl bromoacetate and subsequent hydrolysis.

Fragments **4** and **7** were coupled *via* Steglich reaction in dichloromethane to yield **8**. The allyl protecting group was removed in a two-step reaction with Wilkinson catalyst and HgCl₂/HgO to obtain **9**. Finally, the reaction with methacryloyl chloride gave the targeted monomer, **m(AZO-Naph)**.

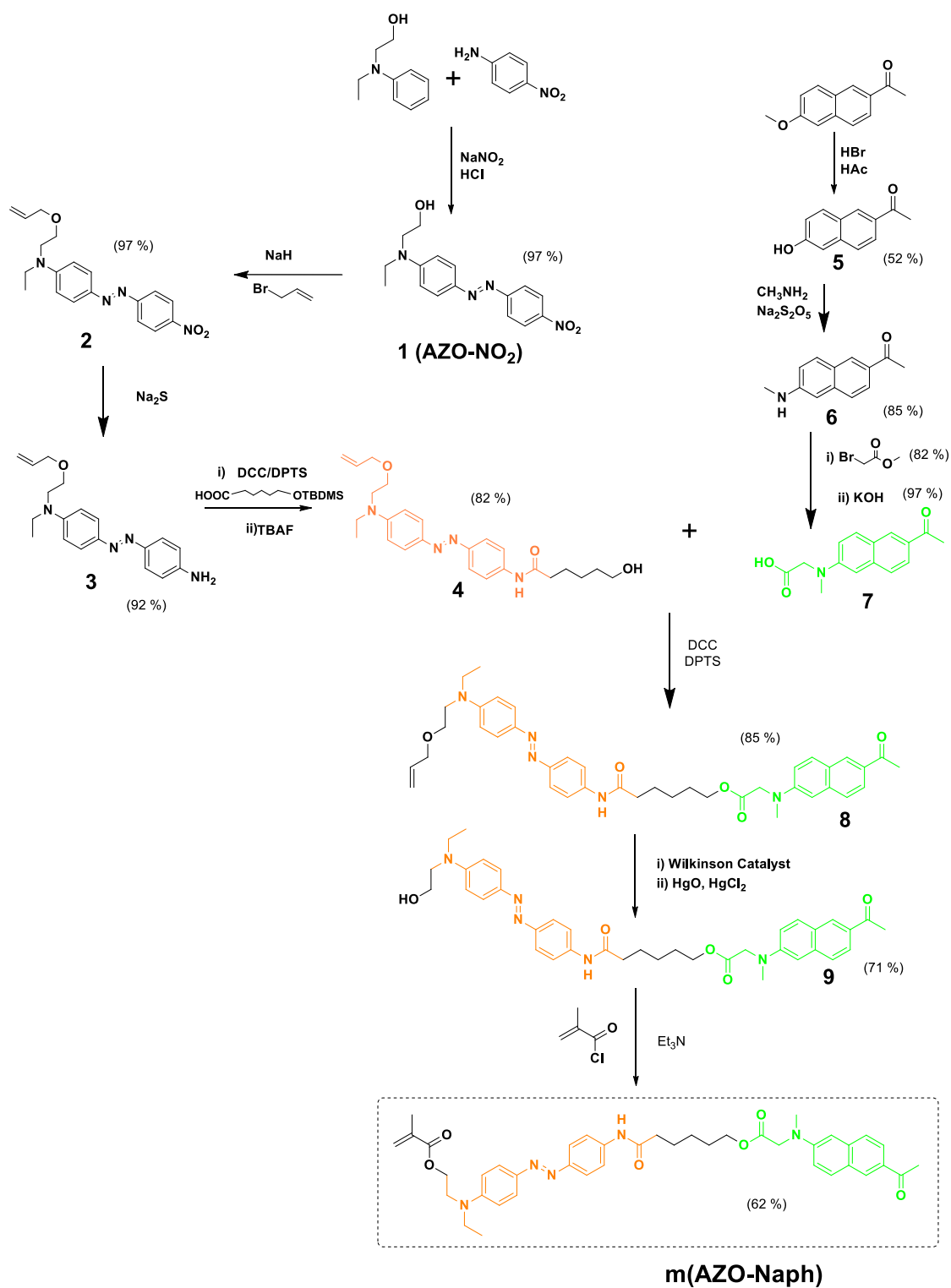


Figure 3.4. Synthesis of the monomer *m*(AZO-Naph)

RAFT polymerisation of *m*(AZO-Naph) was initially attempted with a commercially available macro-CTA of PEG functionalised with 4-cyano-4-

(phenylthiocarbonylthio)pentanoate, as it was previously used with other azobenzene-containing methacrylic monomers (see **Chapter 2**). However, all the attempts to achieve BCs with this macro-CTA were unsuccessful. It has been described that the presence of amine and amide groups might hydrolyse partially or totally thiocarbonylthio CTA groups.³ Therefore, the CTA group was changed to 2-cyano-2-propyl dodecyl trithiocarbonate as it has been reported that this CTA group is more resistant towards the hydrolysis provoked by nitrogen atoms and more convenient for monomers containing amide or amine functionalities.³ Therefore, PEG of 5000 g/mol available in our laboratory was modified by a Steglich esterification using 4-cyano-4-((dodecylthio) thiocarbonylthio)pentanoic acid to obtain the corresponding **PEG5k-trithioCTA** macro-CTA. The ¹H NMR spectrum is collected in **Figure 3.5**. The formation of the ester bond was corroborated from the presence of a new signal at 4.25 ppm that corresponds with the methylenic protons adjacent to the ester group. Relative integration of the PEG signals and terminal CTA groups was also in concordance with the proposed structure.

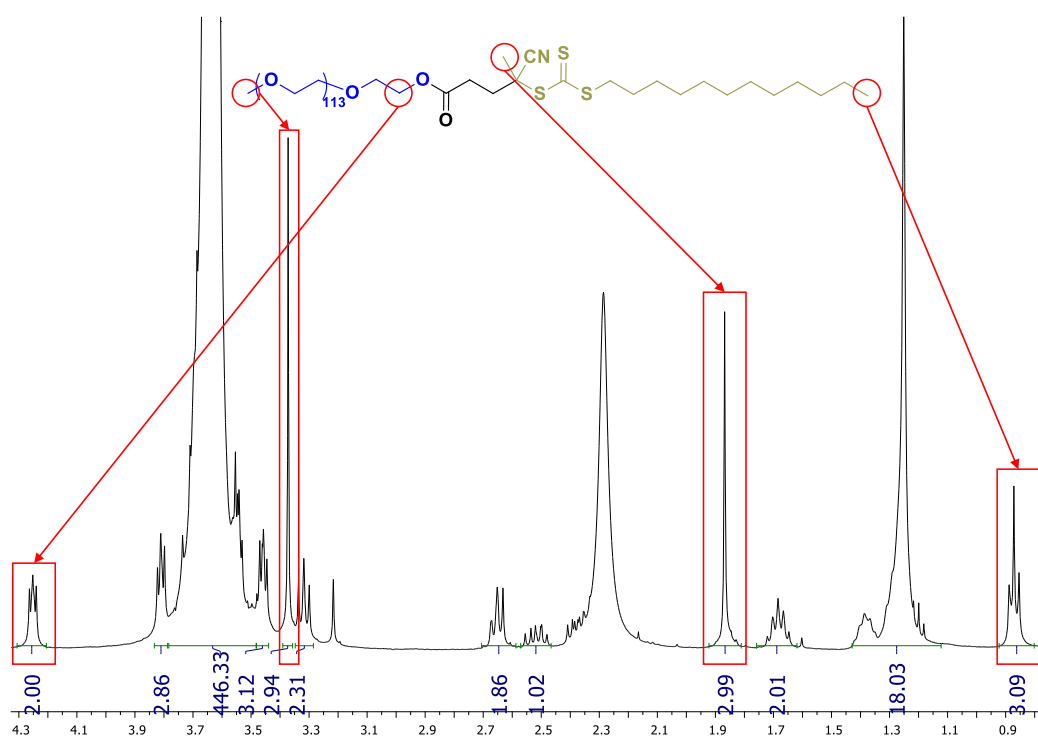


Figure 3.5. ¹H NMR in CDCl₃ of PEG5k-trithioCTA

RAFT polymerisation of **m(AZO-Naph)** was then carried out in freshly distilled DMF at 70 °C using AIBN as thermal initiator (**Figure 3.6**). m_{th} was adjusted to 10. The polymerisation crude was precipitated twice into cold diethyl ether yielding **PEG5k-*b*-p(AZO-Naph)**.

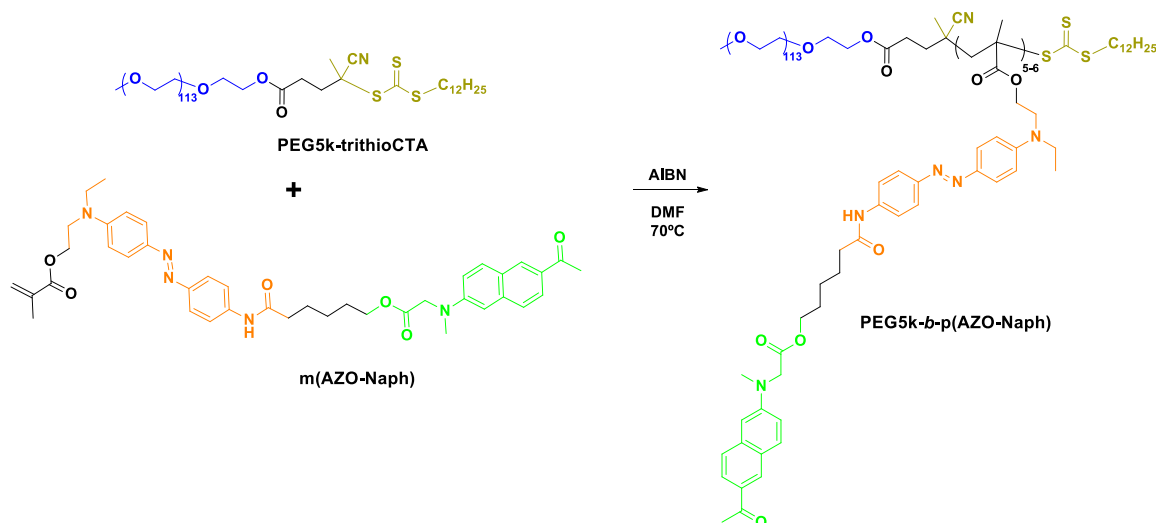


Figure 3.6. Polymerisation of **m(AZO-Naph)** to obtain **PEG5k-*b*-p(AZO-Naph)**

SEC traces showed a shift of the mass distribution peak to lower elution times (when compared with the macro-CTA), which was in concordance with the expected increase of the molar mass (**Figure 3.7**). The average number molar mass $M_{n,SEC}$ determined by SEC, calibrated using PMMA standards and a light scattering detector, was 8670 g/mol and dispersity $\mathcal{D} = 1.06$. By 1H NMR an average degree of polymerisation (m) of around 6 was estimated for the hydrophobic block **p(AZO-Naph)** (**Figure 3.8**), which corresponds to an average $M_{n,NMR} = 9300$ g/mol (as the sum of PEG and **p(AZO-Naph)** blocks), which agreed with SEC measurements.

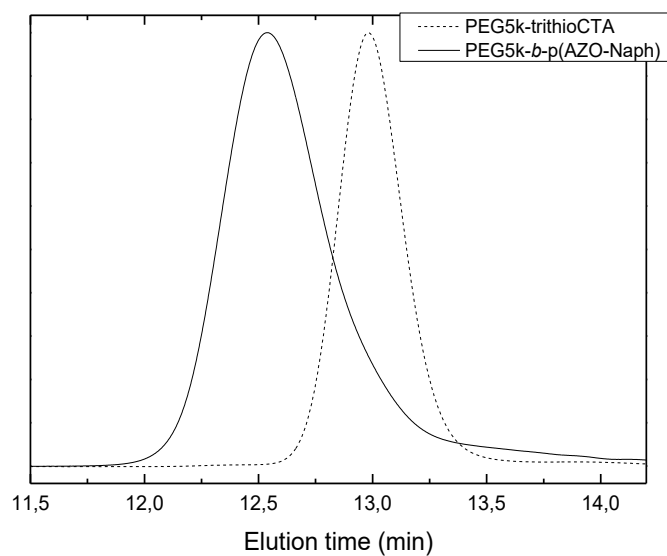


Figure 3.7. SEC traces for PEG5k-trithioCTA and PEG5k-b-p(AZO-Naph)

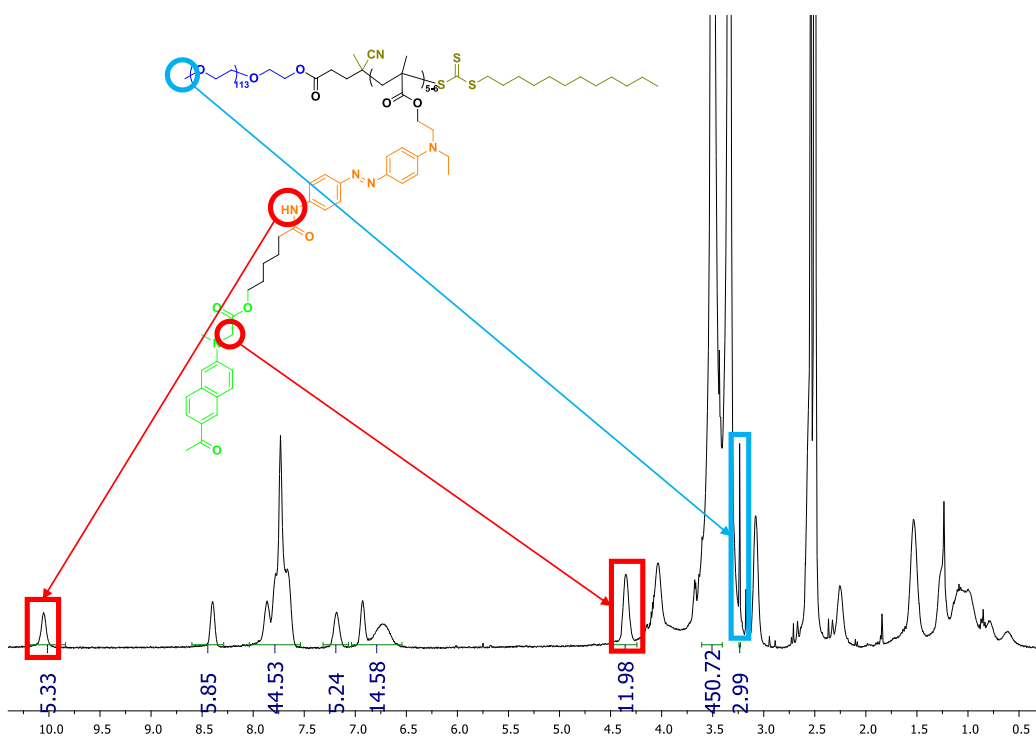


Figure 3.8. ^1H NMR in DMSO-d_6 of PEG5k-b-p(AZO-Naph)

Thermal properties of the synthesised macro-CTA and derived BC were evaluated by TGA and DSC. Data are gathered in **Table 3.1**. Both polymers presented good

thermal stability with decomposition temperatures above 180 °C. The presence of volatiles was discarded. Thermal transitions were evaluated by DSC at a rate of 10 °C/min. Data were collected from first scan. Both **PEG5k-trithioCTA** and **PEG5k-*b*-p(AZO-Naph)** presented melting temperatures of 57 and 43 °C, respectively.

Table 3.1. Thermal properties of PEG5k-trithioCTA and PEG5k-*b*-p(AZO-Naph)

Polymer	TGA ^a	T _m (ΔH _m) ^b
PEG5k-trithioCTA	229	57 (169)
PEG5k-<i>b</i>-p(AZO-Naph)	185	43 (60)

^a Decomposition temperature (in °C) associated to mass loss determined by TGA given at the onset of the weight loss curve

^b Melting temperature (in °C) given at the maximum of the peak and associated melting enthalpy (in J/g), in brackets, determined by DSC on the first heating scan at 10 °C/min

PEG5k-*b*-p(AZO-Naph) was self-assembled by the co-solvent method using THF-water. The process was followed by turbidimetry and the sample was dialysed against water once the water addition was completed. This dispersion was studied by TEM and spherical micelles were detected whose hydrodynamic diameter (D_h) was 22 ± 7 nm as determined by DLS (**Figure 3.9**).

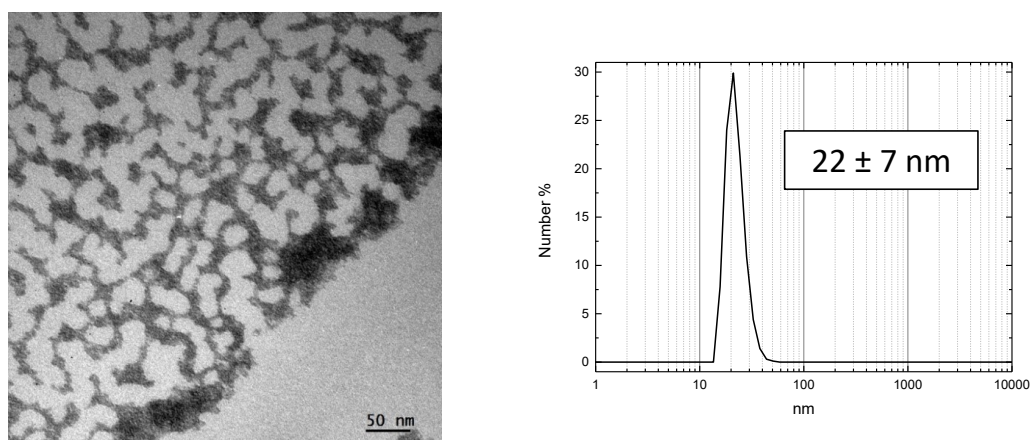


Figure 3.9. Representative TEM image and DLS distribution of PEG5k-*b*-p(AZO-Naph) micelles in water

CAC of **PEG5k-*b*-p(AZO-Naph)** was determined both by fluorescence spectroscopy, using Nile Red, and by DLS with calculated values of 58 and 54 $\mu\text{g/mL}$ respectively (**Figure 3.10**), which were in good agreement.

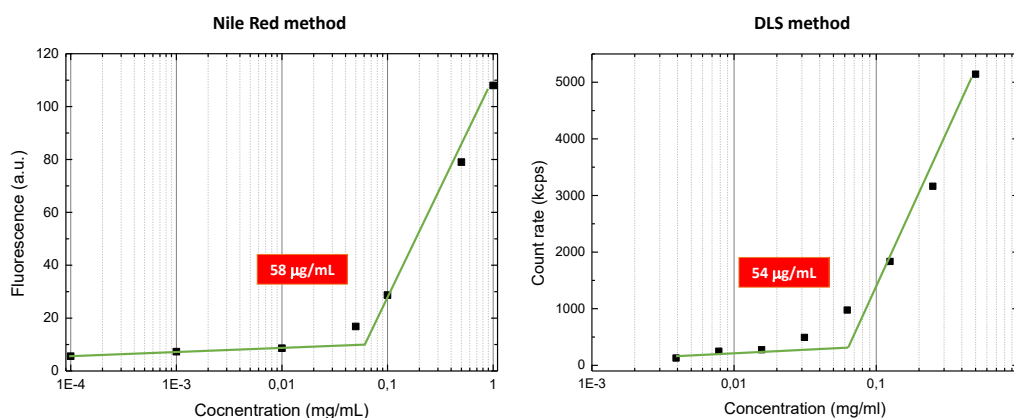


Figure 3.10. CAC for PEG5k-*b*-p(AZO-Naph) using fluorescence spectroscopy (Nile Red) and DLS

3.2.2. SUPRAMOLECULAR AMPHIPHILIC BLOCK COPOLYMER HAVING THE AZO-NAPH BICHROMOPHORE

As an alternative to the synthesis of the covalent BC, the supramolecular approach was also evaluated. Even if this approach also requires the laborious synthesis of a bichromophoric moiety, compositional variations are easily affordable. In our lab, amphiphilic BCs have previously been reported with a polymethacrylic block with diacylaminopyridine (DAP) side units.^{4,5} We demonstrated that this polymer is an excellent platform for supramolecular functionalisation using thymine complementary units able to form three H-bonds. Therefore, a thymine derivative of **AZO-Naph** was prepared starting from compound **9** and 2-(5-methyl-2,4-dioxo-3,4-dihydropyrimidin-1(2*H*)-yl)acetic acid *via* a Steglich reaction, yielding **thm(AZO-Naph)** (**Figure 3.11**).

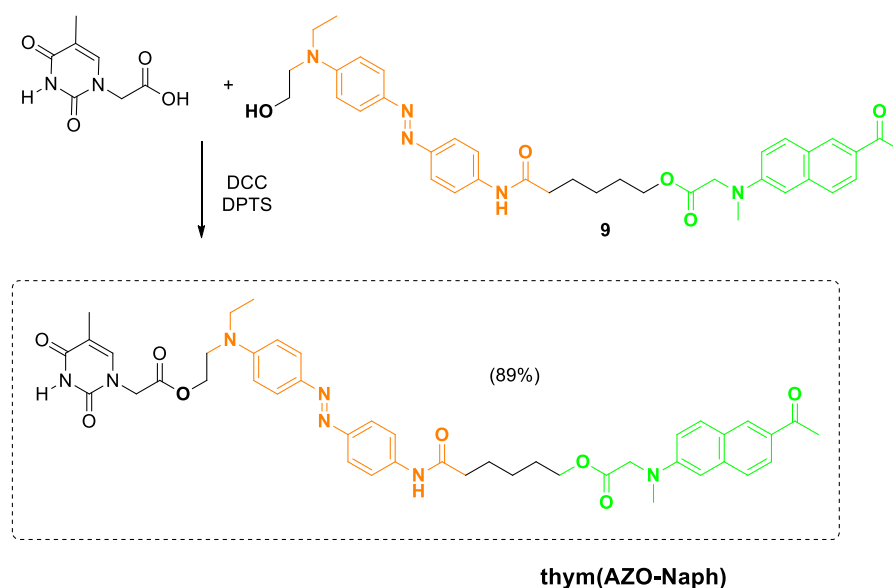


Figure 3.11. Synthesis of *thym(AZO-Naph)*

Then, a supramolecular side chain functionalised BC was prepared from **PEG10k-*b*-PDAP** (Figure 3.12). This amphiphilic BC precursor with a PEG hydrophilic block of 10000 g/mol molar mass was prepared as previously reported.⁴ According to ¹H NMR analysis, average degree of polymerisation (*m*) of the PDAP block was 32, which corresponds with average number molar masses (*M_{n,NMR}*) 22000 g/mol calculated as the sum of the molar masses of both blocks. The supramolecular BC was prepared by dissolving **PEG10k-*b*-PDAP** and **thym(AZO-Naph)** in THF using a 1:1 DAP:thymine molar ratio. The solvent was slowly evaporated by shaking the mixture at room temperature and eventually dried under vacuum, giving rise to **PEG10k-*b*-PDAP·thym(AZO-Naph)** (Figure 3.12). H-bonding recognition between DAP and thymine in solution was evaluated by ¹H NMR (Figure 3.13) in which a shift to lower fields was observed for the atoms involved in the H-bonding as consequence of their deshielding due to the non-covalent interaction.

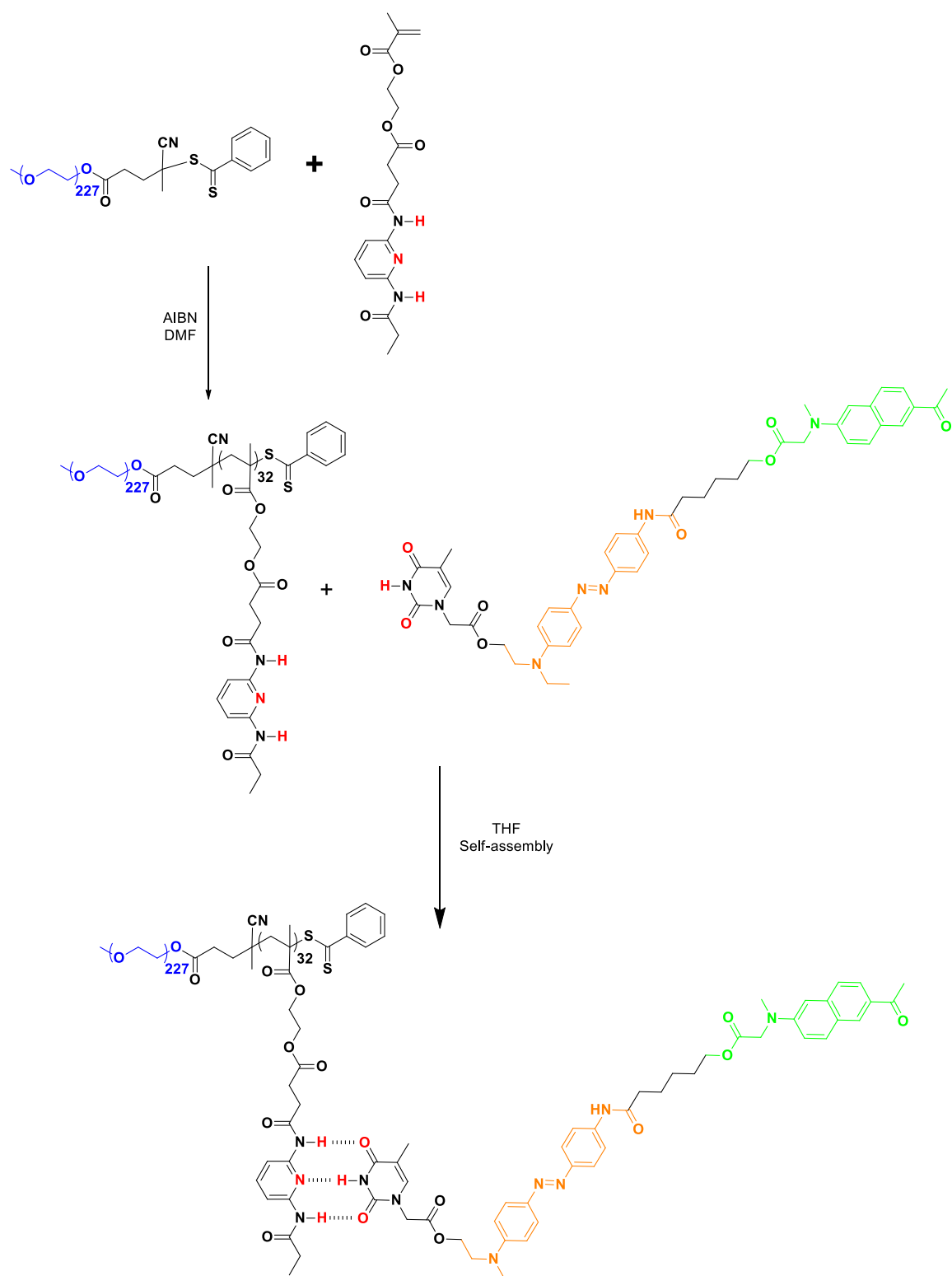


Figure 3.12. Synthesis of supramolecular BC PEG10k-b-PDAP·thym(AZO-Naph)

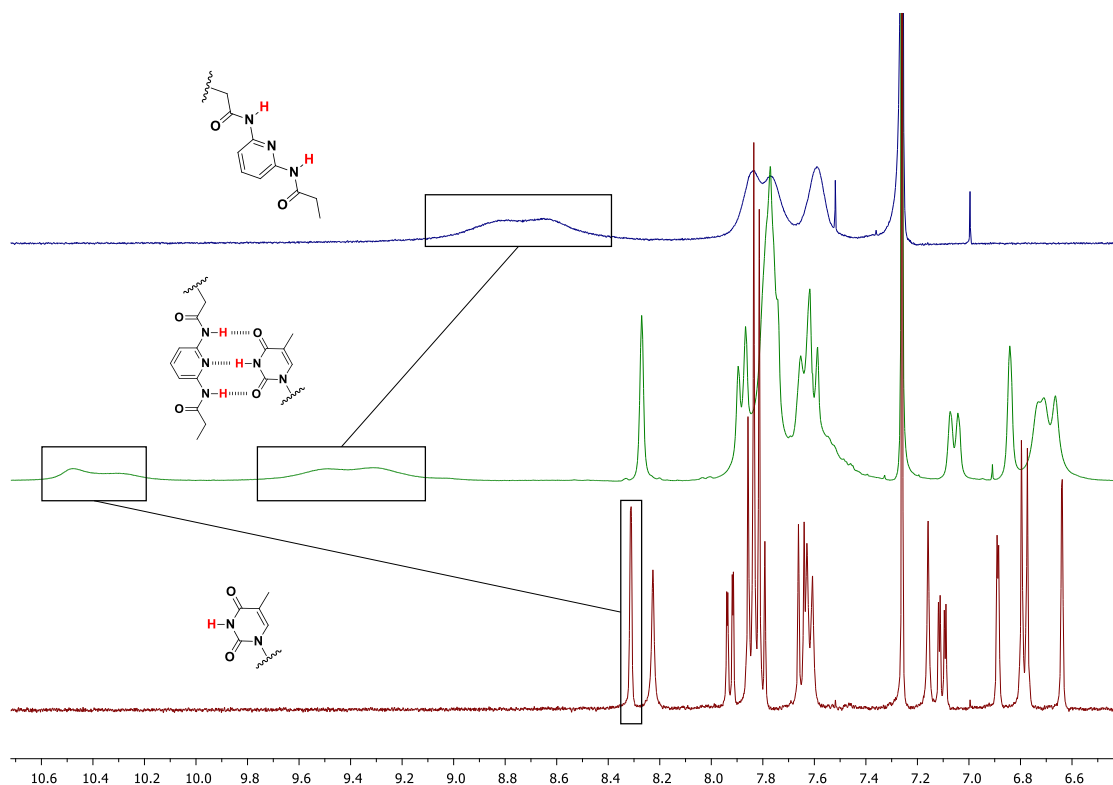


Figure 3.13. ^1H NMR study in CDCl_3 of the interaction between DAP and thymine. In red, protons shifted after complexation.

The preparation of self-assemblies from this BC was also attempted by the co-solvent method using THF, acetone, DMSO or DMF and subsequent slow addition of milliQ water. However, in all attempts an orange precipitate was detected upon water addition even when an addition pump was used in order to gain a good control of the water addition. The precipitate was filtered off yielding a colourless solution, which evidenced that the solid separated from the solution was mainly **thym(AZO-Naph)**. Consequently, this supramolecular BC was discarded for additional experiments.

3.2.3. COVALENT AMPHIPHILIC BLOCK COPOLYMERS WITH AZO- NO_2

With the aim of simplifying the synthesis of chromophores, alternative BCs were investigated based on **AZO- NO_2** that has been widely used in the design of

photoresponsive materials.^{6,7} **AZO-NO₂** has its main absorption band shifted from the UV region to *ca.* 400-500 nm. Besides, a naphthalene with a similar chemical structure to that in **AZO-Naph** was used as a potential sensitiser of the azobenzene isomerisation. Therefore, methacrylic monomers with **AZO-NO₂** and **Naph** moieties were synthesised according to **Figure 3.14**. **m(AZO-NO₂)** by reaction of **AZO-NO₂** with methacryloyl chloride in dichloromethane. **m(Naph)** was prepared starting from compound **5**. Using the Bucherer reaction, compound **5** with sodium metabisulfite and 2-(methylamino)ethanol in water at 140 °C gave **10**, that was finally esterified with methacryloyl chloride in dichloromethane to yield **m(Naph)**.

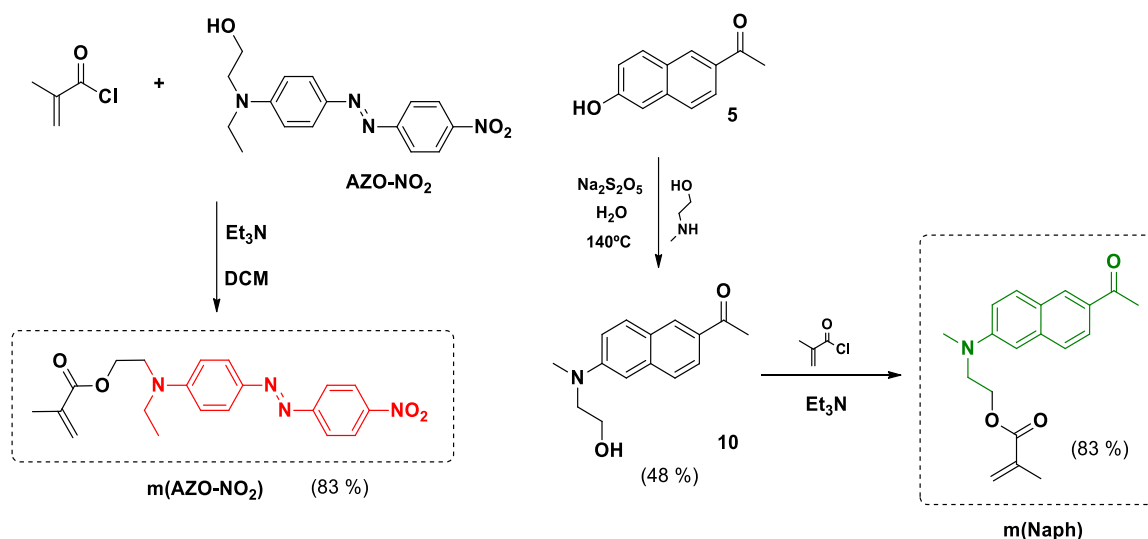


Figure 3.14. Synthesis of *m*(AZO-NO₂) and *m*(Naph)

According to the results described in **Chapter 2**, two series of covalent BCs were prepared by RAFT polymerisation using the commercially available PEG macro-CTAs of 2000 and 10000 g/mol average molar masses with the 4-cyano-4-(phenylthiocarbonylthio)pentanoate terminal group (**Figure 3.15**). BCs with **AZO-NO₂** and **Naph** repeating units randomly distributed along the hydrophobic segment in a 3/1 molar proportion were prepared to explore the potential antenna effect without introducing an excessive amount of naphthalene that could affect the photoresponse properties of the BC. Additionally, two BCs were prepared, one with each monomer, to be used as reference. Polymerisations were carried out in freshly distilled DMF at 70 °C using AIBN as thermal initiator. Theoretical degrees

of polymerisation (m/p_{th}) were adjusted to 25 and 60 for **PEG2k** and **PEG10k**, respectively.

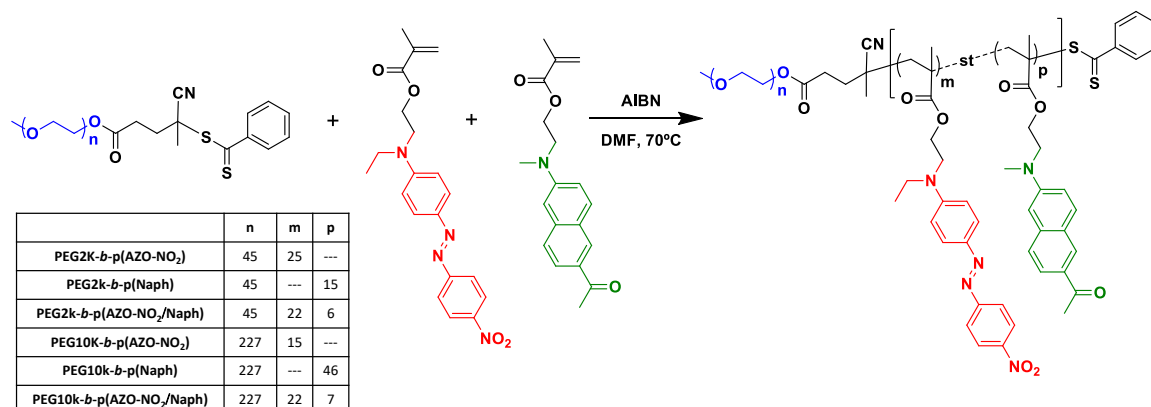


Figure 3.15. General synthesis of BCs from *m*(AZO-NO₂) and *m*(Naph)

The evolution of polymerisations was tracked by SEC. SEC traces for **PEG2k** BCs are shown in **Figure 3.16**. Monomodal mass distributions shifted to lower retention times when compared to the corresponding macro-CTA as expected. $M_{n,SEC}$ were calculated using PMMA standards and a light scattering detector and their values are shown in **Table 3.2**. Dispersity values (\mathcal{D}) between 1.0 and 1.1 were determined, which are consistent with a controlled polymerisation process. Similar results were obtained for BCs based on the **PEG10k**.

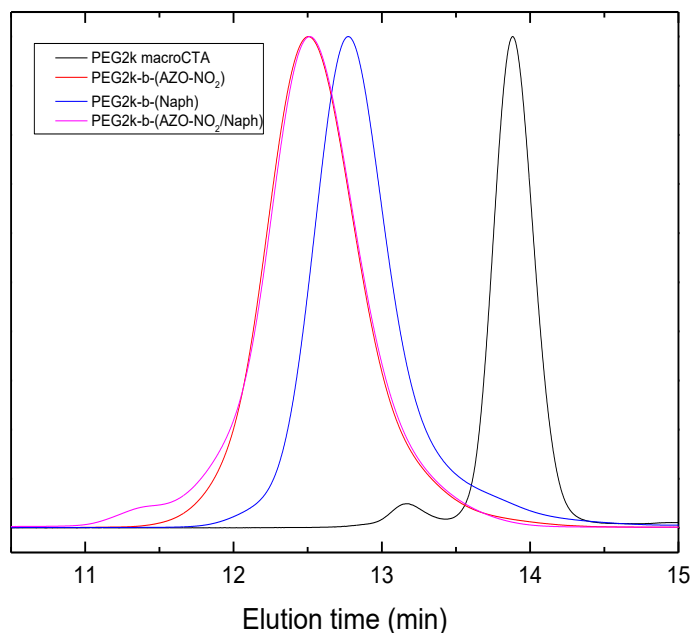


Figure 3.16. SEC traces for PEG2k based BCs

Average degrees of polymerisation (m for $p(\text{AZO-NO}_2)$ and p for $p(\text{Naph})$ segments) and related average number molar masses ($M_{n,\text{NMR}}$), given as the sum of the molar masses of both blocks, were estimated by ^1H NMR. The integration of methylenic protons of PEG (ca. 3.6 ppm) (terminal methyl group was not well defined enough to be used as reference) and well defined peaks corresponding to protons of the azobenzene and/or naphthalene repeating units were compared. Values are collected in **Table 3.2**. In **Figure 3.17**, ^1H NMR spectrum of **PEG10k-*b*- $p(\text{Naph})$** is shown as an example. In this case, the methyl group 2.48 ppm of the acetyl radical at the **Naph** unit was used to calculate a degree of polymerisation of approx. 46. In the case of **AZO-NO₂** units, aromatic signals were used. Experimental m/p and m/p_{th} were in better concordance when **PEG2k-CTA** was used. With **PEG10k-CTA** major differences between theoretical and experimental m/p were observed.

Table 3.2. Molar masses of AZO-NO₂/Naph covalent BCs calculated by ¹H NMR and SEC

Polymer	m/p _{th} ^a	m/p ^b	M _{n,NMR} ^c	M _{n,SEC}	<i>D</i>
PEG2k- <i>b</i> -p(AZO-NO ₂)	25/0	25/0	11550	10191	1.05
PEG2k- <i>b</i> -p(Naph)	0/25	0/16	7000	8018	1.03
PEG2k- <i>b</i> -p(AZO-NO ₂ /Naph)	21/7	22/6	12300	10027	1.06
PEG10k- <i>b</i> -p(AZO-NO ₂)	60/0	15/0	15700	12449	1.08
PEG10k- <i>b</i> -p(Naph)	0/60	0/46	24300	23350	1.09
PEG10k- <i>b</i> -p(AZO-NO ₂ /Naph)	45/15	22/7	20600	21035	1.12

^a Theoretical degree of polymerisation calculated from the [monomer]₀/[macro-CTA]₀ assuming full monomer conversion. m: azobenzene; p: naphthalene

^b Experimental degree of polymerisation of the hydrophobic block estimated by ¹H NMR end group analysis. m: azobenzene; p: naphthalene

^c Molar mass of BC as the sum of the molar mass of PEG and hydrophobic blocks calculated using m determined by ¹H NMR ($M_n = M_{\text{PEG}} + m \times M_{\text{m(AZO-NO}_2)} + p \times M_{\text{m(Naph)}}$). For PEG, commercial value was used

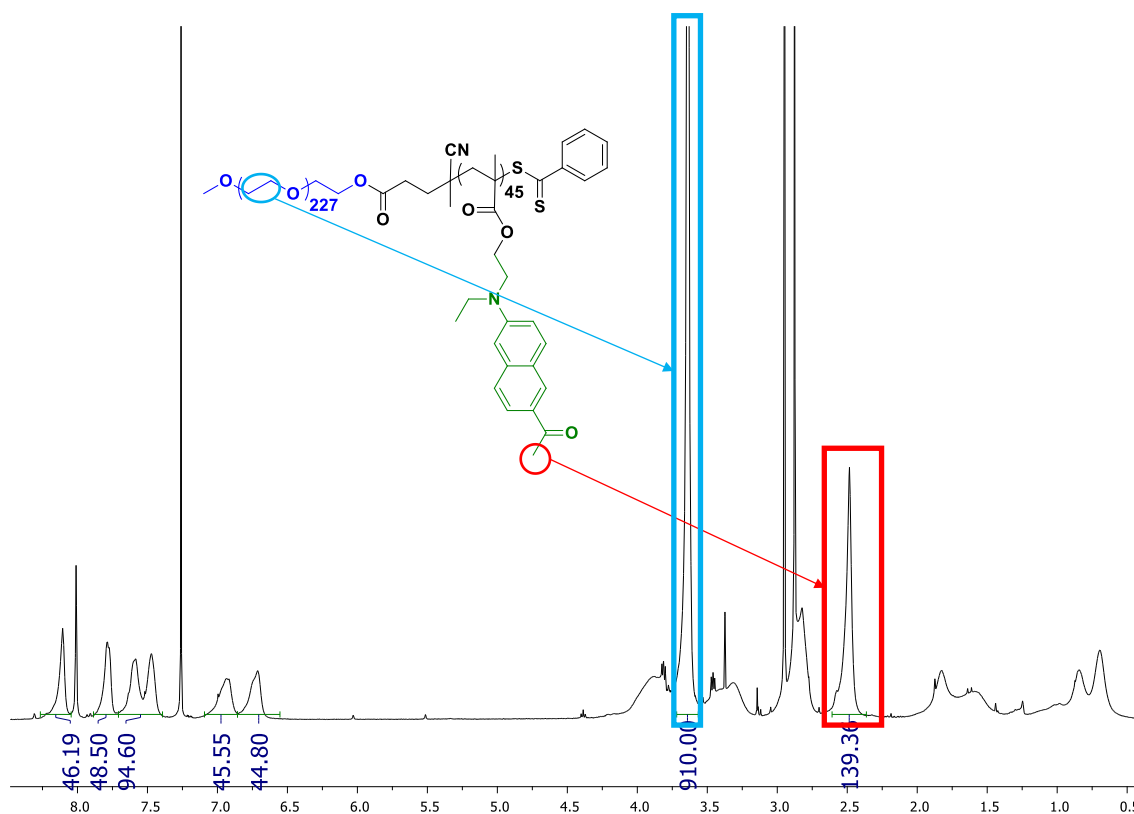


Figure 3.17. ¹H NMR spectrum in CDCl₃ of PEG10k-*b*-p(Naph)

Thermal properties in bulk of these polymers were determined by TGA and DSC and relevant data are presented in **Table 3.3**. The polymers had good thermal stability and, according to TGA, weight loss was not observed at temperatures below 280 °C. According to DSC, BCs of **PEG2k** series show two transitions, the T_g corresponding to the hydrophobic blocks as well as the T_m of PEG block, except for **PEG2k-*b*-p(AZO-NO₂)**, which allows us to think that blocks are immiscible. For **PEG2k-*b*-p(AZO-NO₂/Naph)** a small crystallisation was observed at 46 °C in all the heating scans. In the case of **PEG10k** BCs, the thermal behaviour was dominated by the **PEG10k** block with the T_m appearing close to that of the macroinitiator T_m . T_g could not be determined probably due to the minor proportion of hydrophobic blocks in these BCs.

Table 3.3. Thermal properties of the covalent BCs of AZO-NO₂/Naph system

Polymer	TGA ^a	T_g ^b	T_m (ΔH_m) ^c
PEG2k-<i>b</i>-p(AZO-NO₂)	288	62	----
PEG2k-<i>b</i>-p(Naph)	281	23	46 (24)
PEG2k-<i>b</i>-p(AZO-NO₂/Naph)	283	67	45 (0.8)
PEG10k-<i>b</i>-p(AZO-NO₂)	302	----	55 (94)
PEG10k-<i>b</i>-p(Naph)	293	----	52 (50)
PEG10k-<i>b</i>-p(AZO-NO₂/Naph)	299	----	54 (60)

^a Decomposition temperature (in °C) associated to mass loss determined by TGA given at the onset of the weight loss curve

^b Glass transition temperature (in °C) determined by DSC on the first heating scan at 10 °C/min given at the half height of the baseline jump

^c Melting temperature (in °C) given at the maximum of the peak and associated melting enthalpy (in J/g), in brackets, determined by DSC on the first heating scan at 10 °C/min

Self-assembly properties of these amphiphilic BCs were evaluated using the co-solvent method, as described in **Chapter 2**, using THF as organic common solvent and the self-assemblies were characterised by TEM and DLS. Representative TEM images and DLS curves for **PEG2k** series are shown in

Figure 3.18. Vesicles were formed for all the BCs. In the case of **PEG2k-*b*-*p*(Naph)**, smaller vesicles were observed in TEM images together with a residual population of spherical micelles that were not detected by DLS. It has to be mentioned that vesicles usually appeared as deflated or broken in TEM images because of the rupture of their membranes under the ultrahigh vacuum of the microscope.

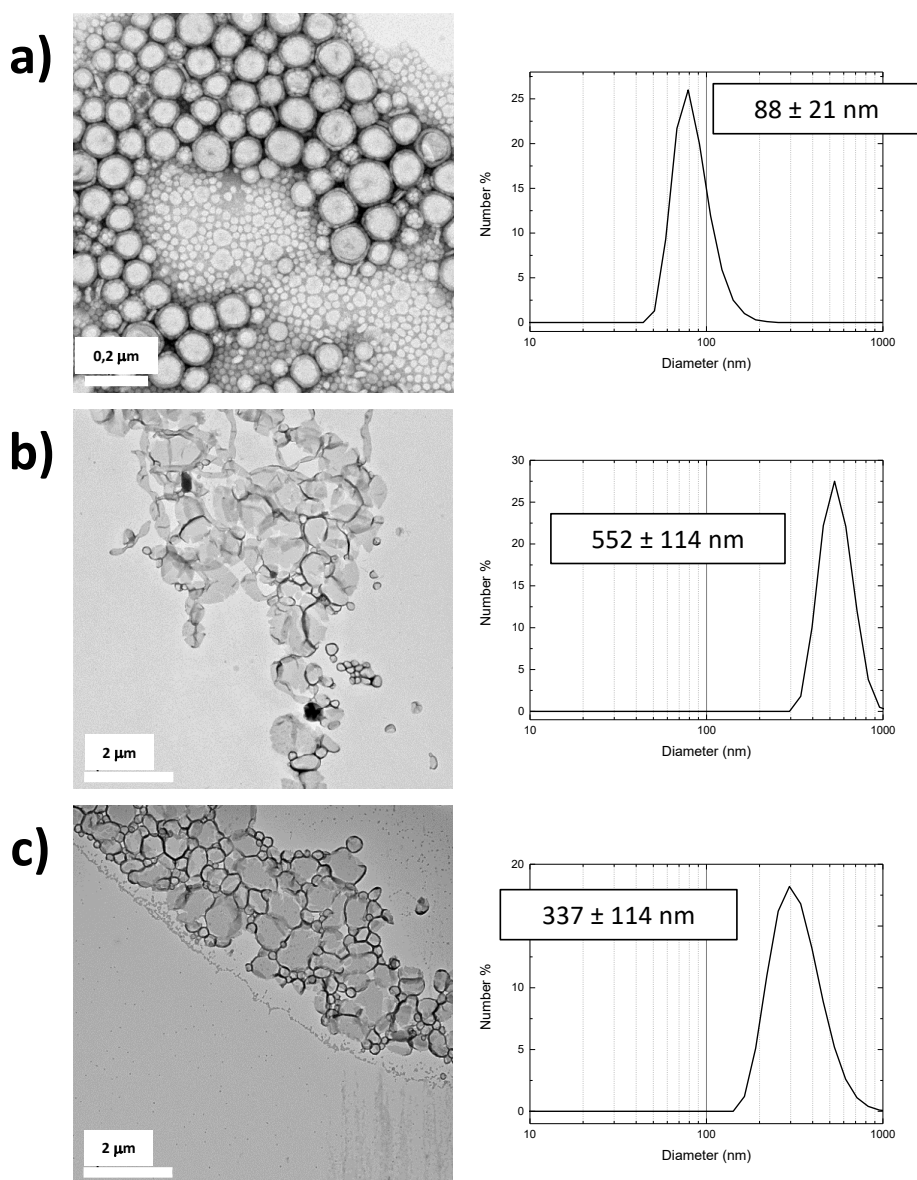


Figure 3.18. Representative TEM images and DLS distributions for a) PEG2k-*b*-*p*(Naph), b) PEG2k-*b*-*p*(AZO-NO₂) and c) PEG2k-*b*-*p*(AZO-NO₂/Naph)

In the case of BCs derived from the **PEG10k** macro-CTA, all the studied BCs formed spherical micelles with relatively homogeneous D_h around 35-50 nm (**Figure 3.19**).

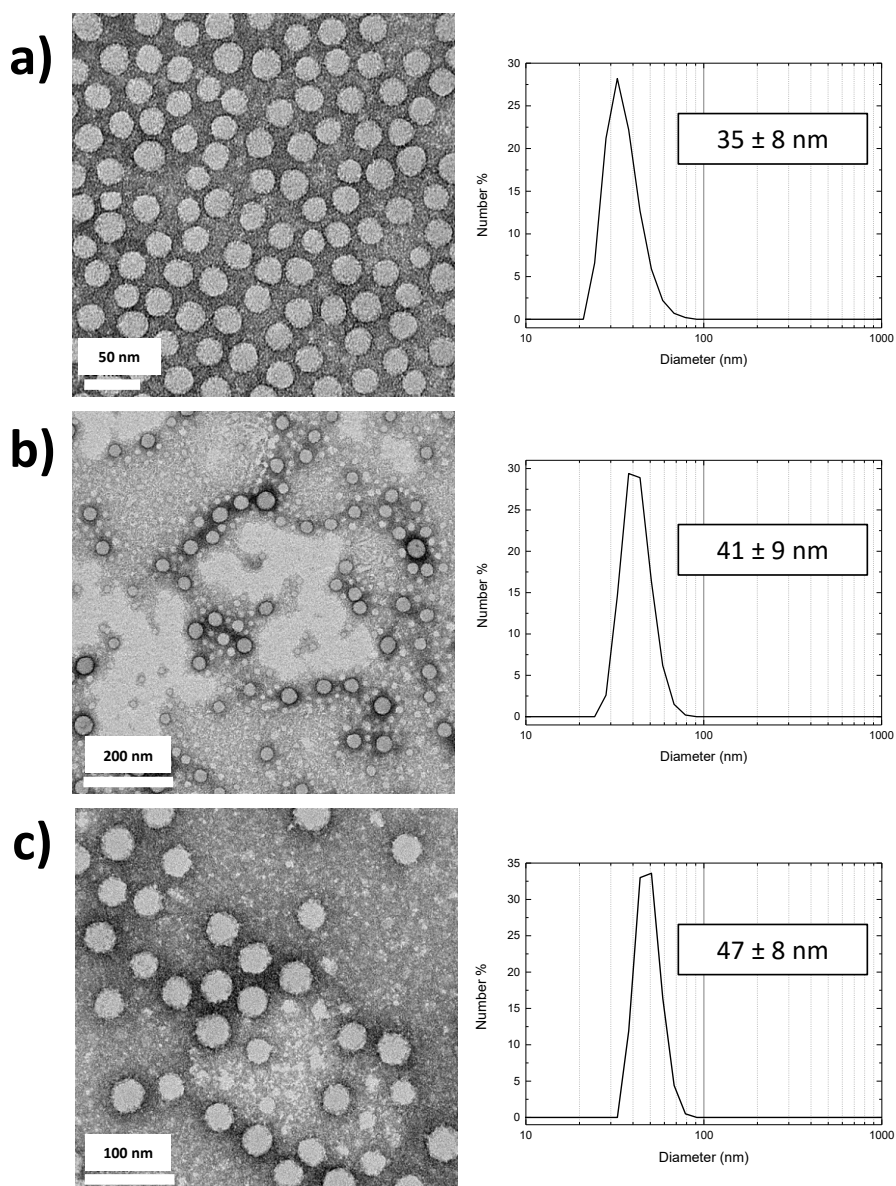


Figure 3.19. Representative TEM images and DLS distributions for a) *PEG10k-b-p(Naph)*, b) *PEG10k-b-p(AZO-NO₂)* and c) *PEG10k-b-p(AZO-NO₂/Naph)*

The CAC was evaluated by DLS or by fluorescence spectroscopy (using Nile Red) depending on the polymer. As shown in **Figure 3.20**, in which CAC is calculated for **PEG2k-*b*-p(Naph)** and **PEG10k-*b*-p(Naph)** using Nile Red as fluorescent dye,

the CAC values can be calculated at the intersection of the linear fit of both tendencies of the Nile Red emission at 610 nm. Values of 67 and 82 $\mu\text{g/mL}$ were obtained respectively. The use of this method with BCs having **AZO-NO₂** has a major drawback because the spectral overlap of the azobenzene absorption with the excitation of Nile Red (550 nm). Therefore, CAC values of azobenzene containing polymers were determined by DLS as described in **Chapter 2**. For **PEG2k-*b*-p(AZO-NO₂)** and **PEG2k-*b*-p(AZO-NO₂/Naph)** nonlinear regressions were obtained probably due to intermediate aggregates during the vesicles disassembly. For **PEG10k-*b*-p(AZO-NO₂)** and **PEG10k-*b*-p(AZO-NO₂/Naph)** low values were determined around 4-8 $\mu\text{g/mL}$ that might be due to antiparallel interaction between **AZO-NO₂** units when self-assembled structures are formed.

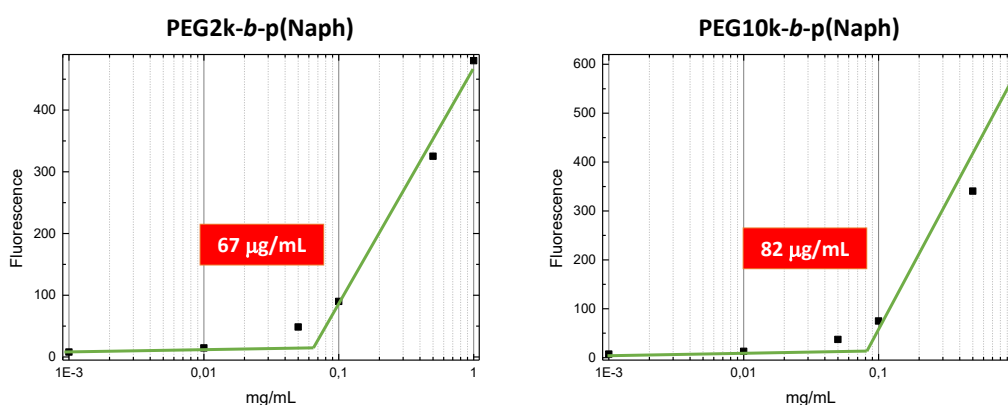


Figure 3.20. Determination of CAC by fluorescence spectroscopy using Nile Red

3.2.4. SUPRAMOLECULAR AMPHIPHILIC BLOCK COPOLYMERS WITH AZO-NO₂

As described in **Section 3.2.2.**, supramolecular chemistry is a versatile alternative in which starting from a single macromolecule it is possible to easily prepare materials with tailored properties just by changing the functionality of the complementary units. Thymines **thym(AZO-NO₂)** and **thym(Naph)** were prepared starting from **AZO-NO₂** and compound **7** (**Figure 3.21**). The thymine was introduced using 2-(5-methyl-2,4-dioxo-3,4-dihydropyrimidin-1(2H)-yl)acetic acid in which the corresponding chromophore was attached *via* Steglich esterification.

In the case of **thym(Naph)** an aliphatic spacer was previously introduced (yielding **11**) between both carboxylic groups.

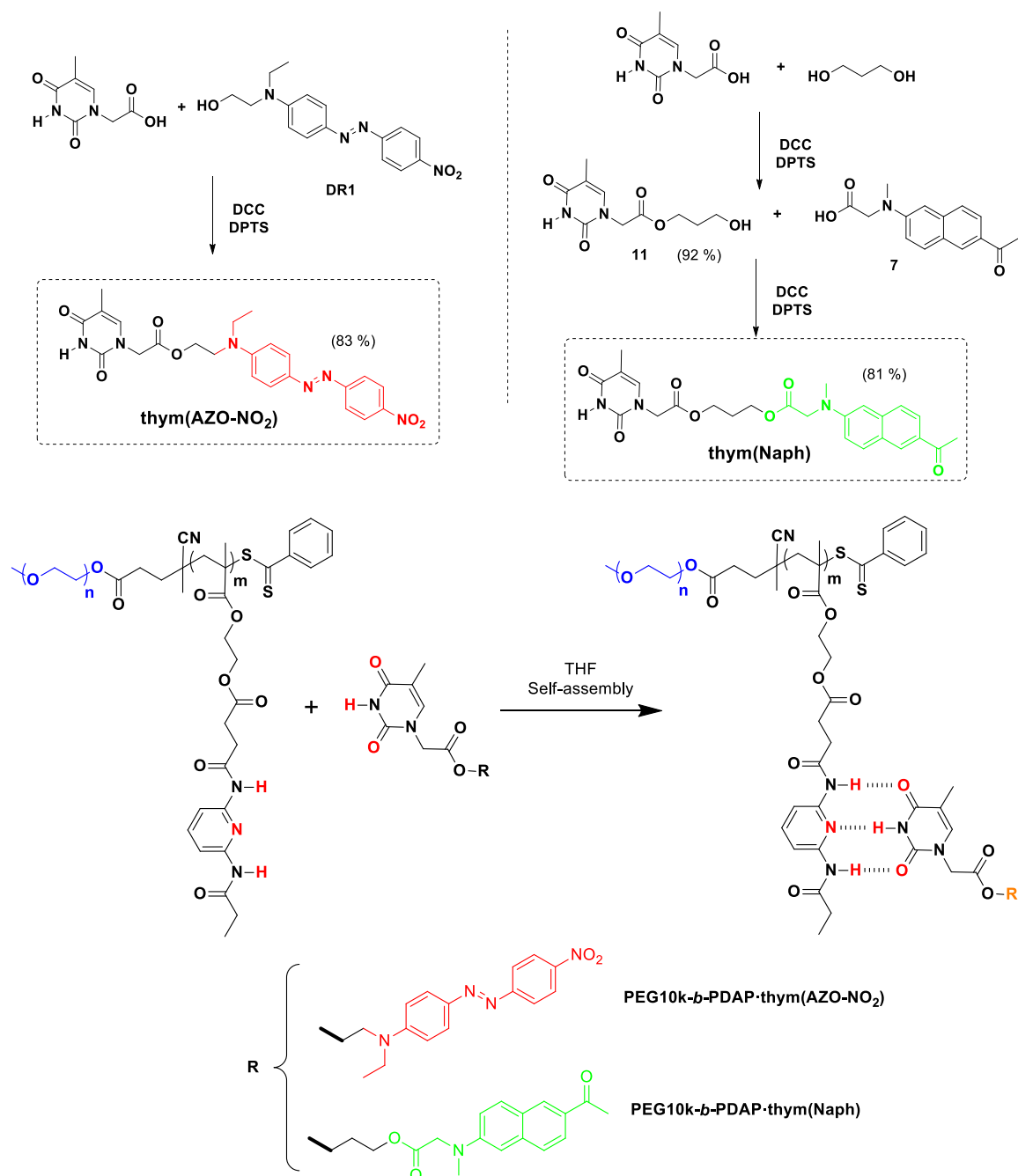


Figure 3.21. Synthesis of thym(AZO-NO₂) and thym(Naph) and BCs prepared from PEG10k-*b*-PDAP and thym(AZO-NO₂) and thym(Naph)

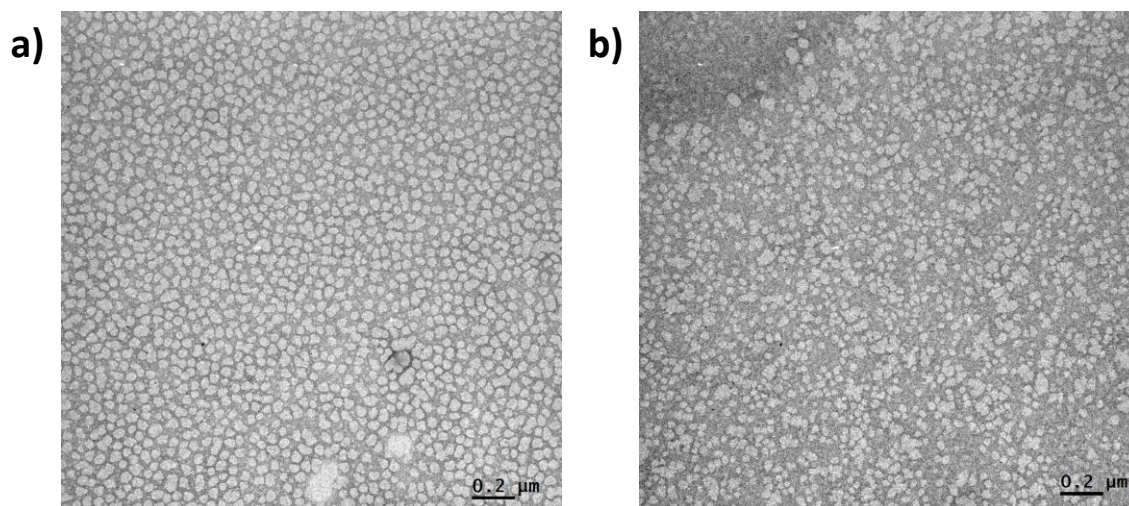


Figure 3.22. Representative TEM images of a) PEG10k-b-PDAP and b) PEG2k-b-PDAP self-assemblies in water

A new BC, **PEG2k-b-PDAP**, was prepared with $n = 45$ and $m = 9$. Then, **PEG10k-b-PDAP** ($n = 227$ and $m = 32$), used in **Section 3.2.1.**, and **PEG2k-b-PDAP** were self-assembled starting from THF (5 mg of polymer in 1 mL of THF) and adding 2.5 mL of water at a rate of 0.75 mL/h with the help of an addition pump. Spherical micelles were formed according to TEM observations in concordance with earlier reports, in which diameters of 32 and 21 nm were determined respectively for both polymers (**Figure 3.22**; **Error! No se encuentra el origen de la referencia.**).^{4,5}

PEG10k-b-PDAP was first used as scaffold, in which thymine were attached, in order to optimise the experimental conditions of self-assembly process. BCs were prepared from a THF solution of **PEG10k-b-PDAP** and the corresponding thymine(s) using a 1:1 DAP/Thym molar ratio (**Figure 3.21**). The hydrogen bonding interaction of the thymine-DAP pair was confirmed by ¹H NMR in CDCl₃ by comparing the supramolecular BC spectra with those of its components at the same concentration (**Figure 3.23**) to discard variations due to concentration effects. Proton resonances of H atoms involved in the H-bonds (labelled in red) shifted to a lower field as consequence of the deshielding produced by the H-bonding interaction. Some modifications in aromatic rings were also observed probably due to π - π stacking interactions in solution between naphthalene units.

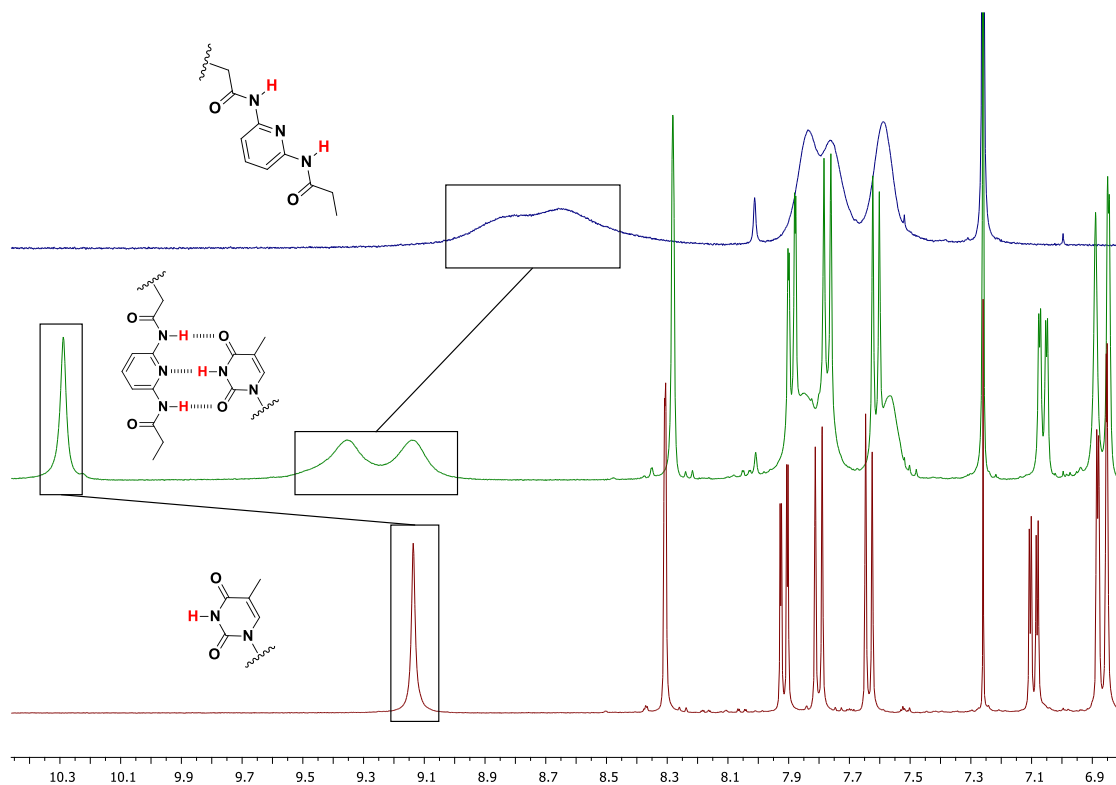


Figure 3.23. ^1H NMR in CDCl_3 analysis of the DAP-thym interaction in $\text{PEG10k-b-PDAP}\cdot\text{thym(Naph)}$. In red, atoms involved in the H-bond.

Next, $\text{PEG10k-b-PDAP}\cdot\text{thym(AZO-NO}_2)$ and $\text{PEG10k-b-PDAP}\cdot\text{thym(Naph)}$ were also self-assembled using the same experimental procedure of PEG10k-b-PDAP . Initially stable dispersions of $\text{PEG10k-b-PDAP}\cdot\text{thym(AZO-NO}_2)$ and $\text{PEG10k-b-PDAP}\cdot\text{thym(Naph)}$ were obtained that precipitated during the dialysis, probably due to partial precipitation of $\text{thym(AZO-NO}_2)$ and thym(Naph) . Samples were filtered to remove the solid and stable dispersions were eventually obtained. $\text{PEG10k-b-PDAP}\cdot\text{thym(AZO-NO}_2)$ dispersion was red coloured, which was indicative of the partial internalisation of $\text{thym(AZO-NO}_2)$ into the self-assemblies. For $\text{PEG10k-b-PDAP}\cdot\text{thym(Naph)}$, a colourless solution was obtained that became fluorescent under 365 nm light, which was also an evidence of the presence of thym(Naph) in the self-assembled structures (Figure 3.24). In both cases, spherical micelles of around 40 nm of diameter were obtained according to DLS and TEM observations (Figure 3.25).

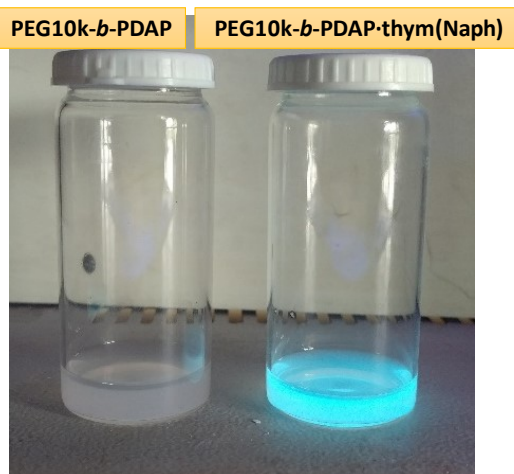


Figure 3.24. PEG10k-b-PDAP and PEG10k-b-PDAP·thym(Naph) nanostructures illuminated at 365 nm light

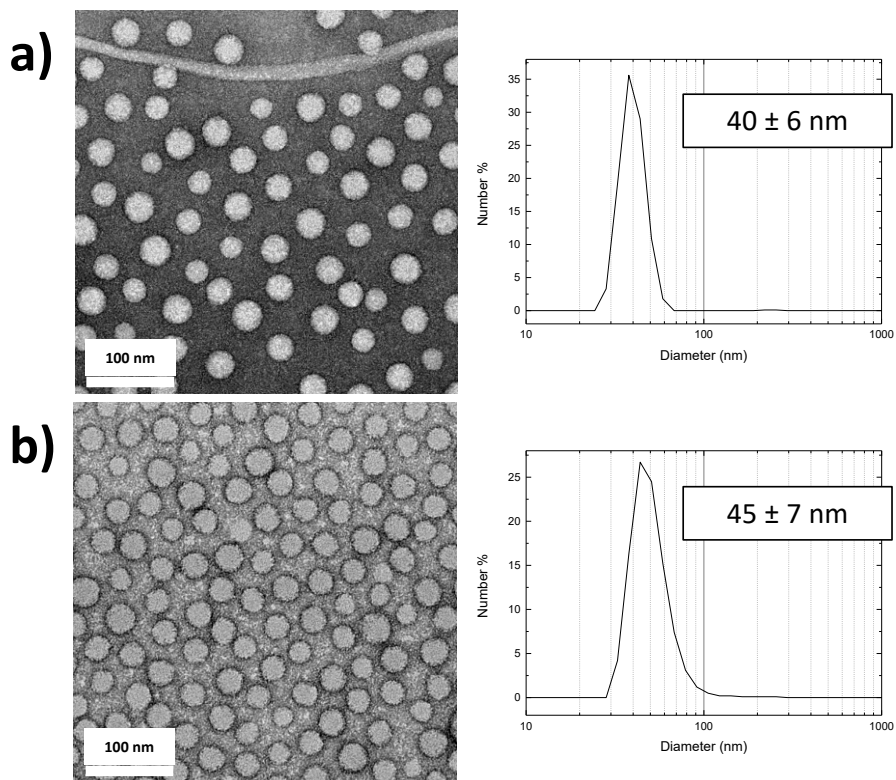


Figure 3.25. Representative TEM images and DLS distributions of the resulting water solution of a) PEG10k-b-PDAP·thym(AZO-NO₂) and b) PEG10k-b-PDAP·thym(Naph) micelles after dialysis and filtration of the precipitate (see above)

With the aim of avoiding the partial precipitation of thymines, supramolecular BCs from **PEG10k-b-PDAP** and **thym(AZO-NO₂)** were prepared using a 1:0.5

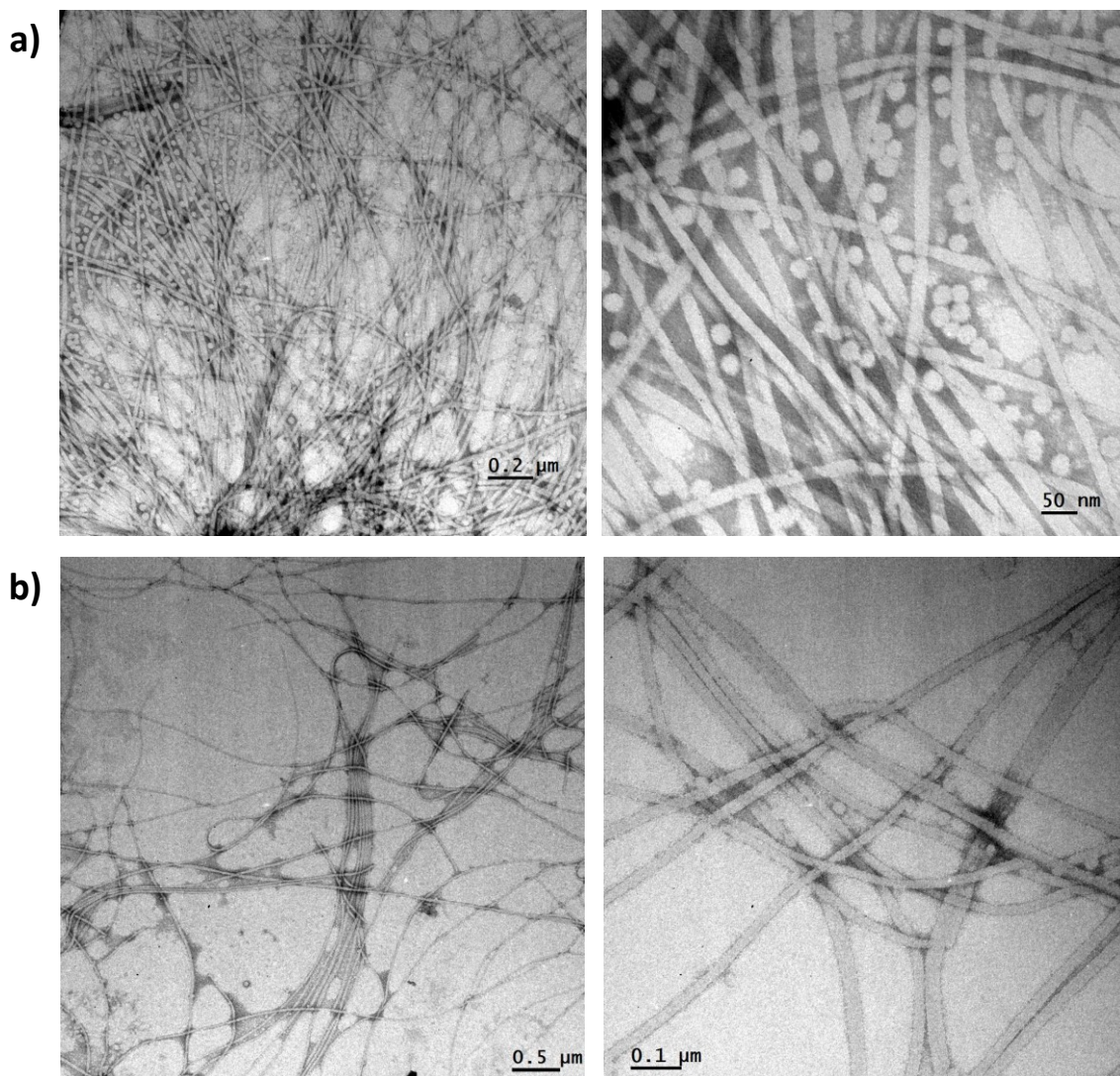


Figure 3.27. Representative TEM images of
a) PEG10k-b-PDAP·thym(AZO-NO₂)_{50%} micelles and fibrillar structures in water and b) PEG2k-b-PDAP·thym(AZO-NO₂)_{50%} micelles and fibrillar structures in water

With the aim of discarding that both **PEG10k-b-PDAP**, or **PEG2k-b-PDAP**, and **thym(AZO-NO₂)** were separately self-assembled yielding spherical micelles and fibrillar structures respectively, a last experiment was performed. **Thym(AZO-NO₂)** alone was attempted to be self-assembled in water but a precipitate was obtained that, after filtration, led to a colourless solution. Consequently, the nanostructures observed by TEM seem to correspond to the self-assembly of the supramolecular BCs, and the inclusion of **thym(AZO-NO₂)** has an effect in the hydrophobic/hydrophilic balance and the morphology of the self-assemblies.

3.3. LIGHT RESPONSIVENESS

3.3.1. STUDY OF THE PHOTORESPONSE OF PEG5k-*b*-p(AZO-NAPH)

Irradiation experiments were first carried out in THF solution in order to gain information about the azobenzene isomerisation. One-photon studies were performed as a preliminary study of the possible two-photon irradiation of these materials, that requires of a high intensity pulsed laser. For this purpose, the photoresponse was evaluated at 365 nm (excitation of naphthalene) and 420 nm (direct excitation of azobenzene).

UV-Vis spectrum of **PEG5k-*b*-p(AZO-Naph)** in THF was registered and a maximum at 418 nm was found, that fits with the π - π^* azobenzene band. Shoulders at low wavelengths *ca.* 360 nm were observed, that corresponds with the naphthalene unit.¹ When 365 nm light was used, expecting an antenna effect from the naphthalene that might cause the azobenzene to isomerise, almost no changes were observed (**Figure 3.28a**). Therefore, there seems to be no antenna effect or the photoisomerisation is very slow under these conditions. When this solution was irradiated using a 420 nm LED light source (**Figure 3.28b**), a photostationary state was reached only after 5 s, in which a decrease of azobenzene main band was observed together the shifting of the maximum to 455 nm due to *trans* to *cis* isomerisation. Furthermore, absorption increased above 490 nm where an isosbestic point could be found. The *cis* azobenzene fast reversed to *trans* isomer in the dark, which is a characteristic of these systems.

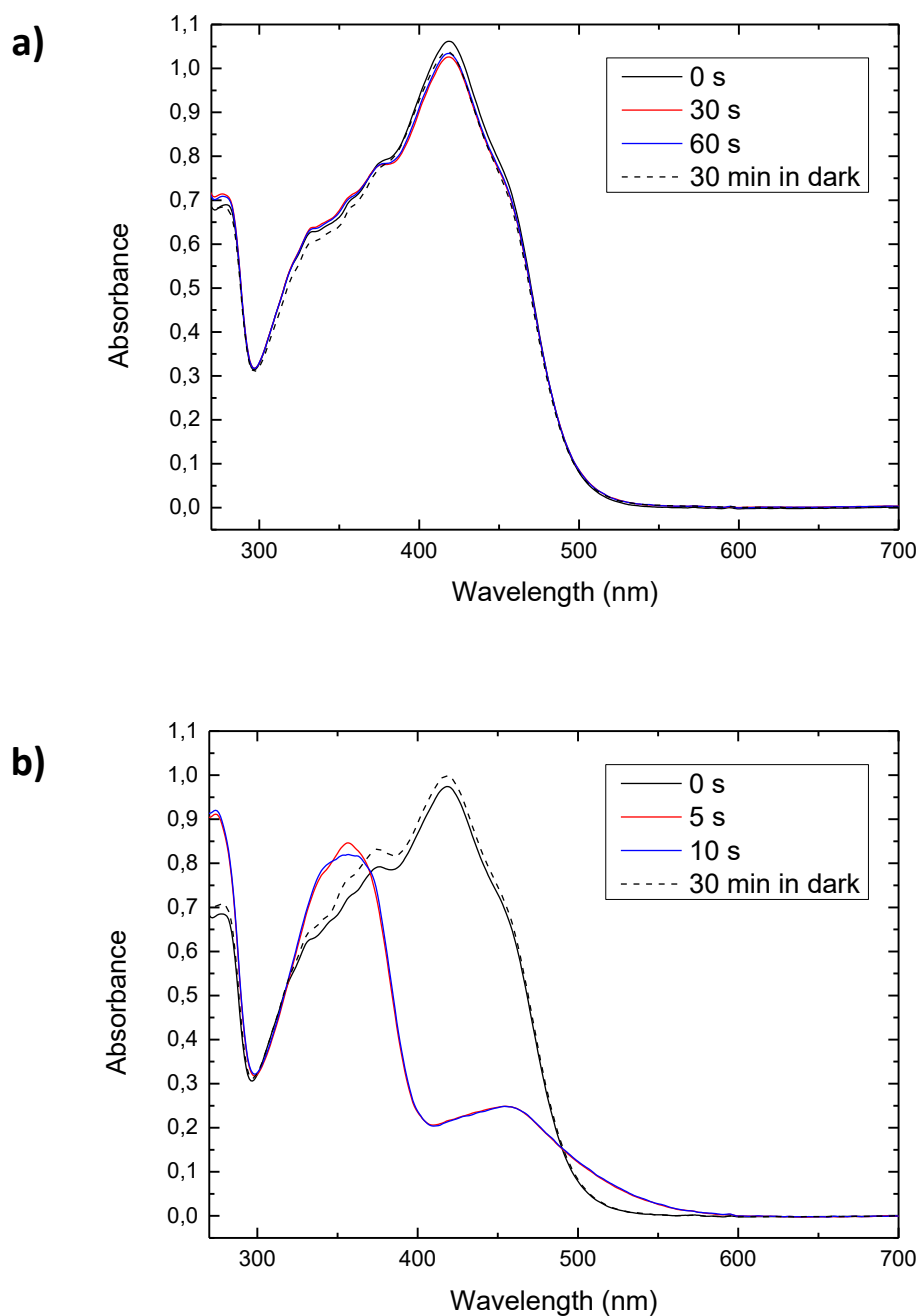


Figure 3.28. UV-Vis spectra of PEG5k-b-p(AZO-Naph) in THF solution (1 mg/mL) registered upon (a) 365 nm and (b) 420 nm light irradiation and storing in the dark

Micelles aqueous dispersions of **PEG5k-b-p(AZO-Naph)** were then irradiated either at 365 nm (excitation of naphthalene) or at 420 nm (direct excitation of azobenzene) (**Figure 3.29**). Before irradiation, the UV-vis spectrum presented a

less resolved broad band when compared to THF solution with a maximum at 382 nm and a shoulder at *ca.* 420 that could fit with azobenzene maximum found in THF solution. Contrary to what happens in solution, similar changes on the UV-vis spectra were observed upon irradiation both at 365 and 420 nm, being changes slightly more pronounced when micelles were irradiated at 420 nm. A decrease in the absorbance at 420 nm together with a slight increase at *ca.* 550 nm were evident after a few seconds, which likely might be due to *trans* to *cis* photoisomerisation of azobenzene. The fact that isomerisation was also observable under 365 nm irradiation, unlike what was observed in solution, might indicate that the antenna effect is assisted by locating azobenzene and naphthalene in a confined space. In spite of this, morphological changes were not observed in TEM images or DLS with micelles of approx. 22 nm of diameter still visible. This could be due to an insufficient change in polarity provoked by the photoisomerisation that was not able to induce morphological changes.

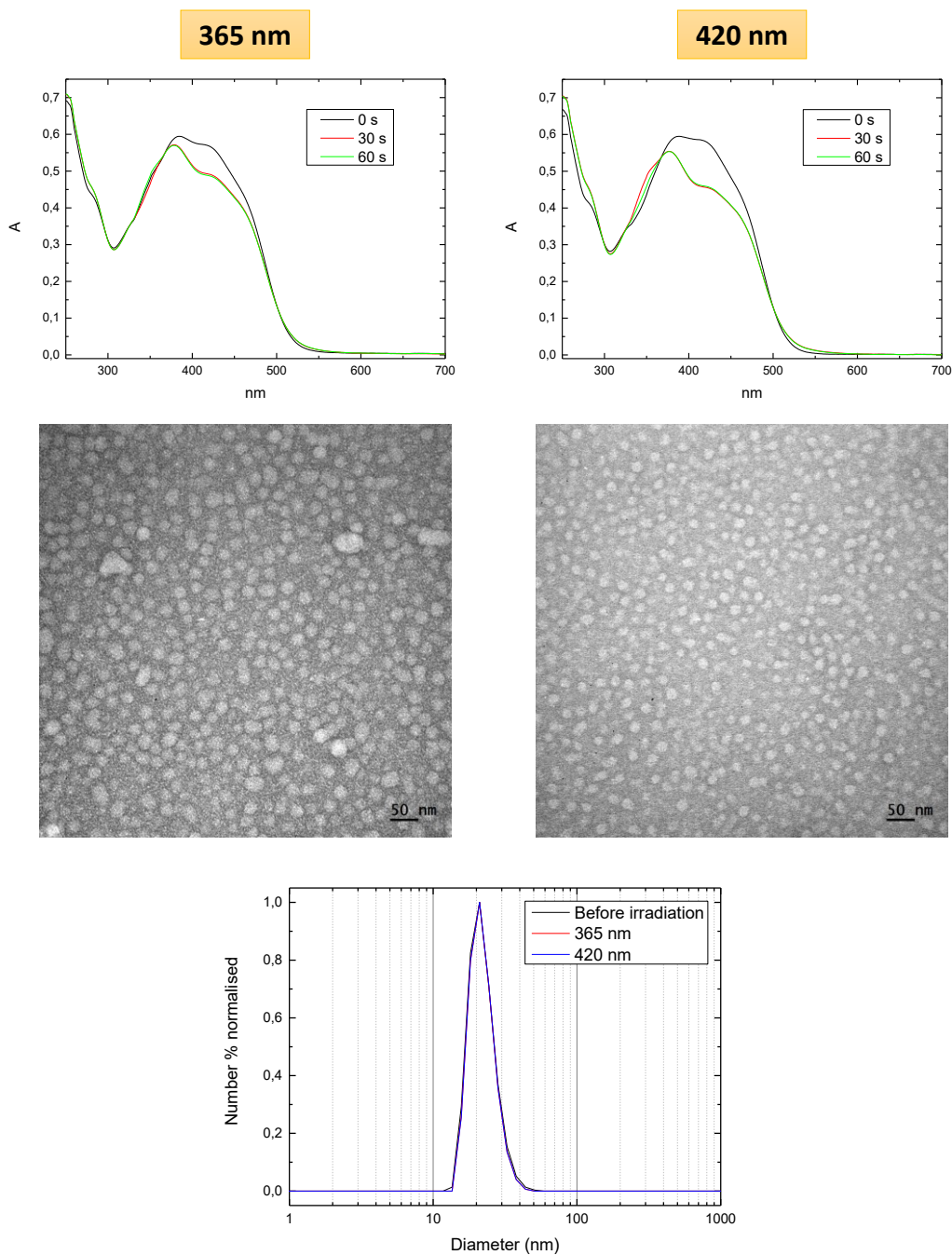


Figure 3.29. Photoresponse studies for PEG5k-b-p(AZO-Naph)

Nile Red was loaded into the **PEG5k-b-p(AZO-Naph)** micelles, which were then illuminated at 420 nm since isomerisation seemed to be slightly larger than at 365 nm. After 10 s, the initial Nile Red emission had almost disappeared (**Figure 3.30**), although this fluorescence was recovered after 24 h, which could be indicative that Nile Red was not released. However, the decrease of Nile Red fluorescence was indicative that some changes were produced in micelles upon

light illumination, mainly associated to the polarity changes by *trans* to *cis* isomerisation.

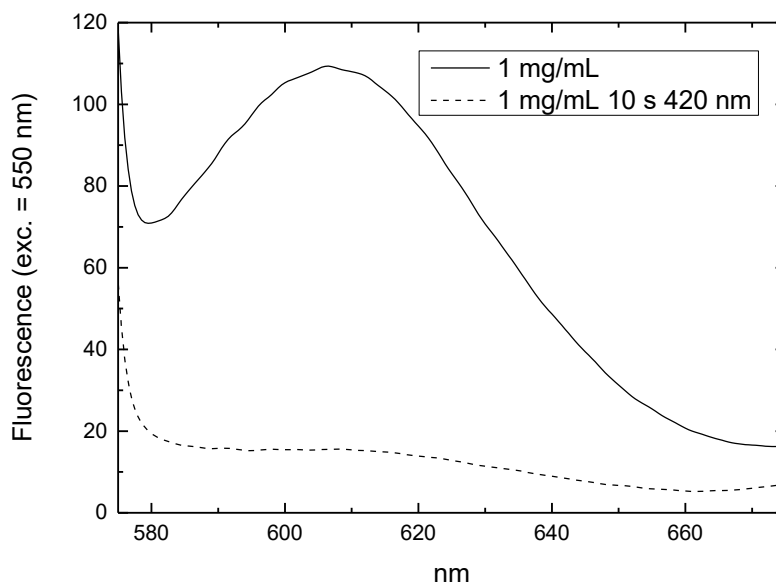


Figure 3.30. Fluorescence spectra ($\lambda_{exc} = 550 \text{ nm}$) of Nile Red loaded micelles of **PEG5k-b-p(AZO-Naph)** before and after 10 s of irradiation with 420 nm light

3.3.2. STUDY OF THE PHOTORESPONSE OF AZO-NO₂/NAPH BCs

Irradiation experiments with **AZO-NO₂/Naph** BCs were carried out in THF solution at 365 and 420 nm irradiation (indirect and direct azobenzene excitation, respectively). Additionally, samples were also irradiated at 530 nm, because **AZO-NO₂** has a significant absorption at this wavelength.

Before irradiation, **p(AZO-NO₂)** block absorption was evaluated registering **PEG2k-b-p(AZO-NO₂)** in THF solution as a model and the maximum was located at 465 nm. However, after several minutes of irradiation no photoisomerisation was detected at any of these three wavelengths, probably because the life time of *cis* state in solution for this chromophore is in the scale on nanoseconds, which is characteristic of push-pull azobenzenes, making difficult to detect it.¹⁰ Spectra at different times of irradiation with 420 nm light are shown in **Figure 3.31** as an example.

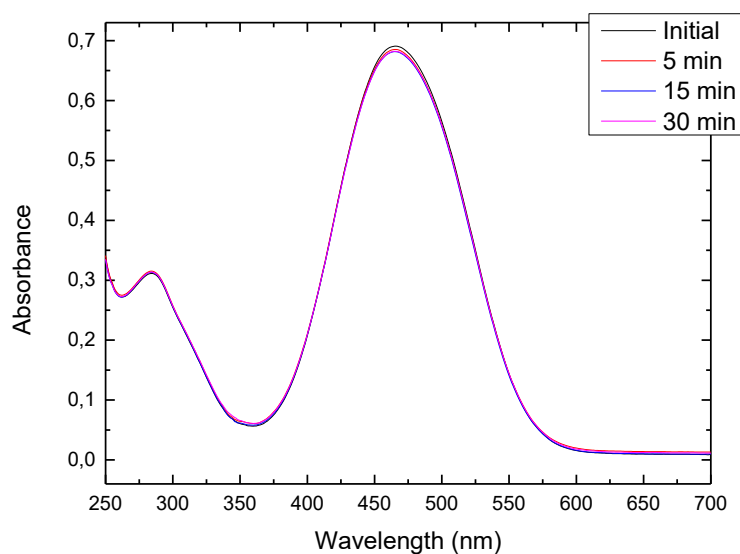


Figure 3.31. UV-Vis spectra of PEG2k-b-p(AZO-NO₂) in THF solution (0.25 mg/mL) after different times of irradiation with 420 nm light

p(AZO-NO₂/Naph) block absorption was also evaluated in THF solution, using PEG2k-b-p(AZO-NO₂/Naph) as a model. The UV-Vis spectra at different times of irradiation were registered. Before irradiation, a maximum was located at ca. 465 nm that corresponds with AZO-NO₂ and a small band at 350 nm, not present in PEG2k-b-p(AZO-NO₂), which corresponds with the naphthalene. As in PEG2k-b-p(AZO-NO₂), the photoisomerisation was not observed after irradiation with any wavelength. In Figure 3.32, UV-Vis spectra registered at different times of irradiation with 420 nm light are shown as an example.

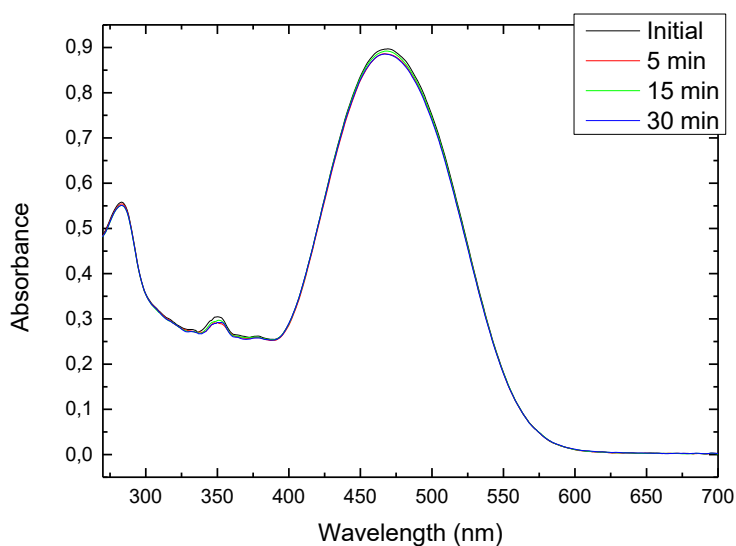


Figure 3.32. UV-Vis spectra of PEG2k-b-p(AZO-NO₂/Naph) in THF solution (0.3 mg/mL) after different times of irradiation with 420 nm light

Self-assembled BCs were evaluated upon the same wavelengths that THF solutions. The photoresponse of the micelles obtained from BCs with **PEG10k** were first studied by irradiating aqueous dispersion of the self-assemblies for different time intervals. Before irradiation, micellar water solutions of **PEG10k-b-p(AZO-NO₂)** showed similar UV-Vis spectrum to that of the BC in THF solution (**Figure 3.33**). When samples were irradiated at 365 or 530 nm almost no modification on the position or the intensity of the main band was observed. However, after 420 nm irradiation a remarkable absorbance decrease at the π - π^* transition of the *trans* isomer together with an absorbance increase at *ca.* 350 nm was observed. Besides, a slight absorbance increase at about 600 nm with an isosbestic point at 586 nm was observed that can be indicative of *trans* to *cis* isomerisation of azobenzene. These spectral changes associated to *trans* to *cis* isomerisation of the azobenzene were not observed in solution. In this case spectral changes due to photoisomerisation might be due to the confinement of the azobenzenes into the vesicle membrane that hinders the back isomerisation thus increasing the lifetime of the *cis* isomer. However, the absence of spectral changes when samples were irradiated at 365 or 530 nm, seems to suggest that *trans* to *cis* isomerisation does not occur under these conditions. The irradiated samples at

420 were studied by TEM, but no clear changes were observed for the micellar morphology, although some modifications were occasionally detected after 420 nm, when micelles appeared to be deformed. Furthermore, by irradiating at 530 nm some amorphous material appeared on the TEM grid although no changes in UV-Vis spectra were detected. In DLS, a shift to minor diameter was observed after 420 nm, which was in concordance with the UV-Vis spectra and TEM images.

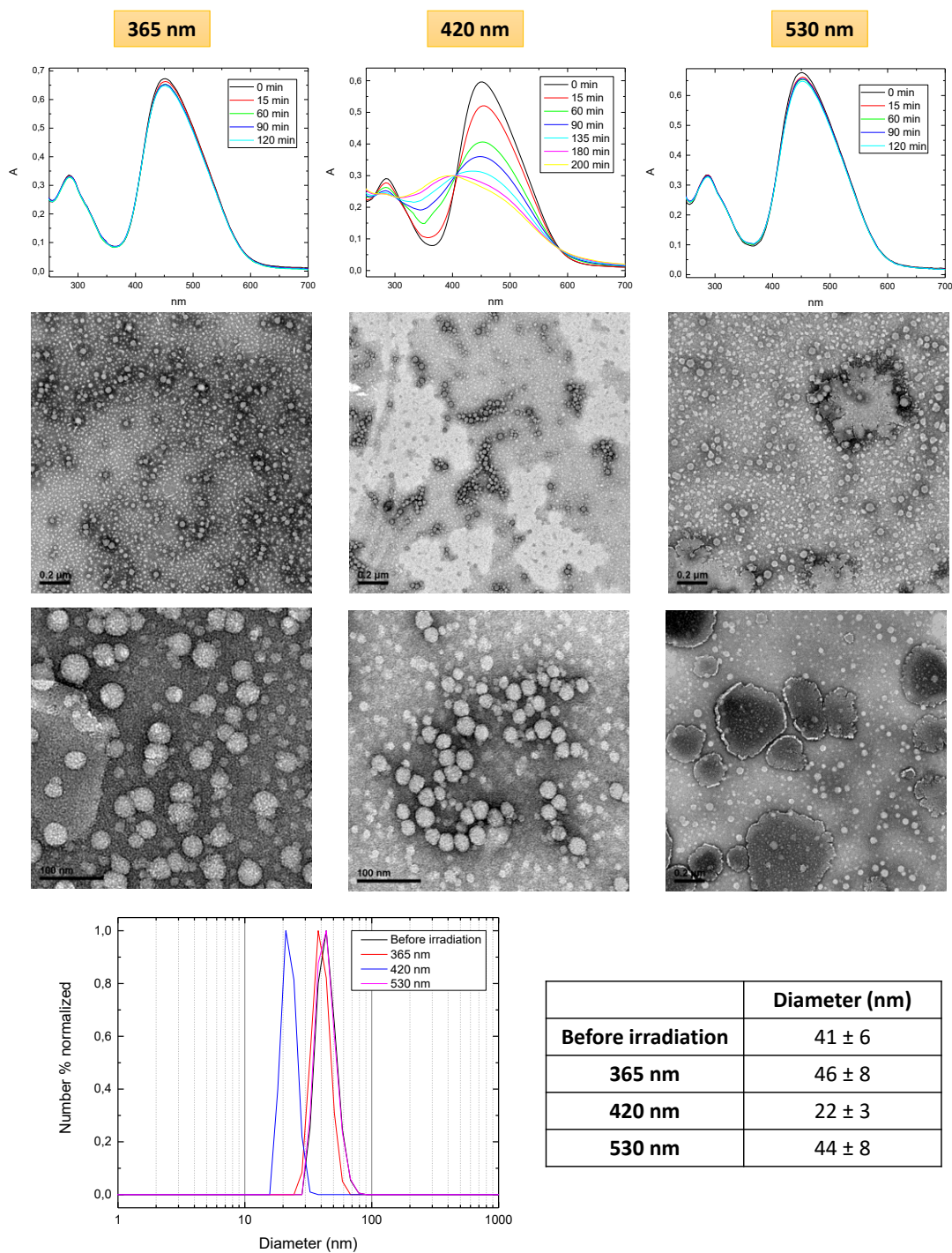


Figure 3.33. Photoresponse studies for PEG10k-b-p(AZO-NO₂)

Micelles of **PEG10k-b-p(AZO-NO₂/Naph)** were also investigated (**Figure 3.34**). Before irradiation, UV-Vis showed a broad band with two maxima, one at 462 nm (that corresponds with azobenzene) and another band at ca. 360 nm (that corresponds to naphthalene). Under light exposure at 365 or 530 nm almost no

changes were observable in UV-Vis spectra. However, using 420 nm light a decrease in the maximum of the AZO-NO₂ band together with an increase of absorption around 350 nm were evident and the presence of an isosbestic point at 590 nm. In all cases, micelles were still visible in TEM images, although some modifications similar to those of **PEG10k-*b*-p(AZO-NO₂)** after 420 and 530 nm irradiation were observed. Again, a shift to minor diameters was also observed in DLS after 420 nm irradiation.

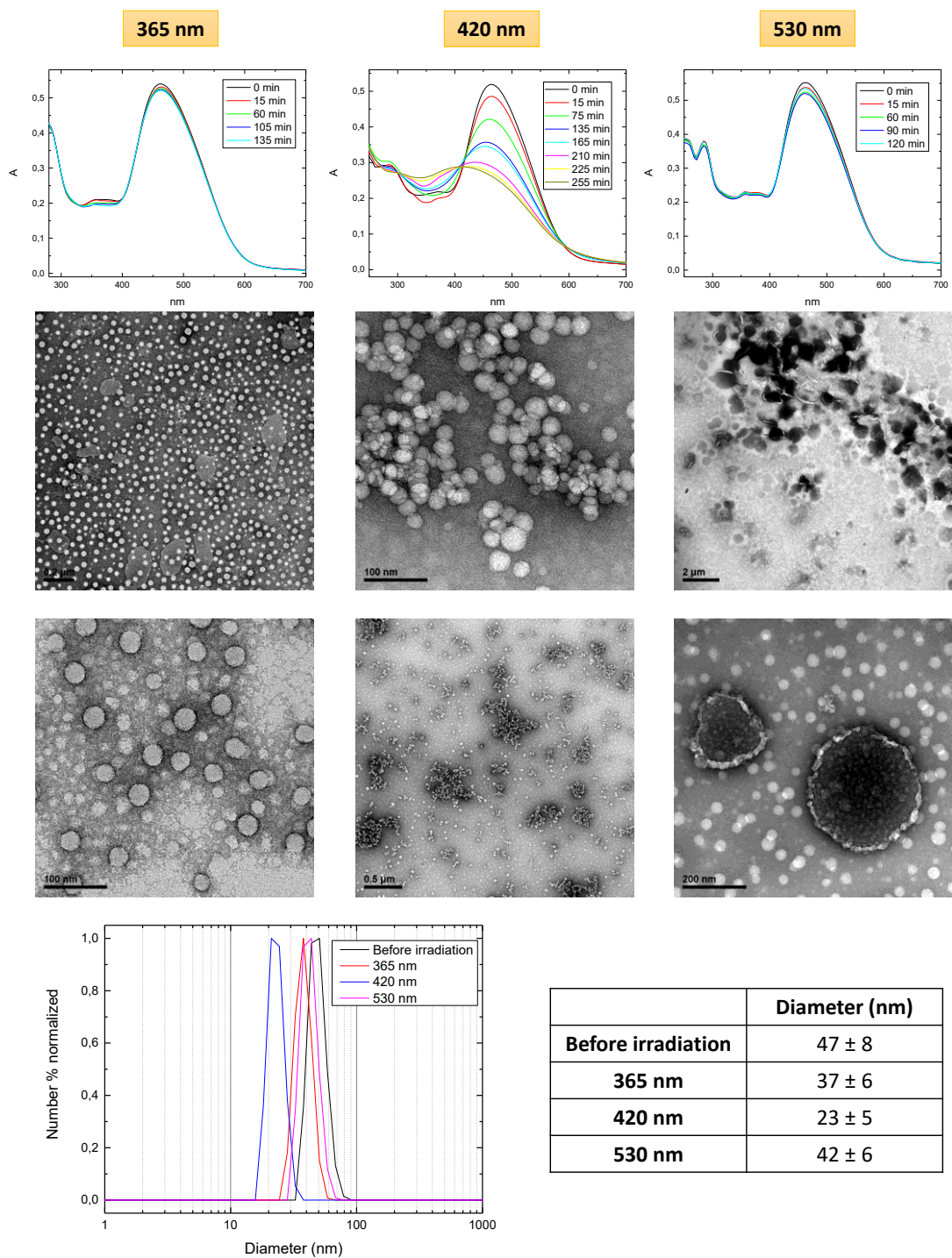


Figure 3.34. Photoresponse studies for PEG10k-b-p(AZO-NO₂/Naph)

In this case, Nile Red was not encapsulated since it presents overlapping problems, as it presented in **Chapter 2**. Consequently the use of Nile Red as a fluorescent probe for controlled release could not be performed.

Then, vesicles dispersions of **PEG2k** series were evaluated. For the aqueous dispersion of **PEG2k-*b*-p(AZO-NO₂)** vesicles, a broad band having an ill-defined maximum at *ca.* 500 nm was recorded by UV-vis as well as a large light scattering (**Figure 3.35**). A minor decrease of the main absorption band was registered after irradiation at 365 nm. The decrease was more significant upon irradiation at 420 and 530 nm, in particular at 420 nm. Irradiated samples were studied by TEM and DLS. In the three cases, vesicles together with amorphous material were observed in TEM photographs in comparison with non-irradiated samples. In DLS, a shift to minor diameters was registered after irradiation with the three wavelengths which might be indicative of changes on the vesicles morphology.

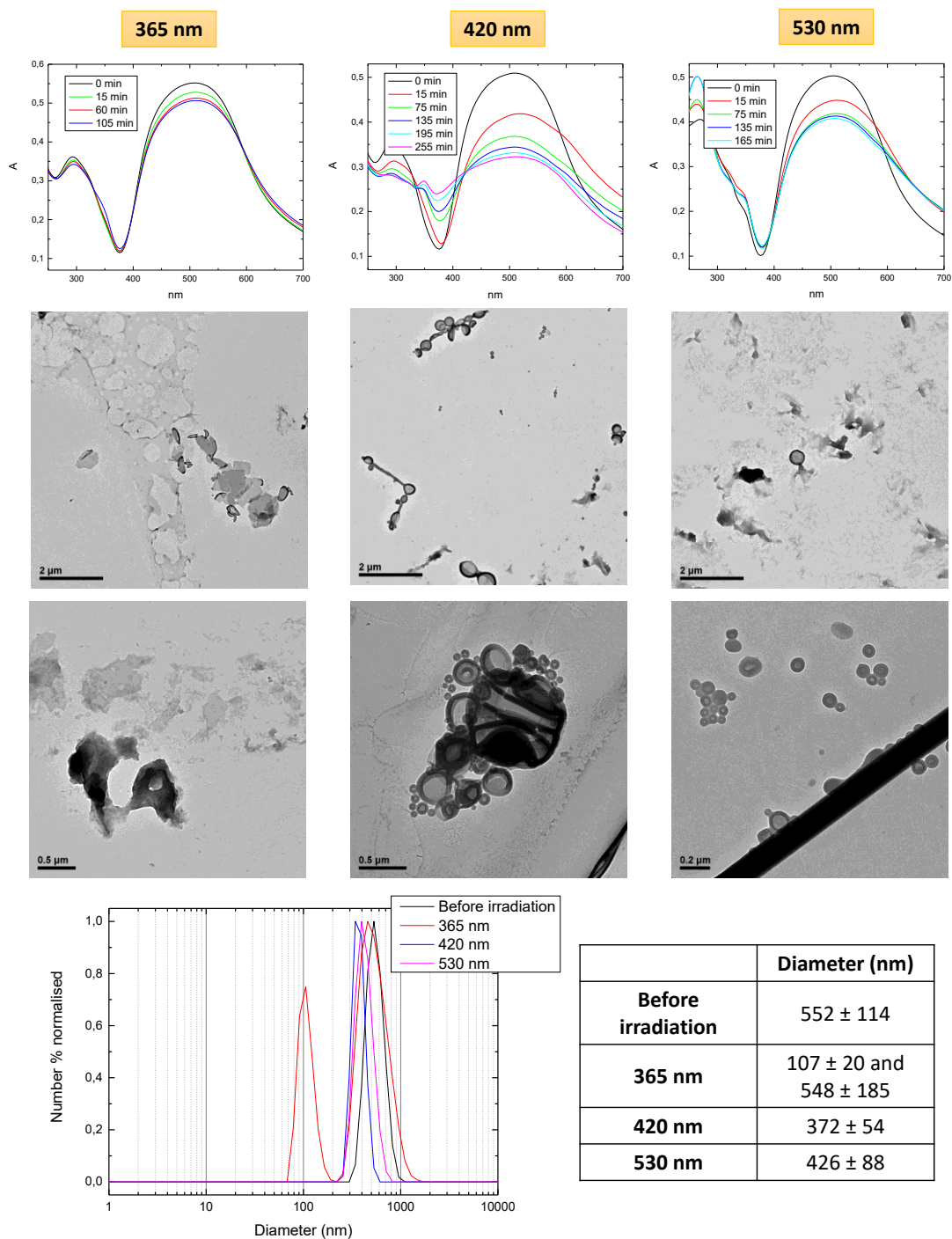


Figure 3.35. Photoresponse studies for vesicles derived from *PEG2k-b-p(AZO-NO₂)*

For **PEG2k-b-p(AZO-NO₂/Naph)** similar UV-vis spectral variations were observed when compared to **PEG10k-b-p(AZO-NO₂/Naph)**. The initial spectrum of the vesicles in water (before irradiation) was similar to that of THF solution (**Figure 3.36**). The absorption band corresponding to the **AZO-NO₂** chromophore was

centred at approx. 482 nm and some absorption registered in the 360 nm zone and associated to naphthalene. Minor modifications in the UV-Vis spectra were registered when irradiating with 365 and 530 nm light. However, an evident decrease of azobenzene band was visible after 420 nm illumination.

TEM inspection of the irradiated samples showed no appreciable morphological changes after 365 and 530 nm irradiation but under 420 nm irradiation a smaller number of vesicles together with amorphous material were observed in comparison with non-irradiated sample. DLS measurements indicated slight changes on average hydrodynamic diameters (D_h) and sizes distributions for 420 and 520 nm irradiation, but not for 365 nm irradiation in which DLS distribution kept almost the same. A diameter decrease of approx. 140 nm was determined after 420 nm irradiation, which was in concordance with TEM modifications. After 530 nm irradiation, a decrease of 174 nm was registered, which suggested that some modifications occurred even if they were not observed in TEM images.

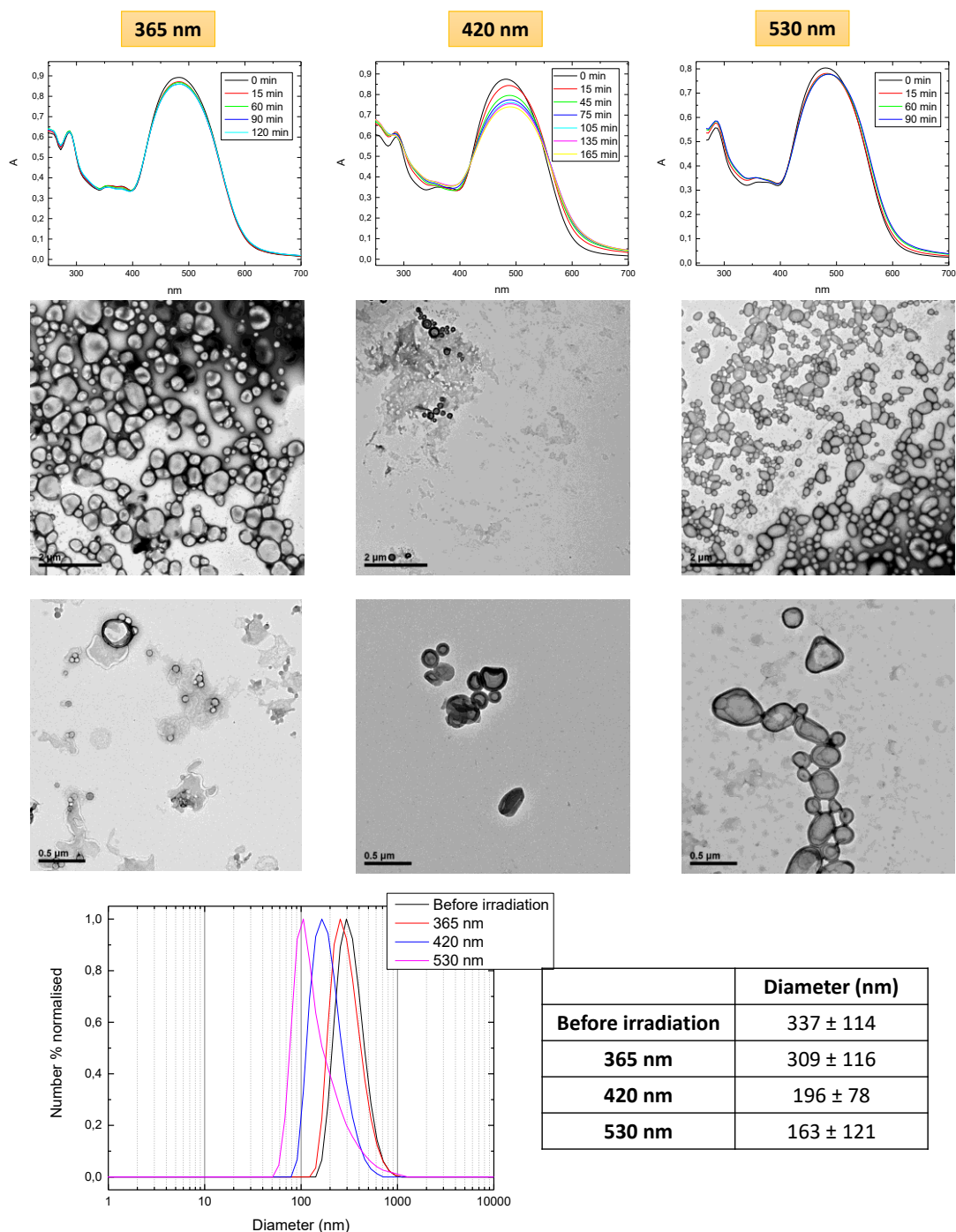


Figure 3.36. Photoresponse studies for *PEG2k-b-p(AZO-NO₂/Naph)*

As a model of hydrophilic compound, the encapsulation and light stimulated release of Rhodamine B (RhB) was studied with vesicles from **PEG2k-b-p(AZO-NO₂)** and **PEG2k-b-p(AZO-NO₂/Naph)**. As in **Chapter 2**, vesicles were formed in the presence of RhB. Non-encapsulated RhB was removed by dialysis against water by refreshing the dialysis water until was finally colourless.

Once RhB was encapsulated within the aqueous hollow cavity of **PEG2k-*b*-p(AZO-NO₂)** vesicles, three aliquots were separated so that one (aliquot 1) was kept in dark and used as blank while the other two were irradiated for 1 h with 420 nm light (aliquot 2) and with 530 nm (aliquot 3), because significant modifications in UV-Vis spectra were observed only for these wavelengths. To evaluate the RhB release, all the three samples were dialysed in small vials against water and the dialysis water inspected after 14 h. The dialysis medium of the reference aliquot kept in dark was colourless at the naked eye meanwhile the other two (dialysis medium from aliquots irradiated at 420 or 530 nm) were slightly pink. The presence of RhB in the dialysis medium was determined by fluorescence spectroscopy as shown in **Figure 3.37a**. Even if some RhB was released by physical diffusion, RhB release was clearly triggered by light mostly under 420 nm light than under 530 nm. Similar results and conclusions were drawn for **PEG2k-*b*-p(AZO-NO₂/Naph)** under the same set of experiments (**Figure 3.37b**).

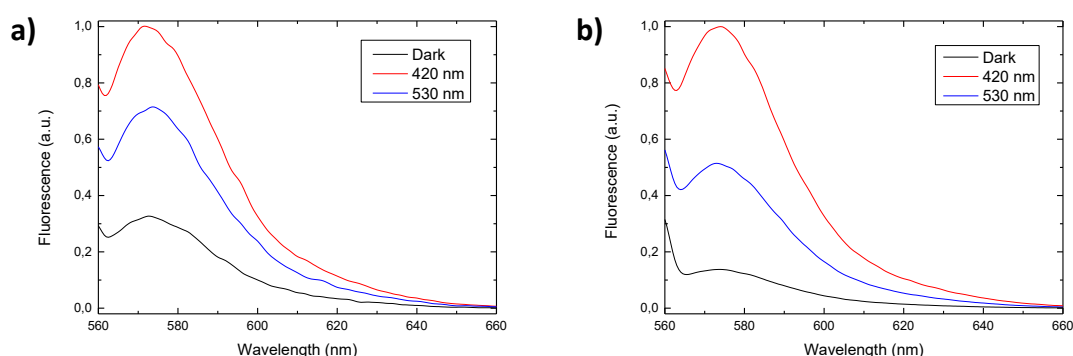


Figure 3.37. Fluorescence spectra ($\lambda_{exc} = 553 \text{ nm}$) of the dialysis water of RhB loaded vesicles of a) **PEG2k-*b*-p(AZO-NO₂)** and b) **PEG2k-*b*-p(AZO-NO₂/Naph)** under light irradiation with 420 and 530 nm

In view of these experiments it can be deduced that only when the azobenzene is directly irradiated is possible to stimulate its photoisomerisation and modification of the vesicles with concurrent release of the fluorescent probe. Accordingly, light of 420 nm is more efficient for the photostimulated release process as it better matches the maximum of the **AZO-NO₂** absorption band while the introduction of naphthalene did not seem to improve the light response of the materials.

3.4. CONCLUSIONS

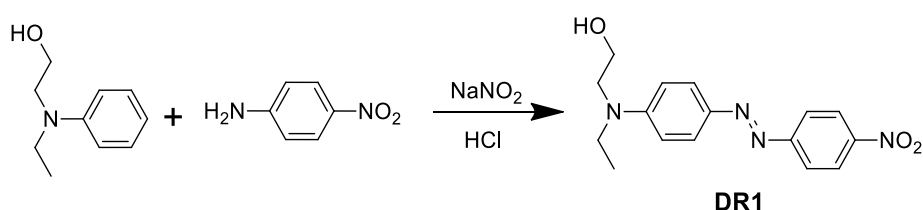
Summary and conclusions of this work are the following:

- The synthesis of BCs based on PEG as hydrophilic block and a polymethacrylic block with pendant azobenzene and/or naphthalene units, has been approached by RAFT polymerisation. On one hand, a bichromophoric moiety simultaneously containing an azobenzene and a naphthalene derivative (**AZO-Naph**) was attached to the polymeric structure. On the other hand, homo and block copolymers containing an **AZO-NO₂** and/or naphthalene units attached to the polymeric structure
- The self-assembly properties of the BCs in water, as selective solvent, were studied. Either stable micelle or vesicle solutions were obtained depending on the composition of the BCs, in particular when covalent BCs were used.
- Supramolecular chemistry has been proved as an alternative to covalent chemistry in the preparation of BCs, allowing the preparation of several polymers starting from a unique one containing DAP acting as scaffold after the complexation with different thymine units. These supramolecular were self-assembled and stable dispersions were obtained under some conditions, although the obtained structures were not of interest to our goals.
- The response of micelles and vesicles, self-assembled from covalent BCs, to different wavelengths of UV-Vis spectrum has been evaluated. Specifically, good results were observed after direct irradiation with visible light at 420 and 530 nm wavelengths, especially at 420 nm, that affected directly to azobenzene moieties. On the other hand, the inclusion of naphthalene did not provide of a good photoresponse using UV light.
- Encapsulation and controlled release experiments have been performed, showing the potential of these systems as drug nanocarriers. RhB was encapsulated into polymeric vesicles and released after irradiation at 420 and 530 nm.

3.5. EXPERIMENTAL SECTION

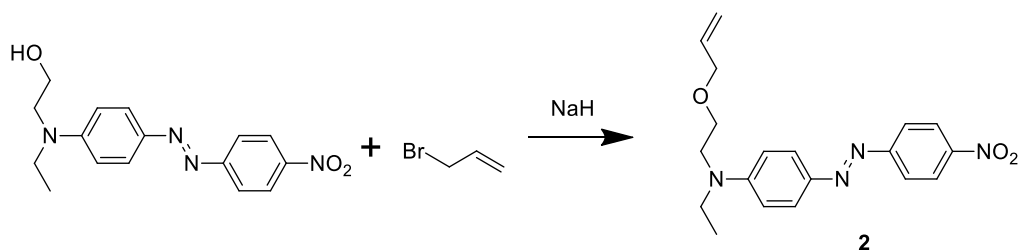
3.5.1. SYNTHESIS AND CHEMICAL CHARACTERISATION

Synthesis of 2-(ethyl(4-((4-nitrophenyl)diazenyl)phenyl)amino)ethanol (AZO-NO₂)



p-Nitroaniline (10.00 g, 72 mmol) was dissolved in 12% HCl (160 mL) and the solution cooled down below 5°C. Then, NaNO₂ (4.50 g, 74 mmol) dissolved in distilled water (50 mL) was added dropwise while temperature was kept below 5°C. After 30 min stirring, 2-(ethylphenylamino)ethanol (11.88 g, 74 mmol) in NaOH 2M (50 mL) was added and the mixture stirred at room temperature for 1 h. NaHCO₃ was added until reaching neutral pH. Finally, the obtained solid was filtered and washed with hexane to yield a red powder. Yield: 97%. ¹H NMR (400 MHz, CDCl₃) δ 8.34 – 8.28 (m, 2H), 7.97 – 7.91 (m, 4H), 6.89 – 6.72 (m, 2H), 3.90 (t, *J* = 5.8 Hz, 2H), 3.63 (t, *J* = 5.9 Hz, 2H), 3.58 (q, *J* = 7.1 Hz, 2H), 1.26 (t, *J* = 7.1 Hz, 3H).

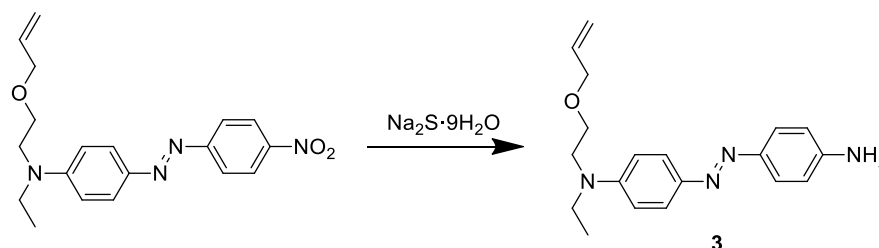
Synthesis of *N*-(2-(allyloxy)ethyl)-*N*-ethyl-4-((4-nitrophenyl)diazenyl)aniline (2)



NaH (60% dispersion in mineral oil, 840 mg, 35.1 mmol) was added to a solution of **AZO-NO₂** (5 g, 16 mmol) in anhydrous DMF (50 mL), the reaction was stirred for 5 min and then allyl bromide (2.8 mL, 33.4 mmol) was added dropwise. The reaction was carried out at room temperature and followed by TLC until was

completed. Then, the reaction was quenched with saturated NH_4Cl (50 mL). Aqueous phase was extracted with ethyl acetate, and combined organic layers were washed with brine and dried with anhydrous MgSO_4 . The solution was filtered and concentrated under vacuum. The crude was purified by column chromatography using silica gel and hexane/ethyl acetate (1/1) as eluent to obtain the product as a red solid. Yield: 97%. ^1H NMR (400 MHz, CDCl_3) δ 8.35 – 8.27 (m, 2H), 7.96 – 7.84 (m, 4H), 6.81 – 6.73 (m, 2H), 5.90 (ddt, $J = 17.2, 10.4, 5.5$ Hz, 1H), 5.28 (ddt, $J = 17.2, 3.7, 1.6$ Hz, 1H), 5.19 (ddt, $J = 10.4, 3.4, 1.4$ Hz, 1H), 4.01 (ddd, $J = 5.5, 1.4, 1.4$ Hz, 2H), 3.70 – 3.61 (m, 4H), 3.56 (q, $J = 7.1$ Hz, 2H), 1.25 (t, $J = 7.1$ Hz, 3H). ^{13}C NMR (100 MHz, CDCl_3): δ 156.9, 151.6, 147.4, 143.7, 134.5, 126.4, 124.8, 122.7, 117.3, 111.4, 72.4, 67.8, 50.4, 46.1, 12.3.

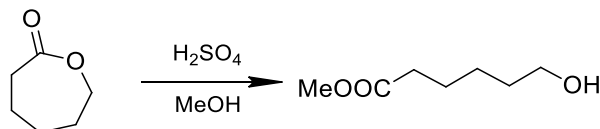
Synthesis of *N*-(2-(allyloxy)ethyl)-4-((4-aminophenyl)diazenyl)-*N*-ethylaniline (3)



2 (5.28 g, 15.1 mmol) was dissolved in a 7:3 degassed mixture of dioxane and water (160 mL) under Ar atmosphere. The reaction was heated to 90°C and sodium sulphide (6.00 g, 25.4 mmol) was added portion-wise over 30 min. The reaction was followed by TLC (ethyl acetate) and once the reaction was completed, it was poured into a saturated aqueous solution of NaHCO_3 . The reaction was extracted with DCM (3 x 100 mL) and the combined organic layers were washed with brine, dried over MgSO_4 filtered and evaporated under vacuum. The residue was purified by silica column chromatography using hexane/ethyl acetate 3/1 as eluent to give an orange powder. Yield: 92%. ^1H NMR (400 MHz, CDCl_3): δ 7.87 – 7.51 (m, 4H), 6.99 – 6.64 (m, 4H), 5.91 (ddt, $J = 17.2, 10.4, 5.5$ Hz, 1H), 5.28 (ddt, $J = 17.2, 3.7, 1.6$ Hz, 1H), 5.19 (ddt, $J = 10.4, 3.4, 1.4$ Hz, 1H), 4.01 (ddd, $J = 5.5, 1.4, 1.4$ Hz, 2H), 3.70 – 3.61 (m, 4H), 3.50 (q, $J = 7.1$ Hz, 2H), 1.21 (t, $J = 7.1$ Hz, 3H); ^{13}C NMR

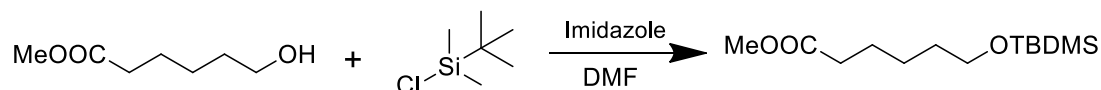
(100 MHz, CDCl₃): δ 149.5, 148.2, 146.2, 143.7, 134.7, 124.6, 124.2, 117.2, 115.0, 111.4, 72.4, 67.9, 50.4, 45.9, 12.4.

Synthesis of methyl 6-hydroxyhexanoate



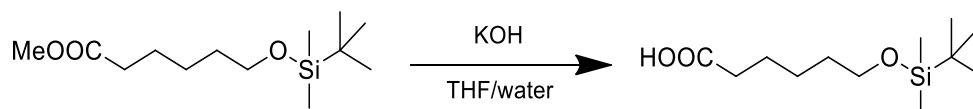
Caprolactone (4.00 g, 35 mmol) was dissolved in a mixture of H₂SO₄ (50 mL) and MeOH (200 mL), and the reaction was allowed to proceed during 14 h at reflux. Then, MeOH was partially evaporated under vacuum, distilled water (200 mL) was added, and the mixture extracted with DCM (3x150 mL). Combined organic phases were washed with brine, dried over anhydrous MgSO₄, filtered and concentrated under vacuum, obtaining the desired product as a colourless oil. Yield: 76%. ¹H NMR (300 MHz, DMSO) δ 4.33 (t, *J* = 5.1 Hz, 1H), 3.58 (s, 3H), 3.37 (dt, *J* = 11.8, *J* = 6.1 Hz, 2H), 2.28 (t, *J* = 7.4 Hz, 2H), 1.61 – 1.45 (m, 2H), 1.45 – 1.34 (m, 2H), 1.34 – 1.21 (m, 2H).

Synthesis of methyl 6-((*tert*-butyldimethylsilyl)oxy)hexanoate



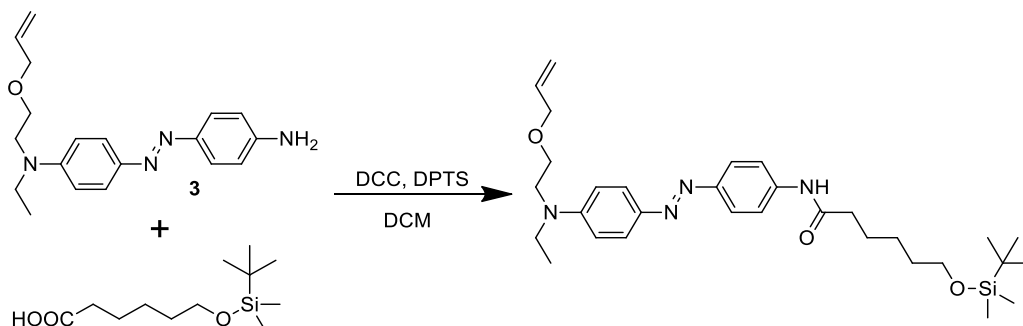
Methyl 6-hydroxyhexanoate (3.00 g, 20.5 mmol), imidazole (2.70 g, 41 mmol) and *tert*-butylchlorodimethylsilane (3.10 g, 20.5 mmol) were dissolved in dried DMF (7 mL). The reaction was carried out at room temperature during 14 h. Then, organic phase was extracted with DCM (3x100 mL), and washed with HCl 1M (1x100 mL), saturated NaHCO₃ (1x100 mL) and brine. The organic solution was dried over anhydrous MgSO₄, filtered and concentrated under vacuum to isolate the desired product as a colourless oil. Yield: 98%: ¹H NMR (400 MHz, CDCl₃) δ 3.62 (s, 3H), 3.56 (t, *J* = 6.4 Hz, 2H), 2.27 (t, *J* = 7.5 Hz, 2H), 1.70 – 1.55 (m, 2H), 1.55 – 1.45 (m, 2H), 1.43 – 1.31 (m, 2H), 0.85 (s, 9H), 0.00 (s, 6H). ¹³C NMR (101 MHz, CDCl₃) δ 174.20, 62.99, 51.45, 34.15, 32.54, 26.02, 25.75, 25.52, 24.86, - 5.25.

Synthesis of 6-((*tert*-butyldimethylsilyl)oxy)hexanoic acid



6-((*tert*-butyldimethylsilyl)oxy)hexanoate (905 mg, 2.74 mmol) and NaOH 5M (0.56 mL, 2.8 mmol) were stirred in a mixture of THF/water/MeOH (2/1/2) (2 mL). Once the solution became homogeneous, it was neutralised with HCl 10% and extracted with DCM (3x50 mL). Then, the combined organic extracts were washed with brine, dried over anhydrous MgSO₄, filtered and concentrated under vacuum to render a colourless oil. Yield: 98%. ¹H NMR (300 MHz, CDCl₃) δ 3.63 (t, *J* = 6.4 Hz, 2H), 2.38 (t, *J* = 7.5 Hz, 2H), 1.77 – 1.62 (m, 2H), 1.62 – 1.49 (m, 2H), 1.49 – 1.36 (m, 2H), 0.91 (s, 9H), 0.06 (s, 6H). ¹³C NMR (75 MHz, CDCl₃) δ 179.74, 63.06, 34.14, 32.56, 26.11, 25.50, 24.65, 18.50, - 5.14.

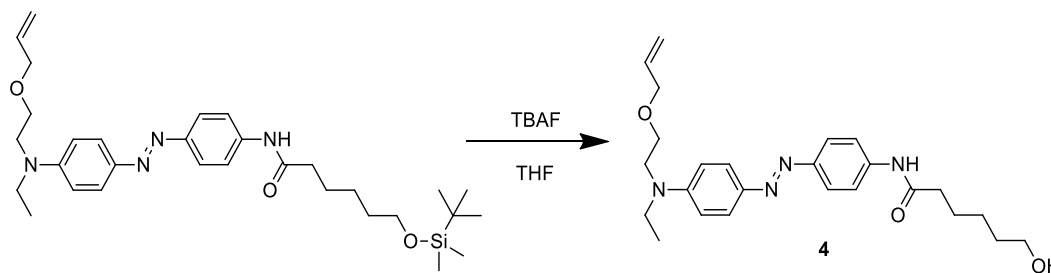
Synthesis of *N*-(4-((4-((2-(allyloxy)ethyl) (ethyl)amino)phenyl)diazenyl)phenyl)-6-((*tert*-butyldimethylsilyl)oxy)hexanamide



Compound **3** (500 mg, 1.54 mmol), 6-((*tert*-butyldimethylsilyl)oxy)hexanoic acid (455 mg, 1.85 mmol) and DPTS (240 mg, 0.77 mmol) were dissolved in DCM (10 mL) and the reaction flask cooled into an ice bath. Then, DCC (476 mg, 2.31 mmol) was added and after 30 min the ice bath was removed. The reaction was allowed to proceed for 14 h. The white solid was filtered off and the reaction crude concentrated under vacuum. The residue was purified by silica column chromatography using DCM/ethyl acetate (8/2) as eluent, obtaining the product as an orange powder. ¹H NMR (400 MHz, Acetone-*d*⁶) δ 9.31 (s, 1H), 7.87 – 7.73 (m,

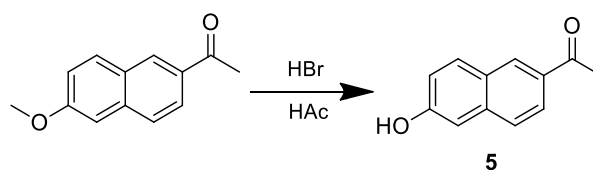
6H), 6.89 – 6.82 (m, 2H), 5.91 (ddt, $J = 17.3, 10.5, 5.3$ Hz, 1H), 5.27 (ddt, $J = 17.3, 3.7, 1.8$ Hz, 1H), 5.12 (ddt, $J = 10.5, 3.4, 1.4$ Hz, 1H), 4.01 (ddd, $J = 5.3, 1.6, 1.6$ Hz, 2H), 4.00 (t, $J = 1.6$ Hz, 2H), 3.71 – 3.63 (m, 6H), 3.58 (q, $J = 7.1$ Hz, 2H), 2.41 (t, $J = 7.1$ Hz, 2H), 1.78 – 1.65 (m, 2H), 1.60 – 1.49 (m, 2H), 1.49 – 1.39 (m, 2H), 1.20 (q, $J = 7.0$ Hz, 3H), 0.89 (s, 9H), 0.05 (s, 6H). ^{13}C NMR (101 MHz, Acetone- d_6) δ 172.18, 151.31, 149.76, 144.16, 141.88, 136.21, 125.69, 123.64, 120.18, 116.51, 112.26, 72.60, 68.80, 63.61, 60.64, 50.99, 46.39, 37.94, 33.52, 26.41, 20.95, 18.92, 14.62, 12.55, -5.03.

Synthesis of *N*-(4-((4-((2-(allyloxy)ethyl)(ethyl)amino)phenyl)diazenyl)phenyl)-6-hydroxyhexanamide (4)



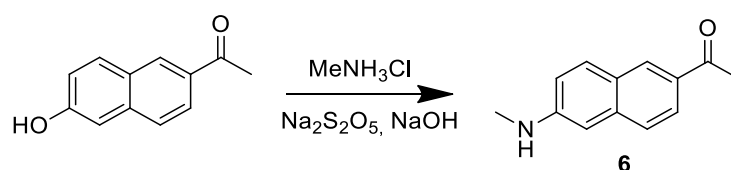
N-(4-((4-((2-(allyloxy)ethyl) (ethyl)amino)phenyl)diazenyl) phenyl)-6-((tert-butyl)dimethylsilyloxy)hexanamide (900 mg, 1.63 mmol) and acetic acid (98 mg, 1.63 mmol) were dissolved in anhydrous THF (5 mL). The flask was cooled down in an ice bath. Then TBAF (425 mg, 1.63 mmol) was dissolved in anhydrous THF (2 mL) and added dropwise into the flask under Ar atmosphere. The reaction was stirred for 24 h, the reaction crude concentrated under vacuum and the residue purified by silica column chromatography using ethyl acetate as eluent. Yield: 82%. ^1H NMR (400 MHz, CDCl_3) δ 7.94 – 7.79 (m, 4H), 7.72 – 7.62 (m, 2H), 6.81 – 6.72 (m, 2H), 5.89 (ddt, $J = 17.3, 10.5, 5.3$ Hz, 1H), 5.27 (dd, $J = 17.2, 1.6$ Hz, 1H), 5.18 (dd, $J = 10.4, 1.5$ Hz, 1H), 4.00 (ddd, $J = 5.3, 1.6, 1.6$ Hz, 2H), 3.71 – 3.59 (m, 6H), 3.53 (q, $J = 7.0$ Hz, 2H), 2.41 (t, $J = 7.4$ Hz, 2H), 1.83 – 1.77 (m, 2H), 1.66 – 1.57 (m, 2H), 1.52 – 1.43 (m, 2H), 1.22 (t, $J = 7.0$ Hz, 3H).

Synthesis of 1-(6-hydroxynaphthalen-2-yl)ethanone (**5**)



HBr (48%wt) (16.7 mL, 150 mmol) was added to 1-(6-methoxynaphthalen-2-yl)ethanone (3.00 g, 15 mmol) in acetic acid (30 mL) and the solution stirred at 100°C for 12 h. The reaction was concentrated under vacuum and the crude dissolved in ethyl acetate, washed with saturated NaHCO₃ solution and brine, dried over anhydrous MgSO₄, filtered and concentrated again under vacuum. The residue was purified by silica column chromatography using hexane/ethyl acetate (1/1) as eluent, obtaining the product as a white powder. Yield: 52%. ¹H NMR (400 MHz, Acetone-d₆) δ 9.04 (s, 1H), 8.52 (d, *J* = 1.2 Hz, 1H), 7.97 (d, *J* = 8.8 Hz, 1H), 7.94 (dd, *J* = 8.7, *J* = 1.8 Hz, 1H), 7.75 (d, *J* = 8.7 Hz, 1H), 7.27 (d, *J* = 2.3 Hz, 1H), 7.24 (dd, *J* = 8.8, 2.4 Hz, 1H), 2.65 (s, 3H). ¹³C NMR (101 MHz, Acetone-d₆) δ 197.56, 158.68, 138.51, 133.23, 132.47, 131.26, 128.34, 127.36, 125.10, 120.21, 110.02, 26.60.

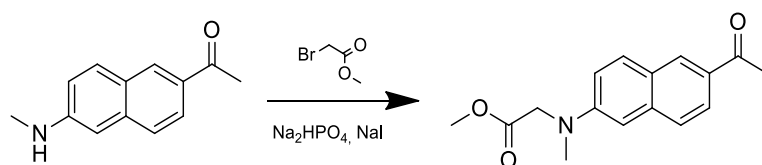
Synthesis of 1-(6-(methylamino)naphthalen-2-yl)ethanone (**6**)



A mixture of compound **5** (1.00 g, 5.4 mmol), methylamine hydrochloride (2.2 g, 26.2 mmol), Na₂S₂O₅ (2.05 g, 10.8 mmol) and NaOH (1.1 g, 26.2 mmol) in water (30 mL) sealed in an ace pressure tube was stirred at 140 °C for 48 h. The solid was filtered, washed with water, dried under vacuum and purified by silica column chromatography using DCM/ethyl acetate (9/1) as eluant. The product was obtained as a yellowish solid. Yield: 85 %. ¹H NMR (400 MHz, Acetone-d₆) δ 8.38 (d, *J* = 1.5 Hz, 1H), 7.87 (dd, *J* = 8.7, 1.8 Hz, 1H), 7.77 (d, *J* = 8.9 Hz, 1H), 7.64 (d, *J* = 8.8 Hz, 1H), 7.06 (dd, *J* = 8.9, 2.3 Hz, 1H), 6.80 (d, *J* = 2.2 Hz, 1H), 5.66 (s,

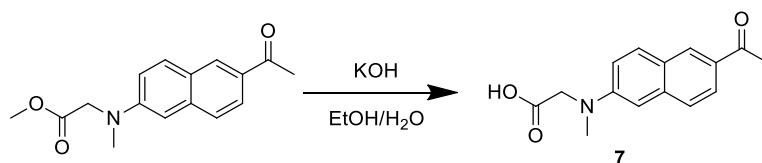
1H), 2.92 (d, $J = 5.1$ Hz, 3H), 2.60 (s, 3H). ^{13}C NMR (75 MHz, Acetone- d^6) δ 197.07, 151.04, 139.27, 131.33, 131.27, 131.20, 126.54, 126.47, 125.11, 119.60, 102.76, 30.16, 26.39.

Synthesis of methyl 2-((6-acetylnaphthalen-2-yl)(methyl)amino)acetate



A solution of **6** (600 mg, 33 mmol), methyl bromoacetate (342 mg, 4.5 mmol), NaI (166 mg, 1.12 mmol) and Na₂HPO₄ (640 mg, 4.5 mmol) in acetonitrile (30 mL) was stirred under reflux for 18 h. The reaction crude was diluted with ethyl acetate (100 mL) and washed with brine, dried over anhydrous MgSO₄, filtered and concentrated under vacuum. The residue was purified by silica column chromatography using DCM/ethyl acetate (95/5) as eluent to yield a white powder. Yield: 82%. ^1H NMR (400 MHz, Acetone- d^6) δ 8.43 (d, $J = 1.4$ Hz, 1H), 7.89 (d, $J = 8.8$ Hz, 2H), 7.69 (d, $J = 8.8$ Hz, 1H), 7.24 (dd, $J = 9.1, 2.7$ Hz, 1H), 7.03 (d, $J = 2.6$ Hz, 1H), 4.37 (s, 2H), 3.68 (s, 3H), 3.21 (s, 3H), 2.62 (s, 3H). ^{13}C NMR (101 MHz, Acetone- d^6) δ 197.17, 171.46, 150.15, 138.47, 132.02, 131.54, 131.08, 127.07, 126.39, 125.03, 116.84, 106.43, 54.12, 52.05, 39.64, 26.42.

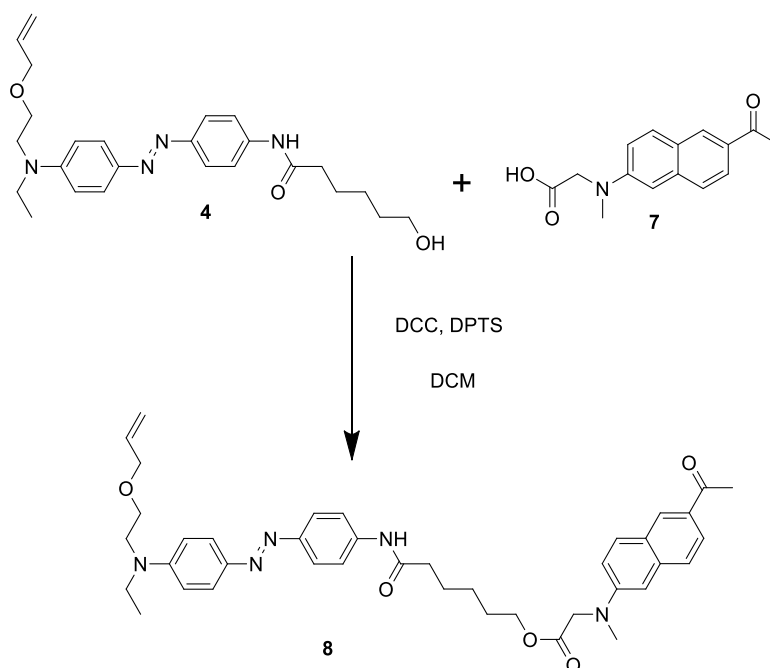
Synthesis of 2-((6-acetylnaphthalen-2-yl)(methyl)amino)acetic acid (**7**)



Methyl 2-((6-acetylnaphthalen-2-yl)(methyl)amino)acetate (400 mg, 1.47 mmol) and KOH (160 mg, 2.9 mmol) were dissolved in a mixture ethanol/water (10 mL of ethanol + 2 mL of distilled water). The reaction was stirred for 5 h, and then diluted with water and neutralised with HCl. The solid was isolated by filtration, washed with water and recrystallised from methanol. Yield: 97%. ^1H NMR (300 MHz, Acetone- d^6) δ 8.43 (d, $J = 1.5$ Hz, 1H), 7.94 – 7.85 (m, 2H), 7.70 (d, $J = 8.7$ Hz,

1H), 7.27 (dd, $J = 9.1, 2.6$ Hz, 1H), 7.04 (d, $J = 2.6$ Hz, 1H), 4.35 (s, 2H), 3.22 (s, 3H), 2.62 (s, $J = 3.0$ Hz, 3H). ^{13}C NMR (75 MHz, Acetone- d_6) δ 197.20, 171.85, 150.30, 138.50, 131.94, 131.52, 131.10, 127.03, 126.33, 125.01, 116.87, 106.35, 53.98, 39.67, 26.42.

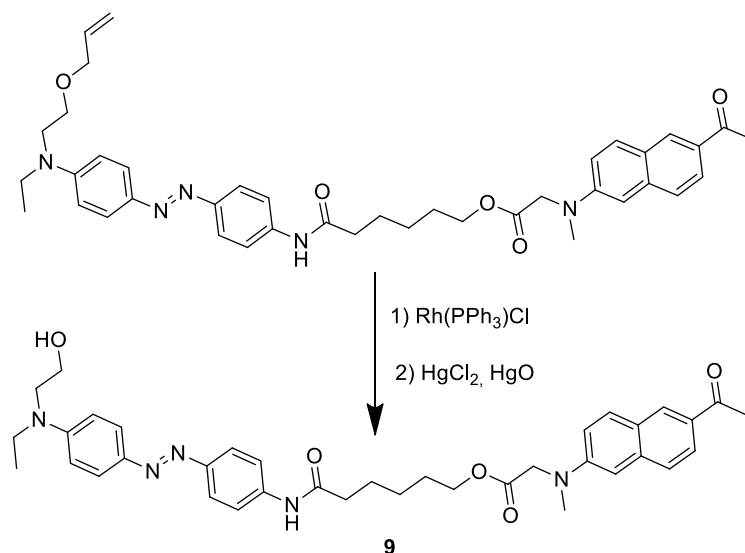
Synthesis of 6-((4-((4-((2-(allyloxy)ethyl)(ethyl)amino)phenyl)diazenyl)phenyl)amino)-6-oxohexyl 2-((6-acetylnaphthalen-2-yl)(methyl)amino)acetate (8)



A dispersion of **4** (120 mg, 0.28 mmol), **7** (84 mg, 0.32 mmol) and DPTS (40 mg, 0.12 mmol) in dry DCM (10 mL) was cooled in an ice bath. Then, EDC (80 mg, 0.42 mmol) was added and the mixture was stirred for 30 min. Then, the reaction was warmed up to room temperature and stirred for 24 h. The reaction crude was diluted with DCM (50 mL), washed with water (2x50 mL), brine (1x50 mL), dried over anhydrous MgSO_4 , filtered and concentrated under vacuum. The residue was purified by silica column chromatography using DCM/ethyl acetate (8/2) as eluent to give an orange solid. Yield: 85%. ^1H NMR (300 MHz, Acetone- d_6) δ 9.26 (s, 1H), 8.41 (d, $J = 1.3$ Hz, 1H), 7.93 – 7.85 (m, 2H), 7.85 – 7.76 (m, 6H), 7.69 (d, $J = 8.7$ Hz, 1H), 7.24 (dd, $J = 9.1, 2.6$ Hz, 1H), 7.02 (d, $J = 2.5$ Hz, 1H), 6.90 – 6.81 (m, 2H), 5.91 (ddt, $J = 17.3, 10.5, 5.3$ Hz, 1H), 5.27 (ddt, $J = 17.3, 3.7, 1.8$ Hz, 1H),

5.12 (ddt, $J = 10.5, 3.4, 1.4$ Hz, 1H), 4.36 (s, 2H), 4.13 (t, $J = 6.4$ Hz, 2H), 4.01 (dt, $J = 5.3, 1.5$ Hz, 2H), 3.70 – 3.63 (m, 4H), 3.58 (q, $J = 7.0$ Hz, 2H), 3.21 (s, 3H), 2.59 (s, 3H), 2.33 (t, $J = 7.4$ Hz, 2H), 1.73 – 1.59 (m, 4H), 1.44 – 1.33 (m, 2H), 1.21 (t, $J = 7.0$ Hz, 3H). ^{13}C NMR (75 MHz, Acetone- d_6) δ 197.29, 172.04, 171.18, 151.33, 150.31, 149.81, 144.18, 141.80, 138.55, 136.20, 132.13, 131.64, 131.14, 127.16, 126.49, 125.67, 125.14, 123.63, 120.22, 116.97, 116.49, 112.27, 106.57, 72.58, 68.79, 65.28, 54.59, 50.97, 46.36, 39.88, 37.57, 29.26, 26.50, 26.32, 25.73, 12.52.

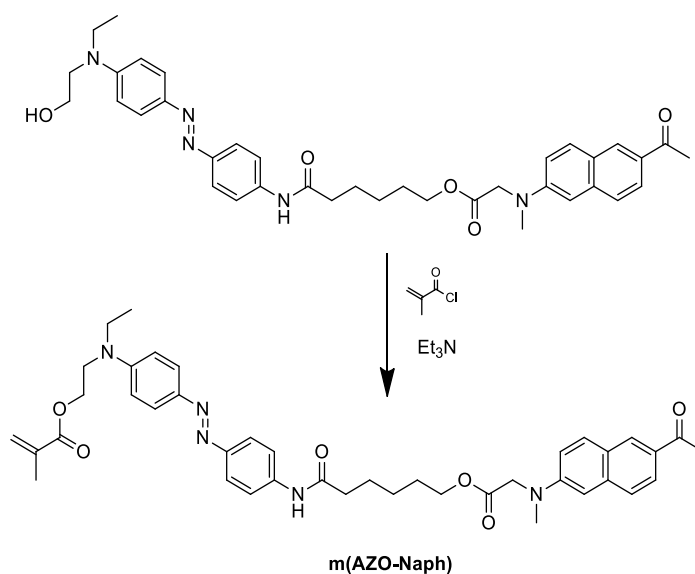
Synthesis of 6-((4-((4-(ethyl(2-hydroxyethyl)amino)phenyl)diazenyl)phenyl)amino)-6-oxohexyl 2-((6-acetylnaphthalen-2-yl)(methyl)amino)acetate (9)



Compound **8** (100 mg, 0.147 mmol) and Rh(PPh₃)Cl (16.6 mg, 0.017 mmol) were stirred for 2 h at 100°C in a mixture of ethanol/water (15 mL/2 mL). Afterwards, the solvent was evaporated under reduced pressure. Then, HgO (58.7 mg, 0.272 mmol) and HgCl₂ (59 mg, 0.221 mmol) were added to the reaction flask, dissolved in a mixture of acetone/water (60 mL/6 mL) and refluxed for 1.5 h. The reaction crude was filtered through a pad of Celite®, the solvent evaporated and the residue solved in DCM (50 mL). The organic solution was washed with aqueous 50% KI (50 mL) and brine, dried over anhydrous MgSO₄, filtered and concentrated under vacuum. The residue was purified by silica column chromatography using DCM/ethyl acetate (3/2) as eluent rendering an orange powder that was recrystallised from ethanol. Yield: 71%. ^1H NMR (400 MHz, Acetone- d_6) δ 9.26 (s,

1H), 8.42 (d, $J = 1.5$ Hz, 1H), 7.92 – 7.86 (m, 2H), 7.84 – 7.76 (m, 6H), 7.69 (d, $J = 8.8$ Hz, 1H), 7.24 (dd, $J = 9.1, 2.6$ Hz, 1H), 7.02 (d, $J = 2.6$ Hz, 1H), 6.88 – 6.82 (m, 2H), 4.36 (s, 2H), 4.13 (t, $J = 6.4$ Hz, 2H), 3.93 (t, $J = 5.6$ Hz, 1H), 3.78 (q, $J = 6.2$ Hz, 2H), 3.61 – 3.54 (m, 4H), 3.21 (s, 3H), 2.60 (s, 3H), 2.33 (t, $J = 7.4$ Hz, 2H), 1.72 – 1.59 (m, 5H), 1.45 – 1.31 (m, 2H), 1.21 (t, $J = 7.1$ Hz, 3H). ^{13}C NMR (75 MHz, Acetone- d_6) δ 197.31, 172.07, 171.23, 151.59, 150.37, 149.88, 144.14, 141.83, 138.61, 132.20, 131.69, 131.19, 127.21, 126.55, 125.73, 125.20, 123.67, 120.27, 117.03, 112.26, 106.63, 65.33, 60.25, 54.64, 53.52, 46.42, 39.94, 37.63, 29.32, 26.55, 26.38, 25.79, 12.54.

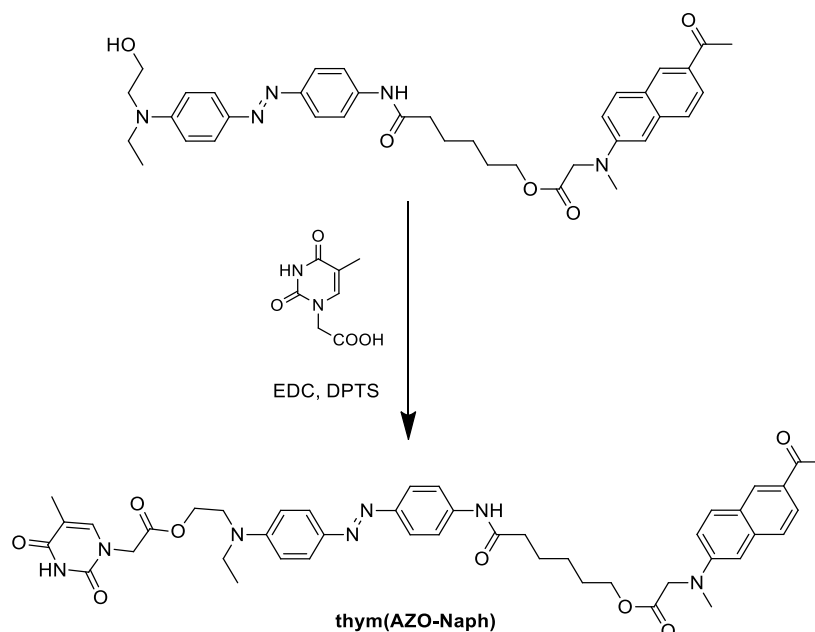
Synthesis of 2-((4-((4-(6-(2-((6-acetylnaphthalen-2-yl)(methyl)amino)acetoxy)hexanamido)phenyl)diazenyl)phenyl)(ethyl)amino)ethyl methacrylate (m(AZO-Naph))



Compound **9** (80 mg, 0.125 mmol) and trimethylamine (20 mg, 0.188 mmol) were dissolved in dry DCM (5 mL) and cooled into an ice bath under Ar atmosphere. Then, methacryloyl chloride (15.7 mg, 0.15 mmol) was added into the flask. The reaction was stirred for 24 h. The reaction was washed with saturated NaHCO_3 and brine, dried over MgSO_4 , filtered and evaporated under reduced pressure. The residue was purified by silica column chromatography using DCM/ethyl acetate (9/1) as eluent. Yield: 62 %. IR (KBr), ν (cm^{-1}): 3341, 1736, 1719, 1702, 1617, 1592, 1530, 1360, 1189, 849, 831, 547. ^1H NMR (400 MHz, Acetone) δ 9.27 (s,

1H), 8.41 (d, J = 1.4 Hz, 1H), 7.88 (dd, J = 8.7, 1.6 Hz, 2H), 7.85 – 7.77 (m, 6H), 7.69 (d, J = 8.8 Hz, 1H), 7.23 (dd, J = 9.1, 2.6 Hz, 1H), 7.01 (d, J = 2.5 Hz, 1H), 6.95 – 6.89 (m, 2H), 6.07 (dd, J = 1.7, 1.0 Hz, 1H), 5.64 – 5.60 (m, 1H), 4.40 – 4.32 (m, 4H), 4.12 (t, J = 6.2 Hz, 2H), 3.79 (t, J = 5.9 Hz, 2H), 3.59 (q, J = 7.0 Hz, 2H), 3.20 (s, 3H), 2.59 (s, 3H), 2.33 (t, J = 7.4 Hz, 2H), 1.90 (dd, J = 1.5, 1.1 Hz, 3H), 1.73 – 1.56 (m, 4H), 1.42 – 1.31 (m, 2H), 1.22 (t, J = 7.0 Hz, 1H). ¹³C NMR (75 MHz, Acetone) δ 197.14, 171.92, 171.07, 167.51, 151.09, 150.19, 149.59, 144.26, 141.83, 138.44, 137.19, 131.97, 131.54, 131.08, 127.05, 126.35, 126.05, 125.56, 125.02, 123.61, 120.06, 119.97, 116.85, 112.35, 106.44, 71.22, 65.17, 62.86, 54.44, 49.30, 45.91, 39.80, 37.47, 26.44, 26.23, 25.63, 18.44, 12.44.

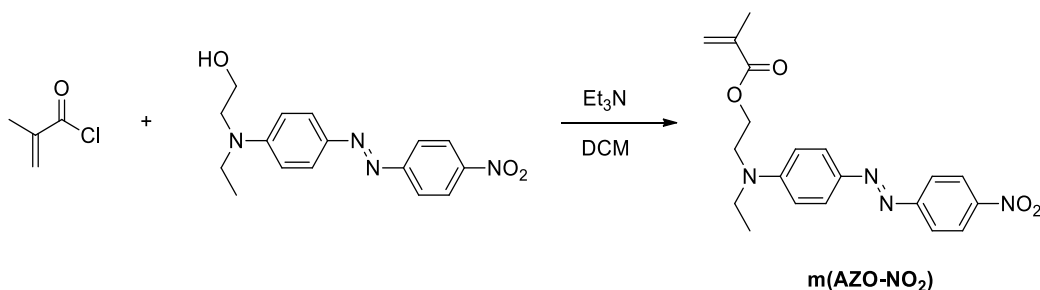
Synthesis of 2-((4-((4-(6-(2-((6-acetylnaphthalen-2-yl)(methyl)amino)acetoxy)hexanamido)phenyl)diazenyl)phenyl)(ethyl)amino)ethyl 2-(5-methyl-2,4-dioxo-3,4-dihydropyrimidin-1(2H)-yl)acetate (thym(AZO-Naph))



Compound **9** (60 mg, 0.09 mmol), thymine-1-acetic acid (21 mg, 0.09 mmol) and DPTS (9 mg, 0.0021 mmol) were dissolved in DCM (10 mL) and cooled down in an ice bath. Then, EDC (24 mg, 0.12 mmol) was added. After 30 min, the ice bath was removed and the reaction was allowed to proceed for 24 h at room temperature. The reaction crude was washed with water (20 mL) and brine, dried over anhydrous MgSO₄, filtered and the solvent evaporated under vacuum. The

residue was purified by silica column chromatography using DCM/ethyl acetate (1/1 as eluent), obtaining an orange powder. IR (KBr), ν (cm^{-1}): 3344, 2948, 1748, 1724, 1701, 1660, 1618, 1592, 1510, 1385, 1198, 1137, 842, 553. Yield: 89%. ^1H NMR (300 MHz, DMSO) δ 11.39 (s, 1H), 10.09 (s, 1H), 8.43 (d, $J = 1.5$ Hz, 1H), 7.90 (d, $J = 9.1$ Hz, 1H), 7.86 – 7.65 (m, 8H), 7.42 (q, $J = 1.2$ Hz, 1H), 7.22 (dd, $J = 9.2, 2.6$ Hz, 1H), 6.96 (d, $J = 2.4$ Hz, 1H), 6.89 – 6.82 (m, 2H), 4.47 (s, 2H), 4.39 (s, 2H), 4.31 (t, $J = 5.4$ Hz, 2H), 4.08 (t, $J = 6.4$ Hz, 2H), 3.69 (t, $J = 5.1$ Hz, 2H), 3.47 (q, $J = 6.8$ Hz, 3H), 3.11 (s, 3H), 2.59 (s, 3H), 2.28 (t, $J = 7.3$ Hz, 2H), 1.74 (d, $J = 1.1$ Hz, 3H), 1.65 – 1.51 (m, 4H), 1.29 (m, 2H), 1.13 (t, $J = 6.9$ Hz, 3H). ^{13}C NMR (75 MHz, DMSO) δ 197.01, 171.35, 170.37, 168.29, 164.27, 150.92, 149.82, 149.06, 147.93, 142.64, 141.44, 140.74, 137.06, 130.65, 130.40, 130.34, 126.03, 124.85, 124.63, 124.01, 122.60, 119.22, 116.04, 111.39, 108.64, 105.16, 64.23, 62.84, 53.27, 48.50, 48.05, 44.85, 39.10, 36.25, 27.93, 26.36, 25.00, 24.56, 11.96, 11.88.

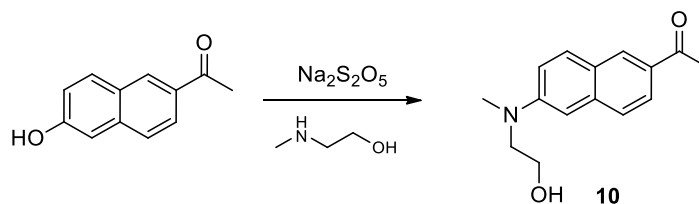
Synthesis of 2-(ethyl(4-((4-nitrophenyl)diazenyl)phenyl)amino)ethyl methacrylate (m(AZO-NO₂))



AZO-NO₂ (2.00 g, 6.37 mmol) and trimethylamine (0.77 g, 7.69 mmol) were dissolved in DCM (75 mL) and cooled to 0°C under argon atmosphere. Then, methacryloyl chloride (0.79 g, 7.64 mmol) was added dropwise and the reaction was stirred for 12 h. Then, the organic solution was washed with aqueous 10% NH₄Cl and brine, and dried with MgSO₄. The solvent was evaporated and the residue purified using silica gel column chromatography eluting with hexane/ethyl acetate (9/1), obtaining a red powder. Yield: 83 %. IR (KBr), ν (cm^{-1}): 2927, 1719, 1601, 1511, 1390, 1511, 1390, 1338, 1158, 1135, 1105, 823, 754, 686. ^1H NMR (300 MHz, CDCl₃) δ 8.37 – 8.28 (m, 2H), 8.05 – 7.94 (m, 4H), 6.88 (m, 2H), 6.13 –

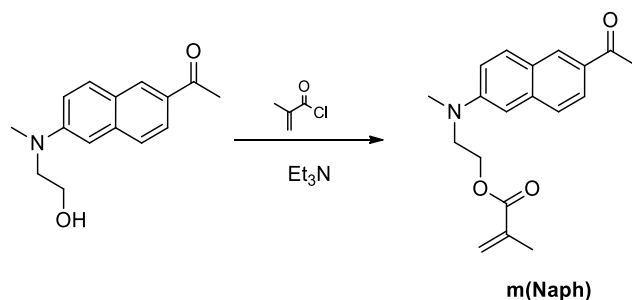
6.07 (m, 1H), 5.62 – 5.56 (m, 1H), 4.39 (t, $J = 6.2$ Hz, 2H), 3.76 (t, $J = 6.2$ Hz, 2H), 3.58 (q, $J = 7.1$ Hz, 2H), 1.94 (dd, $J = 1.4, 1.0$ Hz, 3H), 1.28 (t, $J = 7.1$ Hz, 3H). ^{13}C NMR (101 MHz, CDCl_3) δ 167.43, 156.88, 151.42, 147.56, 143.98, 136.01, 126.40, 124.81, 122.80, 122.77, 111.63, 77.48, 77.16, 76.84, 61.84, 48.90, 45.77, 18.46, 12.41.

Synthesis of 1-(6-((2-hydroxyethyl)(methyl)amino)naphthalen-2-yl)ethanone (10)



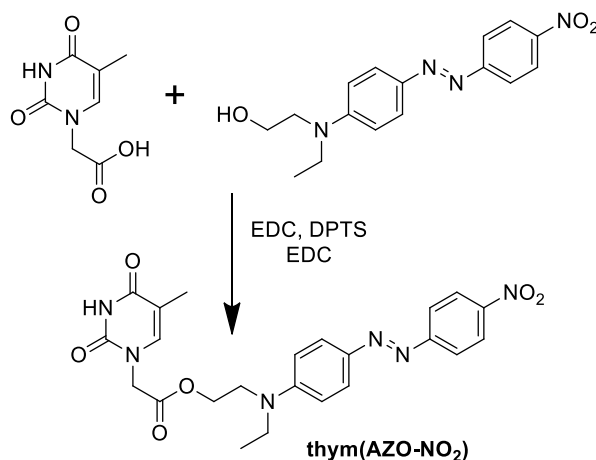
A suspension of **5** (1.00 g, 5.37 mmol), 2-(methylamino)ethanol (8.60 g, 107.5 mmol) and $\text{Na}_2\text{S}_2\text{O}_5$ (5.10 g, 26.9 mmol) in water (50 mL) in an ace pressure tube was stirred at 140 °C for 72 h. Then, the resulting final solution was extracted with DCM (3 x 50 mL) and the combined organic phases were washed with brine and dried with MgSO_4 . The solvent was evaporated and the residue was purified by silica gel chromatography eluting with hexane/ethyl acetate (1/1) rendering a yellow powder. Yield: 48%. ^1H NMR (400 MHz, CDCl_3) δ 8.27 (s, 1H), 7.89 (dd, $J = 8.7, 1.7$ Hz, 1H), 7.75 (d, $J = 9.1$ Hz, 1H), 7.59 (d, $J = 8.7$ Hz, 1H), 7.20 (dd, $J = 9.1, 2.5$ Hz, 1H), 6.90 (d, $J = 2.2$ Hz, 1H), 3.89 (t, $J = 5.6$ Hz, 2H), 3.63 (t, $J = 5.7$ Hz, 2H), 3.11 (s, 3H), 2.64 (s, 3H). ^{13}C NMR (101 MHz, CDCl_3) δ 198.01, 149.77, 137.78, 131.00, 130.94, 130.44, 126.31, 125.35, 124.73, 116.55, 105.68, 60.38, 54.98, 39.07, 26.51.

Synthesis of 2-((6-acetylnaphthalen-2-yl)(methyl)amino)ethyl methacrylate (m(Naph))



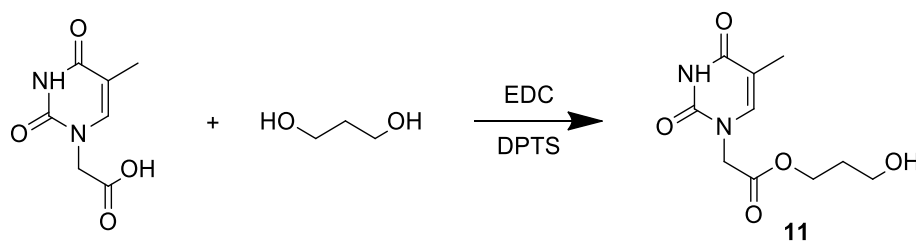
Methacryloyl chloride (200 mg, 1.97 mmol) was added dropwise to a solution of **10** (400 mg; 1.64 mmol) and trimethylamine (243 mg, 2.46 mmol) in DCM (10 mL) at 0°C under argon atmosphere. The reaction was stirred for 12 h. Then, organic phase was washed with NH₄Cl 10% and brine, and dried with MgSO₄. The solvent was evaporated and the residue purified using silica gel column chromatography eluting with DCM, obtaining a yellow powder. Yield: 83 %. IR (KBr), ν (cm⁻¹): 2925, 1713, 1661, 1623, 1508, 1360, 1287, 1213, 1170, 1148, 843. ¹H NMR (400 MHz, CDCl₃) δ 8.31 (d, J = 1.4 Hz, 1H), 7.92 (dd, J = 8.7, 1.8 Hz, 1H), 7.80 (d, J = 9.1 Hz, 1H), 7.63 (d, J = 8.7 Hz, 1H), 7.20 (dd, J = 9.1, 2.6 Hz, 1H), 6.91 (d, J = 2.4 Hz, 1H), 6.03 (dq, J = 1.4, 1.0 Hz, 1H), 5.52 (dq, J = 3.1, 1.5 Hz, 1H), 4.39 (t, J = 5.9 Hz, 2H), 3.80 (t, J = 5.9 Hz, 2H), 3.14 (s, 3H), 2.67 (s, 3H), 1.89 – 1.87 (m, 3H). ¹³C NMR (101 MHz, CDCl₃) δ 197.86, 167.45, 149.00, 137.81, 136.06, 131.15, 131.01, 130.41, 126.25, 125.36, 124.82, 116.12, 105.61, 62.02, 51.12, 38.98, 26.55, 18.39.

Synthesis of 2-(ethyl(4-((4-nitrophenyl)diazenyl)phenyl)amino)ethyl 2-(5-methyl-2,4-dioxo-3,4-dihydropyrimidin-1(2H)-yl)acetate (thym(AZO-NO₂))



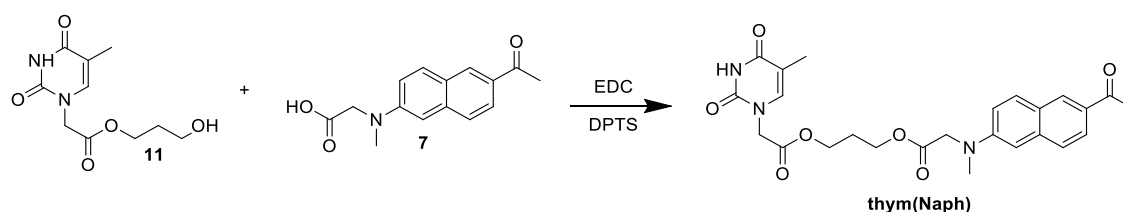
AZO-NO₂ (200 mg, 0.636 mmol), thymine-1-acetic acid (117 mg, 0.636 mmol) and DPTS (56 mg, 0.19 mmol) were dissolved in DCM (20 mL) and the solution cooled in an ice bath. Then, EDC (158 mg, 0.827 mmol) was added and the reaction was stirred for 24 h. The organic solution was washed with water and brine, dried over MgSO₄, filtered, the solvent evaporated. The residue was purified by silica column chromatography using DCM/ethyl acetate (7/3) as eluent yielding the product as a red powder. IR (KBr), ν (cm⁻¹): 1740, 1720, 1683, 1601, 1518, 1333, 1248, 1215, 1140, 1101, 858, 831, 764, 533. Yield: 83 %. ¹H NMR (400 MHz, DMSO) δ 11.41 (s, 1H), 8.48 – 8.26 (m, 2H), 8.07 – 7.90 (m, 2H), 7.88 – 7.82 (m, 2H), 7.42 (q, J = 1.2 Hz, 1H), 6.95 – 6.85 (m, 2H), 4.47 (s, 2H), 4.33 (t, J = 5.5 Hz, 2H), 3.73 (t, J = 5.4 Hz, 2H), 3.52 (q, J = 7.1 Hz, 2H), 1.73 (d, J = 1.2 Hz, 3H), 1.14 (t, J = 7.0 Hz, 3H). ¹³C NMR (101 MHz, DMSO) δ 168.29, 164.25, 156.17, 151.49, 150.92, 146.91, 142.88, 141.43, 126.10, 124.98, 122.51, 111.66, 108.62, 62.78, 48.48, 48.10, 45.03, 11.95, 11.89.

Synthesis of 3-hydroxypropyl 2-(5-methyl-2,4-dioxo-3,4-dihydropyrimidin-1(2H)-yl)acetate (**11**)



Thymine-1-acetic acid (1.00 g, 5.43 mmol), 1,3-propanediol (1.28 g, 16 mmol) and DMAP (200 mg, 1.63 mmol) were dissolved in DCM (50 mL) under Ar atmosphere. Then, EDC (1.24 g, 6.49 mmol) in DCM (5 mL) was added dropwise. The reaction was stirred for 24 h. Then, the solution was washed with water and brine, dried over MgSO₄ and the solid was filtered off. The solvent was evaporated and the residue purified by silica column chromatography using DCM/MeOH (9.5/0.5) as eluent rendering the product as a white powder. Yield: 92 %. ¹H NMR (300 MHz, DMSO) δ 11.37 (s, 1H), 7.50 (q, J = 1.2 Hz, 1H), 4.52 (t, J = 5.2 Hz, 1H), 4.47 (s, 2H), 4.16 (t, J = 6.5 Hz, 2H), 3.45 (t, J = 6.5 Hz, 2H), 1.81 – 1.67 (m, 5H).

Synthesis of 3-(2-((6-acetylnaphthalen-2-yl)(methyl)amino)acetoxyl)propyl 2-(5-methyl-2,4-dioxo-3,4-dihydropyrimidin-1(2H)-yl)acetate (thym(Naph))



EDC (48 mg, 0.249 mmol) in DCM (1 mL) was added dropwise to a solution of **7** (53 mg, 0.207 mmol), **11** (50 mg, 0.207 mmol) and DMAP (7.6 mg, 0.062 mmol) in DCM (5 mL) under Ar atmosphere. The reaction was maintained stirred for 24 h. Then, the solution was washed with water and brine, dried over MgSO₄ and the solid was filtered off. The solvent was removed under reduced pressure and the residue purified by silica column chromatography using DCM/ethyl acetate (9/1) as eluent giving the desired product as a white powder. Yield: 81 %. IR (KBr), ν (cm⁻¹): 3415, 2926, 1739, 1697, 1664, 1620, 1463, 1211, 854, 797, 761, 468.

¹H NMR (400 MHz, CDCl₃) δ 9.14 (s, 1H), 8.31 (d, J = 1.4 Hz, 1H), 7.92 (dd, J = 8.7, 1.8 Hz, 1H), 7.80 (d, J = 9.1 Hz, 1H), 7.64 (d, J = 8.7 Hz, 1H), 7.09 (dd, J = 9.1, 2.6 Hz, 1H), 6.88 (d, J = 2.5 Hz, 1H), 6.85 (d, J = 1.2 Hz, 1H), 4.33 (s, 2H), 4.23 – 4.18 (m, 4H), 4.16 (t, J = 6.3 Hz, 2H), 3.19 (s, 3H), 2.66 (s, 3H), 1.99 – 1.92 (m, 2H), 1.86 (d, J = 1.1 Hz, 3H). ¹³C NMR (101 MHz, CDCl₃) δ 197.95, 170.61, 167.56, 164.15, 150.94, 148.81, 140.19, 137.57, 131.45, 131.12, 130.39, 126.56, 125.74, 124.80, 115.86, 111.39, 106.12, 77.16, 62.17, 61.16, 54.43, 48.70, 39.89, 29.80, 27.87, 26.56, 12.36.

General procedure for RAFT polymerisation of (AZO-NO₂/Naph) monomers

Monomers, macro-CTA and AIBN (see the table below for further details) were placed into a Schlenk flask and dissolved in DMF (1 mL per 100 mg of reagents weight). The charged flask was degassed *via* three freeze-pump-thaw cycles and flushed with argon. Then, the flask was introduced into a bath at 70 °C and the polymerisation was allowed to proceed for 24 h. Polymerisation crude was precipitated into cold diethyl ether and the solid isolated by filtration. Polymer was further purified by preparative size exclusion chromatography (SEC) in THF using a BioBeads® resin to remove the unreacted monomer.

Polymer	macro-CTA mass (mmol)	m(AZO-NO ₂) mass (mmol)	m(Naph) mass (mmol)	AIBN mass (mmol)
PEG2k- <i>b</i> -p(AZO-NO ₂)	62 mg (0.0314) ¹	300 mg (0.785)	-----	0.5 mg (0.00314)
PEG2k- <i>b</i> -p(Naph)	51 mg (0.025) ¹	-----	200 mg (0.643)	0.4 mg (0.0025)
PEG2k- <i>b</i> -p(AZO-NO ₂ /Naph)	100 mg (0.05) ¹	400 mg (1.05)	108 mg (0.35)	0.8 mg (0.005)
PEG10k- <i>b</i> -p(AZO-NO ₂)	130 mg (0.013) ²	130 mg (0.785)	-----	0.2 mg (0.0013)
PEG10k- <i>b</i> -p(Naph)	107 mg (0.0107) ²	-----	200 mg (0.64)	0.17 mg (0.00107)

PEG10k-b-p(AZO-NO₂/Naph)	214 mg (0.0214) ²	374 mg (0.96)	100 mg (0.3215)	0.35 mg (0.0024)
--	---------------------------------	------------------	--------------------	---------------------

¹ PEG of 2000 g/mol

² PEG of 10000 g/mol

Characterisation data for PEG2k-b-p(AZO-NO₂): IR (KBr), ν (cm⁻¹): 2868, 1728, 1600, 1514, 1389, 1132, 856. ¹H NMR (400 MHz, CDCl₃) δ 8.08, 7.70, 6.68, 4.19, 4.06, 3.64, 3.38, 1.79, 1.10, 0.81.

Characterisation data for PEG2k-b-p(Naph): IR (KBr), ν (cm⁻¹): 2883, 1728, 1686, 1618, 1506, 1384, 1358, 1280, 1112, 846. ¹H NMR (300 MHz, CDCl₃) δ 8.13, 7.81, 7.62, 7.50, 6.96, 6.74, 3.87, 3.64, 3.38, 2.88, 2.51, 1.62, 0.86, 0.71.

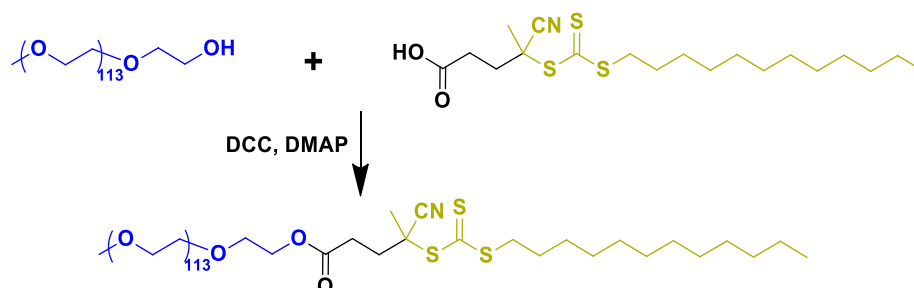
Characterisation data for PEG2k-b-p(AZO-NO₂/Naph): IR (KBr), ν (cm⁻¹): 2871, 1729, 1600, 1515, 1387, 1338, 1133, 857. ¹H NMR (400 MHz, DMSO) δ 8.06, 7.64, 7.04, 6.69, 3.91, 3.49, 3.22, 2.87, 0.94, 0.60.

Characterisation data for PEG10k-b-p(AZO-NO₂): IR (KBr), ν (cm⁻¹): 2884, 1729, 1600, 1516, 1467, 1341, 1279, 1101, 961, 841. ¹H NMR (400 MHz, CDCl₃) δ 8.14, 7.75, 6.73, 4.06, 3.64, 3.37, 1.91, 1.10, 0.81.

Characterisation data for PEG10k-b-p(Naph): IR (KBr), ν (cm⁻¹): 2884, 1728, 1668, 1618, 1506, 1384, 1342, 1342, 1280, 1103, 962, 843. ¹H NMR (400 MHz, CDCl₃) δ 8.11, 7.79, 7.58, 7.47, 6.93, 6.71, 3.88, 3.64, 3.37, 2.48, 1.82, 1.64, 0.87, 0.84, 0.69.

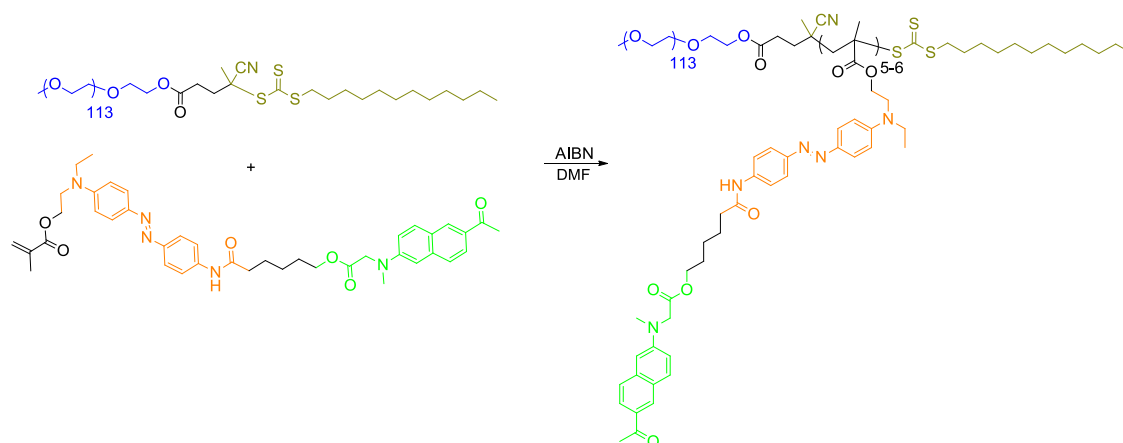
Characterisation data for PEG10k-b-p(AZO-NO₂/Naph): IR (KBr), ν (cm⁻¹): 2883, 1730, 1600, 1515, 1341, 1102, 962, 856. ¹H NMR (400 MHz, DMSO) δ 8.07, 7.64, 7.05, 6.69, 3.91, 3.50, 3.24, 2.86, 0.94, 0.63.

Synthesis of PEG5k-trithioCTA



Monomethyl polyethylene glycol ($M_n = 5000$ g/mol) (2.50 g, 0.5 mmol), 4-cyano-4-[(dodecylsulfanylthiocarbonyl)sulfanyl]pentanoic acid (604 mg, 1.5 mmol) and DMAP (19 mg, 0.15 mmol) were added to a round-bottom flask and dissolved in DCM (20 mL). Then, DCC (300 mg, 1.5 mmol) was dissolved in DCM (5 mL) and added dropwise under argon atmosphere. The reaction was stirred for 24 h. The formed solid was filtered off and the solution concentrated under vacuum and precipitated twice into cold diethyl ether. The solid was filtered and dried. The product was obtained as a yellow powder. Yield: 60%. IR (KBr), ν (cm^{-1}): 2889, 1467, 1359, 1343, 1280, 1114, 1060, 964, 842. ^1H NMR (400 MHz, CDCl_3) δ 4.25, 3.64, 3.37, 3.32, 2.65, 2.50, 1.87, 1.68, 1.39, 1.25, 0.87.

Synthesis of PEG5k-*b*-p(AZO-Naph)



PEG5k-trithioCTA (50 mg, 0.00925 mmol), m(AZO-Naph) (65 mg, 0.0925 mmol) and AIBN (0.15 mg, 0.000925 mmol) were placed into a Schlenk flask and dissolved in DMF (1 mL). The flask was degassed *via* three freeze-pump-thaw cycles and flushed with argon. Then, the flask was introduced into a bath at 70 °C

and the polymerisation was allowed to proceed for 24 h. Polymerisation crude was precipitated twice into cold diethyl ether and the polymer isolated as an orange powdery solid. IR (KBr), ν (cm^{-1}): 2888, 1736, 1671, 1599, 1467, 1343, 1280, 1150, 1109, 963, 842. ^1H NMR (400 MHz, DMSO) δ 10.05, 8.40, 7.73, 7.18, 6.93, 6.73, 4.35, 4.04, 3.51, 3.24, 3.08, 2.25, 1.53, 1.24, 1.01, 0.80, 0.61.

3.5.2. PREPARATION AND CHARACTERISATION OF POLYMER AGGREGATES

Preparation of supramolecular polymers

Both polymer and thymine derived compounds were weighted and dissolved in THF. The solvent was slowly evaporated at room temperature. Finally, the resultant supramolecular polymers were dried under vacuum.

Preparation of polymeric nanocarriers via co-solvent method

5 mg of BC was dissolved in THF or DMSO and then, Milli-Q water was added dropwise (10 μL per drop) and the cuvette stirred while turbidity was followed by UV-Vis spectroscopy measuring the scattering of the solution at 650 nm. Once turbidity reached a plateau, the mixture was dialysed against water using a Spectra/Por® membrane (MWCO = 1000 g/mol) during 3 days. The polymeric nanocarriers solution was diluted to 5 mL to obtain a 1 mg/mL concentration of nanocarriers.

Preparation of TEM grids

10 μL of a 1 mg/mL nanocarriers solution was applied onto a TEM grid. After 30 s, the drop was removed with filter paper by capillarity. A 10 μL of a uranyl acetate solution was applied following the same procedure and removed in the same way. Finally, the TEM grid was dried sipping the possible remains of water using a micropipette tip joined to a vacuum pump.

Irradiation experiments

The solution to be irradiated was introduced in UV cuvettes and placed at a distance of 10 cm from a LED light source of a 420 or 530 nm, or from a UV lamp of 365 nm depending on the experiment. UV-Vis spectra were registered at different times of irradiation.

Determination of CAC using DLS

DLS measurement were performed at different concentrations (from 0.0001 to 1 mg/mL). Attenuator was set in such a way that count rate at 0.1 mg/mL was around 2000 - 4000 kcps and kept in that configuration for all the experiments as well as the laser beam was positioned in a fixed position, in order to assure the same conditions in every measurement. Then, count rate was represented against concentration in logarithmic scale. The onset corresponds with CAC value.

Determination of CAC using Nile Red

120 μL of a $5 \cdot 10^{-6}$ M solution of Nile Red in DCM was added into vials and DCM was allowed to evaporate. Vials were dried under vacuum and then 600 μL of nanocarriers solution from 10^{-4} to 1 mg/mL were introduced into the vials and stirred for 24 h. Nile Red fluorescence spectra were registered from 560 to 700 nm, exciting at 550 nm. Fluorescence maxima were represented against concentration in logarithmic scale and the onset was determined as the CAC value.

Encapsulation of Rhodamine B

5 mg of polymer was dissolved in THF (1 mL). Then, a solution of RhB in water (2.5 mL at a concentration of 1 mg/mL) was added into the polymer solution at a rate of 1 mL/h. The resulting solution was dialysed against water until water was completely colourless. Finally, the solution was diluted until concentration of self-assemblies was 1 mg/mL.

Controlled release of Rhodamine B

RhB loaded vesicles solution was split in different aliquots and then, kept in dark or irradiated with a proper wavelength depending on the experiment. Then, aliquot was placed into a dialysis membrane, which is introduced into a vial filled with water. The vial was closed and allowed to dialyse overnight. Fluorescence of water was registered, exciting at 554 nm.

3.6. REFERENCES

1. Izquierdo-Serra, M. *et al.* Two-Photon Neuronal and Astrocytic Stimulation with Azobenzene-Based Photoswitches. *J. Am. Chem. Soc.* **136**, 8693–8701 (2014).
2. Rastetter, W. H. & Phillion, D. P. Template-driven macrolide closures. *J. Org. Chem.* **46**, 3209–3214 (1981).
3. Janoschka, T., Teichler, A., Krieg, A., Hager, M. D. & Schubert, U. S. Polymerization of free secondary amine bearing monomers by RAFT polymerization and other controlled radical techniques. *J. Polym. Sci. Part Polym. Chem.* **50**, 1394–1407 (2012).
4. Concellón, A. *et al.* Polymeric micelles from block copolymers containing 2,6-diacylaminopyridine units for encapsulation of hydrophobic drugs. *RSC Adv* **6**, 24066–24075 (2016).
5. Concellón, A. *et al.* Light-Responsive Self-Assembled Materials by Supramolecular Post-Functionalization via Hydrogen Bonding of Amphiphilic Block Copolymers. *Macromolecules* **49**, 7825–7836 (2016).
6. Kim, D. Y., Tripathy, S. K., Li, L. & Kumar, J. Laser-induced holographic surface relief gratings on nonlinear optical polymer films. *Appl. Phys. Lett.* **66**, 1166–1168 (1995).
7. Wu, S. *et al.* Block copolymers of PS-b-PEO co-assembled with azobenzene-containing homopolymers and their photoresponsive properties. *Soft Matter* **7**, 11535 (2011).
8. Ortiz-Palacios, J. *et al.* Incorporation of novel azobenzene dyes bearing oligo(ethylene glycol) spacers into first generation dendrimers. *Dyes Pigments* **116**, 1–12 (2015).

9. Ortíz-Palacios, J., Zaragoza-Galán, G., Aguilar-Ortíz, E., Rodríguez-Alba, E. & Rivera, E. Synthesis, characterization and optical properties of novel dendronized azo-dyes containing a fullerene C₆₀ unit and well-defined oligo(ethylene glycol) segments. *RSC Adv* **7**, 16751–16762 (2017).
10. Poprawa-Smoluch, M. *et al.* Photoisomerization of Disperse Red 1 Studied with Transient Absorption Spectroscopy and Quantum Chemical Calculations. *J. Phys. Chem. A* **110**, 11926–11937 (2006).
11. Blanchard, P. M., Gilbert, A. & Mitchell, G. R. Photoinduced protonation of azo dyes in halogenated solvents and polymers. *J. Mater. Chem.* **3**, 1015 (1993).

**CHAPTER 4: AMPHIPHILIC
BLOCK COPOLYMERS BASED
ON GUANINE**

4.1. INTRODUCTION AND AIMS

In an attempt to improve the stability of light responsive supramolecular block copolymers, new systems based on guanine-cytosine motifs have been prepared as an alternative to 2,6-diacylaminopyridine—thymine pair used in **Chapter 3**, since it has been described that guanine-cytosine interactions are stronger than DAP-thymine ones.¹ Therefore, the main aim of this Chapter was to prepare supramolecular polymers based on guanine-cytosine complementary interactions and to study their self-assembly properties. As it was remarked in the General Introduction, Chapter 1, there are not many examples of guanine based polymers and they still remain a synthetic challenge.^{2,3}

Accordingly, amphiphilic BCs have been prepared from a guanine based methacrylate by RAFT polymerisation using two PEG macroinitiators of 2000 and 10000 g/mol average molar masses (with degrees of polymerisation of 45 and 227, respectively). Besides, two azobenzenes with a terminal cytosine unit have also been prepared. 4-Isobutyloxy-4-alkyloxyazobenzene has been used previously in our group to prepare both covalent and supramolecular polymers and its behaviour under 365 nm illumination is well established.^{4,5} Additionally, on the basis of the results presented in **Chapter 2**, an *ortho*-tetramethoxyazobenzene with the cytosine unit, **cyt-tetraAZO-N**, was studied because it is able to isomerise upon exposure to 530 and 625 nm visible light.⁶ The general structure of the target polymers is represented in **Figure 4.1**.

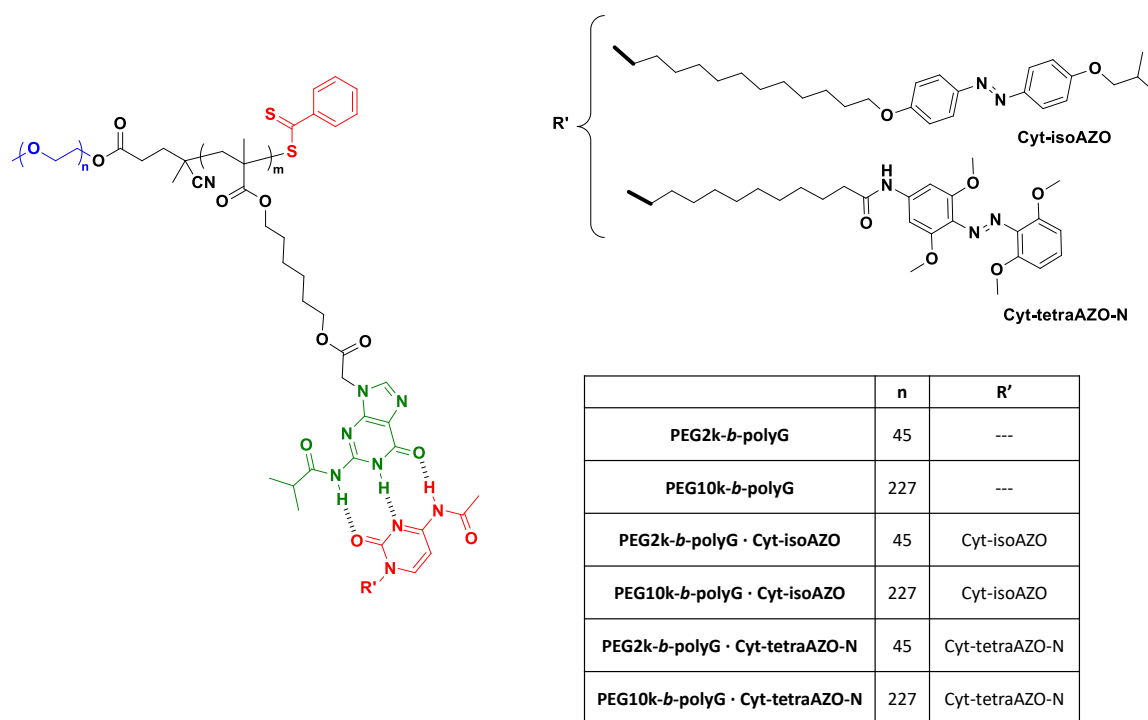


Figure 4.1. General structure of the guanine-cytosine supramolecular amphiphilic BCs

The addressed tasks were the following:

- Synthesis and chemical characterisation of the guanine methacrylate monomer
- Synthesis and chemical characterisation of the cytosine functionalised azobenzenes
- Study of the cytosine-guanine interaction in solution
- Preparation and characterisation of the guanine containing block copolymers
- Study of the self-assembly properties of amphiphilic block copolymers in water and characterisation of the self-assemblies
- Functionalisation of guanine containing BCs with cytosine units and self-assembly studies of the resulting supramolecular BCs

4.2. SYNTHESIS AND CHARACTERISATION OF AMPHIPHILIC BLOCK COPOLYMERS

4.2.1. SYNTHESIS OF GUANINE AND CYTOSINE MONOMERS

The guanine methacrylate monomer **meth-G** was prepared in several steps from commercial guanine as shown in **Figure 4.2**. The amino group of the guanine was initially acylated to increase its solubility. In a first attempt, guanine was treated with acetic anhydride in DMF at 150 °C, obtaining the acetylated compound **1**. Subsequent reaction of compound **1** with *tert*-butyl bromoacetate and sodium hydride in DMF at room temperature gave the aimed compound but in a very low yield since a mixture of products, due to the substitution in different nitrogen atoms, was obtained. Alternatively, guanine was treated with isobutyric anhydride giving rise to the acetylated compound **2**. Due to the larger steric hindrance of the isobutyric group, reaction with *tert*-butyl bromoacetate yielded only the N7 and N9 alkylated regioisomers. From this mixture, the desired N9-alkylated regioisomer, tagged as **3**, was isolated by recrystallisation from ethyl acetate, as described in the literature.⁷ Removal of the *tert*-butyl group with triethylsilane and trifluoroacetic acid at room temperature in dichloromethane⁸ and subsequent Steglich reaction with 6-hydroxyhexyl methacrylate (**5**) in dichloromethane gave the target **meth-G** monomer, in which the methacrylic polymerisable group was linked to the guanine motif through a hexamethylenic flexible spacer.

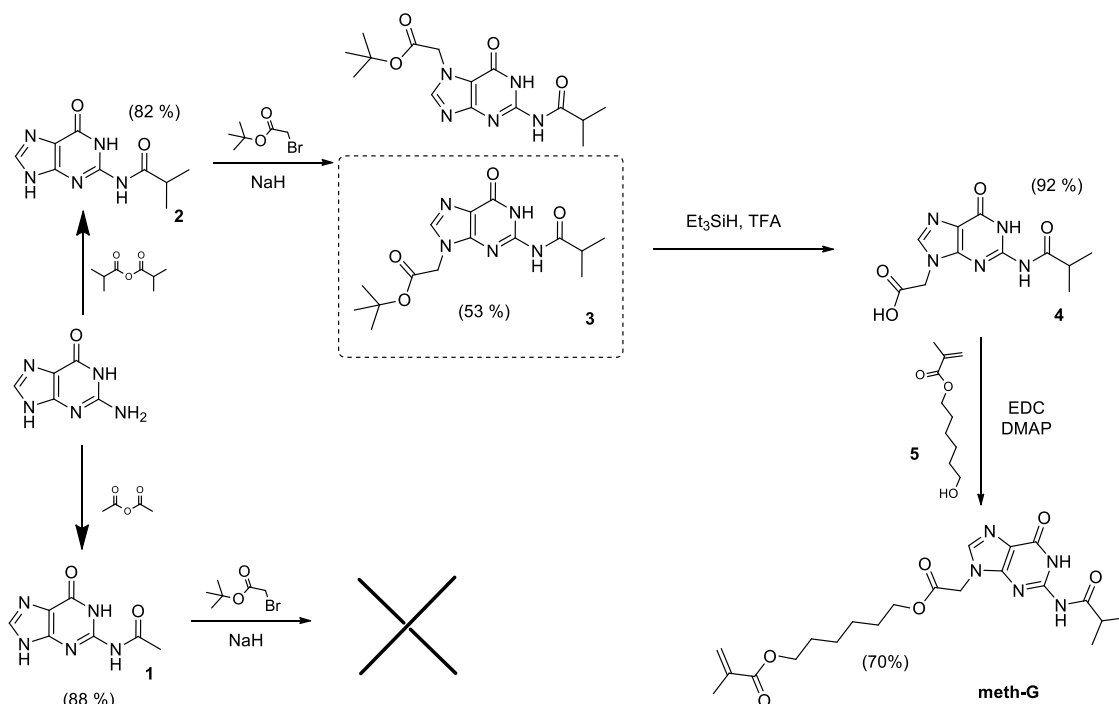


Figure 4.2. Synthesis of meth-G

Azobenzenes were prepared with a cytosine unit connected through an aliphatic flexible spacer. **Cyt-isoAZO** was prepared as shown in **Figure 4.3** where the starting azobenzene **7** was synthesised as previously reported.⁴ A Williamson reaction with 1,12-dibromododecane in acetone at 60°C gave azobenzene **8** to which the acetylcytosine **9** (obtained according to an adapted procedure)⁹ was anchored *via* substitution of the terminal bromide in DMF at 80°C, obtaining the desired **cyt-isoAZO**. Chemical structure of the *N*-alkylated **cyt-isoAZO**, was corroborated by ¹H-¹³C HSQC NMR experiments (**Figure 4.4**). It could be seen how the resonance at 3.86 ppm in ¹H NMR spectrum correlated with the one at 50.8 ppm in the ¹³C NMR spectrum, which was indicative of the formation of the *N*-CH₂- bond and not of the *O*-CH₂- bond (corresponding to *O*-alkylated) for which a correlation peak above 60 ppm in the ¹³C NMR should be expected.

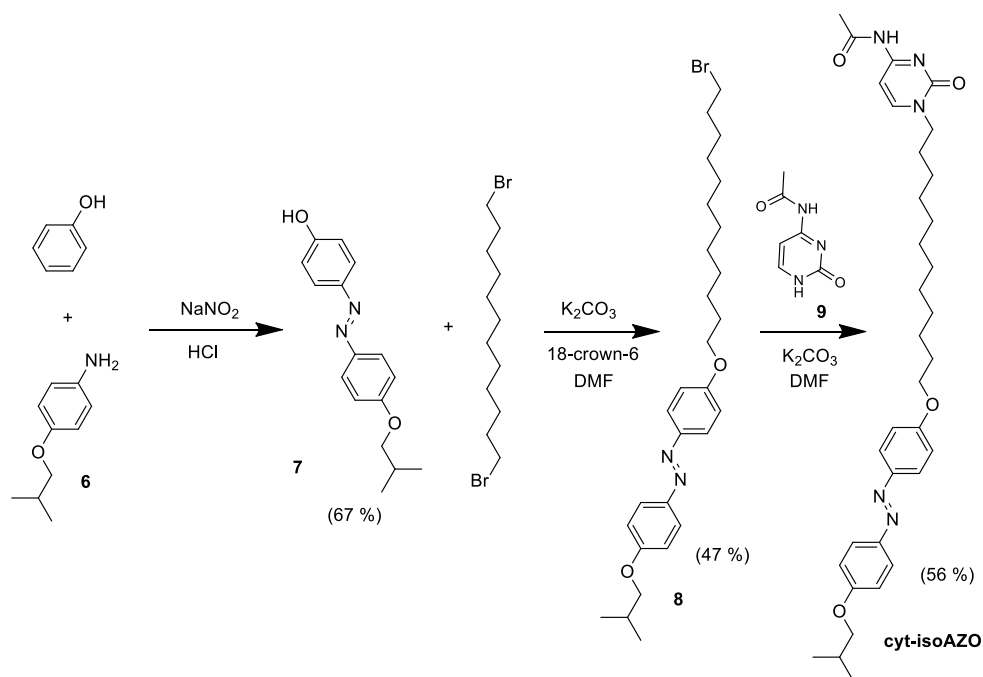


Figure 4.3. Synthesis scheme of cyt-isoAZO

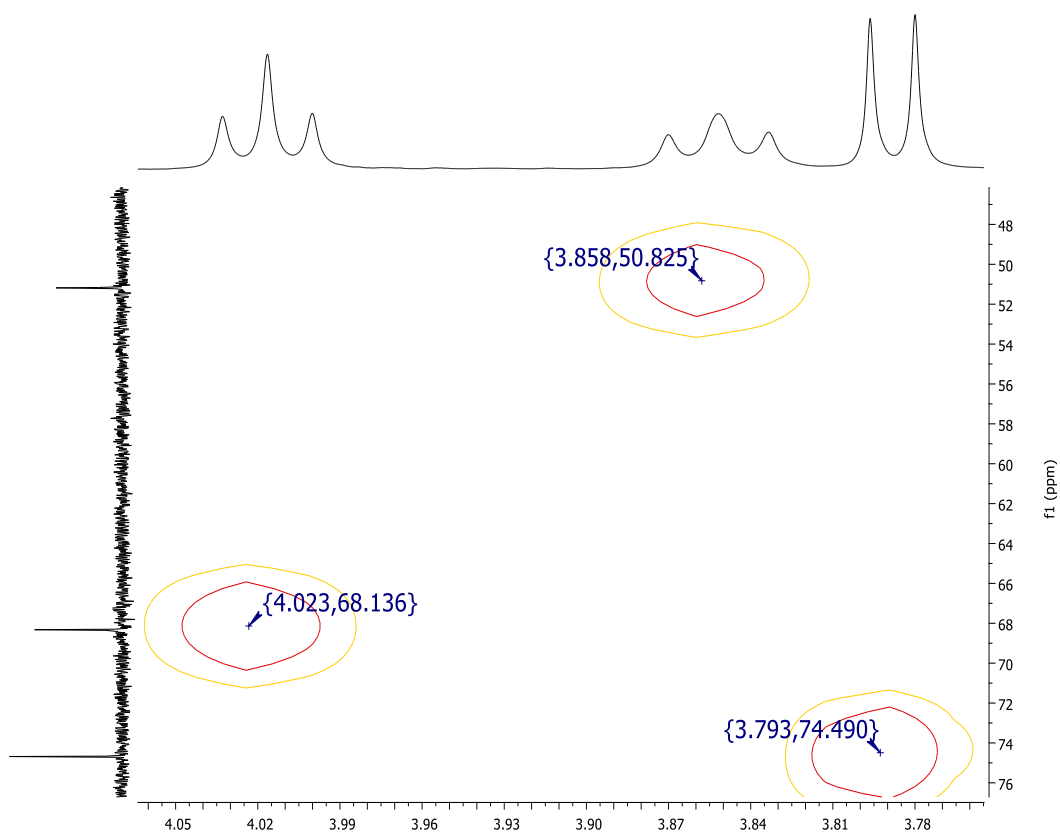


Figure 4.4. ^1H - ^{13}C HSQC magnification of cyt-isoAZO in CDCl_3

Cyt-tetraAZO-N was prepared in a similar way using 4-amino-2,2',6,6'-tetramethoxyazobenzene whose synthesis was described in **Chapter 2 (Figure 4.5)**. The aliphatic spacer was incorporated by an amidation reaction with 11-bromoundecanoic acid using EDC and DMAP in DCM, rendering compound **10** that after a substitution reaction with the acetyl cytosine **9** gave the target **cyt-tetraAZO-N** whose chemical structure was properly characterised using ^1H - ^{13}C HSQC NMR experiments.

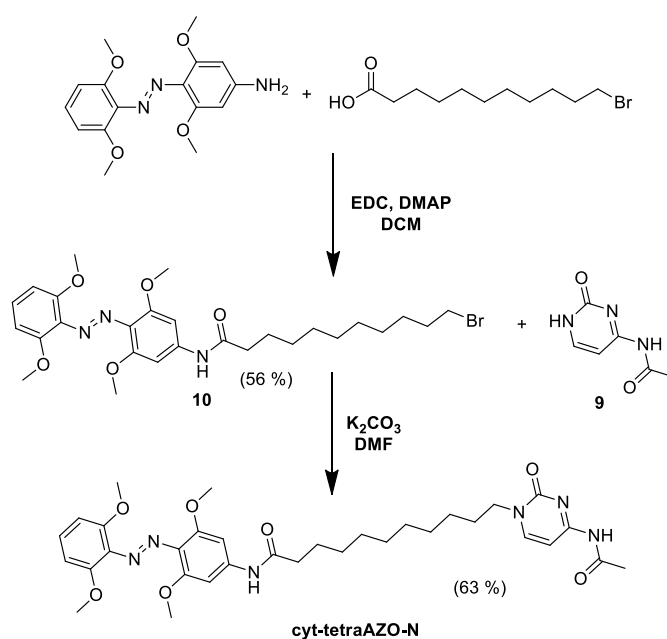


Figure 4.5. Synthesis of *cyt-tetraAZO-N*

H-bonding recognition in solution of the guanine-cytosine pair was confirmed by ^1H NMR from a 1:1 molar ratio mixture of **meth-G** and **cyt-isoAZO** in CDCl_3 . As it can be seen in **Figure 4.6**, the proton resonances of the N–H bonds in the guanine and cytosine units involved in the interaction (labelled in red in **Figure 4.6**) shifted to lower fields, as consequence of a deshielding associated to the formation of the H-bonds.

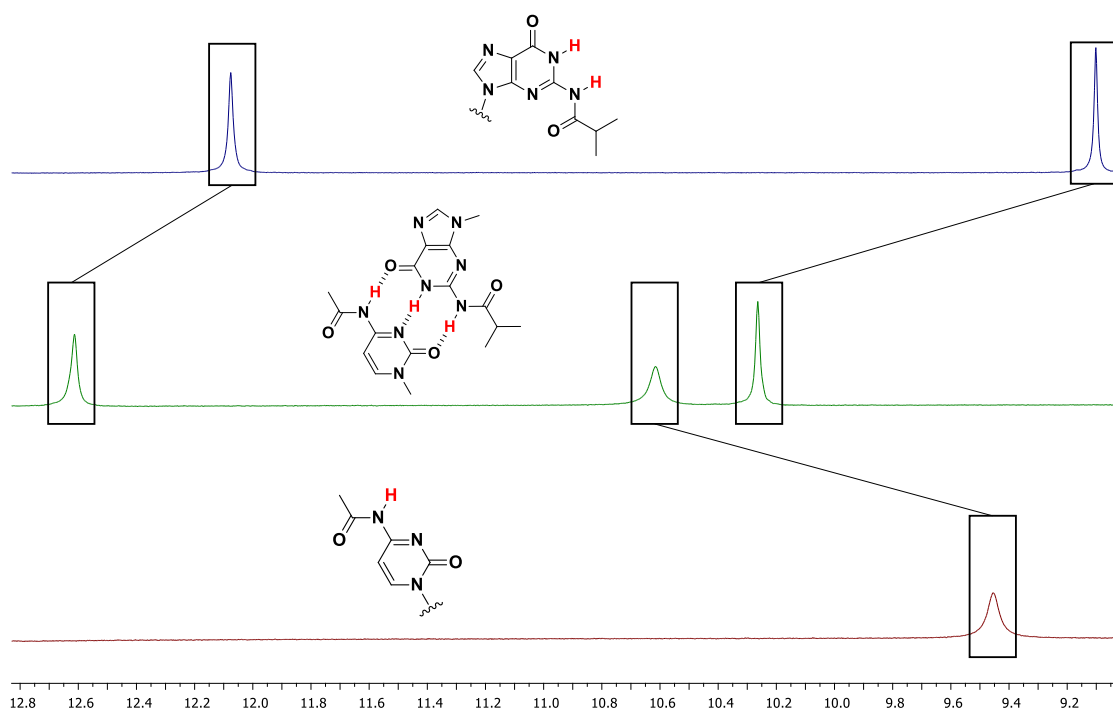


Figure 4.6. ¹H NMR spectra (region from 9.1 to 12.8 ppm) of meth-G, cyt-isoAZO and a 1:1 molar mixture of both in CDCl₃. In red, atoms involved in the H-bonding

The interaction was also studied at different temperatures, between 25-55 °C, by ¹H NMR in CDCl₃. When increasing the temperature, the proton resonances associated to the H-bonding shifted to lower chemical shifts and the signals became broad (**Figure 4.7**). This was related with a weakening of the H-bonding interaction accompanying the increase of thermal energy in the system.

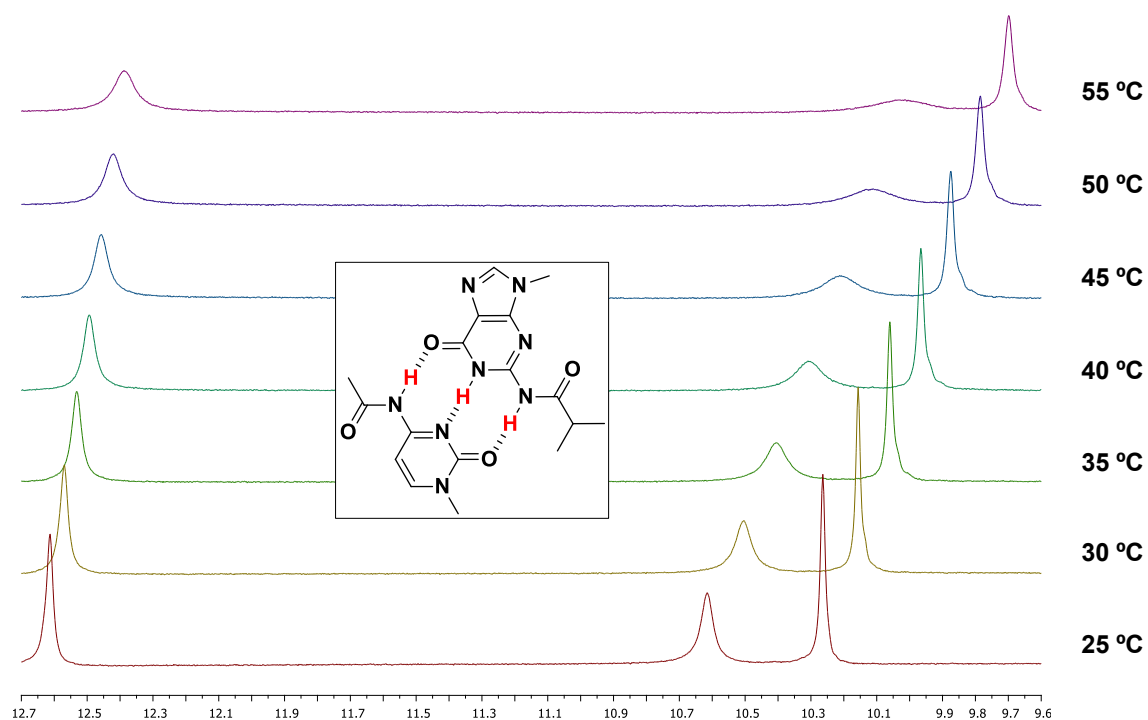


Figure 4.7. Variable temperature ^1H NMR spectra (region from 9.6 to 12.7 ppm) in CDCl_3 of cytosine-guanine complex

4.2.2. SYNTHESIS OF AMPHIPHILIC BLOCK COPOLYMERS

BCs were prepared by RAFT polymerisation of **meth-G** as described in Chapter 2 using **PEG2k-CTA** and **PEG10k-CTA**, with 4-cyano-4-(thiobenzoylthio)pentanoate terminal groups and AIBN as thermal initiator. The general chemical structure of guanine BCs is represented in **Figure 4.8**. The polymerisations were carried out in DMF at 70 °C using $[\text{macroCTA}] / [\text{meth-G}] / [\text{AIBN}]$ in 1 / 35 / 0.1 ratio what represents a $m_{\text{th}} = 35$ for the guanine block (polyG). This in turn corresponds to a $M_{n,\text{th}}$ of 25600 and 17600 g/mol, for **PEG10k-CTA** and **PEG2k-CTA**, respectively, calculated as the sum of the PEG and polyG blocks. BCs were isolated by precipitating polymer into a cold mixture of diethyl ether and methanol (9/1) in order to remove the non-reacted monomer and DMF.

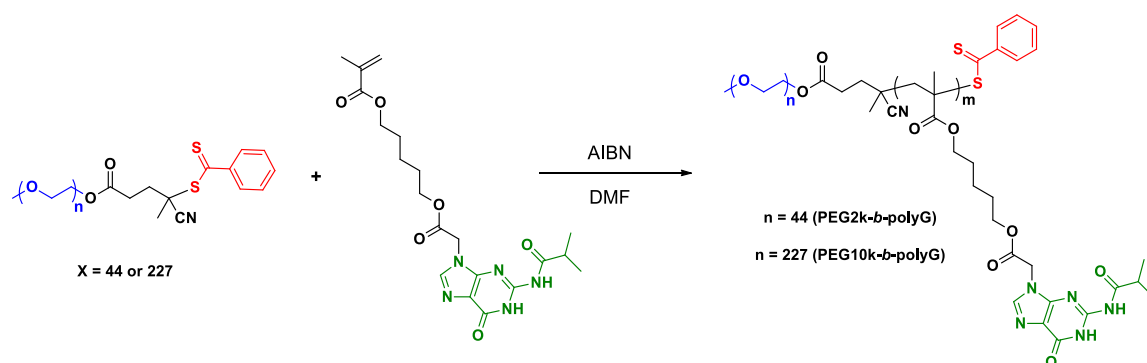


Figure 4.8. General synthesis of the guanine containing polymers

SEC characterisation was performed in DMF, because of the insolubility of the BCs in THF, but these experiments were unsuccessful and SEC trace could not be registered. Average degree of polymerisation of the polyG, m was estimated by end group analysis using $^1\text{H NMR}$. In this case, the relative integration of the methylenic groups of PEG, at 3.50 ppm, and aromatic and methylenic protons of the guanine, at 7.93 and 4.99 ppm peaks, were compared (**Figure 4.9**). From m , average number molar masses ($M_{n,\text{NMR}}$) were calculated as the sum of both blocks, as well as the hydrophobic/hydrophilic weight ratios. Results are shown in **Table 4.1**.

Table 4.1. Molar masses of the polyG BCs

Polymer	m_{th}^{a}	m^{b}	$M_{n,\text{NMR}}^{\text{c}}$	Hydrophilic/Hydrophobic weight ratio
PEG2k-<i>b</i>-polyG	35	32	16300	12/88
PEG10k-<i>b</i>-polyG	35	10	14800	67/23

^a Theoretical degree of polymerisation calculated from the $[\text{monomer}]_0/[\text{macro-CTA}]_0$ assuming full monomer conversion

^b Experimental degree of polymerisation of the polyG block estimated by $^1\text{H NMR}$ end group analysis

^c Molar mass of BC as the sum of the molar mass of PEG and polyG blocks calculated using m determined by $^1\text{H NMR}$ ($M_n = M_{\text{PEG}} + m \cdot M_{\text{monomer}}$). For PEG, commercial value was used

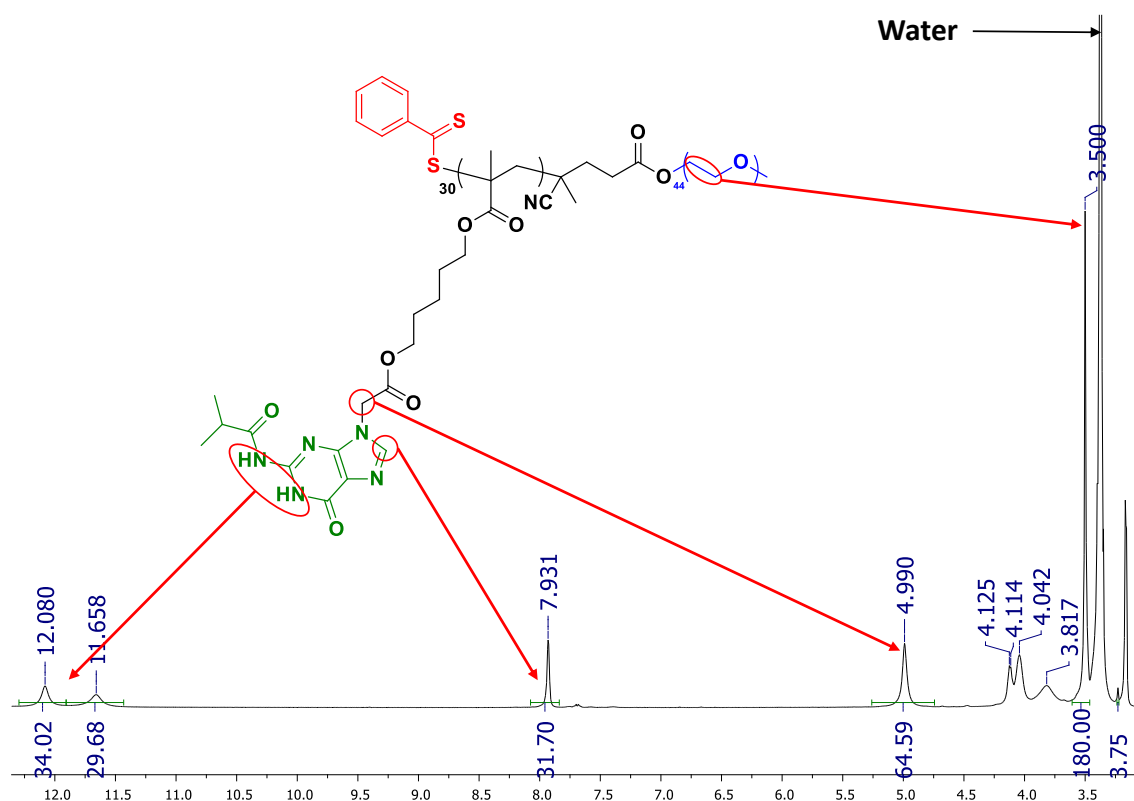


Figure 4.9. ^1H NMR in CDCl_3 of PEG2k-*b*-polyG

With **PEG2k-CTA**, an average $m = 32$ was determined, while for **PEG10k-CTA**, $m = 10$ (polymerised twice yielding similar results). The discrepancy between m_{th} and m when using **PEG10k-CTA** was also described in previous Chapters and seems to be associated to the macroCTA.

Thermal characterisation of the BCs was performed by TGA and DSC. Relevant data are gathered in **Table 4.2**.

Table 4.2. Thermal properties of the polyG BCs

Polymer	TGA ^a	T _g ^b	T _m (ΔH_m) ^c
PEG2k-<i>b</i>-polyG	172	45	---
PEG10k-<i>b</i>-polyG	268	---	54 (120 J/g)

^a Decomposition temperature (in $^{\circ}\text{C}$) associated to mass loss determined by TGA given at the onset of the weight loss curve

- ^b Glass transition temperature (in °C) determined by DSC on the first heating scan at 10 °C/min given at the half height of the baseline jump
- ^c Melting temperature (in °C) given at the maximum of the peak and associated melting enthalpy (in J/g), in brackets, determined by DSC on the first heating scan at 10 °C/min

DSC was performed at a rate of 10 °C/min. **PEG2k-*b*-polyG** was amorphous and a T_g was observed at 45 °C in the first scan, in contrast with **PEG2k-CTA** that had a T_m at 49 °C. **PEG10k-*b*-polyG** had a T_m at 54 °C that can be associated with the T_m of the macroinitiator (at 59 °C), due to its mayor proportion in this BC compared with **PEG2k-*b*-polyG**. As in **Chapter 2**, a unique transition was observed in each BC which might be indicative of, at least, partial compatibility between blocks.

4.3. SELF-ASSEMBLY IN WATER OF AMPHIPHILIC BLOCK COPOLYMERS

4.3.1 SELF-ASSEMBLY OF BLOCK COPOLYMERS

As the guanine moieties interacts with each other through H-bonding,¹⁰ self-assembly of **PEG10k-*b*-polyG** and **PEG2k-*b*-polyG**, were first investigated. Because BCs are only soluble in highly polar solvent such as DMF or DMSO, but not in THF or dioxane, self-assemblies were prepared by the co-solvent method using either DMF or DMSO and water. Turbidity curves are presented in **Figure 4.10**.

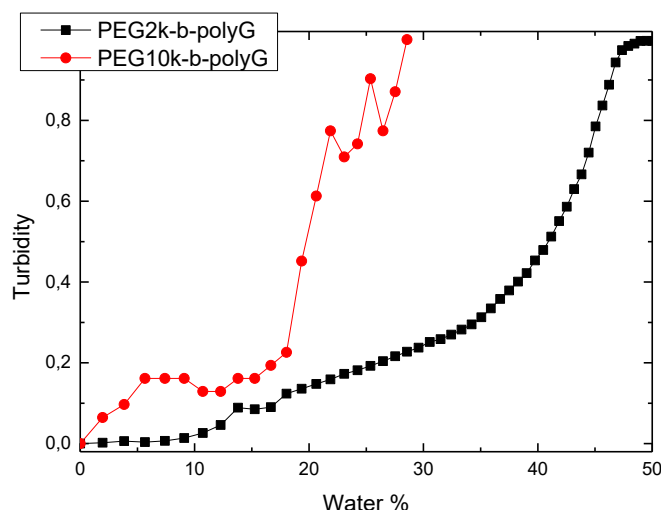


Figure 4.10. Turbidity curves registered PEG2k-*b*-polyG and PEG10k-*b*-polyG

With **PEG10k-*b*-polyG**, precipitation was observed when water was added over a solution of 5 mg/mL of the polymer in DMSO. Nevertheless, an apparently clear solution was obtained after the addition of water over a DMF solution of the BC, which is *a priori* indicative that stable polymeric self-assemblies were formed. The final dispersion was dialysed to remove the organic solvent and then diluted to obtain a 1 mg/mL concentration of the BC. This dispersion was studied by TEM and DLS. TEM grids stained with uranyl acetate during 30 s showed spherical

micelles that by DLS had an average hydrodynamic diameter of 40 ± 15 nm (Figure 4.11).

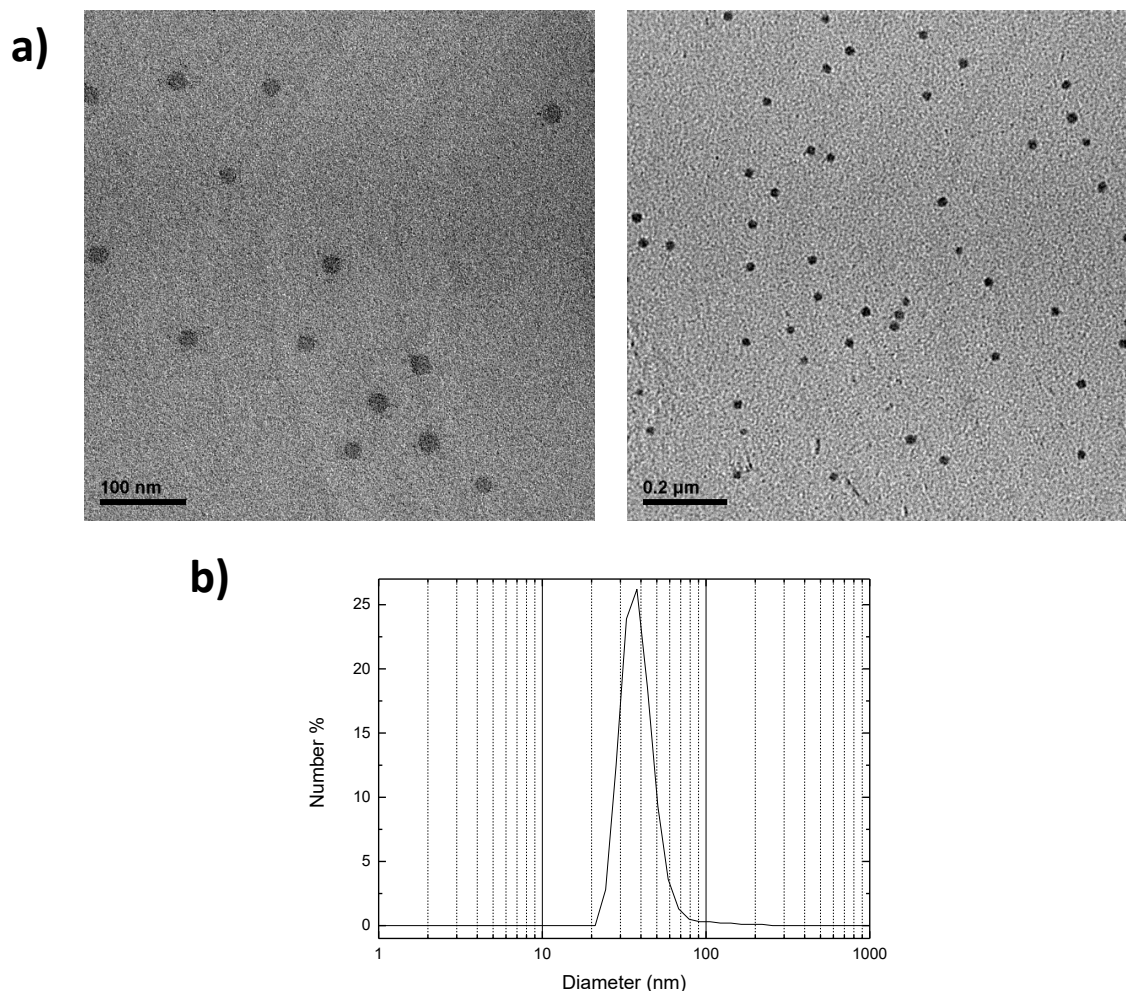


Figure 4.11. a) Representative TEM images and b) DLS number distribution of PEG10k-b-polyG micelles in water dispersion (1 mg/mL)

PEG2k-b-polyG was able to form stable dispersions using both DMF and DMSO at initial concentration of the BCs of 5 mg/mL. Employing DMF, large black spheres together with some amorphous material were observed by TEM (Figure 4.12a). However, DLS measurements were unstable probably due to the presence of the amorphous material. When using DMSO, black spheres were also observed in TEM images but not amorphous material (Figure 4.12b). From the images, self-assemblies were intense stained. Therefore, new TEM grids were prepared

that were stained only 10 s where contrast of images was improved (**Figure 4.12c**). Spherical self-assemblies were observed with D_h values of 323 ± 122 nm according to DLS.

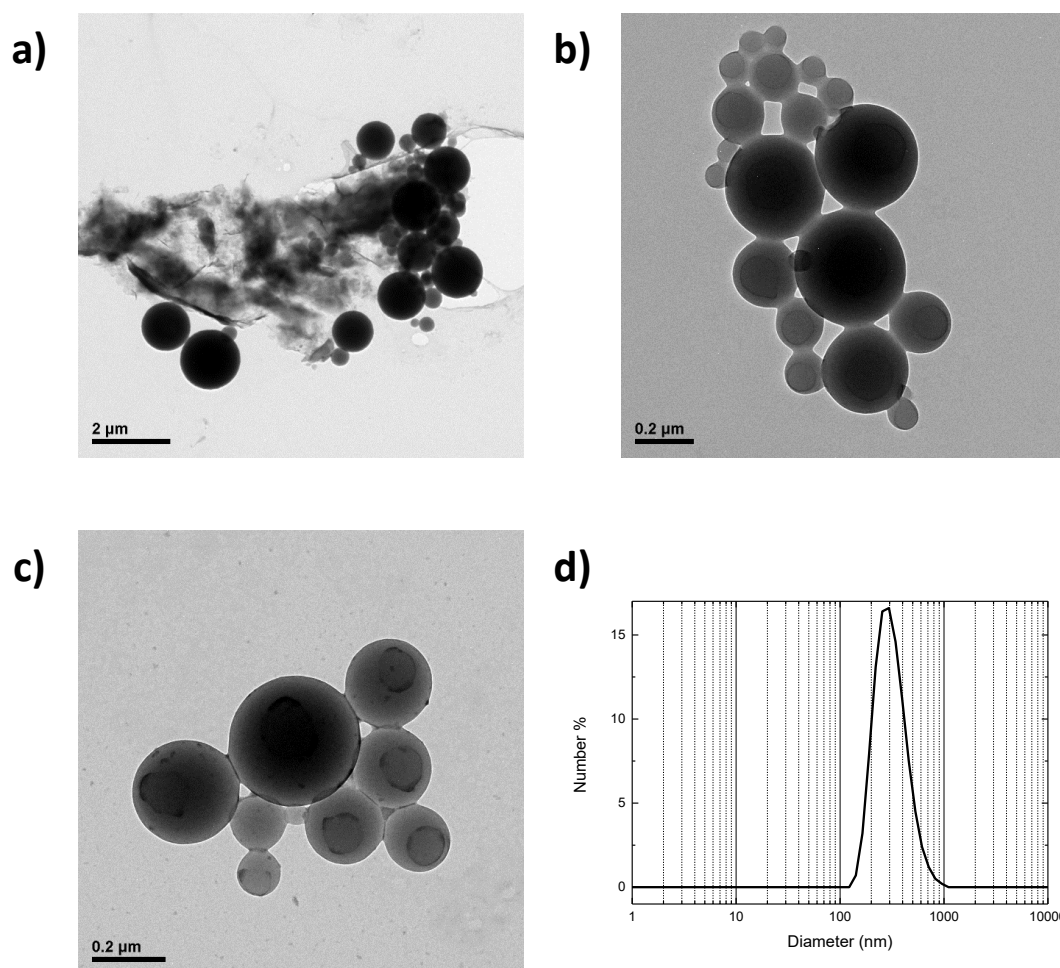


Figure 4.12. Representative TEM images of PEG2k-b-polyG spheres in water dispersion (1 mg/mL) formed by the co-solvent using a) DMF-water b) DMSO-water and stained for 30 s and c) DMSO-water and stained for 10 s and d) DLS of aggregates in water dispersion

CAC values were determined by fluorescence spectroscopy using Nile Red, as it was described in **Chapter 3**. In **Figure 4.13**, CAC determination for **PEG2k-b-polyG** is shown as an example. For **PEG2k-b-polyG**, CAC value was $8 \mu\text{g/mL}$, while for **PEG10k-b-polyG**, it was $87 \mu\text{g/mL}$. Both values were in concordance with values of reference for BCs in literature,¹¹ being lower in case of **PEG2k-b-polyG**. This can be due to the higher hydrophobic/hydrophilic balance of this BC.¹²

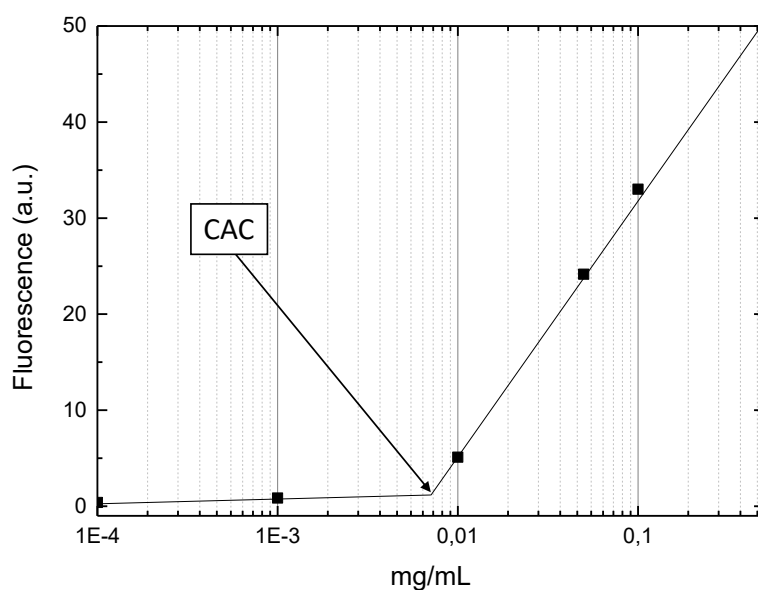


Figure 4.13. Plot of the emission intensity of Nile Red at 630 nm ($\lambda_{exc}=550$ nm) versus the log of the PEG2k-b-polyG concentration

4.3.2. SELF-ASSEMBLY OF SUPRAMOLECULAR BLOCK COPOLYMERS

The simplest methodology to obtain bulk samples of supramolecular BCs usually consists on dissolving both counterparts in a common solvent that is slowly evaporated to isolate the supramolecular material, as in **Chapter 3**. However, as the synthesised polyG BCs were only soluble in DMF and DMSO, this approach was restricted due to the low volatility of the solvents. For this reason, the preparation of supramolecular polymers was approached in THF and chloroform, assuming that the guanine-cytosine molecular recognition would occur along with an increase of the solubility of the BCs. However, it was not possible to completely dissolve the components even by stirring for several hours. Consequently, it was not possible to isolate the supramolecular BCs in order to the study of their bulk properties.

Consequently, self-assembly of supramolecular BCs was approached from solutions of polymers and cytosine-azobenzene derivatives, *i.e.* without isolating the solid supramolecular BCs. Four supramolecular polymer solutions in DMF or

DMSO were prepared by combining **PEG2k-*b*-polyG** and **PEG10k-*b*-polyG** and **Cyt-isoAZO** and **Cyt-tetraAZO-N** (Figure 4.14).

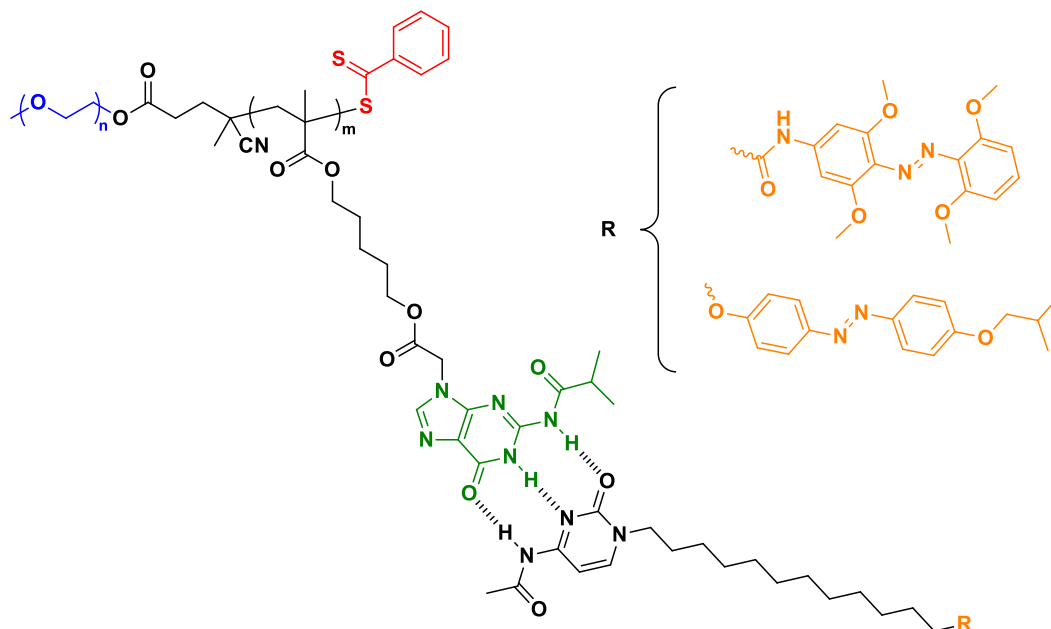


Figure 4.14. General structure of the aimed supramolecular polymers

Aggregates from the supramolecular BCs resulting from the guanine-cytosine interactions were obtained using the co-solvent method. In order to gain control over the addition of water, an addition pump was used instead of manual addition. Addition rate of water was set at 0.75 mL/h, and a total of 2.5 mL of Milli-Q water was added to the organic solution. Then, samples were dialysed against water and finally diluted to obtain a solution concentration of 1 mg/mL of the supramolecular BC.

Initially, **cyt-isoAZO** containing BCs were attempted starting from DMF but the whole supramolecular BCs were not completely soluble and then DMSO was used instead. Nevertheless, the formation of self-assembled structures was not successful and an orange precipitate was formed throughout the addition of water.

However, for **cyt-tetraAZO-N** stable dispersions were obtained using DMF. In the case of **PEG10k-*b*-polyG · Cyt-tetraAZO-N**, micelles were obtained according to TEM images (Figure 4.15) and a D_h of 40 ± 9 nm was determined in DLS

observations. For **PEG2k-*b*-polyG · Cyt-tetraAZO-N**, spheres were observed in TEM images (staining time = 10 s) (**Figure 4.16**) with a D_h of 545 ± 88 nm according to DLS experiments.

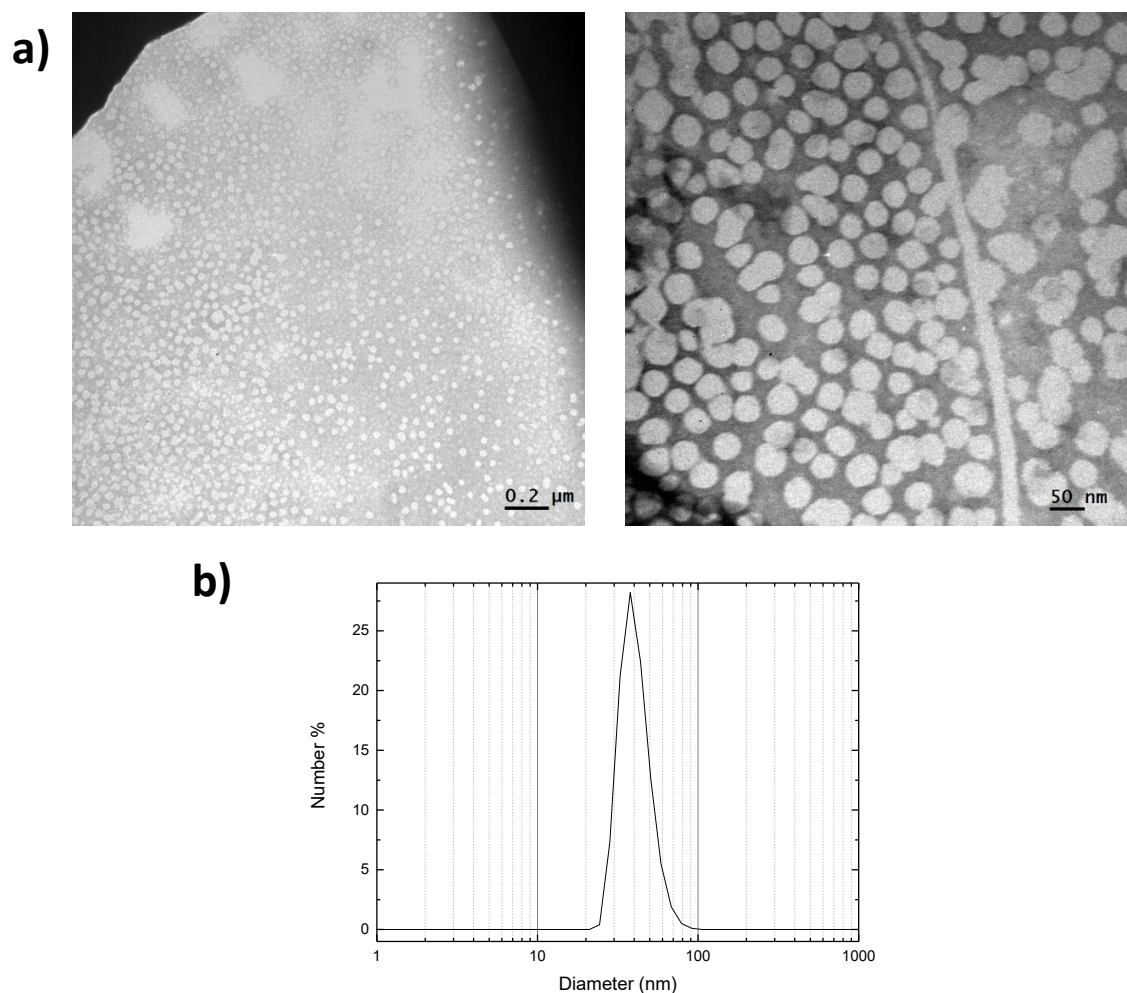


Figure 4.15. Representative a) TEM images of PEG10k-*b*-polyG·Cyt-tetraAZO-N micelles in water dispersion (1 mg/mL) (staining time = 30 s) and b) DLS number distribution of PEG10k-*b*-polyG·Cyt-tetraAZO-N micelles in water dispersion

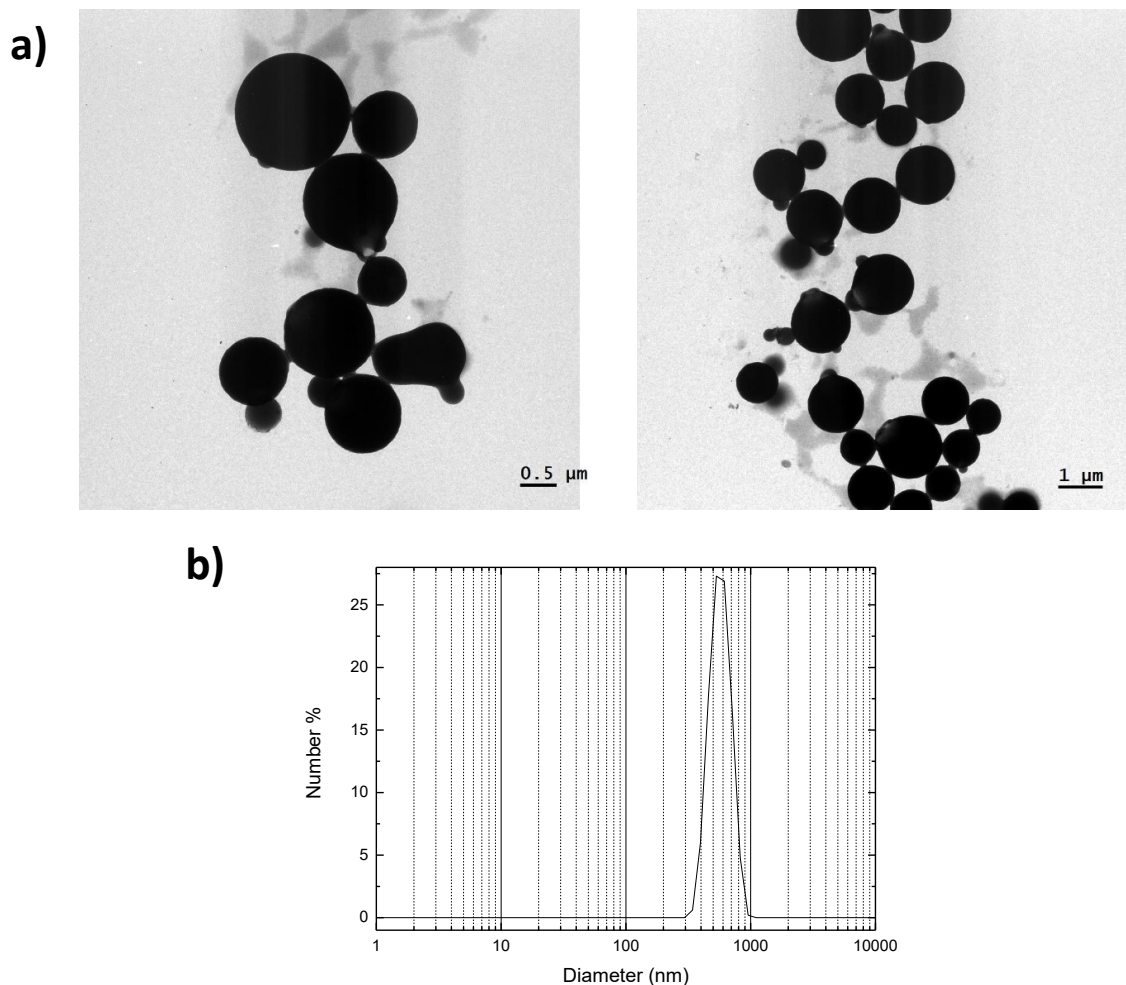


Figure 4.16. Representative a) TEM images of PEG2k-b-polyG·Cyt-tetraAZO-N spheres in water dispersion (1 mg/mL) and b) DLS number distribution of PEG2k-b-polyG·Cyt-tetraAZO-N spheres in water dispersion

Then, UV-Vis spectrum of **PEG10-b-polyG** micelles in water was registered (**Figure 4.17**) as reference, in order to compare with the subsequent supramolecular polymers spectra, and two maxima at 260 and 280 nm were found.

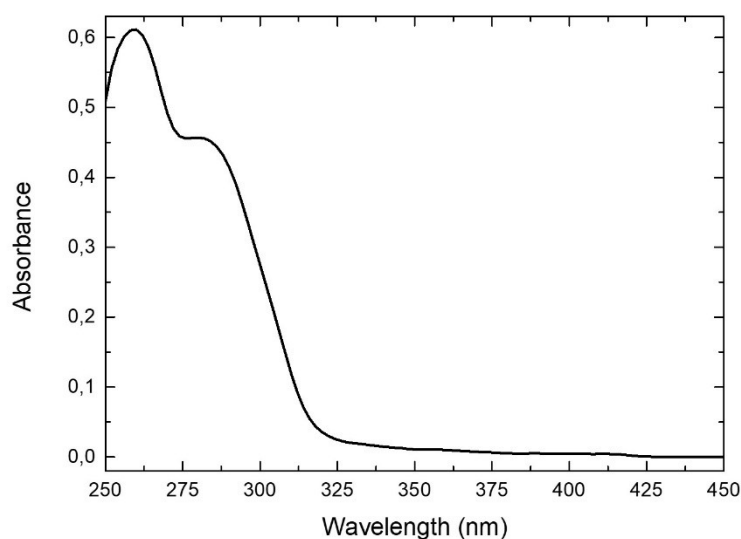


Figure 4.17. UV-Vis spectrum of PEG10k-*b*-polyG micelles in water dispersion (0.5 mg/mL)

On the basis of the previous results shown in **Chapter 2**, photoresponse of **PEG10k-*b*-polyG · Cyt-tetraAZO-N** and **PEG2k-*b*-polyG · Cyt-tetraAZO-N** was evaluated upon 530 nm light. Spectra at different times of irradiation are shown in **Figure 4.18a** and in **Figure 4.18b**.

Before irradiation ($t=0$ min), the UV-vis spectrum of **PEG10k-*b*-polyG · Cyt-tetraAZO-N** presented a maximum absorption corresponding to the polyG band at *ca.* 280 nm that overlapped the π - π^* transition band of the azobenzene, which appeared as a shoulder at *ca.* 325 nm. A weak signal at 450 nm corresponded to the n - π^* transition band of the *trans* isomer of **tetraAZO-N** chromophore. After irradiation with 530 nm light, π - π^* band slightly decreased as well as the n - π^* band was blue-shifted.

For **PEG2k-*b*-polyG · Cyt-tetraAZO-N**, a maxima at about 280 nm that might be due to **polyG**, and at about 386 nm corresponding to the π - π^* transition band of azobenzene were visible. This last band was red shifted compared to the maximum register in solution and might be due to the presence of *J*-aggregates in the self-assembled structures. The n - π^* transition band appeared as a shoulder at *ca.* 500 nm. Nevertheless, it has to be taken into account the scattering of the samples,

which led to highly distorted spectra. After irradiation, a small decrease was observed in π - π^* band together with a blue-shifting of n - π^* band

Self-assembled structures were studied after irradiation and no significant morphological modifications were appreciated in TEM images neither for **PEG10k-*b*-polyG · Cyt-tetraAZO-N** (Figure 4.19) nor for **PEG2k-*b*-polyG · Cyt-tetraAZO-N** (Figure 4.20). Regarding DLS, no changes were observed for **PEG10k-*b*-polyG · Cyt-tetraAZO-N** but a shift from 545 ± 88 nm to 427 ± 70 nm was observed for **PEG2k-*b*-polyG · Cyt-tetraAZO-N** after 3 minutes of irradiation with 530 nm, which could be an evidence of some light induced modifications not observed in TEM.

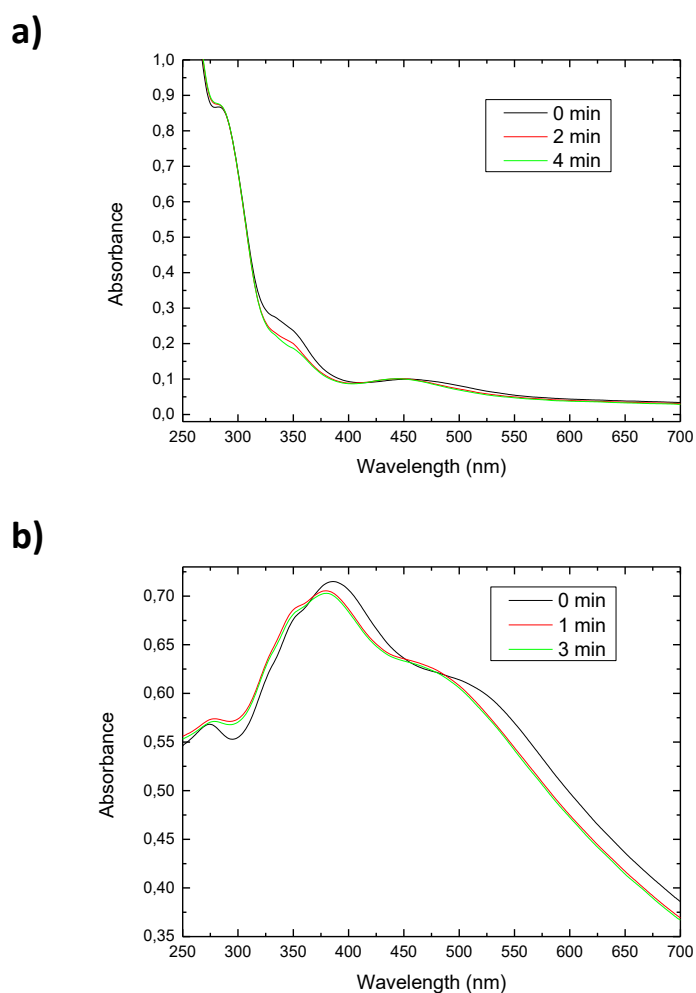


Figure 4.18. Spectra at different times of irradiation with 530 nm of
a) PEG10k-*b*-polyG · Cyt-tetraAZO-N micelles in water dispersion (1 mg/mL) and
b) PEG2k-*b*-polyG · Cyt-tetraAZO-N vesicles in water dispersion (1 mg/mL)

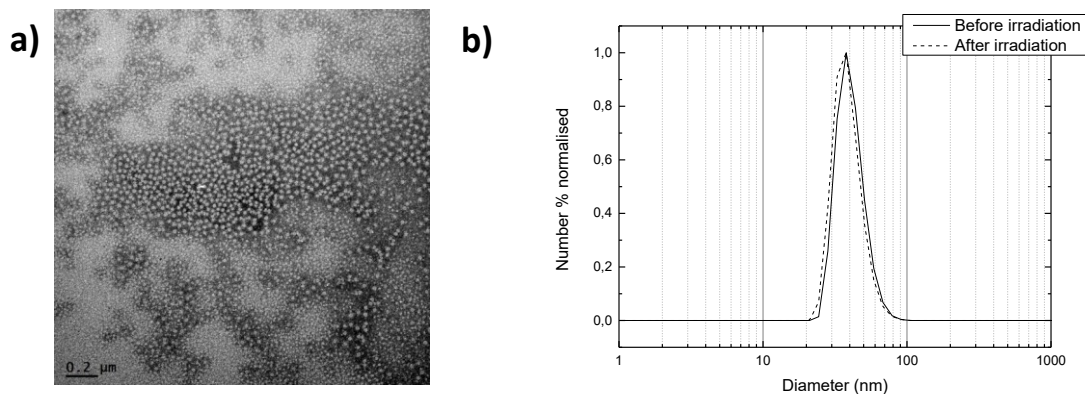


Figure 4.19. Representative a) TEM images and b) DLS number distribution of PEG10k-b-polyG·Cyt-tetraAZO-N micelles in water dispersion (1 mg/mL) after irradiation with 530 nm

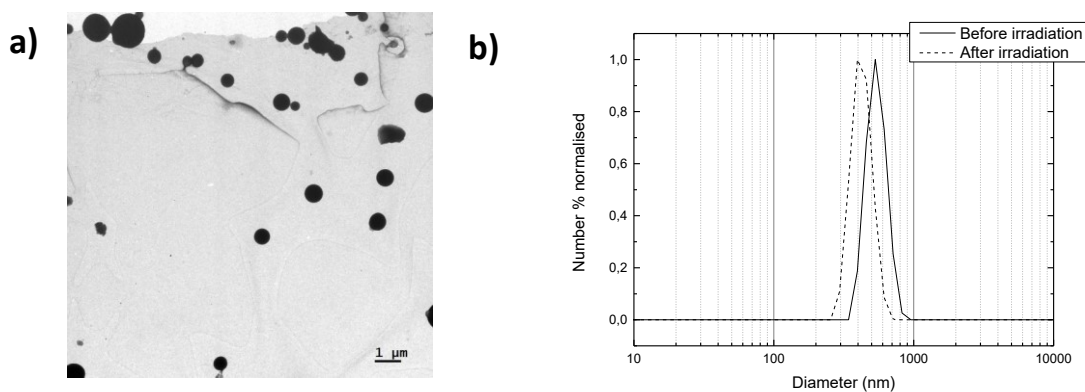


Figure 4.20. Representative a) TEM images and b) DLS number distribution of PEG2k-b-polyG·Cyt-tetraAZO-N vesicles in water dispersion (1 mg/mL) after irradiation with 530 nm

4.4. CONCLUSIONS

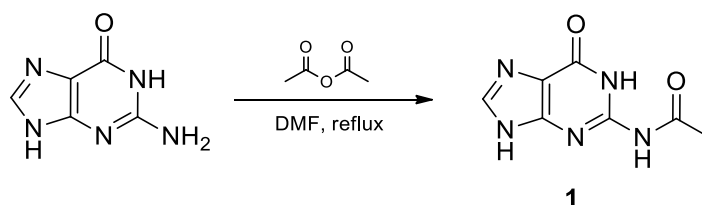
Summary and main conclusions of this Chapter are the following:

- Novel guanine-based amphiphilic block copolymers have been prepared being the first described to the best of our knowledge. These BCs have been prepared by RAFT polymerisation using PEG macroCTA. The macroCTA with a lower degree of polymerisation affords better results.
- These BCs have been modified in organic solution using cytosine derived molecules, due to the G-C interaction.
- Guanine-based block copolymers were self-assembled in water before and after functionalisation with cytosine molecules and stable dispersions were obtained.

4.5. EXPERIMENTAL SECTION

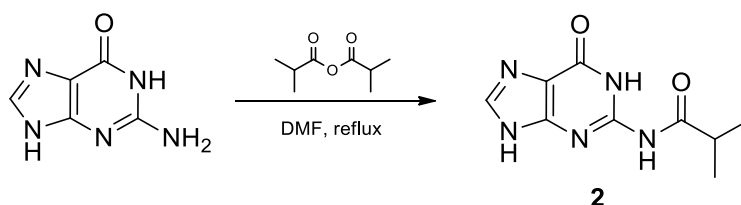
4.5.1. SYNTHESIS AND CHEMICAL CHARACTERISATION

Synthesis of N-(6-oxo-6,9-dihydro-1H-purin-2-yl)acetamide (1)



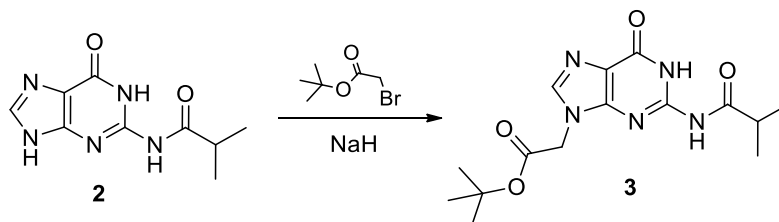
Guanine (5.0 g, 33 mmol) and acetic anhydride (8.4 g, 82.7 mmol) were dissolved in dry DMF (100 mL). The temperature was set at 150 °C and the reaction was allowed to stir until the reaction became clear (2-3 h approx.). Then, DMF was removed under reduced pressure and the crude was purified recrystallising in ethanol/water (1/1). The solid was filtered and dried obtaining a white powder. Yield: 88%. ¹H NMR (400 MHz, DMSO) δ 12.11 (s, 1H), 11.95 (s, 1H), 7.93 (s, 1H), 2.16 (s, 3H).

Synthesis of N-(6-oxo-6,9-dihydro-1H-purin-2-yl)isobutyramide (2)



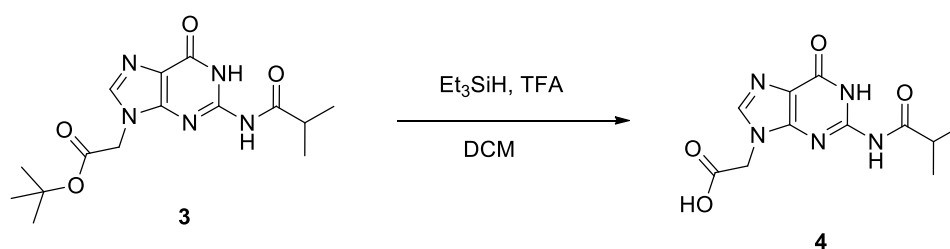
Guanine (7.56 g, 50 mmol) and butyric anhydride (21.36 g, 135 mmol) were dissolved in dry DMF (100 mL). The temperature was set at 150 °C and allowed to stir until the reaction became clear. Then, DMF was removed under reduced pressure and the crude was purified by recrystallisation in ethanol/water (1/1). The solid was filtered and dried, obtaining a white powder. Yield: 82%. ¹H NMR (400 MHz, DMSO) δ 12.07 (s, 1H), 11.63 (s, 1H), 8.02 (s, 1H), 2.81 – 2.68 (sep, *J* = 6.8 Hz, 1H), 1.11 (d, *J* = 6.8 Hz, 6H).

Synthesis of tert-butyl 2-(2-isobutyramido-6-oxo-1H-purin-9(6H)-yl)acetate (3)



Compound **2** (3.3 g, 14.9 mmol) was dissolved in dry DMF (75 mL) and the flask was placed into an ice bath. NaH (360 mg, 14.9 mmol) was added and the reaction was allowed to stir for 30 minutes. *Tert*-butyl bromoacetate (2 mL) was added dropwise and, then, the ice bath was removed and the reaction was stirred during 2 h. DMF was distilled off under reduced pressure and the crude was purified by recrystallisation in ethyl acetate, obtaining the product as a white powder. Yield: 53%. IR (KBr), ν (cm^{-1}): 2977, 1681, 1606, 1557, 1410, 1367, 1253, 1197, 1157, 780. ^1H NMR (300 MHz, DMSO) δ 12.10 (s, 1H), 11.65 (s, 1H), 7.95 (s, 1H), 4.88 (s, 2H), 2.77 (sep, $J = 6.7$ Hz, 1H), 1.42 (s, 9H), 1.11 (d, $J = 6.8$ Hz, 6H).

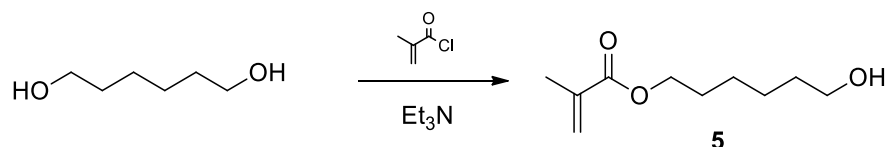
Synthesis of 2-(2-isobutyramido-6-oxo-1H-purin-9(6H)-yl)acetic acid (4)



Compound **3** (2.0 g, 5.97 mmol) was suspended in DCM (10 mL) and triethylsilane (4.8 mL, 30 mmol) was added. The flask was cooled to 0 °C in an ice bath and trifluoroacetic acid (15 mL) was added over a period of 5 min. After 30 min, the ice bath was removed and the reaction was allowed to stir for 2 h at room temperature. Then, diethyl ether (100 mL) was added and evaporated under reduced pressure until a foam was obtained. This foam was dispersed in diethyl ether (50 mL) and the solid was filtered and washed several times with diethyl ether, obtaining a white powder. Yield: 92 %. IR (KBr), ν (cm^{-1}): 3419, 3134, 1682, 1608, 1411, 1253, 1195, 1155, 786. ^1H NMR (300 MHz, DMSO) δ 12.12 (s, 1H), 11.70 (s, 1H), 8.04 (s, 1H),

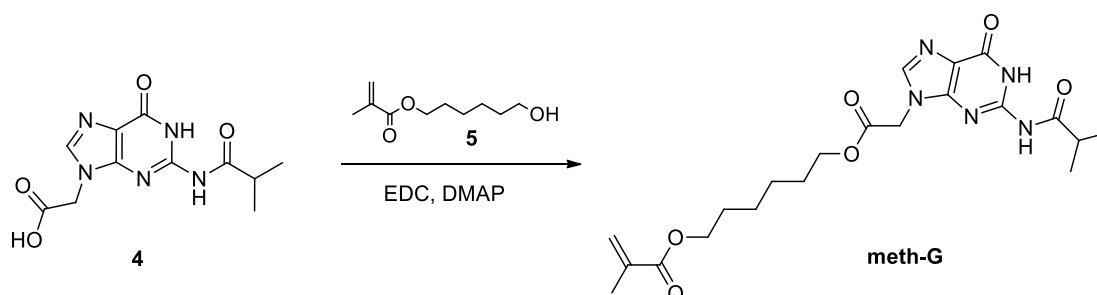
4.91 (s, 2H), 2.76 (sep, $J = 6.8$ Hz, 1H), 1.11 (d, $J = 6.8$ Hz, 6H). ^{13}C NMR (75 MHz, DMSO) δ 180.22, 168.97, 154.64, 148.93, 148.25, 140.32, 119.15, 44.54, 34.73, 18.86.

Synthesis of 6-hydroxyhexyl methacrylate (**5**)



1,6-hexanediol (11.3 g, 96 mmol) and Et₃N (5.0 g, 48 mmol) were placed into a flask under argon atmosphere and dissolved in DCM (100 mL). Then, methacryloyl chloride (5.0 g, 48 mmol) was added dropwise and the reaction stirred overnight. The solution was washed with saturated NaHCO₃ solution (100 mL), brine (100 mL) and dried with MgSO₄. The solvent was removed and the crude was purified by silica column chromatography using hexane/ethyl acetate (9/1) as eluent, obtaining a colourless oil. Yield: 66 %. ^1H NMR (400 MHz, CDCl₃) δ 6.08 (dd, $J = 1.6, 1.0$ Hz, 1H), 5.54 (dt, $J = 1.6, 1.6$ Hz, 1H), 4.14 (t, $J = 6.6$ Hz, 2H), 3.63 (t, $J = 6.6, 2\text{H}$), 1.93 (dd, $J = 1.6, 1.0$ Hz, 3H), 1.74 – 1.64 (m, 2H), 1.60 – 1.53 (m, 2H), 1.45 – 1.36 (m, 4H). ^{13}C NMR (101 MHz, CDCl₃) δ 167.69, 136.59, 125.34, 64.76, 62.84, 32.67, 28.69, 25.88, 25.48, 18.40.

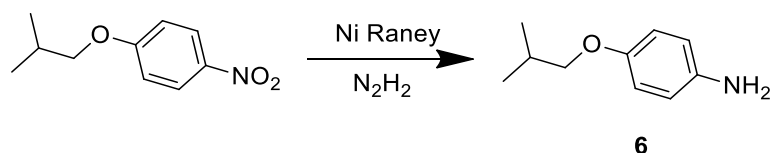
Synthesis of 6-(2-(2-isobutyramido-6-oxo-1H-purin-9(6H)-yl)acetoxyl)hexyl methacrylate (meth-G)



Compound **5** (600 mg, 3.22 mmol), compound **4** (900 mg, 3.22 mmol) and DMAP (118 mg, 0.6 mmol) were dissolved in dry DMF (15 mL) under argon atmosphere

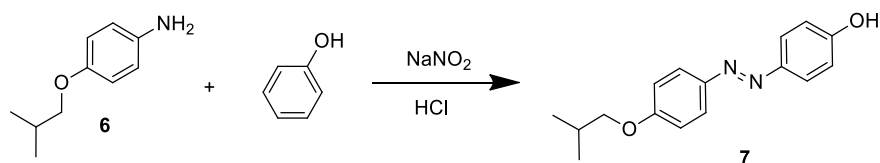
and the flask was cooled to 0 °C. Then, EDC (740 mg, 3.87 mmol) was added and the reaction stirred at this temperature for 30 min. Then, the ice bath was removed and the reaction was further stirred overnight. The mixture was diluted with ethyl acetate (200 mL) and washed with water (3 x 100 mL). The organic phase was washed with brine, dried over MgSO₄ and the solvent evaporated. The crude was purified by silica column chromatography using DCM/methanol (9.5/0.5) as eluent, obtaining a white solid. Yield: 70 %. IR (KBr), ν (cm⁻¹): 3145, 2932, 1757, 1717, 1663, 1613, 1569, 1482, 1411, 1198, 1155, 787. ¹H NMR (400 MHz, CDCl₃) δ 12.16 (s, 1H), 9.77 (s, 1H), 7.75 (s, 1H), 6.09 (dt, *J* = 1.5, 0.9 Hz, 1H), 5.56 (dt, *J* = 1.5, 1.5 Hz, 1H), 4.18 – 4.06 (m, 4H), 2.86 (sep, *J* = 6.9 Hz, 1H), 1.93 (dd, *J* = 1.5, 0.9 Hz, 3H), 1.72 – 1.56 (m, 4H), 1.43 – 1.27 (m, 4H), 1.24 (d, *J* = 6.9 Hz, 6H). ¹³C NMR (101 MHz, CDCl₃) δ 179.51, 167.89, 167.25, 155.77, 148.99, 148.27, 139.59, 136.46, 125.69, 120.55, 66.15, 64.58, 44.51, 36.28, 28.34, 28.27, 25.46, 25.28, 19.13, 18.41.

Synthesis of 4-isobutyloxyaniline (6)



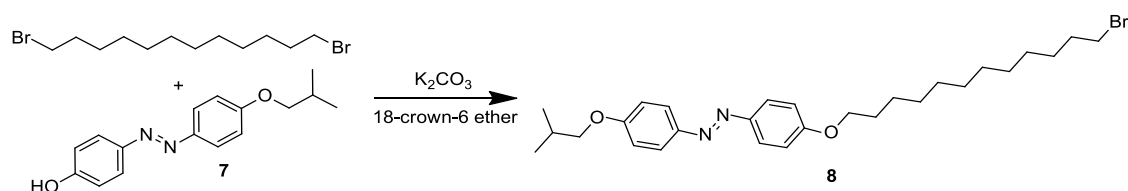
4-Isobutyloxynitrobenzene (7.0 g, 35.9 mmol) and hydrazine monohydrate (3.5 mL, 71.7 mmol) were dissolved in ethanol (70 mL). The solution was heated to 40 °C, and then activated Ni Raney was added carefully until no bubbling was observed. The reaction was stirred while following its progress by TLC. Once the reaction was completed, the reaction was filtered through a pad of Celite[®] and the ethanol was eliminated by evaporating. The crude was redissolved in diethyl ether (100 mL), washed with water (100 mL) and brine (100 mL). The organic phase was dried over MgSO₄, the solid filtered off and the solvent evaporated. Yield: 88 %. ¹H NMR (CDCl₃, 400MHz) δ (ppm): 6.75-6.73 (m, 2H), 6.65-6.62 (m, 2H), 3.64 (d, *J* = 6,5 Hz, 2H), 3,40 (s broad, 2H), 2.04 - 2.11 (m, 1H), 1.00 (d, *J* = 6,7 Hz, 6H).

Synthesis of 4-isobutyloxy-4'-hydroxyazobenzene (7)



A solution of NaNO₂ (2.2 g, 31.5 mmol) in water (20 mL) was added dropwise over a solution of the aniline **6** (5.2 g, 31.2 mmol) in HCl 6M (15 mL) cooled in an ice bath. Then, a solution of phenol (2.96 g, 31.5 mmol) in 2M NaOH (25 mL) was added dropwise while keeping temperature below 5°C. The product was precipitated after 24 h of stirring by addition of HCl until pH=7. The solid was filtered and further purified by silica column chromatography using DCM as eluent, obtaining an orange powder. Yield: 67 %. ¹H NMR (CDCl₃, 400MHz) δ (ppm) 7.87 - 7.85 (m, 4H), 7.84 - 7.82 (m, 4H), 3.81 (d, *J* = 6,5 Hz, 2H), 2.07 - 2.13 (m, 1H), 1.05 (d, *J* = 6,7 Hz, 6H). ¹³C NMR (CDCl₃, 100 MHz) δ (ppm) 161.4, 157.6, 146.8, 124.6, 124.4, 115.8, 114.7, 74.7, 28.3, 19.3.

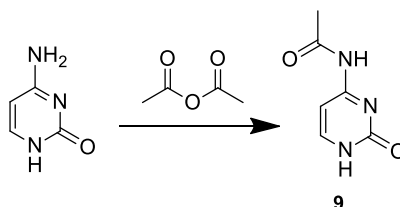
Synthesis of 4-isobutyloxy-4'-(12-bromododecyl)oxy)azobenzene (8)



A suspension of 1,11-dibromoundecane (4.9 g, 14.8 mmol), K₂CO₃ (4.0 g) and 18-crown-6 ether (a spoon tip) in acetone (60 mL) was stirred into a round bottom flask at 60 °C. Then, azobenzene **7** (4 g, 14.8 mmol) was dissolved in acetone (10 mL) and added dropwise into the reaction flask. The reaction was heated at reflux for 20 h. The solvent was evaporated and the residue dissolved in DCM (100 mL). The resulting organic solution was washed with water (100 mL) and brine (100 mL), and dried over MgSO₄. The solid was filtered off and the solvent evaporated. The residue was purified by silica column chromatography using hexane/DCM (3/1) as eluent. Yield: 47 %. ¹H NMR (300 MHz, CDCl₃) δ 8.09 – 7.71 (m, 4H), 7.12 – 6.87 (m, 4H), 4.03 (t, *J* = 6.6 Hz, 2H), 3.80 (d, *J* = 6.5 Hz, 2H), 3.41 (t, *J* = 6.9 Hz, 2H), 2.19 – 2.05 (m, 1H), 1.92 – 1.74 (m, 4H), 1.56 – 1.23 (m, 16H), 1.05 (d, *J* = 6.7 Hz,

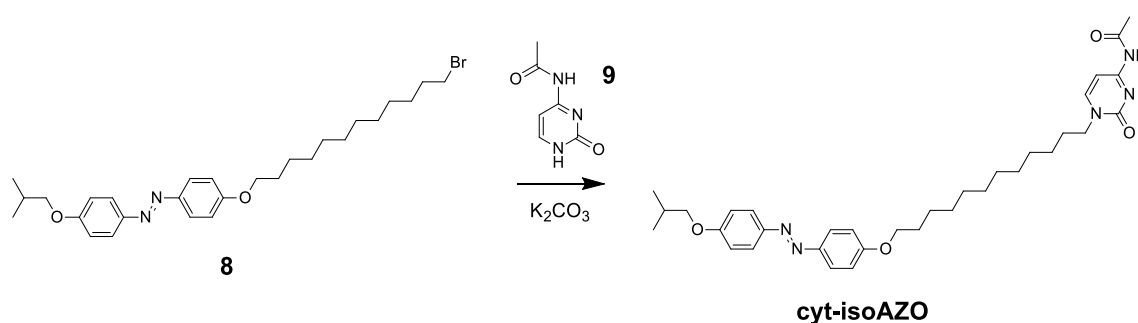
6H). ^{13}C NMR (CDCl_3 , 75 MHz) δ (ppm) 161.4, 161.3, 147.1, 147.1, 124.4, 114.8, 74.8, 68.5, 34.2, 33.0, 29.7, 29.6, 29.5, 29.4, 28.9, 28.4, 28.3, 26.2, 19.4

Synthesis of acetylcytosine (**9**)



Acetic anhydride (6 mL) was added dropwise over a solution of cytosine (2.0 g, 18 mmol) in DMF (50 mL) under argon atmosphere heated to 150 °C. The reaction was stirred for 2 h. Then, the reaction was cooled to room temperature and a saturated NaHCO_3 solution was added until no bubbles were observed. The formed solid was filtered, washed with water and dried. Yield: 86 %. ^1H NMR (400 MHz, DMSO) δ 7.80 (d, $J = 7.0$ Hz, 1H), 7.09 (d, $J = 7.0$ Hz, 1H), 2.08 (s, 3H). ^{13}C NMR (101 MHz, DMSO) δ 170.98, 163.30, 156.28, 147.23, 94.58, 24.38.

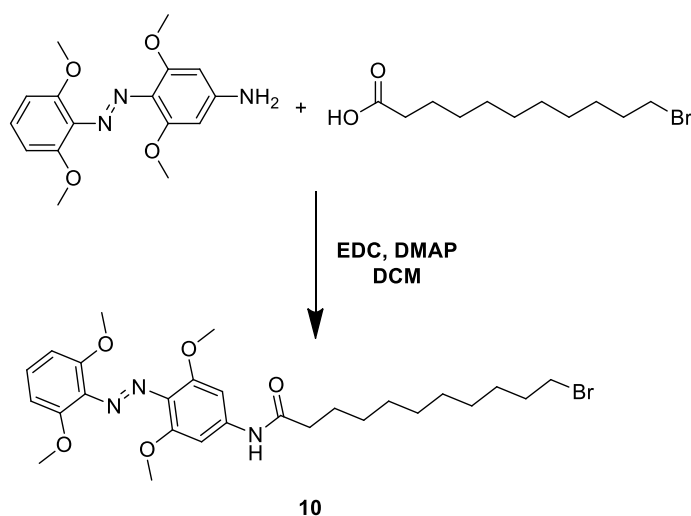
Synthesis of *N*-(1-(12-(4-((4-isobutoxyphenyl)diazenyl)phenoxy)dodecyl)-2-oxo-1,2-dihydropyrimidin-4-yl)acetamide (cyt-isoAZO)



Acetylcytosine **9** (250 mg, 1.63 mmol) and K_2CO_3 (340 mg, 2.46 mmol) were suspended in dry DMF (15 mL). The solution was allowed to stir for 30 min. Then, azobenzene **8** (1.25 g, 2.41 mmol) was added and the mixture heated to 80 °C. The reaction was allowed to proceed for 16 h and then poured into CHCl_3 (200 mL). The organic solution was washed with water (3x200 mL) and brine (200 mL), dried over MgSO_4 , and the solvent evaporated. The crude was purified by silica

column chromatography eluting first with DCM/ethyl acetate (9/1) and then with DCM/MeOH (9/1). The product was obtained as an orange powder. Yield: 56 %. IR (KBr), ν (cm^{-1}): 3321, 2971, 2849, 1691, 1663, 1601, 1580, 1555, 1499, 1471, 1383, 1243, 1147, 1032, 838, 787. ^1H NMR (400 MHz, CDCl_3) δ 7.89 – 7.81 (m, 4H), 7.62 (d, J = 7.0 Hz, 1H), 7.39 (d, J = 7.2 Hz, 1H), 7.02 – 6.94 (m, 4H), 4.02 (t, J = 6.5 Hz, 2H), 3.85 (t, J = 7.3 Hz, 2H), 3.79 (d, J = 6.6 Hz, 2H), 2.29 (s, 3H), 2.11 (sep, J = 6.7 Hz, 1H), 1.84 – 1.76 (m, 2H), 1.73 (m, 2H), 1.52 – 1.41 (m, 2H), 1.40 – 1.21 (m, 16H), 1.04 (d, J = 6.7 Hz, 6H). ^{13}C NMR (75 MHz, CDCl_3) δ 171.08, 162.76, 161.39, 161.26, 155.90, 148.78, 147.01, 147.00, 124.40, 114.78, 114.77, 96.70, 74.77, 68.41, 51.22, 29.62, 29.57, 29.49, 29.31, 29.07, 28.41, 26.64, 26.13, 25.02, 19.38.

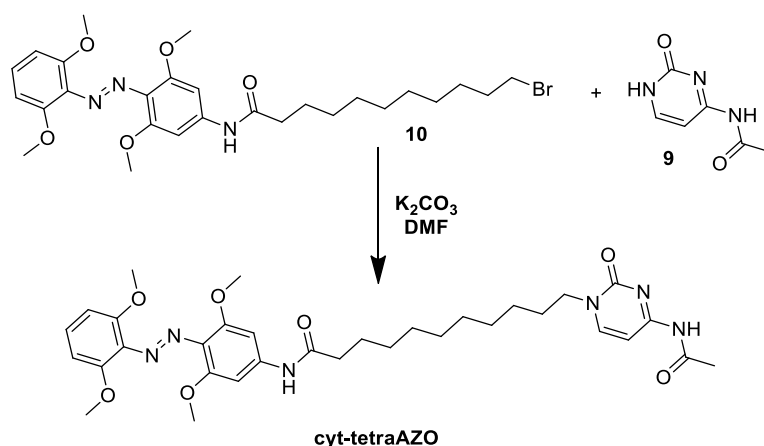
Synthesis of 11-bromo-*N*-(4-((2,6-dimethoxyphenyl)diazenyl)-3,5-dimethoxyphenyl)undecanamide (10)



A solution of *ortho*-tetramethoxyazobenzene (840 mg, 2.64 mmol) (see compound **1** in **Chapter 2**), 1-bromoundecanoic acid (700 mg, 2.64 mmol) and DMAP (40 mg, 0.32 mmol) in DCM (5 mL) was cooled in an ice bath and then EDC (506 mg, 2.64 mmol) was added into the flask under argon atmosphere. The ice bath was removed after 30 min and the reaction was maintained at room temperature for 24 h. The reaction solution was washed with water and brine, dried over MgSO_4 , and the solvent rotary-evaporated. The resultant crude was purified by silica column chromatography using DCM as eluent to yield a red powder. Yield: 56 %.

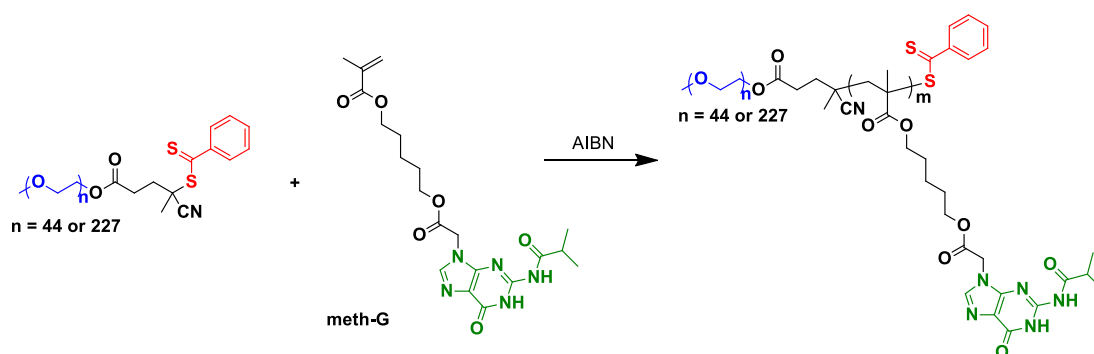
^1H NMR (400 MHz, DMSO) δ 10.09 (s, 1H), 7.25 (t, J = 8.4 Hz, 1H), 7.14 (s, 2H), 6.76 (d, J = 8.5 Hz, 2H), 3.71 (s, 6H), 3.70 (s, 6H), 3.52 (t, J = 6.7 Hz, 2H), 2.33 (t, J = 7.4 Hz, 2H), 1.84 – 1.74 (m, 2H), 1.66 – 1.55 (m, 2H), 1.44 – 1.21 (m, 12H).

Synthesis of 11-(4-acetamido-2-oxopyrimidin-1(2H)-yl)-N-(4-((2,6-dimethoxyphenyl)diazenyl)-3,5-dimethoxyphenyl)undecanamide (cyt-tetraAZO-N):



A suspension of compound **9** (200 mg, 1.42 mmol) and K_2CO_3 (300 mg, 2.13 mmol) in dry DMF (15 mL) was stirred for 30 min. Then, compound **10** (800 mg, 1.42 mmol) was added, the flask heated to 80 °C and the reaction allowed to evolve for 16 h. The reaction crude was poured into CHCl_3 (200 mL) and the resulting organic solution washed with water (3x200 mL) and brine (200 mL), dried over MgSO_4 and evaporated to dryness. The crude was purified by silica column chromatography eluting first with DCM/ethyl acetate (9/1) and then with DCM/MeOH (9/1). The product was obtained as an orange powder. Yield: 63 %. IR (KBr), ν (cm^{-1}): 2925, 2853, 1658, 1597, 1492, 1406, 1372, 1307, 1256, 1233, 1127, 1109. ^1H NMR (400 MHz, DMSO) δ 10.77 (s, 1H), 10.10 (s, 1H), 8.07 (d, J = 7.2 Hz, 1H), 7.24 (t, J = 8.4 Hz, 1H), 7.16 – 7.10 (m, 3H), 6.76 (d, J = 8.5 Hz, 2H), 3.76 (t, J = 7.2 Hz, 2H), 3.71 (s, 6H), 3.70 (s, 6H), 2.33 (t, J = 7.4 Hz, 2H), 1.70 – 1.51 (m, 4H), 1.36 – 1.18 (m, 12H). ^{13}C NMR (75 MHz, DMSO) δ 171.83, 170.86, 162.16, 155.18, 152.92, 151.19, 150.18, 141.62, 134.18, 128.59, 105.34, 95.67, 94.84, 56.09, 55.90, 49.51, 36.61, 28.87, 28.83, 28.77, 28.68, 28.59, 28.26, 25.88, 24.93, 24.29.

Synthesis of PEG(X)k-*b*-polyG (X = 2 or 10):



Meth-G (200 mg, 0.447 mmol), **PEG(X)k-CTA** (25.6 mg of PEG2k or 125 mg of PEG10k, 0.0127 mmol) and AIBN (0.2 mg, 0.00127 mmol) were dissolved in DMF (2 mL) into a Schlenk flask. The flask was degassed *via* three freeze-pump-thaw cycles and the polymerisation was carried out at 70°C for 24 h. The polymer was precipitated into cold ethyl ether/methanol (180+20 mL) and isolated by filtration to obtain a pink powder.

*PEG2k-*b*-polyG*: IR (KBr), ν (cm^{-1}): 3176, 2937, 1683, 1610, 1563, 1411, 1198, 1155, 783. ^1H NMR (400 MHz, DMSO) δ 12.08, 11.66, 7.93, 4.99, 4.13, 4.11, 4.04, 3.82, 3.50, 3.23, 1.49, 1.21, 1.08, 0.87, 0.73.

*PEG10k-*b*-polyG*: IR (KBr), ν (cm^{-1}): 2890, 1686, 1613, 1562, 1467, 1343, 1280, 1242, 1114, 963, 842. ^1H NMR (400 MHz, DMSO) δ 12.08, 11.66, 7.95, 4.99, 4.13, 4.11, 4.04, 3.82, 3.50, 3.23, 1.48, 1.21, 1.08, 0.87, 0.73.

4.5.2. PREPARATION AND CHARACTERISATION OF POLYMER AGGREGATES

Preparation of polymer aggregates by the co-solvent method

Procedure A

5 mg of block copolymer were dissolved in DMF or DMSO and then, Milli-Q water was added dropwise while turbidity was followed by UV-Vis spectroscopy measuring the scattering of the solution at 650 nm. Once turbidity has reached a plateau, the mixture was dialysed against water using a Spectra/Por® membrane

(MWCO = 1000 g/mol) during 3 days. The nanoparticles solution was diluted to a total volume of 5 mL to obtain a final concentration of 1 mg/mL of the polymer in water.

Procedure B

5 mg of polymer were dissolved in 1 mL of DMF. Then, 2.5 mL of Milli-Q water were added using a syringe pump at a rate of 0.75 mL/h. Then, DMF was removed by dialysis against water using a Spectra/Por® membrane (MWCO = 1000 g/mol) during 3 days. The nanoparticles solution was diluted to a total volume of 5 mL to obtain a final concentration of 1 mg/mL of the polymer in water.

Preparation of TEM grids

10 μL of a 1 mg/mL nanoparticles solution was applied onto a TEM grid. After 10 or 30 s (depending on the sample), the drop was removed with filter paper by capillarity. A 10 μL of a uranyl acetate solution was applied following the same procedure and removed in the same way. Finally, the TEM grid was dried by sipping the possible remains of water using a micropipette tip joined to a vacuum pump.

Determination of CAC using Nile Red

120 μL of a stock solution of $5 \cdot 10^{-6}$ M solution of Nile Red in DCM were added to a series vials, and DCM was evaporated first at room temperature and later under vacuum. Then 600 μL of a solution of nanoparticles with a concentration ranging from 10^{-4} to 1 mg/mL were added to each vials and stirred for 24 h. Nile Red fluorescence spectra were registered from 560 to 700 nm, exciting at 550 nm. Fluorescence maxima were represented against concentration in logarithmic scale giving rise to a non-linear function in which the onset corresponds to the CAC value.

4.6. REFERENCES

1. Yang, L., Tan, X., Wang, Z. & Zhang, X. Supramolecular Polymers: Historical Development, Preparation, Characterization, and Functions. *Chem. Rev.* **115**, 7196–7239 (2015).
2. Spijker, H. J., van Delft, F. L. & van Hest, J. C. M. Atom Transfer Radical Polymerization of Adenine, Thymine, Cytosine, and Guanine Nucleobase Monomers. *Macromolecules* **40**, 12–18 (2007).
3. Kim, J. C. *et al.* Synthesis, physicochemical characteristics, and biocompatibility of self-assemble polymers bearing guanine, cytosine, uracil, and thymine moieties. *J. Polym. Sci. Part Polym. Chem.* **53**, 1151–1160 (2015).
4. Blasco, E., Barrio, J. del, Sánchez-Somolinos, C., Piñol, M. & Oriol, L. Light induced molecular release from vesicles based on amphiphilic linear-dendritic block copolymers. *Polym. Chem.* **4**, 2246 (2013).
5. Concellón, A. *et al.* Light-Responsive Self-Assembled Materials by Supramolecular Post-Functionalization via Hydrogen Bonding of Amphiphilic Block Copolymers. *Macromolecules* **49**, 7825–7836 (2016).
6. Wang, D., Wagner, M., Butt, H.-J. & Wu, S. Supramolecular hydrogels constructed by red-light-responsive host–guest interactions for photo-controlled protein release in deep tissue. *Soft Matter* **11**, 7656–7662 (2015).
7. Englund, E. A., Xu, Q., Witschi, M. A. & Appella, D. H. PNA–DNA Duplexes, Triplexes, and Quadruplexes Are Stabilized with *trans*-Cyclopentane Units. *J. Am. Chem. Soc.* **128**, 16456–16457 (2006).
8. Liu, Z.-C. *et al.* Synthesis of photolabile o-nitroveratryloxycarbonyl (NVOC) protected peptide nucleic acid monomers. *Tetrahedron* **61**, 7967–7973 (2005).

9. Shatila, R. S. & Bouhadir, K. H. Two simple protocols for the preparation of diallylaminoethyl-substituted nucleic bases: a comparison. *Tetrahedron Lett.* **47**, 1767–1770 (2006).
10. Newmark, R. A. & Cantor, C. R. Nuclear magnetic resonance study of the interactions of guanosine and cytidine in dimethyl sulfoxide. *J. Am. Chem. Soc.* **90**, 5010–5017 (1968).
11. Mynar, J. L. *et al.* Two-photon degradable supramolecular assemblies of linear-dendritic copolymers. *Chem. Commun.* 2081 (2007). doi:10.1039/b701681f
12. Yasugi, K., Nagasaki, Y., Kato, M. & Kataoka, K. Preparation and characterization of polymer micelles from poly(ethylene glycol)-poly(D,L-lactide) block copolymers as potential drug carrier. *J. Controlled Release* **62**, 89–100 (1999).

CONCLUSIONES

Capítulo 2

Se han preparado nuevos copolímeros bloque anfífilos basados en unidades de azobenceno con respuesta a la luz visible, mediante polimerización RAFT. Estos copolímeros bloque han sido ensamblados en agua dando lugar a micelas o vesículas dependiendo de la proporción entre los bloques hidrófilo e hidrófilo. Se ha estudiado la fotorrespuesta de estos sistemas a luz de 530 y 625 nm, siendo esta última más lenta, pero de gran interés en aplicaciones biológicas. En el caso de las vesículas, se encapsuló y liberó Rodamina B de forma controlada mediante estímulos lumínicos.

Capítulo 3

Se han sintetizado copolímeros bloque anfífilos basados en derivados de 4-alkilaminoazobenceno, sensibles a longitudes de onda fuera de la región UV, en combinación con unidades sensibilizadoras derivadas de naftaleno mediante polimerización RAFT. Estos copolímeros han sido autoensamblados en agua, formando micelas o vesículas dependiendo de la proporción entre ambos bloques. Se estudió además la fotorrespuesta de los autoensamblados, obteniéndose mejores comportamientos cuando se producía la excitación directa de los derivados de azobenceno, así como la capacidad de las vesículas de encapsular y liberar Rodamina B mediante el uso de luz.

También se evaluó la posibilidad de usar la química supramolecular como alternativa sintética para la preparación de estos sistemas. Aunque esta estrategia fue satisfactoria, las estructuras obtenidas tras el autoensamblado en agua no fueron de interés para nuestros objetivos.

Capítulo 4

Se han preparado nuevos copolímeros bloque anfífilos basados en guanina mediante polimerización RAFT. Éstos han sido funcionalizados con azobencenos con grupos citosina terminales en disolución acuosa. Todos estos sistemas han sido autoensamblados en agua dando lugar a dispersiones estables.

APPENDIX: TECHNIQUES AND INSTRUMENTS

Nuclear Magnetic Resonance (NMR)

^1H NMR and ^{13}C NMR were registered on a Bruker AV-400 (400 MHz) or on a Bruker ARX-300 (300 MHz).

Infrared spectroscopy

Spectra were registered on a Bruker FT-IR using KBr pellets.

Size exclusion chromatography (SEC)

SEC was performed on a Waters e2695 Alliance liquid chromatography system using a Waters 2424 evaporation light scattering detector and a Waters 2998 PDA detector. Measurements were performed in THF with a flow of 1 mL/min using PMMA standards for calibration or in DMF with a flow of 0.5 mL/min using PS standards for calibration.

UV-Vis spectroscopy

UV-Vis spectra were recorded on a ATI-Unicam UV4-200 spectrometer.

Fluorescence spectroscopy

Fluorescence measurements were recorded using a Perkin Elmer LS 50B fluorescence spectrophotometer.

Thermogravimetry (TGA)

TGA were performed using a TA Instruments Q5000IR under nitrogen atmosphere.

Differential Scanning Calorimetry (DSC)

Thermal transitions were determined using a DSC Q-2000 from TA instruments with powdered samples. Glass transitions temperatures were determined at half height point of the baseline jump and the melting temperatures at the maximum of the corresponding peaks.

Transmission Electronic Microscopy (TEM)

TEM was performed in a JEOL-2000 FXIII (200 kV) or in a JEOL JEM 1010 (100 kV). Samples were stained using uranyl acetate for 30 s or 10 s depending on the sample.

Dynamic light scattering (DLS)

DLS measurements were carried out in a Malvern Instrument Nano ZS with a He-Ne laser of 633 nm wavelength, a detector angle of 173° at 25 °C. Size measurements were registered three times to ensure consistency.

Light irradiation

Samples were placed into a UV cuvette and irradiated locating the cuvette 10 cm away from the irradiation source. A Phillips PL-9W was used as 365 nm source. For 420, 530 or 625 nm, a Mightex LCS-0420-12-22, a Mightex LCS-0530-15-22 (30 $\mu\text{W}/\text{cm}^2$) or a Mightex LCS-0625-07-22 (30 $\mu\text{W}/\text{cm}^2$) high power LED were used, respectively.